Faculty of Engineering and Science

Isolation and Microencapsulation of Phosphate Solubilizing Microorganisms for Enhanced Agricultural Growth on Peat

Hii Yiik Siang

0000-0003-0972-2993

This thesis is presented for the Degree of

Doctor of Philosophy

of

Curtin University

September 2020

DECLARATION

To the best of my knowledge and belief, this thesis contains no material previously published by any other person except where due acknowledgement has been made. This thesis contains no material which has been accepted for the award of any other degree or diploma in any university.

Signature :

Name : Hii Yiik Siang

Date : 2nd September 2020

ACKNOWLEDGEMENT

First and foremost, all praise, honor and glory to my Lord for His guidance and the strength He has given to me. Without His guidance, I would not be able to complete it.

Most importantly, I am very grateful to have receive support from the Curtin Malaysia Postgraduate Research Scholarship throughout my research. I am also thankful for Sarawak Biodiversity Centre (SBC) in granting the permission (Permit No SBC-EP-0055-SCYS) to isolate bacteria from peat collected from Sibu, Sarawak. Moreover, I would like to extend my deepest appreciation to my main supervisor, A/P Dr. Stephanie Chan for her supervision, encouragement and excellent advices during the period of my study. I would also like to thank my co-supervisor Dr. Lau Shiew Wei for her valuable suggestions and support and Prof. Michael Danquah for his guidance and helpful suggestions. Besides, I would like to thank A/P Dr. Law Ming Chiat for his supervision in my numerical modeling.

I also appreciate the help I received from laboratory technicians for their technical assistance. Other than that, I would like to express my appreciation to my friends in Curtin University, Carol Lai and Ignatius Phang for their kindness and useful advices. To my parents, aunts and siblings, I am greatly grateful for their endless love and faith in me. Additionally, I am also deeply grateful to my church members at the Miri Gospel Chapel Church for their unconditional love and support.

PUBLICATION FROM THESIS

Hii, Yiik Siang, Yen San Chan, Shiew Wei Lau, and Danquah Michael. "Isolation and characterization of phosphate solubilizing microorganisms from peat." *Biocatalysis and Agricultural Biotechnology* (2020): 101643.

Hii, Yiik Siang, Yen San Chan, Ming Chiat Law and Shiew Wei Lau. “Microencapsulation of *Staphylococcus haemolyticus* HCLB02 via novel impinging aerosol method: Optimization and Kinetic Study" - Submitting

Hii, Yiik Siang, Ming Chiat Law and Yen San Chan. “Modeling of Counterflow Sprays for the Microencapsulation of Phosphate Solubilizing Microorganisms." – Submitting

ABSTRACT

The utilization of peatland for agriculture is largely constrained by the low soil fertility. Crops require nutrients to survive and phosphorus is an essential macronutrient for plants growth. However, phosphorus tends to form complexes with calcium, aluminium and iron. These complexes have low solubility which limits the plant intake. Hence, phosphate solubilizing microorganisms (PSMs) have attracted the attention of agriculturists as PSMs have the competence to solubilize and mineralize insoluble phosphate complexes. PSMs also have the ability to synthesize growth-promoting hormones, facilitate the uptake of nutrients and prevent plant diseases. Therefore, this thesis firstly focuses on the isolation and identification of native phosphate solubilizing microorganisms (PSMs) from peat in Sarawak, Malaysia. This is the first report on the potential of *Staphylococcus haemolyticus* as PSMs. The solubilization potential of *S. haemolyticus* was optimized by varying the growth nutrients. Optimization was done using one-factor at a time method and the results showed that maximum solubilizing activity was obtained at 10 g/L of glucose, 2.5 g/L of yeast and 5 g/L of magnesium chloride hexahydrate.

The inoculation of PSMs into the soil without proper carrier generally causes the population to decline rapidly. In agriculture, encapsulation technique has been extensively used for protection, controlled release and functionalization of microorganisms. Encapsulated microorganisms provide greater long-term effectiveness as they can be released in a slow and controlled manner. Thus, this study also aimed to encapsulate PSMs in alginate microbeads by using the novel impinging aerosol method with misting nozzle instead of pneumatic nozzle. Experiments were executed by varying 3 process parameters namely alginate flowrate, alginate concentration and calcium chloride concentration. These parameters were optimized by employing the response surface methodology (RSM) with Box-Behnken Design (BBD). The results obtained showed that at 40 ml/min of alginate flowrate, 1.5 % alginate concentration and 0.1 M calcium chloride, the cell viability of PSMs was highest with average mean alginate microbeads size of 236.87 ± 12.25 µm. Then, the cell release of optimized alginate microbeads containing PSMs was studied. The cell release data was fitted to 5 kinetic models and Ritger-Peppas was found

to be the best model that describe the release of PSMs from alginate microbeads with R^2 value of 0.983.

Impinging aerosol is a continuous and scalable method and it is efficient in encapsulating cells. However, factors such as type of nozzles, alginate concentration and flowrate greatly influence the mean size of droplets, spray angle, wall wetting of chamber and spray distribution. Thus, this study also aimed to develop a computational fluid dynamics (CFD) model that could describe the impinging aerosol application. Eulerian-Lagrangian model was developed to study the spray angle, droplets size, fluid film formation on wall and spray distribution. The primary and secondary breakup were modeled using the Huh atomization and Reitz-Diwakar models, respectively while Bai-Gosman wall impingement model was employed for the fluid film formation on chamber wall. The CFD models were validated against experimental data and good agreement was observed for droplets size and spray angle at different flowrate. Then, the developed model was used to predict the spray outcomes with different parameters such as alginate concentration and nozzle orifice size. The CFD results showed that alginate flowrate of 40 ml/min, alginate concentration of 2 % and nozzle orifice size of 0.4 mm or 0.5 mm produced good spray distribution of alginate droplets within calcium chloride mists and minimal fluid film formation were formed. Well-distributed sprays allow the collisions between alginate and calcium chloride droplets which promotes the formation of solidified alginate microbeads. In addition, thinner fluid film ensures high products yield could be obtained.

Keywords: Phosphate solubilizing microorganisms (PSMs), microencapsulation, impinging aerosol method, cell release study and spray breakup model

TABLE OF CONTENTS

LIST OF FIGURES

LIST OF TABLES

ABBREVIATIONS

Analysis of Variance	ANOVA
American Society for Testing and Materials	ASTM
Box-Behnken design	BBD
Bromo phenol blue	BPB
Colony forming unit	CFU
Computational fluid dynamics	CFD
Coefficient of variation	CV
Coefficient of determination	R^2
Central composite design	CCD
Cleaning-in-process	CIP
Deoxyribonucleic acid	DNA
Direct-injection spark-ignition	DISI
Discrete Particle method	DPM
Electro-hydrodynamic atomization	EHDA
Fluid bed drying	FBD
Gibberellins	GA
Gasoline direct injection	GDI
Indole acetic acid	IAA
Kelvin-Helmholtz-Rayleigh-Taylor	KHRT
Linearized Instability Sheet Atomization	LISA
Monosodium glutamate	MSG
National Botanical Research Institute Phosphate	NBRIP
National Center for Biotechnology Information	NCBI
Optical density	OD
Organic acids	OA
Overall absolute percent error	OE
One-factor-at-a-time	OFAT
Phosphorus	P
Phosphate solubilizing microorganisms	PSMs
Pressurized metered dose inhalers	pMDI

Pyrroloquinoline quinone	PQQ
Polymerase chain reaction	PCR
Ribosomal ribonucleic acid	rRNA
Response surface methodology	RSM
Reitz-Diwakar	RD
Sauter Mean Diameter	SMD
Spray drying	SD
Spray-freeze drying	SFD
Standard deviation	SD
Taylor Analogy Breakup	TAB
Tryptic soy agar	TSA
Tryptic soy broth	TSB
Urea water solution	UWS
Ultraviolet	UV
Volume of Fluid	VOF

LIST OF SYMBOLS

Symbols	Description
$\overline{u_i}$	Average fluid velocity [m/s]
ρ	Density of the continuous phase [kg/m^3]
μ	Dynamic viscosity [Pa.s]
τ_{ij}	Reynolds-stress [N/m^2]
ε	Dissipation rate [m^2/s^3]
k	Turbulent kinetic energy [J/kg]
μ_t	Turbulent viscosity [Pa.s]
p	Pressure [Pa]
v_t	Kinematic eddy viscosity [m^2/s]
u	Fluid phase velocity [m/s]
u_p	Droplet velocity [m/s]
ρ_p	Density of the droplet [kg/m^3]
D_p	Droplet diameter [m]
C_D	Drag coefficient [-]
Re_p	Droplet relative Reynolds number [-]
L_t	Turbulent length scale [-]
τ_t	Turbulent time scale [-]
K_{avg}	Liquid jet average turbulent kinetic energy [J/kg]
ε_{avg}	Liquid jet dissipation rate at nozzle exit [m^2/s^3]
L_w	Wavelength of surface instability [-]
τ_A	Atomization time scale [-]
τ_t	Turbulence time scale [-]
τ_w	Wave growth time scale [-]
τ_{spn}	Spontaneous wave growth time [-]
τ_{exp}	Exponential growth time [-]
ρ_l	Liquid density [kg/m^3]
U	Spray velocity [m/s]
D_d	Diameter of the parent droplet [m]

K_A	Break-up rate constant [-]
β	Spray semi-cone angle [°]
β_d and α_d	Randomized angles [°]
D_s	Stable diameter [m]
τ_b	Breakup time scale [-]
We_p	Weber number of particles [-]
σ_p	Surface tension of droplet [N/m]
We_{crit}	Critical Weber number [-]
Q	Volume fraction of the droplets with a diameter smaller than D_p [-]
X	Mean size of droplets for which Q equals 0.6321 [-]
q	Droplet size spread parameter [-]
We_{co}	Collision Weber number [-]
γ	Drop size ratio [-]
u_1 and u_2	Velocities of the colliding drops [m/s]
r_1 and r_2	Droplets corresponding radii [m]
b_{crit}	Critical collision parameter [-]
We_I	Incident Weber number [-]
μ_p	Dynamic viscosity of droplet [Pa.s]
h_f	Film thickness [m]
ρ_f	Film density [kg/m^3]
v_f	Film velocity [m/s]
S_u	Mass source/sink per unit area from droplet impingement [kg/m^2]
V	Volume of film [m^3]
A	Area of film [m^2]
s_m	Momentum source [kg m/s]
p_f	Pressure of film [Pa]
f_b	Body force [N]
T_f	Viscous stress tensor within film [N/m^2]

CHAPTER 1

INTRODUCTION

This thesis proposes the application of phosphate solubilizing microorganisms in solubilizing fixed phosphate on peat-based agriculture. This chapter discusses the challenges on isolation and microencapsulation of PSMs as microbial inoculants for peat providing a framework for the objectives of this project. This chapter covers the background, research gaps, significance, research objectives and finally the thesis organization.

1.1 Background

The world population is anticipated to reach 9.6 billion which has been projected as our planet's maximum capacity by the year 2050 (Parnell et al., 2016). According to Food and Agriculture Organization (2017), global food production in 2050 need to be increased by 50 % as compared to demand in 2012. Due to the shortage of prime land, agriculture has begun planting on peatlands in order to constantly meet the increasing global food demand (Rahman et al., 2014). Malaysia has approximately 2.6 Mha of peatlands of which about 70 % are in Sarawak dominated by oil palm, coconut-cocoa and sago planting (DID, 2017). In 2009, a total of 666, 038 ha of peatland in Malaysia were planted with oil palm which 66 % were in Sarawak (Omar et al., 2010). The two main constraints of peatlands for agriculture development are the low nutrient contents and low pH of 3.2 to 3.7. Generally, soil acidity is accountable to natural and/or anthropogenic processes as shown in Figure 1.1. Acidity of soil is commonly caused by natural process and it can be deteriorated by environmental contamination through the application of fertilizers and acidifying

substances. Moreover, soil pH can be further reduced by the increase of H^+ concentration due to the imbalance in N, S, and C cycles, decomposition of organic material, excessive uptake of cations over anions and the uptake of nitrogen by crops. Mineral stress and infertility in the acidic soils can be ascribed to deficiencies of nutrients and toxicity by metals such as manganese (Mn), iron (Fe) and aluminium (Al). Hence, increasing soil acidity may leads to reduce yields, stunted root growth, poor nodulation of legumes, persistence of acid-tolerant weeds and increases incidence of diseases (Dinkecha, 2019).

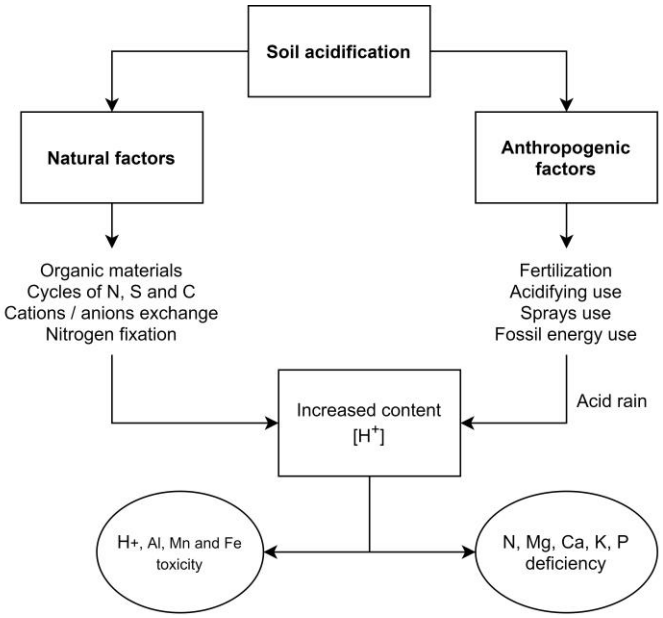

Figure 1.1 Soil acidification due to natural and anthropogenic factors. Adapted from Bojórquez-Quintal et al. (2017)

1.1.1 Phosphorus- An important nutrient for plant growth

Phosphorus (P) is the second important key element after nitrogen as a mineral nutrient in plant requirement. A sufficient supply of phosphorus is important as it aids in photosynthesis, energy transfer, signal induction, macromolecular synthesis and respiration (Maheshwari et al., 2013). P plays notable role in stimulating root development, establishing the primordia of plant reproductive part and increases the disease resistance ability of plant. P deficiency in plants significantly inhibits growth, resulting in stunted plants (Sharma et al., 2013). Figure 1.2 shows the phosphorus cycle in a typical cropping system.

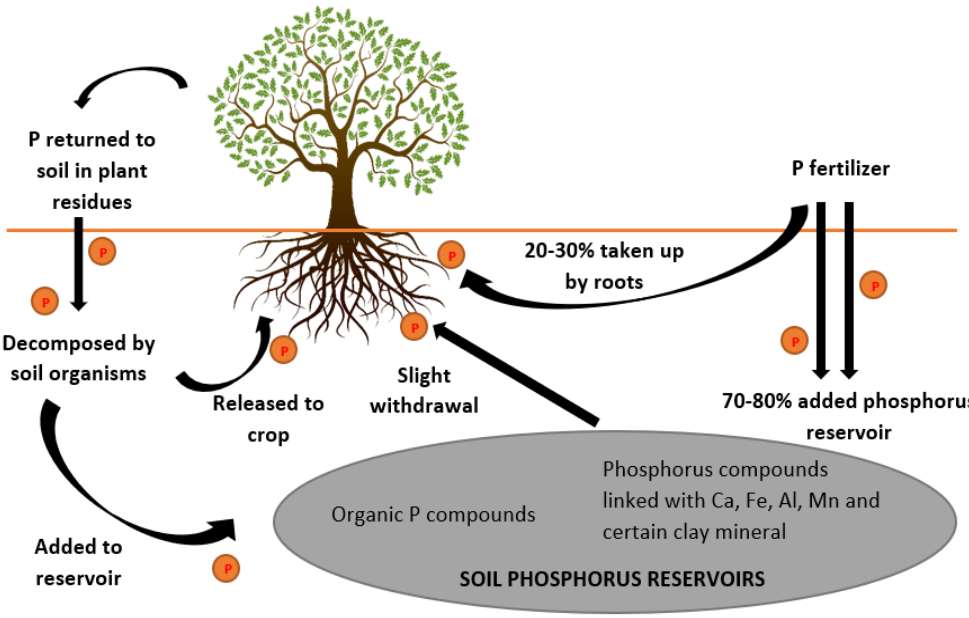

Figure 1.2 The phosphorus cycle in a typical cropping system. Adapted from Glendinning (2000)

As shown in Figure 1.2, P is abundant in soils in both inorganic and organic forms but its availability is limited as it presents mostly in insoluble forms. Direct application of phosphate rock as fertilizer is a very efficient way in correcting P deficiency (Rahman et al., 2014). However, plants can only absorb small amount of phosphate from fertilizer as approximately 70 to 80 % of added P is precipitated by metal-cation complexes (Parnell et al., 2016). Phosphate availability is dependent on soil pH and dominant cations. In acidic soil, the fixation of phosphate by aluminium and iron is very pronounced which limits the availability of soluble phosphate for plant uptake (Selim, 2015). If the soil is alkaline, phosphate is typically bound to calcium, but not as tightly. As reported by Melling (2016), the total P in peat ranges from 637.9 to 819.9 mg kg^{-1} but only about 20-28 % of phosphorus is available for plant uptakes. Similarly, Rahman et al. (2014) elucidated that the available form of P in deep peat ranges from 30-200 mg kg^{-1}. In peat, P is largely found in organic form and it must be mineralized before it is available to the plant (Sulandjari et al., 2019). According to Sutejo et al. (2017), the percentage composition of Al and Fe in fibrous peat were in the range of 1.9 to 12.9 % and 0.7 to 1.0 %, respectively. Besides, Kononen et al. (2015) and Kolli et al. (2010) showed that the composition of Al is approximately 2 to 3-fold more than Fe for tropical peat and 6 to

15-fold for forest peat. Thus, it concludes that concentration of Al-P in peat is higher than Fe-P.

The mining of phosphate minerals and utilization of P fertilizers are not eco-friendly, economically unfeasible and unsustainable. The production of phosphatic fertilizer is costly as it requires 4 million dollars per year (Situmorang et al., 2015) and involves the usage of non-renewable phosphate resources such as rock phosphate and mineral acids such as sulphuric acid as raw materials (Wyciszkiewicz et al., 2015). Bouwman et al. (2013) estimated that the total consumption of phosphate for fertilizer production from 2000 to 2050 will increase by approximately 64 %. In reference to the global dietary trends, Metson et al. (2012) suggested that the annual global phosphate demand will increase by 68 to 148 % in 2050 when compared to 2007 consumption. Studies by Gilbert (2009) and Scholz et al. (2013) showed that the world's resource of rock phosphate is likely to be significantly reduced in the next few decades and the sustainability of current phosphate supply is uncertain. In about 500–600 years, rock phosphate reserve will be depleted at present mining rate which is about 7,100 million tonnes/annum (Sharma et al., 2013). Besides, the excessive usage of phosphatic fertilizer to improve agricultural productivity potentially causes accumulation of toxic elements in the soil (Alori et al., 2017) which further reduces the soil fertility. Frequent fertilization increases the risk of phosphorus leaching as peatland has poor phosphorus adsorption capacity (O'Driscoll et al., 2011; Paavilainen & Paivanen, 2013). Then, the phosphorus in runoff accelerates algal blooms, hypoxia and eutrophication which potentially harms the aquatic ecosystem (Chowdhury et al., 2017). Figure 1.3 shows the conceptual model of P cycling in the soil.

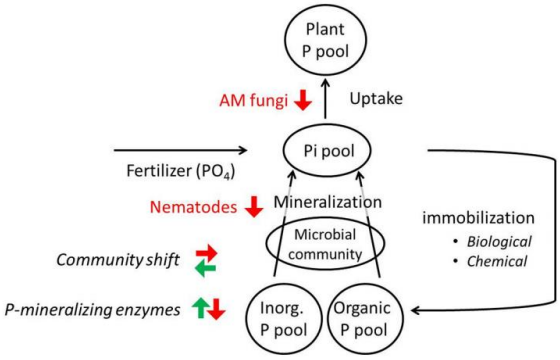

Figure 1.3 Conceptual model of P cycling in the soil (Ikoyi et al., 2018). Reproduced with permission of Elsevier

Referring to Figure 1.3, soil microorganisms play an important role in nutrient cycling in the soil. Soil microorganisms aid in the maintenance of plant available P pools because they mediate to a large extent the solubilization of inorganic P and mineralization of organic P in soils. Ikoyi et al. (2018) investigated the effect of application of P fertilizer on the abundance, diversity and taxonomic composition of microbial community. Their results showed that fertilizer treatments significantly reduced the bacterial, fungal and arbuscular mycorrhization community structures compared to the control. Sample without fertilization had a significantly higher relative abundance of bacterial genera including *Bacillus, Bradyrhizobium, Paenibacillus, Nocardioides* and *Balneimonas* that have been associated with P solubilization. These results suggested that a positive effect of a single phosphate application on plant growth in a soil can be voided by its adverse effect on the soil microbiota and their ecosystem. As frequent phosphate fertilization is unfavorable, there is an urgent need to find a sustainable alternative that is proficient of improving the efficacy of P fertilization, increasing crop yields and reducing ecological pollution caused by P loss from the soil.

1.1.2 Phosphate solubilizing microorganisms (PSMs)

Notably, apart from P fertilization, microbial P solubilization and mineralization are the practicable ways to increase the concentration of plant available P. The presence of various microorganisms in the soil and rhizosphere are effective at releasing soluble P from total soil P through solubilization and mineralization (Bhattacharyya and Jha, 2012). This group of microorganisms is generally known as phosphate solubilizing microorganisms (PSMs). PSMs have the ability to transform phosphate which is fixed in the soil into available forms such as soluble monobasic ($H_2PO_4^-$) and dibasic (HPO_4^{2-}) ions for plant uptake (Rodriguez et al., 2006). Generally, PSMs secrete organic acids (OA) and the acidification of their surrounding leads to the release of P ions from the complexes by H^+ substitution for mineral ions. PSMs also mineralize soil organic P by the production of enzymes that hydrolyze organic forms of phosphate compounds, thereby releasing inorganic phosphorus that will be immobilized by plants. Besides solubilizing P, PSMs also promote plant growth by producing growth-promoting hormones and increasing the efficiency of nitrogen fixation. PSMs also act as biocontrol agents against some plant

pathogens by producing siderophores, antibiotics, hydrogen cyanide and lytic enzymes which inhibits the growth of plant pathogens (Walpola et al., 2012b).

Since the early 1900s, numerous strains of PSMs have been isolated from various sources such as soil, rhizosphere, root nodules, compost and earthworm casts (Singh et al., 2011). Remarkably, these PSMs belong largely to genera such as *Pseudomonas, Fusarium, Azotobacter, Rhizobium, Paenibacillus, Rhodococcus, Serratia, Aspergillus, Bacillus, Flavobacterium, Agrobacterium, Aerobacter* and *Penicillium* (Rodriguez & Fraga, 1999; Maheshwari et al., 2013; Sharma et al., 2013). Numerous media such as Pikovskaya (Pikovskaya, 1948), bromophenol blue dye method (Gupta et al., 1994) and National Botanical Research Institute Phosphate (NBRIP) medium (Nautiyal, 1999) have been developed to screen PSMs. However, these media use calcium phosphate (Ca-P) such as tricalcium phosphate (TCP) as their sole phosphate source and PSMs isolated are able to solubilize Ca-P but only scarce amount can solubilize iron or aluminium phosphate (Fe-P or Al-P). These PSMs are effective in alkaline or calcareous soil in which Ca-P predominate and ineffective in acidic soil in which phosphate forms complexes with Al or Fe ions (Pengnoo et al., 2007).

1.1.3 Microbial encapsulation for improved cell viability

In order to increase the consumption of the P accumulated in soils, PSMs that has the ability in transforming insoluble phosphates to soluble forms can act as biofertilizers. Several authors such as Adesemoye et al. (2009), Khan et al. (2009), Fitriatin et al. (2014) and Etesami and Alikhani (2016) suggested that about 25% to 50% of phosphatic fertilizer requirement could be reduced by the inoculation of PSMs. PSMs are frequently used to inoculate plant material without a proper carrier or in amounts that do not permit for efficient rhizosphere colonization under field conditions. It is challenging for the inoculated PSMs to survive and flourish in soil following inoculation (Backer et al., 2018). It is not easy to induce root colonization via direct inoculation of microorganisms into soil without proper carrier. This is because microorganisms are vulnerable to environmental variations such as soil conditions, fluctuation of pH and temperature, humidity and competition with soil micro and macrofauna (Wu et al., 2012b). Cell immobilization technology has proved to be more advantageous over free cell inoculation (Zohar Perez et

al., 2002). Formulating inoculant containing highly effective PSMs with high rhizosphere colonization rate and long storage life poses a key challenge for commercialization. Suitable formulation is vital for a high-quality inoculant. Good formulations should provide ideal environment to enhance microorganism life on roots to assure maximal benefits after application to the target plants. Formulation of inoculants is a critical matter, but little exploration has been conducted on this issue. There are three fundamental features for all inoculants. Firstly, inoculants need to support the growth of encapsulated PSMs under environmental stresses. Secondly, they should be able to sustain adequate number of viable PSMs (~10^9 CFU/g beads) in good functional condition for an adequate period (Stephens & Rask, 2000). Lastly, inoculants need to deliver sufficient PSMs at the time of inoculation to reach a threshold number of PSMs that is obligatory to obtain a plant response (Date 2001).

There are numerous conventional inoculants such as peat based and liquid formulations. The use of peats as carriers is unfavorable due to its high variability which affects the quality of the final product (Bashan, 1998). Additionally, peat formulations are not capable to maintain high cells density (Schoebitz et al., 2013b). On the other hand, liquid formulations which include suspensions, concentrates and oil-based products are also not desirable because it does not provide a protective environment for the PSMs (Bashan et al. 2002). In fact, encapsulation techniques have been introduced to enhance efficiency of formulations by entrapping microorganisms on matrices. Encapsulation provides proper microenvironment, reduces microbial competition and provides controlled release to assist colonization of plant roots (Young et al., 2006). The most prominent encapsulation techniques are immobilization of cells by spray-drying, emulsion or extrusion methods. Spray drying results in high volume output but the use of high production temperature is unfavorable for the cells viability (Mauriello et al., 1999). Emulsion method is based on emulsification of cell-polymer suspension in vegetable oil. Then, the emulsion is added into an ionic solution ($CaCl_2$) to induce gelation forming micro-hydrogel beads (Krasaekoopt et al., 2003). According to Vemmer and Patel (2013) this technique produces smaller particles with a higher size distribution in comparison with extrusion method. However, Burey et al. (2008) reported that the main disadvantage in this technique is the removal of oil. Extrusion is a simple and cost-effective encapsulation

method as it involves extruding the cell-polymer suspension through a syringe needle. This method uses mild formulation conditions that ensure high cell concentration and viability (Krasaekoopt et al., 2003). The key limitations of this method are the large beads size, scale-up restrictions and non-continuous production (Gouin, 2004). These droplets harden when fall into cross-linking solution and form irregular shape and porosity microbeads (Martins et al., 2007).

1.2 Research Gaps and Significances

The capability of PSMs to solubilize and mineralize insoluble inorganic and organic phosphate is related with the nutritional richness of the soil, the physiological and growth status of the PSMs. In other words, PSMs obtained from soils from environmental extremes such as high acidity, high salinity, high alkalinity, low nutrient or extreme temperature environments have the capability to solubilize more phosphate than PSMs isolated from soils with moderate conditions (Zhu et al., 2011). For example, Selvakumar et al. (2008) isolated PSMs from stressed environment with extreme cold temperature region and their results showed that *Serratia marcescens* greatly improved the nutrient uptake of wheat seedlings and biomass of plant when grown in cold environment. Similarly, Zhu et al. (2011) isolated PSMs from marine environment and the PSMs could survived high sodium chloride (NaCl) concentrations (up to 20 %) and pH range of 4.0–10.0, making it suitable for the saline-alkali soil-based agriculture. As reviewed by Verma et al. (2017), the acidic environments sustain a diverse microbial community with plant growth promotions attributes . A few acidotolerant bacterial genera have been found in acidic environments and their plant growth promotions attributes in low pH conditions are identified (Yadav et al., 2011; Yadav et al., 2014). Generally, the lack of successful commercial PSMs inoculants has been noted and attributed to plant or environmental incompatibility (Leggett et al., 2001). Notably, Taurian et al. (2010) suggested that it is essential to isolate PSMs from ecosystem where the inoculant will be used in order to ensure PSMs have the ability to compete with native microflora and survive the environmental stresses. As reported by Cho and Tiedje (2000), beneficial PSMs are generally native isolates from the location and cropping systems. Various different species of PSMs can be isolated from different locations (Panda et al., 2016). For examples, Pengnoo et al. (2007), Istina et al. (2015) and Situmorang et al. (2015) isolated PSMs in

genera *Burkholderia*, *Ustilago* and *Flavobacterium*, respectively from peat of different location. It can be hypothesized that PSMs isolated from peat could survive the harsh environment of peat and possess the ability to solubilize and mineralize fixed phosphate in soil P reservoir. To the best of my knowledge, there are limited studies on the isolation of PSMs from peat in Malaysia. Thus, it is essential to identify natives PSMs that could be used as microbial inoculants for the peat-based agriculture.

Currently, halo zone formation by bacterial colonies on agar plates has been used as the sole indicator for phosphate solubilization by PSMs. However, this method is only efficient to identify PSMs that could solubilize tricalcium phosphate, $Ca_3(PO_4)_2$. When these isolates are tested for Al-P solubilization in liquid media, these strains show low solubilizing activity. Often, the solubilization of insoluble Al complexes through metal complexing gives no halo zone on the agar plates (Bashan et al., 2013). The formation of halo-zone when Al-P is used as indicator has not yet been reported (Gadagi & Sa, 2002). Notably, colonies that does not produce halo-zone could solubilize numerous type of insoluble inorganic phosphate in broth medium (Sharma et al., 2013). Based on the fact that solubilization of insoluble phosphate is always linked with the reduction in pH, this study employed a method developed by Gadagi et al. (2002), where pH indicator dye, bromo phenol blue (BPB) was added to culture media with Al-P as the phosphate source for the isolation of Al-P solubilizer. The organic acids release by PSMs would turn the blue dye to yellow. An additional test in liquid media to assay Al-P dissolution by PSMs was done to confirm their Al-P solubilizing potential. The isolated PSMs are hypothesized to possess the ability to solubilize the insoluble Al-P in peat releasing soluble phosphate for plants uptake.

In conventional extrusion method, large microbeads with diameter greater than 1 mm are produced. Their relatively large size is disadvantageous for agricultural uses as during sowing, beads might fall far from the seeds. As the released bacteria travel through the soil, they face competition from the native microflora (Bashan et al., 2014). This fundamental difficulty can be solved by the use of microbeads as it would be possible to produce formulation in powder form. These dried microbeads can be directly coated on seeds (Bashan et al., 2014). As reported by Szczech and Maciorowski (2016), the small

size of capsules allows high cell concentration and viability. This is because the small size capsule provides efficient oxygen diffusion, nutrients and metabolites. In this regard, microencapsulation technology is favorable as it is effective and results in an easy release of microorganisms to the targeted site due to the small size and higher surface area. Additionally, the cells mortality rate during the preparation of microbeads is lower in comparison to macrobeads (Bashan, 1998). Remarkably, the microencapsulation of PSMs through the novel impinging aerosol method has attracts the attention of researchers. This method involves the atomization of alginate and $CaCl_2$ solution into fine droplets in an encapsulation chamber using compressed air driven pneumatic nozzles. It is a continuous process and cost effective (Bhandari, 2009). Despite its promising applications and expected benefits, to date, this method has never been evaluated for the production of microbial inoculants. This research was therefore proposed to investigate the optimum process parameters to entrapped sufficient amount of viable PSMs within the desired bead size. The results obtained from this study is anticipated to provide preliminary results on the development of a continuous processes lab scale impinging aerosol spray device for the production of alginate microbeads as carrier for PSMs. The obtained design can then be upscaled for future work in mass production of PSMs-loaded alginate microbeads as biofertilizer.

Impinging aerosol method is an effective and useful encapsulation method for bacteria. However, there are still issues that arise with impinging aerosol method as the spray atomization of alginate and $CaCl_2$ solutions is a complicated process which is affected by factors such as solution viscosity, process parameters and type of nozzles. It is important to optimize these process parameters as it determines the microbeads size, spray angle and spray distribution which affects the encapsulation efficiency, quality and yield of products. In addition, when working with impingement aerosol method in production of microbeads, the main concern is the impingement of spray droplets on encapsulation chamber wall. If the spray angle is large, droplets tend to stick on wall forming fluid film, leading to production losses. It is time consuming to identify the optimized condition of spray through extensive experimental works. Thus, numerical simulation methods are developed to study the engineering issues due to its convenience and high accuracy. The computational fluid dynamics (CFD) is an essential branch of numerical simulation to

solve the governing equation of fluid dynamics by computer and numerical computation to predict the experimental research proficiently (Li et al., 2019). Consequently, this study also aimed to develop a CFD model to predicts the spray behaviors of impinging aerosol with different solution physicochemical characteristics, process parameters and nozzle orifice diameter. The numerical results were validated with experimental results to ensure model could be used to predict the droplet size, spray distribution and fluid film thickness in the production of PSMs-loaded alginate microbeads.

1.3 Research Questions

1. Which PSMs isolated from peat possess the highest phosphate solubilization potential?
2. What is the optimum condition for cell growth and phosphate solubilization activity?
3. What are the optimum parameters to formulate microbeads that facilitate controlled release and environmental stress protection of PSMs? What is the release kinetic of PSMs from microbeads?
4. What are the droplet size of microbeads, spray angle, spray distribution and fluid film thickness under different operating conditions?
5. What are the factors that affects the spray atomization?

1.4 Objectives

1. To isolate PSMs from peat which are able to solubilize insoluble inorganic phosphate.
2. To identify the optimal condition for culture growth and maximal organic acids production.
3. To determine the optimum process parameters to produce microbeads containing at least 10^9 CFU/g of dried beads and study the kinetic release of PSMs from the microbeads.
4. To develop a CFD model using STAR CCM+ to predict droplet size, spray angle, film thickness and spray distribution and validate the CFD model with experimental data by a lab-scale impinging aerosol spray device for its practical applications in microencapsulation of PSMs.
5. To study the effects of alginate flowrate, alginate concentration and nozzle diameter on spray outcomes using the validated CFD model.

1.5 Scope of the study

First, phosphate solubilizing microorganisms (PSMs) were isolated from peat. Then, the phosphate solubilization potential were tested. Three isolates that showed highest solubilizing potential were subjected to DNA sequencing. Then, the effect of time and addition of soluble phosphate on phosphate solubilization were studied. Optimal cultural condition for cell growth that leads to maximal phosphate solubilization was identified. Three parameters namely glucose concentration, yeast concentration and magnesium chloride hexahydrate concentration were studied. Later, the microbeads containing PSMs was produced using the impinging aerosol method. The process parameters namely concentration of alginate, flowrate of alginate and concentration of calcium chloride were optimized by using the response surface methodology (RSM) in order to produce microbeads with viable cells greater than 10^9 CFU/g of dried beads. Then, the area of study focused mainly on the modeling of impinging aerosol method by using Star CCM+ software. The computation fluid dynamics (CFD) results obtained were validated with experimental results. The validated CFD model was then used for parametric studies. The effects of various parameters such as alginate concentration, flowrate, and nozzle orifice size diameter on spray distribution, spray angle, droplet size and fluid formation on wall were studied. The sensitivity analysis on breakup parameters were also investigated to identify the parameters that influenced the breakup mechanisms.

1.6 Thesis layout

This report consists of 7 chapters as shown in Figure 1.4. Chapter 1 gives an overview of the background of phosphate solubilizing microorganisms and cell immobilization technology. Apart from that, objectives of this study were outlined to inform the readers on the aim of the study. Furthermore, the research gaps and significances were identified to enlighten the importance of the current study. As for Chapter 2, it contains literature review on the phosphate solubilizing microorganisms. It also highlighted the mechanisms of inorganic and organic phosphate solubilization. Moreover, the encapsulation technologies were discussed. The numerical simulation for impinging aerosol method was also highlighted. Chapter 3 covers the experimental research methodology. First, the methods used to for PSMs isolation and identification were explained. Then, the

encapsulation method was discussed. Other than that, details on optimization of cell viability using response surface methodology was included. Next part, the methodology for kinetic release study of PSMs from alginate microbeads was included. Next, Chapter 4 focuses on the results and discussion obtained from the experimental study. The optimum process parameters to produce alginate microbeads with high cell viability were determined. Finally, the best kinetic model for cell release from alginate microbeads was identified. Chapter 5 discusses the CFD model and the physics used in the modeling of impinging aerosol encapsulation method. Chapter 6 focuses on the results and findings obtained from numerical study. Lastly, Chapter 7 includes the conclusion of this thesis which includes summary of research findings and recommendations for future work. Appendix consists of all the raw data obtained experimentally and the copyright permissions.

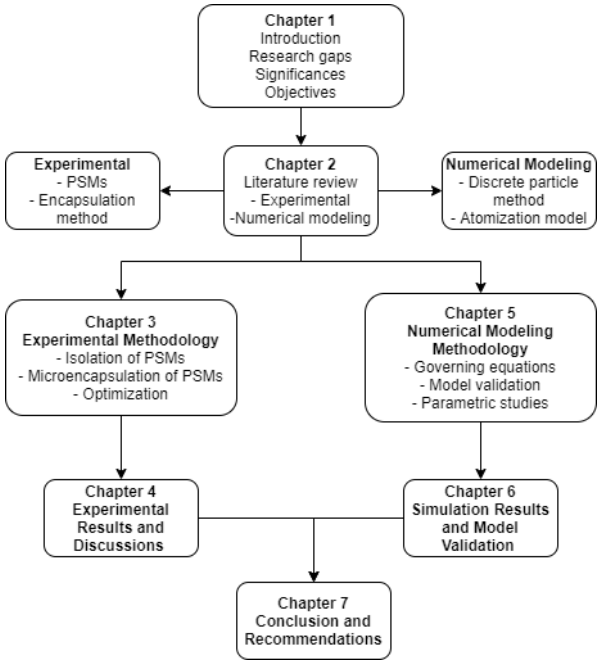

Figure 1.4 Thesis layout flow diagram

1.7 Concluding remark

As the global population increases, there is a need in increasing food production. The decline in arable land has resulted in plantation on peatland. As peatland is low in nutrients, phosphate fertilizers have been used to correct the phosphorus deficiency. Peatland is acidic in nature and thus, the phosphate from fertilizers tend to form complexes with Al and Fe ions, making it unavailable for plant uptake. The usage of fertilizer is not

environmental-friendly which led to the application of PSMs which has the ability to solubilize and mineralize fixed phosphate in soil. It is essential to microencapsulate PSMs prior to inoculation in order to protect the PSMs from the environmental stresses and enable the PSMs to be release to the environment in a controlled manner. Impinging aerosol method is a prominent microencapsulation technique that has gained the attention of researchers in recent years. However, various factors such as flowrate, concentration and size of nozzles orifice greatly affects the spray behaviors. It is time consuming and costly to identify the optimized condition of spray through experimental methods and thus numerical modeling is a useful tool to predict the spray outcomes.

CHAPTER 2

LITERATURE REVIEW

In the previous chapter, the background of PSMs, encapsulation methods and numerical modeling for encapsulation were highlighted. Current chapter focuses on the literature review which provides library evidences and facts to support research question. In this context the following literature review mainly focus on the critical appraisal of past studies related to phosphate solubilizing microorganisms, encapsulation technologies and correlated numerical modeling for spray atomization employed by past researchers.

2.1 Phosphate solubilizing micoorganisms (PSMs)

Phosphate-solubilizing microorganisms (PSMs) is proficient in transforming insoluble P into soluble forms. Pengnoo et al. (2007) isolated PSMs from the rhizosphere of *Melaleuca cajuputi* grown in peat by using $AlPO_4$, $FePO_4$ and phytate as the phosphate sources. Notably, their studies showed that *Ustilago sp.* (fungi) is capable of solubilizing $AlPO_4$, $FePO_4$ and phytate. Situmorang et al. (2015) isolated PSMs from the peat of oil palm plantation in Indonesia. Their studies used TCP as the phosphate source and their findings showed that *Burkholderia sp.* has the highest phosphate solubilization capability. Besides, Istina et al. (2015) screened the PSMs from peat by using $AlPO_4$ as the phosphate source. The results obtained showed that *Penicillium aculeatum* (fungi) has the Al-P phosphate solubilization potential. The application of *P. aculeatum* on oil palm seedlings increased the seedling height, dry weight of roots and phosphate uptake by 3 %, 5 % and

10 %, respectively. They also concluded that bacteria that has the ability to solubilize phytate is a potential candidate for phosphate suppliers in acidic peat.

2.2 Phosphate Solubilization Mechanisms

Several mechanisms have been used to explain the microbial solubilization of inorganic phosphate. Phosphate solubilization occurs mainly by acidification of medium, chelation of the cations bound to phosphate and mineralization (Osorio, 2011).

2.2.1 Acidification of medium

The acidification of medium is associated with the production of organic acids by PSMs via oxidative respiration or decomposition of organic carbons (Sharma et al., 2013). These organic acids convert the phosphate minerals into $H_2PO_4^-$ or HPO_4^{-2} by H^+ substitution for the cation bound to phosphate (Goldstein, 1994). Solubilization without acid production is due to the H^+ excretion accompanying respiration or NH_4^+ assimilation (Osorio, 2011). This mechanism only applies to calcium phosphate as its solubility increases exponentially with decreasing pH making it easier to be solubilized (Bashan et al., 2013). The reaction scheme in the case of calcium phosphate resulting in the formation of more soluble phosphate can be represented by Equation 2.1.

$$Ca_3\left(PO_4\right)_2 + 2H^+ \leftrightarrow 2CaHPO_4 + Ca^{2+} \tag{2.1}$$

Notably, gluconic acid is the most common agent of inorganic phosphate solubilization (Rodriguez et al., 1999; Kalayu, 2019) and it is a primary organic acid releases by *Pseudomonas sp.*, *Rhizobium sp.*, and *Burkolderia sp.* Carbon source such as glucose is the main precursor for the synthesis of gluconic acid. Glucose dehydrogenase and co-factor pyrroloquinoline quinone (PQQ) breakdown glucose to gluconic acid. Gluconic acid can be further oxidized to 2-keto gluconic acid by gluconate dehydrogenase. Other organic acids produced by PSMs in the solubilization of phosphate are 2-ketogluconic acid, oxalic acid, citric acid, lactic acid, tartaric acid and aspartic acid (Ahmed & Shahab, 2011). The potential of *Bacillus sp.* and *Staphylococcus sp.* in ammonium production was reported by Orhan (2016). Similarly, Biswas et al. (2018) isolated PSMs from the gut of the earthworm and their results showed that *Bacillus megaterium*, *Staphylococcus*

haemolyticus and *Bacillus licheniformis* produce ammonia which supports the growth of a *Vigna radiata* plant. Table 2.1 summarized some of the organic acids released by PSMs.

Table 2.1 Organic acids released by PSMs in phosphate solubilization

Phosphate solubilizing microorganisms	**Organic acids**	**References**
Bacillus megaterium	Citric, lactic and propionic acids	Chen et al. (2006)
Serratia marcescens	Citric, gluconic and succinic, lactic acids	
Arthrobacter sp.	Citric and lactic acids	
Rhodococcus erythropolis	Gluconic acid	
Pseudomonas sp.	Gluconic, oxalic, formic, 2-ketogluconic, lactic and malic acids	Vyas and Gulati (2009)
Staphylococcus warneri	Gluconic, citric and succinic acids	Acevedo et al. (2014)
Pantoea sp., Acinetobacter sp. and *Enterococcus sp.*	Gluconic acid	Anzuay et al. (2017)
Serratia sp.	Malic, lactic and acetic acid	Behera et al. (2017)
Alcaligenes aquatilits	Citric acid	Pande et al. (2017)
Burkholderia cepacia	Gluconic and formic acids	
Paenibacillus sp.	Tartaric, oxalic, formic, malic, acetic, citric and succinic acid	Chawngthu et al. (2020)
Bacillus cereus	Tartaric, oxalic, formic, gluconic, malic, acetic, citric and succinic acid	

2.2.2 Chelation

Chelating agents such as organic acids, H_2S, CO_2 and mineral acids are also correlated with phosphate solubilization (Kuhad et al., 2011). In the case of metal chelation, a chelating ligand or anion forms two or more bonds with the metal forming a ring structure. Thus, transforming an insoluble phosphate mineral into the metal complex and releases phosphate anions (Bashan et al., 2013). Organic acid anions with oxygen containing hydroxyl and carboxyl groups have the ability to form stable complexes with cations such as Ca^{2+}, Fe^{2+}, Fe^{3+}, and Al^{3+} that are often bound with phosphate in poorly forms (Ahmed et al., 2011). The reactions of calcium, iron, aluminium phosphate can be explained by Equations 2.2, 2.3 and 2.4, respectively (Bashan et al., 2013).

$$Ca_3(PO_4)_2 + 3mH_nX \leftrightarrow 3[CaX_m]^{2-mn} + 2HPO_4^{2-} + (3mn-2)H^+ \quad (2.2)$$

$$FePO_4 + mH_nX \leftrightarrow [FeX_m]^{3-mn} + HPO_4^{2-} + (mn-1)H^+ \quad (2.3)$$

$$AlPO_4 + mH_nX \leftrightarrow [AlX_m]^{3-mn} + HPO_4^{2-} + (mn-1)H^+ \quad (2.4)$$

Studies by Illmer et al. (1995) showed that *A.niger, Pseudomonas sp., Penicillium sp.* are effective in solubilizing aluminium phosphate via organic acids production. Khan et al. (2013) reported that *Penicillium rugulosum* solubilizes insoluble P by mineral acids such as HCl, nitric acid, and sulfuric acids produces by chemoautrophs and the H^+ pump. As conveyed by Bashan et al. (2013), chelation of phosphate minerals seems to be the main mechanism for aluminium and iron phosphate. These results were in agreement with Merbach et al. (2009) where it is testified that acidification of medium cannot account for phosphate solubilization of aluminium and iron phosphate. This is because the solubility of iron phosphate and aluminium phosphate decreases with lower pH as shown in Figure 2.1. At low pH, it can be seen that the solubility of Fe-P is very low when compared to Al-P. At peat pH which is about 3.2 to 3.7, it can be reasoned that the Fe-P solubilization is negligible and therefore, low P solubilization by PSMs is expected. Based on the studies by Collavino et al. (2010), Anzuay et al. (2017) and Li et al. (2017), the solubilization of Al-P by PSMs was approximately two-fold more than Fe-P as it was considerably more soluble. Thus, this study focused on the solubilizing of Al-P by PSMs.

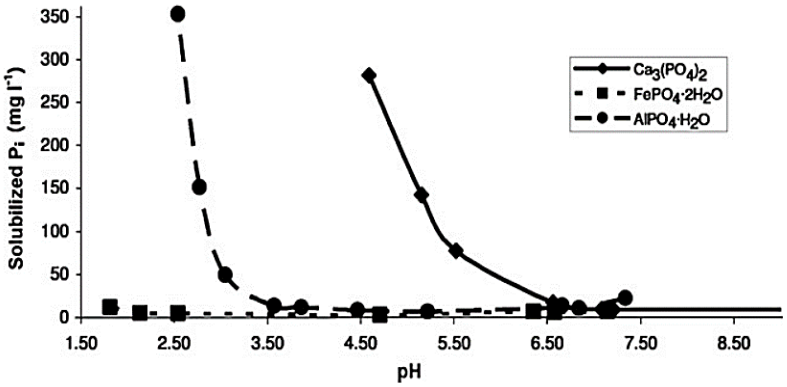

Figure 2.1 Solubilization of phosphate from Ca, Al, and Fe phosphates as a function of pH (Bashan et al., 2013). Reproduced with permission of Springer Nature

2.2.3 Mineralization

Organic phosphorus may constitute 4 - 90 % of total phosphorus in soil (Khan et al., 2009). Phytate, the most stable organic phosphorus is about 50 % of total of the organic phosphorus. Other organic phosphorus is present in the form of phosphomonoesters, phosphodiesters and phosphotriesters (Rodriguez et al., 1999). Organic phosphorus must be hydrolysed to inorganic phosphate before it can be utilized and taken up by plants. Organic phosphorus can be mineralized and catalysed to $H_2PO_4^-$ or HPO_4^{-2} by enzymes such as phosphatases, phytases, phosphonatases and C–P lyases (Iqbal Hussain et al., 2013; Sharma et al., 2013). *Aspergillus sp.*, *Penicillium sp.* and *Trichoderma sp.* are the most reported phytase-producing fungus. Bacteria such as *Bacillus* and *Streptomyces sp.* secrete extracellular enzymes such as phosphoesterases, phosphodiesterases, phytases, and phospholipases which has the ability to mineralize complex organic phosphates (Kalayu, 2019). Some examples of PSMs which have the potential to release phosphate from different organic phosphorus are summarized in Table 2.2. Phosphatases dephosphorylate phosphoester or phosphoanhydride bonds of organic matter. Depending on their pH optima, these enzymes are divided into acid and alkaline phosphatases. Typically, acid phosphatases predominate in acid soils, whereas alkaline phosphatases are more abundant in neutral and alkaline soils (Sharma et al., 2013). Phytases specifically cause release of phosphate from phytate (Ahmed et al., 2011). Phosphonatases and C–P lyases cleave the C–P bond of organophosphonates (Rodriguez et al., 2006).

Table 2.2 Phosphate mineralization from P-substrates by some soil bacterial species

Isolates	**Phosphate source**	**Enzyme**	**References**
Caulobacter sp., Enterobacter aerogenes, Escherichia blattae, Klebsiella pneumoniae, Pseudomonas aeruginosa, Raoultella planticola, Serratia sp., Burkholderia cepacian, Leclercia adecarboxylata and Pseudomonas putida	Non-specific	Acid phosphatase	Behera et al. (2017), Fraser et al. (2017), Story and Brigmon (2017), Teng et al. (2019)
Serratia sp., Acetobactor sp., B. laevolacticus, Klebsiella terrigena, Pseudomonas sp., Enterobacter sp., B. Amyloliquefaciens, Advenella sp. Acromobacter sp., Tetrathiobacter sp. and Bacillus sp.	Phytate	Phytase	Kumar et al. (2013), Singh et al. (2014), Kalsi et al. (2016)
Escherichia coli, Pseudomonas stutzeri, Ochrobactrum anthropi, Sinorhizobium meliloti, Agrobacterium radiobacter, Buckholderia pseudomallei	Phosphonates	C-P Lyase	He et al. (2009), Hove-Jensen et al. (2014)

2.3 Mode of plant growth promotion by PSMs

PSMs apply various approaches in plant growth promotion which include abiotic stress tolerance in plants, nutrient fixation for plant, the production of plant growth regulators,

the production of siderophores and the production of protection enzyme (García-Fraile et al., 2015). Figure 2.2 represents the schematic representation of plant growth promotions by PSMs.

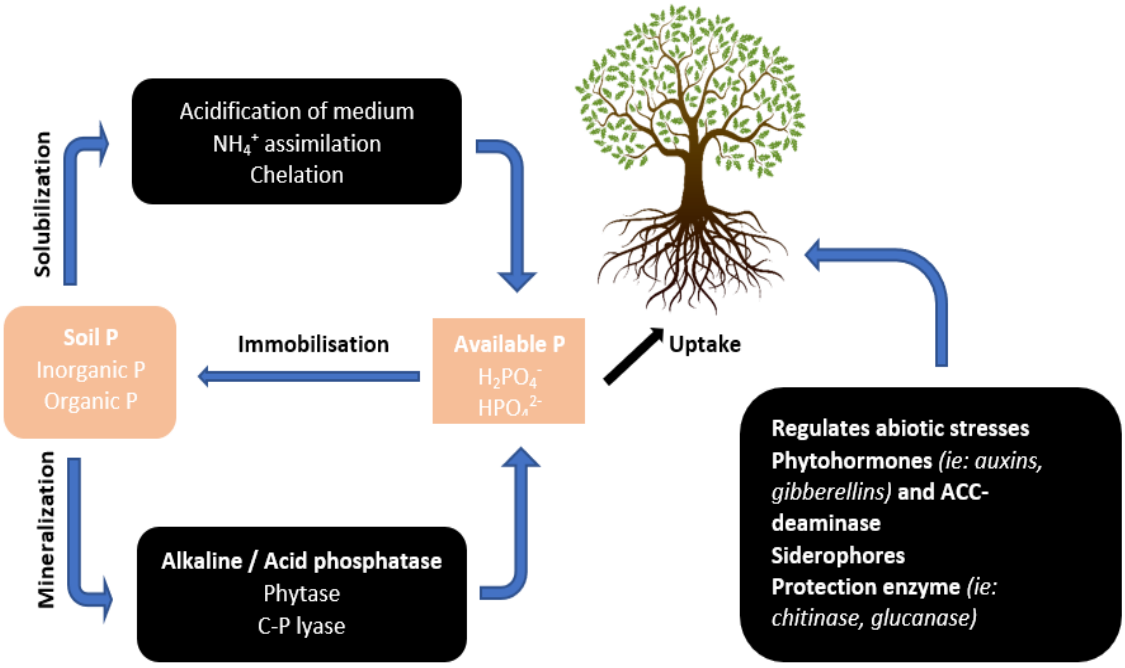

Figure 2.2 Schematic representation of plant growth promotions by PSMs (Sharma et al., 2013; García-Fraile et al., 2015; Vejan et al., 2016)

Abiotic stresses such as high salinity, extreme temperature, deficient or excessive water and high concentration of heavy metals are the key sources of crop yield reduction. The intensity of abiotic stress differs depending on the type of soil and plant's susceptibility to diseases (Vejan et al., 2016). For example, various researchers have isolated halotolerant or halophile PSMs for the application in salt-affected soils. Halotolerant PSMs regulate salt stress by formation of soil aggregates, breaking down organic matters or maintaining nutrient cycling, and transformation of organic compounds (Kirk et al., 2004). Orhan and Gulluce (2015) isolated *Bacillus sp, Staphylococcus sp., Halomonas sp.*, which showed high salt tolerance and substantial enzyme activities that can enhance soil fertility and the cycling of soil nutrient. Arshad et al. (2019) also isolated *Pseudomonas plecoglossicida* as chromium tolerant PSMs. *P. plecoglossicida* was able to tolerate Cr stress, effective in solubilizing phosphate and produced indole acetic acid (IAA) that promotes plant growth. PSMs also increase plant growth by enhancing P uptake efficiency of plants by

transforming the fixed forms of P to an available form (Satyaprakash et al., 2017) and promotes the efficiency of nitrogen fixation (Sharma et al., 2013).

PSMs also enhance plant growth through generation of phytohormones such as auxins and gibberellins (GA) (Vejan et al., 2016). Auxin is one of the essential molecules that regulates most plant processes and the most common auxin in plants is IAA. According to Spaepen et al. (2007) various processes in plant growth and development are controlled by IAA. By increasing the IAA levels, primary root length decreases, root hair formation increases and enhances the formation of lateral roots empowering plants to have better access to nutrients in soil. GA promotes seed germination, floral induction, flower and fruit development, steam and leaf growth and shoot elongation (Spaepen & Vanderleyden, 2011). Afzal and Bano (2008) reported phosphate solubilization by *Rhizobium sp.* and *Pseudomonas sp.* was due to the production of IAA and GA. In addition, enzyme ACC deaminase regulates the level of plant ethylene which governs the development of leaves, flowers, and fruits. Banerjee et al. (2019) testified that *Bacillus safensis, Bacillus flexus* and *Staphylococcus haemolyticus* promotes the growth of *Vigna radiata* plant through IAA, GA, ammonia, ACC deaminase production and phosphate solubilization activity. PSMs also secrete siderophores, a high-affinity iron chelating compounds that forms stable Fe^{3+} hexacoordinated complexes releasing phosphate ions (Khan et al., 2014). When Fe concentration is inadequate, siderophores offer plants with Fe and thus, increasing their development. As elucidated by Mushtaq et al. (2019), IAA and siderophores production coupled with phosphate solubilization activity by *Staphylococcus haemolyticus, Bacillus sp.,* and *Pseudomonas sp.* promotes plant growth. PSMs also guard plants by preventing phytopathogens through the production of hydrogen cyanate (HCN), antibiotics and antifungal metabolites such as chitinase and glucanase (Vejan et al., 2016). Table 2.3 summarized the various plant growth promoting mechanisms by different PSMs reported in recent years.

Table 2.3 Summary of various plant growth promoting mechanisms by different PSMs

Organisms	**Ecological niche**	**Plant growth promoting mechanisms**	**References**
Staphyloccus haemolyticus, *Staphylococcus pasteuri* and *Micrococcus sp.*	Fly ash	Phosphate solubilization IAA production Phosphatase production High mercury tolerance	Ghosh et al. (2015)
Bacillus megaterium	Acidic soils	Phosphate solubilization High antifungal activity	Panda et al. (2016)
Bacillus megaterium, *Staphylococcus haemolyticus* and *Bacillus licheniformis*	Gut of earthworm	Phosphate solubilization IAA production Ammonium ions production Copper and zinc tolerance	Biswas et al. (2018)
Pseudomonas plecoglossicida and *Staphylococci saprophyticus*	Chromium-rich soil	Phosphate solubilization *P. plecoglossicida* produced IAA High chromium tolerance	Arshad et al. (2019)
Bacillus safensis, *Bacillus flexus* and *Staphylococcus haemolyticus*	Gut of earthworm	Phosphate solubilization IAA and GA production Ammonia production ACC deaminase activity Copper, chromium and zinc ions tolerance	Banerjee et al. (2019)
Staphylococcus haemolyticus *Bacillus sp.*, and *Pseudomonas sp.*	Leaves of citrus	Phosphate solubilization IAA production Siderophores production	Mushtaq et al. (2019)

Table 2.3 (Cont'd) Summary of various plant growth promoting mechanisms by different PSMs

Organisms	Ecological niche	Plant growth promoting mechanisms	References
Trichoderma spp.	Amazon soils	Phosphate solubilization Phosphatase and phytase production	Bononi et al. (2020)
Bacillus, Burkholderia, Paenibacillus sp.	Paddy Field	Phosphate solubilization IAA production Acid phosphatase production	Chawngthu et al. (2020)
Bacillus sp.	Rhizosphere, leaf and sap	Phosphate solubilization IAA production	Sousa et al. (2020)

2.4 Miroencapsulation technology for PSMs

Microencapsulation is a mechanical or physicochemical procedure to entrap an active agent into a suitable wall material. This results in the production of spherical microbeads with a thin but strong and semipermeable membrane (Frakolaki et al., 2020). Microencapsulation provides a matrix that provides cell protection, promotes control release and functionalization of microorganisms (John et al., 2011). Generally, encapsulation protects cell by lessening the exposure to abiotic and biotic stresses. It also improves their stability and viability in the production and storage. Additionally, encapsulation also offers more protection during rehydration process (Schoebitz & Belchí, 2016). In order to warrant high cell viability, relatively mild conditions is needed for the microencapsulation process (Rathore et al., 2013). This section presents different techniques for microencapsulation of microbial which include extrusion, coacervation, emulsification, spray drying, spray freeze drying, fluidized bed and impinging aerosol method.

2.4.1 Extrusion, Emulsification and Coacervation

Extrusion is a well-known encapsulation technique where bioactive agents are entrapped into matrix such as alginate and carrageenan (Burgain et al., 2011). It forces the passage

of solution encompassing the cells through small openings or nozzles by using suitable droplet-generating devices. The cells are firstly mixed with biopolymer solution and then extruded through the nozzle at high pressure. The droplets formed are then collected in $CaCl_2$ solution which acts as a gelation bath (Liu et al., 2019a). Microbeads are formed immediately entrapping cells in a 3D network that forms from the ionic cross-linking of polymer with Ca^{2+} ions. Extrusion method is easy to handle, simple and low cost at small scale. Additionally, the microbeads produced has small size distribution and the operating conditions are mild to ensure high cell viability (Frakolaki et al., 2020). The two main disadvantages of this technique are the large size of the formed particles (2–5 mm) (Chan et al., 2011) and the slow particle formation limits the application in large scale (Ching et al., 2017).

To date, alginate is the most common raw material used in encapsulations of microorganisms. Alginate is a naturally occurring polymer available in large sustainable quantities (Draget et al. 2002; Yabur et al. 2007). Alginates are linear copolymer of 1,4-linked β-D-mannuronic acid (M) and α-L-guluronic acid (G) residues extracted from various species of algae (Sohail et al., 2011). The preparation of alginate beads containing bacteria can be achieved easily with minimal amounts of chemicals and equipment at room temperature. Alginate formulation is beneficial as it is nontoxic, biodegradable, low costs and slow-release in nature (Bashan et al. 2002; Zohar-Perez et al. 2002). These microbial inoculants can be enhanced by incorporating additives such as starch, skim milk or humic acid to improve cell survival and promote bacteria growth (Schoebitz et al., 2013b). Various researchers such as Bashan et al. (2002), Trivedi et al. (2005), Wu et al. (2014), and Santos et al. (2020) had encapsulated PSMs using alginate and beads size ranging from 1 to 4 mm were formed. In order to reduce the beads size, extrusion can be achieved via pulsation or vibration of the jet flow through coaxial flow or an electrostatic field (Ching et al., 2017). The size and sphericity of beads can be modified through the temperature, concentration and flow rate of the biopolymer solution, needle size, the distance between the outlet and the gelling bath and the piezoelectric parameters. Kim et al. (2017) encapsulated *Lactobacillus acidophilus* using phytic acid and chitosan with an electrostatic extrusion method. The encapsulation efficiency was 95.5 % with narrow size

distribution of 1.33 ± 0.09 mm. Besides, the beads formed had spherical shapes and smooth surfaces.

Emulsifcation is accomplished via the mixture of polymer with another immiscible liquid. This method is based on the interactions and association between the discontinuous and the continuous phases. In short, the process includes the mixing of cells in water-based polymer suspension (dispersed phase). Then, it is added with large quantity of organic or oil (continuous phase). The homogenization of the mixture is aided with a surfactant and results in the formation of water-in-oil emulsion. Gel beads are then formed within the oil phase when the polymer gets insolubilized. These gel beads are then collected via centrifugation or filtration (Frakolaki et al., 2020). The insolubilization mechanism highly dependent on the characteristics of the wall material and it can be induced by addition of cross-linking agent to the emulsion or lowering the temperature of emulsion. The emulsion technique offers high cell viability and small beads size and thus suitable to be applied at industrial level (Frakolaki et al., 2020). Tu et al. (2015) microencapsulated *Bacillus subtilis* by using gelatin as polymer, soybean oil for the organic phase, Span 80 as surfactant and $CaCl_2$ as cross-linker. At a gelatin concentration of 1.5 %, maximum encapsulation efficiency obtained was 93.44 %. Moreover, after 120 d storage at 25 °C, the cell viability of encapsulated *Bacillus subtilis* could be kept at more than 10^8 CFU/mL. Liffourrena and Lucchesi (2018) immobilized *P. putida* with alginate and perlite. Liquid paraffin was used to form the organic phase, Tween 20 as surfactant and cross-linking with $CaCl_2$. For all perlite concentrations tested, microbead size obtained was in the range of 90 to 120 μm and the cell concentration was 10^8 CFU/g microbeads. Nevertheless, this technique is unfavourable as it leads to wide range of particle size, shape and oil residues on the surface of beads (Rathore et al. 2013; Burgain et al. 2013).

Coacervation is divided into simple or complex. Simple coacervation includes only one type of polymer with the addition of strongly hydrophilic agents to the colloidal solution. Microbeads is obtained by adding an electrolyte or water-miscible non-solvent to the dissolved polymer (e.g., ethanol) (Schoebitz et al., 2016). On the other hand, complex coacervation is a three-phase system involving the solvent, the active material and the coating material. In general, this process involves four steps: (a) preparation of an aqueous

solution of two or more polymers; (b) mixing hydrophobic phase to the aqueous solution of one polymer and homogenizing the resultant mixture so that a stable emulsion is produced; (c) change of pH and temperature to a certain required level to induce coacervation and phase separation; and (d) hardening of the polymer matrices using elevated temperature, desolvation agent, or cross-linker (Timilsena et al., 2019). Coacervation can be controlled by several factors which include the molecular weight, conformation, charge density and composition of core and shell material, the total solid percentage and the dispersion conditions such as pressure, shearing, temperature, pH and ionic strength (Gaonkar et al., 2014). This method requires low temperatures, mild agitation and nontoxic solvents. The advantages of coacervation are high loading capacity, high encapsulation efficiency and optimal controlled-release properties due to its water immiscibility of the microbeads (Bosnea et al., 2014; Frakolaki et al., 2020). Hynes et al. (2010) encapsulated *Colletotrichum truncatum* through complex coacervate. Their results showed that soya lecithin as surfactant promoted greatest retention of *Colletotrichum truncatum* (88 %) in the invert emulsion. Wall ingredients of 1 % gelatin and 2 % gum arabic were most effective for *Colletotrichum truncatum* retention. In addition, when preparing the emulsion, optimal retention of *Colletotrichum truncatum* was obtained with a water:oil ratio of 1:1.8 to 1: 3.7 and stirring speed of 300 rpm. Complex coacervate Marques da Silva et al. (2018) produced microbeads containing *B. lactis* by complex coacervation in gelatin and gum arabic and high encapsulation efficiency of 86.04 % and 99.52 % was obtained, respectively. Small microbeads size between 100.12 and 203.32 μm were obtained with storage life of more than 90 days at room temperature. Despite its high encapsulation efficiency, coacervation technique is not suitable for microbial inoculants production as it is complex and costly. The additional drying process in coacervation is harmful to the cells and it is also difficult to scale-up (Chávarri et al., 2012). A comparative flow chart of extrusion, emulsification and coacervation is presented in Figure 2.3.

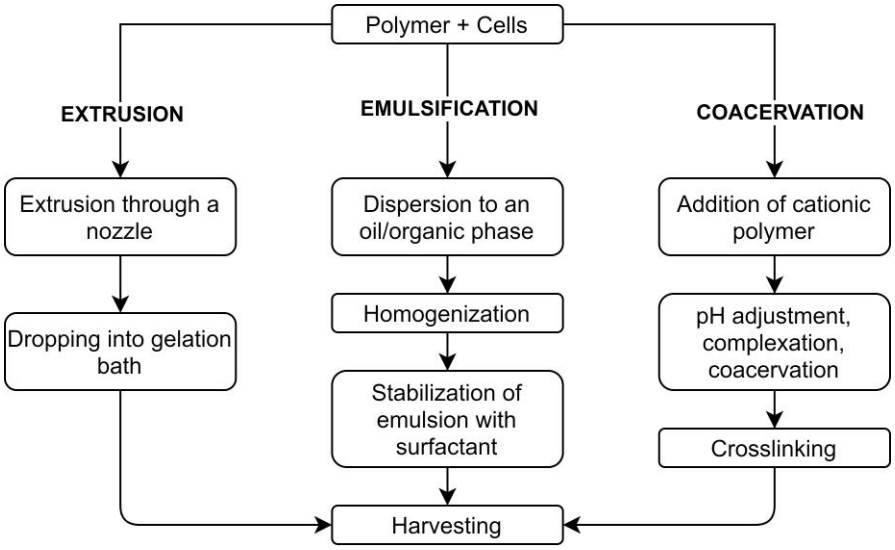

Figure 2.3 Summary of extrusion, emulsion and coacervation processes (Liu et al., 2019a; Frakolaki et al., 2020)

2.4.2 Spray drying and spray-freeze drying

Spray drying (SD) is one of the most common microencapsulation techniques. It involves the combination mass and heat transfer from the air to the atomized droplets. Generally, the method includes the mixing of cells in polymer and atomization of suspensions through a nozzle. Then, the resulting droplets are evaporated through contact with hot gas or air. Then, the dried particles are collected by separating it from the humid air by using a cyclone or bag filter (Fang & Bhandari, 2012). The main aspects that can affect the effectiveness of this method are the cells characteristics, the dryer characteristics, the feed characteristics such as carrier material and its concentration and operating parameters which include the drying temperature and feed rate (Schutyser et al., 2012). The main advantages of SD are low operating costs, high quality of microbeads, continuous process, high yield, rapid solubility of the microbeads, small size, high stability microbeads, high production rate and easy to scale-up (Schoebitz et al., 2016). However, SD also have some drawbacks such as limitations in the wall material selection and low uniformity of microbeads size. In addition, during dehydration or high drying temperatures, cells are exposed to extreme osmotic stress which significant reduces cell viability and activity (Campos et al., 2014). Generally, with increasing inlet temperature during spray drying the survival of bacteria decreases. Schoebitz et al. (2013c), studied the cell survival of

Serratia sp. using only maltodextrin as wall material with inlet temperature of 145ºC and outlet temperature of 90 ºC. The final cell concentration was very low in comparison with initial cell concentration in culture medium. Campos et al. (2014) encapsulated *Enterobacter sp.* immobilized using alginate and maltodextrin as wall materials and bacterial survival of 91 % was obtained with inlet temperature of 100 ºC and outlet temperature of 65 ºC. Ma et al. (2015) investigated the mean survival rate of *B. subtilis* using maltodextrin as wall material and about 90 % was obtained when spray drying was performed at 145 ºC. For that reason, SD is not a decent cell immobilization method as it causes high cell mortality due to dehydration and high temperature drying. The type of bacteria strain, temperature of the drying process, and formulations compositions are the vital factors for the encapsulation of cells in order to gain an effective microbial inoculant.

Spray-freeze drying (SFD) is a relatively new method that combines spray and freeze-drying. SFD aims to produces dried microbeads without heat. SFD includes the atomization of solution that containing cells through nozzle into the cold vapor phase of a cryogenic liquid such as liquid nitrogen. This results in dispersion of frozen droplets which is then dried through freeze drying (Frakolaki et al., 2020). SFD has been widely used in the microencapsulation of probiotics. Semyonov et al. (2010) studied the survival of *Lactobacillus paracasei* using maltodextrin and trehalose as wall materials and cell viability greater than 60 % was obtained. Her et al. (2015) investigated the cell survival of *Lactobacillus casei* with different protective agents such as sucrose, glucose and buffered peptone water. About 97 % survival rate was obtained at 20 kPa air pressure and when buffered peptone water was used as protective agent. SFD has many advantages in comparison with SD such as provides a controlled microbeads size and larger specific area. Nevertheless, SFD requires higher energy consumption and it is approximately 30 times more costly than SD (Burgain et al., 2011). A comparative flow chart of the SD and SFD is presented in Figure 2.4.

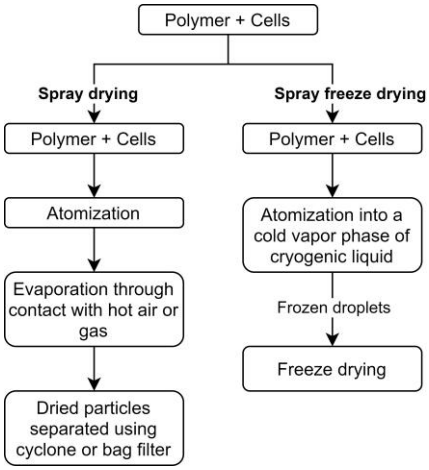

Figure 2.4 Comparative chart of spray drying and spray-freeze drying (Fang et al., 2012; Frakolaki et al., 2020)

2.4.3 Fluid bed drying

The fluid bed drying (FBD) method involves drying, cooling or coating for a wide range of heat-sensitive materials. FBD can be batch or continuous process. Generally, the cells are suspended through an air stream of a certain temperature and humidity. Then, these suspended cells are sprayed with an atomized encapsulating agent. Then, hot air from the bottom dry the aqueous medium and reduces the water activity of the powdered matrix to a favorable level (Frakolaki et al., 2020). The evaporation of water is significantly affected by percentage of water in the medium, spraying speed, temperature, air flow and humidity of the air inlet (Đorđević et al., 2015). Various materials can be utilized as encapsulating agents such as fats, proteins, carbohydrates and gums. The flow chart of this method is presented in Figure 2.5. Wirunpan et al. (2016) studied the survival of *Lactobacillus lactis* in shrimp feed pellet after fluid bed drying. The results indicated that the strain viability depended on the drying temperature. Strain survival was highest at 92.28 % with 50 ºC drying temperature and lowest with 75.94 % at 80 ºC. Moreover, the addition of milk powder and monosodium glutamate (MSG) as protectants was found to effectively enhance the strain survival during drying at high temperature. Gotor-Vila et al. (2017) also elucidated that the use of maltodextrin or potato starch as carriers combined with sucrose and skim milk as protectants is a good tool for reaching an adequate stability and efficacy of *Bacillus amyloliquefaciens* formulated products. This technique requires low energy

consumption and in a batch form it only causes mild heat damage to the cells. Besides, the process can be easily scaled-up, temperature-controlled and modified to provide multilayer coatings (Nag & Das, 2013). Despite the advantages of the fluid bed drying technique, it is not commonly use in microbial inoculant production due to the coalescence of the wet coated material which results in uncontrolled aggregation of the microbeads. The encapsulation of cells is difficult to control and the whole process requires extensive time (Martín et al., 2015).

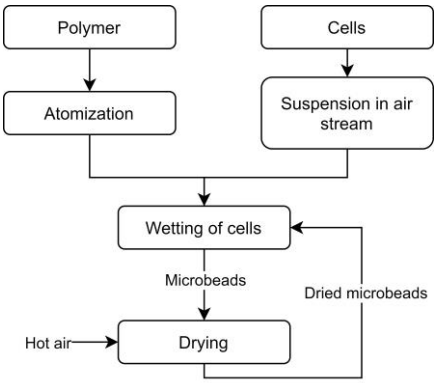

Figure 2.5 Fluid bed coating process (Đorđević et al., 2015)

2.4.4 Electro-hydrodynamic atomization

Electro-hydrodynamic atomization (EHDA) uses a high voltage, a stainless steel needle, a syringe pump to generate particles (electrospray) or fibers (electrospinning) and the particles are collected at a grounded collector (Bhushani & Anandharamakrishnan, 2014). EHDA avoids the use of heat or aggressive solvents representing an alternative to other thermal techniques that lead to some bacteria damages. The central principle of electrospraying is a process of liquid atomization by electrical forces. At low polymer concentration, jet gets destabilized and forms fine droplets. These droplets are highly charged and become dispersed, avoiding the droplet agglomeration. Then, solvent evaporation causes contraction and solidification and finally the microbeads are deposited onto the collector. This process is summarized as shown in Figure 2.6. Electrospraying is cost effective (Ghorani & Tucker, 2015) and the application of the strong electric field does not harm the microbial cells (Bhushani et al., 2014). Under mild and non-thermal conditions, formation of very fine particles can be achieved. The final microbeads size can be controlled through various parameters such as the properties of solution used, the

system design and the operating conditions. Moreover, it exhibits high encapsulation efficiency, high surface-to volume ratio and provides sustained and controlled release of the core material. Zaeim et al. (2017) encapsulated *Lactobacillus plantarum* through electrospraying and the influence of alginate and Tween80 concentration on the microbeads size was studied. Their results showed that increasing in alginate concentration resulted in larger and more uniform microbeads. However, the size of microbeads decreased and their size distribution became narrower by increasing Tween80 concentration. Besides, their results showed high encapsulation yield of 97 %. They further coated the microbeads with chitosan and found that it enhanced the survivability of bacteria during storage and exposure to acid. The main concern of EHDA technique is the dripping of the solution if conditions are not well optimized (Bhushani et al., 2014).

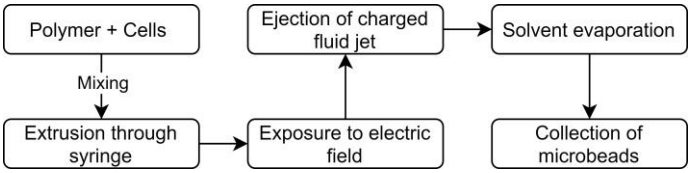

Figure 2.6 Electro-hydrodynamic atomization process (Bhushani et al., 2014)

2.4.5 Impinging aerosol technology

Impinging aerosol method developed by Bhandari (2009) has gained attention of researchers as it is a continuous process and easy to scale up for industrial application. As shown in Figure 2.7, alginate microbeads were produced by oppositely atomizing alginate and cross-linking solution in a reaction chamber. The newly formed calcium alginate microbeads settle and flow out of the chamber. This allows the immediate gelation of alginate microbeads and do not need to be cured in gelation bath over a period of time (Lee et al., 2016). The cross-linked particles produced have an average diameter lower than 40 µm and can be further spray- or freeze-dried. Impinging aerosol method has high encapsulation efficiency (Sohail et al., 2011), high throughput (Martín et al., 2015) and microbeads could be spray or freeze dried. It is suitable for encapsulating heat labile and solvent sensitive materials as it does not involve heat and solvent. Notably, the design of the impinging aerosol method allows the application of different nozzle and adjustable parameters such as distance between nozzles, air pressure and flowrate allow formation of alginate microbeads of narrow size distribution. Spherical alginate microbeads within

the size of 11 to 80 µm can be steadily produced with this method. Moreover, this method minimizes the washout issue encountered in the conventional gelation method where the encapsulated materials diffuses out of the microbeads during curing in the gelation bath. In addition, the implementation of cleaning-in-process (CIP) procedures is easier due to the lack of moving parts in the chamber. This method requires low maintenance, easy to operate and effective in the encapsulation of drugs and probiotic cells. To date, only limited studies on the microencapsulation of probiotics using impinging aerosol method (Sohail et al., 2011; Sohail et al., 2012; Demitri et al., 2017).

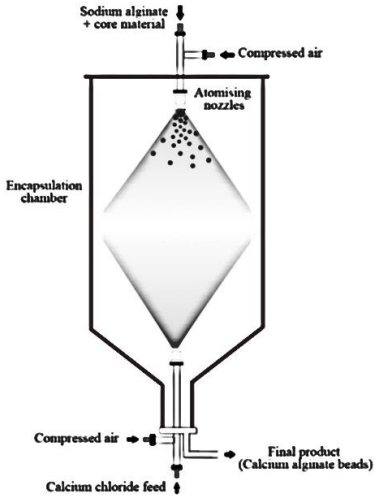

Figure 2.7 Setup and design of the impinging aerosol method for the production of alginate microbeads (Ching et al., 2017). Reproduced with permission of the Taylor & Francis

Sohail et al. (2012) showed that encapsulation *of Lactobacillus rhamnosus GG (LGG) and Lactobacillus acidophilus NCFM* with impinging aerosol method is feasible due to minimal cell loss. Hariyadi et al. (2012) presented that after gastric treatment, high bioactivity of lysozyme and insulin encapsulated by this method was retained. Sohail et al. (2013) encapsulated *Lactobacillus rhamnosus* and *Lactobacillus acidophilus* in alginate microspheres followed by spray- or freeze drying with maltodextrin. Double encapsulated (alginate and maltodextrin) *Lactobacillus rhamnosus* offered improvements in survivability over spray or freeze-dried as compared to free cells (only maltodextrin). Their findings indicate that the alginate matrix protects the cells from membrane damage

by maltodextrin while maltodextrin protects the alginate microbeads from fragmentation during freeze-drying.

The impinging aerosol method provides easy modulation of microbeads release kinetics and encapsulation efficiency by altering the concentration of $CaCl_2$ (Hariyadi et al., 2012). However, numerous parameters such as operating conditions, (flow rate, air pressure and temperature), solution physicochemical characteristics (surface tension, viscosity, and density) and nozzle orifice diameter affects the spray quality of impinging aerosol method (Mandato et al., 2012). Ejim et al. (2010) reported that the increase of the polymer concentrations resulted in an increase of droplet diameter. This could be associated with the increase in both viscosity and surface tension of polymer. For operating conditions, the droplet size increases with mass flow rate, and an increase in air pressure reduces the droplet diameter (Hede et al., 2008). In recent years, the nozzle structure factor attracted much attention. For instance, Zhang et al. (2017) investigated the effect of diameter of nozzle orifices on droplet size distribution. Besides, the atomization of alginate and $CaCl_2$ are driven by pneumatic nozzles. Pneumatic nozzles are identified as two-fluid nozzles as they employ the use of compressed air to atomize the fluid. Air is widely used in the extrusion process because it is obtainable at low cost. Commonly, feed is mixed with air inside or outside the body of the nozzle as shown in Figure 2.8.

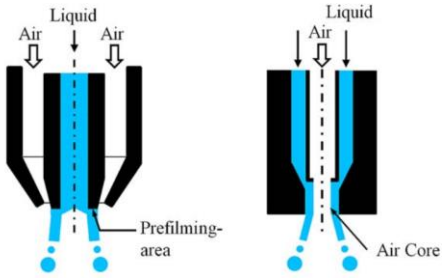

Figure 2.8 Pneumatic nozzle with external mixing (left) and internal mixing (right) (Stähle et al., 2017). Reproduced with permission of John Wiley & Sons

Pressurized air is often used to offer shear force to reduce the size of the droplets and to increase the production rate of the microbeads. Nitrogen gas is applied for application that require sterile or anaerobic conditions during the encapsulation process. Nevertheless, the use of air in direct contact with the alginate solution may not be promising for bioencapsulation. This is because the air is usually generated from an air compressor and

the gas needs to be treated to remove impurities and humidity before it can be supplied to the extrusion system. When an air compressor is used to supply the pressure, a filter is needed to remove any potential contamination from oil. The high cost of compressed air and high energy consumption becomes important to the economics of these nozzles. In order to atomize 1 kg of fluid, approximately 0.5 m^3 of compressed air is needed (Mujumdar, 2014). The nozzles in an air extrusion system are commonly made from glass or stainless steel to ease cleaning and sterilizing processes. This is significant when the nozzles are used for bioencapsulation (Lee et al., 2016). The type of injector used affects the production cost. Generally, stainless steel pneumatic nozzles are costly. Therefore, the adequacy of the injector is essential in the production of alginate microbeads for agricultural purposes. In this present work, microencapsulation of PSMs by employing the impinging aerosol method with slight modification where simple hole type nozzles were used instead of air atomizing nozzle to reduce the cost of production. One of the nozzle types that can be used in impinging aerosol method is the stainless steel misting nozzles as shown in Figure 2.9. These misting nozzles allows high emission velocity with a low flowrate. The pin (impeller), orifice, and nozzle body are designed in such a way that when fluid is extruded through, a very fine mist is created. This kind of arrangement is advantageous for bioencapsulation because the risk of contamination can be minimized as compressed air is not used for extrusion.

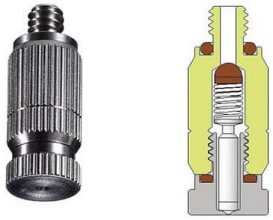

Figure 2.9 Stainless steel mist nozzle (Naturalfog, 2020)

Summary of advantages and disadvantages of various microencapsulation technologies were tabulated in Table 2.4. Referring to Table 2.4, it can be observed that the impinging aerosol method is superior when compared with other encapsulation method. To date, impinging aerosol method has not been used in the encapsulation of the PSMs. Thus, this study aims to employ the impinging aerosol method in the microencapsulation of PSMs. The microencapsulation of various plant growth promoting microorganisms and probiotics with different techniques were summarized in Table 2.5 and Table 2.6.

Table 2.4 Advantages and disadvantages of various encapsulation technologies

Methods	Advantages	Disadvantages	References
Extrusion	• Simple • Low cost • Very narrow size distribution • High cell viability	• Large particle size • Orifice clogging • Unsuitable for large scale applications	Chan et al. (2011), Ching et al. (2017), Frakolaki et al. (2020)
Emulsification	• High cell viability • Small particle size	• Wide size range and shape • Oil residue on particles	Rathore et al. (2013), Burgain et al. (2011), Frakolaki et al. (2020)
Coacervation	• High encapsulation efficiency • Optimal controlled-release properties	• Expensive and complex • Difficult to scale-up • Low cell viability	Chávarri et al. (2012), Bosnea et al. (2014), Frakolaki et al. (2020)
Spray drying	• Economic • Products are dry, stable and have low bulk density • High production rate • Easy to scale-up	• Significant viability and activity losses during drying process	Campos et al. (2014), Schoebitz et al. (2016)
Spray freeze drying	• High cell viability • Controlled particle size and large specific area	• High energy consumption • Costly	Burgain et al. (2011)

Table 2.4. (Cont'd) Advantages and disadvantages of various encapsulation technologies

Methods	• **Advantages**	• **Disadvantages**	
Fluid bed coating	• Low energy consumption • Mild heat damage to the cells • Easy to scale-up	• Uncontrolled aggregation of the particles • Time consuming • Difficult to control	Nag et al. (2013), Martín et al. (2015)
Electro-hydrodynamic atomization	• Small particles • High encapsulation efficiency • Sustained and controlled release of the core material	• High voltage • Dripping of the solution	Bhushani et al. (2014), Bhushani et al. (2014), Ghorani et al. (2015)
Impinging aerosol	• Suitable for heat-sensitive materials • High production yield • A continuous process • Small particle size • Scalable • Easy to operate	• Risk of contamination	Sohail et al. (2011), Martín et al. (2015)

Table 2.5 Microencapsulation of plant growth promoting microorganisms

Cells	**Method (Size)**	**Encapsulating agent**	**References**
Pseudomonas striata, Bacillus polymyxa, and *Azospirillum brasilense*	Extrusion (NR)	Alginate	Gonzalez and Bashan (2000), Viveganandan and Jauhri (2000)
Azospirillum brasilense	Extrusion (1.0 to 3.0 mm)	Alginate	Bashan (1986a), Bashan et al. (2002)
Bacillus subtilis	Extrusion (2.8 mm)	Alginate, humic acid	Young et al. (2006)
Klebsiella oxytoca Rs-5	Extrusion (0.85-1.10 mm)	Alginate	Wu et al. (2011)
P. fluorescens and *Serratia sp.*	Extrusion (NR)	Alginate, potato starch	Schoebitz et al. (2013a)
Raoultella planticola Rs-2	Extrusion (2.21-3.23 mm)	Alginate, starch	Wu et al. (2014)
Saccharomyces cerevisiae	EHDA (192.2 µm)	Alginate, polydopamine	Kim et al. (2015)
Pseudomonas putida	Extrusion (1mm)	Alginate, bentonite, starch	He et al. (2016)
Metarhizium brunneum	Extrusion (3mm)	Alginate, starch	Krell et al. (2018)
Bradyrhizobium japonicum	Extrusion (3mm)	Alginate, sucrose	Chhetri et al. (2019)
Azospirillum brasilense, Burkolderia cepacia, Bacillus sp.	Extrusion (NR)	Alginate	Santos et al. (2020)
Trichoderma spp	Extrusion (3mm)	Alginate	Bhai (2020)

Table 2.5 (Cont.'d) Microencapsulation of plant growth promoting microorganisms

Cells	**Method (Size)**	**Encapsulating agent**	**References**
Bacillus subtilis, Seratia marcescens	EHDA (NR)	Poly(vinyl alcohol) (PVA) and poly-(vinylpyrrolidone) (PVP), Glycerol	Hussain et al. (2019)
Bacillus subtilis	Emulsification (255.1-400.8 µm)	Alginate, gelatin	Tu et al. (2015)
Pseudomonas putida A	Emulsificationµ (90-120 µm)	Alginate, perlite	Liffourrena et al. (2018)
Colletotrichum truncatum	Coacervation (266 to 433 µm)	Nonrefined vegetable oils, soya lecithin, proteins, and carbohydrate	Hynes et al. (2010)
Serratia sp.	Spray drying (NR)	Maltodextrin	Schoebitz et al. (2013c)
Bacillus subtilis	Spray drying (7-14 µm)	Maltodextrin and gum arabic	Ma et al. (2015)
P. fluorescens and A. chroococcum	Fluid bed coating (NR)	Talc	Sahu et al. (2013), Lavanya et al. (2015), Sahu et al. (2016)
Bacillus amyloliquefaciens	Fluid bed coating (NR)	Maltodextrin, potato starch, skim milk, sucrose	Gotor-Vila et al. (2017)

Table 2.6 Microencapsulation of probiotics

Cells	**Method (Size)**	**Encapsulating agent**	**References**
Bifidobacterium longum subsp. infantis	EHDA (1.95-2.47 μm)	Whey protein concentrate, Fibersol®, maltodextrin, zein and polyvynilpyrrolidone (PVP)	Librán et al. (2017)
Lactobacillus plantarum	EHDA (300-550 μm)	Alginate, chitosan	Zaeim et al. (2017)
Lactobacillus paracasei and *Lactobacillus paraplantarum*	Coacervation (1-15 μm)	Whey protein and gum arabic	Bosnea et al. (2014)
Bifidobacterium lactis	Coacervation (100.12 and 203.32 μm)	Gelatin and gum Arabic	Marques da Silva et al. (2018)
Lactobacillus plantarum	Coacervation (3-20 μm)	Gelatin, gum Arabic, sucrose	Zhao et al. (2018)
Lactobacillus rhamnosus and *Lactobacillus acidophilus*	Impinging aerosol (10-40 μm)	Alginate, maltodextrin	Sohail et al. (2011), Sohail et al. (2012), Sohail et al. (2013)
Lactobacillus kefiri	Impinging aerosol (50-70 μm)	Alginate, carboxymethylcellulose	Demitri et al. (2017)
Lactobacillus acidophilus	Spray drying (76.58 μm)	Whey, skim milk	Maciel et al. (2014)
Lactobacillus acidophilus	Spray drying (NR)	Flaxseed mucilage Flaxseed protein	Bustamante et al. (2015)

Table 2.6 (Cont'd) Microencapsulation of probiotics

Cells	Method (Size)	Encapsulating agent	References
Bifidobacterium-BB-12	Spray drying (10.55 and 12.77 μm)	Liquid whey, whey retentate, inulin, polydextrose.	Pinto et al. (2015)
Lactobacillus acidophilus	Emulsification (323-343 μm)	Sodium alginate $CaCO_3$/Ca-EDTA Soybean oil Span 80	Cai et al. (2014)
Lactobacillus casei Shirota	Emulsification and extrusion (0.26-1.79mm)	Alginate, sunflower oil, Tween 80	Semyonov et al. (2010)
Lactobacillus lactis	Fluid bed coating (NR)	Shrimp feed, monosodium glutamate (MSG), milk powder, acacia gum, maltodextrin	Wirunpan et al. (2016)
Lactobacillus paracasei	Spray freeze drying (400-1800 μm)	Maltodextrin and trehalose	Semyonov et al. (2010)
Lactobacillus casei	Spray freeze drying (24.8 μm)	Glucose, sucrose, buffered peptone water	Her et al. (2015)
Lactobacillus plantarum	Spray freeze drying (10-1000 μm)	Whey protein, alginate, fructooligosaccharide	Rajam and Anandharamakrishnan (2015)

2.5 Challenges of microencapsulation

Several authors have been discussing the main advantages of applying microencapsulation techniques in cells protection. However, several parameters such as properties of materials, formulation parameters and operating condition (Paulo & Santos, 2017) affects the final characteristics of microparticles such as mean size, particle size distribution, surface morphology, product yield and encapsulation efficiency. The final properties of microparticles may affect the release rate of cells (Li et al., 2008). Traditionally, one factor-at-time (OFAT) method is used to identify main influencing factors in microencapsulation by studying the influence of one variable while the others remain constant. OFAT requires relative huge number of experiments which is time consuming (Paulo et al., 2017). Thus, design of experiments (DOE) have been used to overcome the main disadvantages of OFAT procedures. The surface response methodology (RSM) is commonly used in microencapsulation. RSM is an effective tool for optimizing the process parameters when there are numerous factors that will affect the response variable. Central composite design (CCD) and Box-Behnken Design (BBD) are the two most popular response surface designs used by researchers (Ebrahimi-Najafabadi et al., 2014). Central composite design (CCD) is generally employed for sequential experiments. It does not involve large number of experiments. CCD requires five levels for each variable and consists of combinations in which all parameters are simultaneously at their highest or lowest level (Wu et al., 2012a). Box-Behnken Design (BBD) only has 3 levels (i.e. low, medium and high, coded as -1, 0 and +1) for each parameter (Cai et al., 2012). The application of RSM for cell microencapsulation optimization processes have been extensively studied by various researchers as tabulated in Table 2.7. Referring to Table 2.7, it can be seen that BBD is widely used to optimize cell viability and encapsulation yield while varying several factors such as concentration of coating materials, operating condition for microencapsulation and concentration of crosslinkers ($CaCl_2$). For example, Chen et al. (2013) employed the BBD method to identify the optimal formulation of highest cell viability of of *Bacillus cereus* microencapsulated by spray drying. Results obtained showed that with 18.3 % maltodextrin and 12.5 % gum arabic as coating materials and spray drying at an outlet temperature of 73.5 ºC, the *B.cereus* could maintain cell viability of 42 %. Trabelsi et al. (2013) studied the effects of sodium alginate

concentration, biomass concentration, and hardening time on encapsulation yield of *Lactobacillus plantarum* using BBD. The ideal conditions were determined to be 2 % of sodium alginate, cell concentration of 10^{10} CFU/ml, and 30 min hardening time. The experimental result these conditions was about 80.98 % which was in close agreement with the estimated value of 82.6 %. Herein, it can be observed that BBD was preferred over CCD in optimization study as it requires less number of runs with high efficiency (Souza et al., 2005). One of the main advantage of employing BBD is that it does not contain combinations where all factors are simultaneously at their highest or lowest levels, avoiding performing experiments under extreme conditions which might results in unsatisfactory outcome (Venegas Mendez, 2013). BBD is highly effective and easier to arrange and interpret when compared with other designs.

Table 2.7 Cell microencapsulation optimization

Core material	**RSM**	**Factors**	**Response**	**References**
Bifidobacterium pseudocatenulatum	CCD	Bovine gelatin, sodium alginate, and genipin	Encapsulation yield, bead strength	Khalil et al. (2019)
Lactobacillus plantarum	BBD	$CaCl_2$ concentration, biomass concentration, and hardening time,	Encapsulation yield	Trabelsi et al. (2013)
Bacillus cereus	BBD	Gum Arabic concentration, maltodextrin concentration and outlet temperature for spray drying	Cell viability	Chen et al. (2013)
Bifidobacterium animalis subsp. lactis	BBD	Alginate, prebiotics mixture and glycerol concentration	Cell viability	Shamekhi et al. (2013)

Table 2.7 (Cont'd) Cell microencapsulation optimization

Core material	RSM	Factors	Response	References
Bifidobacterium bifidum	BBD	Cell/alginate ratio, sodium erythorbate and inulin concentration	Encapsulation yield	Chen et al. (2016)
Bifidobacterium bifidum	BBD	Chitosan concentration, cell/chitosan ratio, stirring time	Viability and encapsulation yield	Shu et al. (2018)
Saccharomyces boulardii	BBD	Alginate, oats bran gum and cell concentration	Encapsulation yield	Ragavan and Das (2018)

2.5.1 Kinetic models of cell release

Evaluation of PSMs release from alginate microbeads is essential to ensure cell release gradually from beads to facilitate colonization of plant roots. The study of kinetic models is generally helpful in explaining release mechanisms which can be useful in the control of cell release. Generally, kinetic models such as zero order, first order, Higuchi, Ritger-Peppas and Weibull are used to study the release profile of cells from alginate beads as shown in Table 2.8. The mechanistic aspects of the release process in swelling-controlled bacterial release from alginate microbeads can be elucidated well using the Ritger–Peppas model, in which the value of "n" characterizes the release mechanism of cells. When $n<0.45$, it indicates Fickian diffusion, $0.45<n<0.89$ represents anomalous (non-fickian) diffusion, $n=0.89$ for case-II transport and $n>0.89$ for super case II transport. Various researches have studied the release of active ingredients, drugs and microorganisms from alginate beads as tabulated in Table 2.9. Referring to Table 2.9, Ritger-Peppas can be considered as the most suitable kinetic models for cell release from alginate microbeads. Most of the researchers obtained high R^2 value ranging from 0.91 to 0.99 for Ritger-Peppas model indicating that the models were well fitted.

Wu et al. (2014) investigated the release of *Raoultella planticola* from alginate-starch microbeads produced with extrusion method and the diffusion exponent "n" for different alginate and starch concentration were all greater than 0.89, indicating the main Case II release mechanism with skeleton corrosion mechanism. The release of cells occurs when the microbeads swell by absorbing water. Their results also revealed that an increase in starch and alginate concentration increased the swelling of the microbeads, which may facilitate the release of the entrapped cells. Feng et al. (2019) showed that the addition of kaolin in starch–alginate beads decreased the swelling ratio and thus, fungal spores release rate decreased. All starch-alginate beads with different kaolin concentration had diffusion exponent 'n' lower than 0.5, indicating a Fickian diffusion mechanism for fungal spores release.

Table 2.8 Kinetic models applied in the study of cell release from alginate beads

Models	**Equations**	**References**	
Zero order	$F = K_0 t$	Costa and Sousa Lobo (2001)	(2.5)
First order	$\ln(1-F) = -K_1 t$	Gibaldi and Feldman (1967)	(2.6)
Higuchi	$F = K_H t^{\frac{1}{2}}$	Paul (2011)	(2.7)
Ritger-Peppas	$\ln F_{60} = \ln K + n \ln t$	Korsmeyer et al. (1983)	(2.8)
Weibull	$\ln\left[-\ln(1-F)\right] = b\ln(t-T_i) - \ln a$	Weibull (1951)	(2.9)

Where F represents the total cumulative bacteria release in time t; F_{60} is first 60 % of the fraction of cell released at time t; $K_{0,}$ K_1, K_H and K are release rate constants related with the features of the bacterial-microbeads system; n is the diffusion exponent indicative of mechanism of release, a is the scale parameter, b is a shape parameter describing the shape of the dissolution, m_{50} is time required for 50 % dissolution.

Table 2.9 Kinetic models to describe release of core material from alginate beads by past researchers

Core material	**Wall coating**	**Kinetic models**	**R^2**	**References**
Raoultella planticola	Alginate, starch and $CaCl_2$	First order	0.74-0.91	Wu et al. (2014)
		Higuchi	0.733-0.93	
		Ritger-Peppas	0.91-0.96	
		n	2.7-3.4	
Raoultella planticola	Alginate, bentonite and $CaCl_2$	First order	0.83-0.99	He et al. (2015)
		Higuchi	0.87-0.99	
		Ritger-Peppas	0.94-0.98	
		n	3.52-4.14	
Metformin HCl	Alginate and polysaccharide	Zero-order	0.997	Nayak et al. (2016)
		First-order	0.864	
		Weibull	0.995	
		Ritger-Peppas	0.996	
		n	1.0	
Stevia rebaudiana extract	Alginate and $CaCl_2$	Zero order	0.82-0.96	Quintal Martínez et al. (2018)
		First order	0.69-0.96	
		Higuchi	0.91-0.98	
		Ritger-Peppas	0.92-0.98	
		n	0.25-0.32	

Table 2.9 (Cont'd) Kinetic models to describe release of core material from alginate beads

Core material	**Wall coating**	**Kinetic models**	**R^2**	**References**
Metronidazole	Alginate and poly-caprolactone	Ritger-Peppas	0.91-0.99	Lan et al. (2013)
		n	0.11-0.39	
Ilex paraguariensis	Alginate, starch and $CaCl_2$	Ritger-Peppas	0.96	López Córdoba et al. (2013)
		n	0.23	
Eucalyptus oil	Alginate and $CaCl_2$	Ritger-Peppas	0.988-0.998	Noppakundilograt et al. (2015)
		n	0.88-1.06	
Tolbutamide	Alginate, starch and $CaCl_2$	Zero-order	0.99	Malakar et al. (2014)
		First-order	0.91-0.93	
		Weibull	0.95-0.97	
		Higuchi	0.56-0.72	
		Ritger-Peppas	0.95-0.98	
		n	0.90 to 1.12	
Vancomycin	Alginate, soy protein isolate, and poly(ethylene oxide)	Ritger-Peppas	0.991	Wongkanya et al. (2017)
		n	1.78	
Gentamicin	Alginate, hyaluronic acid, and gelatin	Ritger-Peppas	0.88-0.92	Ratanavaraporn et al. (2019)
		n	0.46-0.59	
Aspergillus flavus (spore)	Alginate, starch, kaolin and $CaCl_2$	Ritger-Peppas	NR	Feng et al. (2019)
		n	0.24	

2.6 Numerical simulation of Impinging Aerosol Encapsulation

Among a wide range of microencapsulation technologies, novel impinging aerosol method has been successfully used for the microencapsulation of bacteria. The basic operating principle consists of spraying of alginate suspension and cross linking with $CaCl_2$ mist in the opposite direction in encapsulation chamber. Generally, pneumatic nozzles are used for the solution atomization but in this work, misting nozzles were used to reduce the risk of contamination and cost of production in the microencapsulation PSMs. In order to control process efficiency in impinging aerosol method, physical properties of solutions, spray conditions and type of nozzles are the critical factors. In practice, these parameters must be extensively tested to control the spray behaviors including droplet size distribution, spray distribution, spray angle and wall wetting. Therefore, in order to reduce time consumption and expensive cost of extensive experiments, computational fluid dynamics (CFD) analysis had become a very useful tool for spray modeling. Due to the complexity of spray atomization, CFD can be used to observe the small-scale phenomena such as the atomization and breakup of the droplets exiting a spray nozzle. Several authors had used CFD analysis method to simulate spray atomization. Fung et al. (2012) used CFD method to simulate spray atomization from a nasal spray device and Isa et al. (2019) also investigated the spray characteristics of pressure-swirl atomizers for automatic hand sanitizer application using CFD. CFD simulations were also performed on the Spray G geometry to improve the efficiency of the internal combustion engine (Paredi et al., 2018). When working with impingement aerosol method in production of alginate microbeads loaded PSMs, the three main concerns are the size of droplets, quality of spray distribution and the impingement of spray droplets on encapsulation chamber wall. If the spray angle is large, droplets tend to stick on wall forming fluid film, leading to production losses. Thus, it is essential to develop a CFD model to predict the spray behaviors of impinging aerosol.

2.6.1 Numerical Modeling of Multiphase Flow

Numerical approaches such as Eulerian-Eulerian and Eulerian-Lagrangian have been established as a powerful technique to understand or explain the influence of various input variables on process efficiency (Duangkhamchan et al., 2012). In spray application, the

volume of fluid (VOF) and the discrete particle method (DPM) have been used to estimate basic outcomes of spraying nozzles such as spray angle and droplet size distribution. In the Eulerian-Eulerian approach, the VOF is the most popular model. VOF models solve a single set of momentum equations and tracks the volume fraction of each of the fluids throughout the domain for two or more immiscible fluids. Common applications include the estimation of jet breakup and the motion of large bubbles in a liquid. The VOF method keeps track of the volume fraction of each phase present in a simulation. This would suggest that the volume fraction could be used to visualize the spray plume. However, this is very computationally expensive because the cell size needs to be sufficiently small (Chapman, 2020). VOF simulations on single droplet level to study breakup, collisions, agglomeration vaporization heating and acceleration phenomenon has been reviewed in Sirignano (2010). The VOF methodology has been used in several studies and industrial cases to investigate the formation of droplets during primary atomization of a liquid jet in nozzles (Fuster et al., 2009; Tomar et al., 2010). Other innovative application of the VOF methodology is the injection molding of non-Newtonian, low density polyethylene by Salinas et al. (2013).

DPM is an Eulerian-Lagrangian method where the dispersed phase is solved by tracking a large number of droplets through the continuum and gas phase is a continuum phase solved by the Navier–Stokes equations (Khatami et al., 2013). Wang et al. (2004) employed the DPM to study the nitrogen evaporating jet in a gas–solid suspension flow. Parametric studies to assess the effect of the solid catalysts loading on the spray evaporation length were also conducted. Zeoli and Gu (2006) used the DPM to study the droplet breakup during atomization creating fine spherical metal powders. In order to validate the model efficacy, the liquid metal was initialized to large droplet diameters varying from 1 to 5 mm and injected into the gas flow field. Their results showed that the model could provide numerical assessment for the process of spray atomization. DPM was also employed by Mezhericher et al. (2010) to model the drying process of a spray dryer with pressure nozzle atomizer. Their results were validated with experimental data. The model developed was able to capture the temperature profiles of the droplets in drying gas, estimation of mass and moisture content. Khatami et al. (2013) used DPM to simulate the spray atomization from solution for synthesis of sensor film. Air from atomizer and

surrounding air were selected as the continuous phase while methanol as the discrete phase. The developed model has the potential to be used in optimization of operating parameters which include mass flow rate, nozzle diameter and distance from nozzle to substrate for synthesis of thin film for sensor application. Bebe and Andersen (2017) studied the spray angle and penetration length of spraying of water into quiescent air using the DPM. Good agreement was obtained between experimental and simulation results. Fan et al. (2018) employed the DPM to simulate liquid jet in supersonic flow and the influences on numerical results when different breakup models and injection models were employed. Their simulated results have a good match with the experimental data. Besides, the developed model has a great ability to describe the entire spray process including the breakup that occurs near the nozzle exit in the primary breakup region. Bode et al. (2015) developed a DPM model to describe the primary breakup of fuel from Gasoline Direct Injection (GDI) injector, the droplet size distribution and velocity profile obtained showed good agreement with experimental data without excessive tuning of the simulation parameters. Many researchers have attempted spray modeling in various applications by means of DPM as seen in Pimentel et al. (2006), Behjat et al. (2010), Julin et al. (2014), Alkhedhair et al. (2016) and Omar et al. (2016). The numerical predictions on droplet size, droplet velocities and spray penetration obtained by these authors demonstrated good agreement with the experiment results.

2.6.2 Turbulence Modeling

The standard k-ε turbulence model has been extensively used to model the turbulent gas phase induced by the momentum of spray droplets in the application of high-speed sprays (Collazo et al., 2009). However, standard k-ε turbulence model tends to overestimate the turbulent viscosity and is not suitable for the current study of the low-pressure application where flow field is formed by spray droplets in still air. Remarkably, Fogliati et al. (2006) and Fung et al. (2012) employed the realizable k-ε turbulence model in the simulation of paint sprays and nasal spray device at low injection pressure and the simulated results showed good agreement with experimental data. The realizable k−ε turbulence model is more reliable than the standard k−ε for many applications. It is known to predict swirling flows and the spreading rate of jet streams more accurately, which is important when modeling spray nozzles (Persson, 2013). Omar et al. (2016) studied the airflow of aerial

crop spraying system using CFD. They focused on the effect of aircraft speed and nozzle orientation on the spray droplet distribution from a certain height. A more accurate simulation was achieved when the realizable k−ε turbulence was used to model the airflow in the fluid domain.

2.6.3 Spray Modeling

The term spray modeling refers to a subset of discrete phase particle modeling that describes the breakup of a continuous liquid into droplets known as primary and secondary atomization. Primary atomization makes assumptions about the physics inside the nozzle and computes an initial drop size in the region near the nozzle. Secondary atomization models droplets that traverse the domain where they become hydrodynamically unstable and break into smaller droplets (Adapco, 2016). The most common primary atomization models are the Linearized Instability Sheet Atomization (LISA) and Huh model. Generally, LISA has been developed by Schmidt et al. (1999) and Senecal et al. (1999) to model the primary breakup of the liquid film emerging from outwardly opening high-pressure swirl injectors, widely used for liquid-fuel injection in gas turbines, oil furnaces and direct-injection spark-ignited automobile engines. Chryssakis et al. (2002) studied the spray atomization of high-pressure swirl sprays commonly used in commercial Direct-Injection Spark-Ignition (DISI) engines. Measured data which include spray tip penetration, simultaneous spray and air entrainment velocities and droplet size distributions showed satisfactory results when compared against experimental results. In addition, Gavtash et al. (2014) investigated spray atomization of the pressurized metered dose inhalers (pMDI) which is the most extensively used aerosol delivery devices to treat asthma and chronic obstructive pulmonary disease. The model of primary atomization in pMDIs was developed with an internal propellant flow model coupled with LISA framework to estimates the spray velocity and droplet size of pMDIs. Model predictions of spray velocity and droplet size were validated by comparison with experimental data and good agreement was obtained.

Huh model is commonly used to model the breakup of a liquid jet created through a simple hole-type nozzle. According to the Huh atomization model, the spray is modeled by injecting a train of “blob” (parent) parcels which are disaggregated into secondary

(atomized) droplets by the grow of the initial turbulence fluctuations generated on the jet surface because of nozzle flow conditions (Lucchini et al., 2010). Various researchers such as Maes et al. (2016), Paredi et al. (2020), Brusiani et al. (2014), Bode et al. (2015) and Lucchini et al. (2010) employed the Huh model in the modeling of primary atomization of fuel leaving the single or multi-hole injector nozzles. Their model showed was validated against available experimental data for the spray cone angle of steady-flow single-hole experiments and good agreement was obtained. As reported by Maes et al. (2016), the Huh model is very suitable for Eulerian-Lagrangian simulations due to its ability to account for liquid jet turbulence on the atomization process. Thus, the analytical capabilities of Huh model for spray modeling are anticipated to be very high. Paredi et al. (2020) showed that the model developed able to predict gasoline spray evolution under different operating conditions accurately. Aguerre and Nigro (2019) reported that the droplet diameter reduction parameter, k_1 in Huh model allows controlling the Sauter mean diameter of the spray for the first and medium temporal phases of the injection. This parameter controls the Sauter mean diameter (SMD) of the mother droplets resulting from the Huh breakup. Wojdas (2010) reported that by increasing k_1, the breakup rate decrease causing longer atomization. The growth of C_3 and C_4 would have the same effect on the breakup rate, but additionally it would act on the atomization time scale itself, as well as on the spray semi-cone angle β and the simulated shape of the jet.

Secondary droplet break-up is caused by aerodynamic forces such as pressure and friction induced by the relative velocity between the droplets and the surrounding air which can be characterized by the Weber and Ohnesorge numbers. At Ohnesorge numbers lower than 0.1, breakup modes depend only on the Weber number (Fauchais et al., 2014). Various breakup regimes have been identified and each characterized by the shape of the deforming droplets as shown in Table 2.10. Detailed modeling of secondary breakup regime is difficult and thus, the goal of secondary breakup models is to predict when breakup occurs and what diameters result from it. Over the years, there are various secondary breakup models developed such as the Taylor analogy breakup (TAB) model, Reitz-Diwakar (RD) and Kelvin-Helmholtz-Rayleigh-Taylor (KHRT) for the atomization modeling.

Table 2.10 Definition of the critical Weber numbers of the different droplet breakup regimes (Habchi, 2011; Storm & Joos, 2019). Reproduced with permission from Elsevier

Breakup regime	Breakup mechanisms	Range of appearance	Comment
Oscillatory	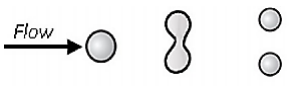	$We_{c0}<We_d<We_{c1}$	We_{c0} ~0.5
Bag		$We_{c1}<We_d<We_{c2}$	$10 < We_{c1} < 16$ $20 < We_{c2} < 45$
Bag-streamer		$We_{c2}<We_d<We_{c3}$	$80 < We_{c3} < 120$
Stripping		$We_{c3}<We_d<We_{c4}$	$350 < We_{c4} < 850$

TAB is a classic method for calculating droplet breakup, which is applicable to many engineering sprays. The TAB model represents an oscillating and distorting droplet as a spring mass system (Taylor, 1963). In this analogy, the surface tension force is represented by the restoring or stabilizing force of the "spring" and the gas aerodynamic force is the source of the external or destabilizing force on the mass. Typically, the TAB model is used at low Weber numbers. An example of a preferred application for this model is the hollow-cone gasoline sprays (Baumgarten, 2006). Tanner (1997) showed that TAB model tends to underpredict droplet sizes of full cone sprays. The RD breakup model works based on two different assumptions where the model assumes that breakup occurs in one of two possible modes, "bag" and "stripping" breakup (Reitz & Diwakar, 1986). As for "bag" breakup, in which the non-uniform pressure field around the droplet causes it to expand in the low-pressure wake region and eventually disintegrate when surface tension forces are overcome. Then, "stripping" breakup, in which liquid is sheared or stripped from the droplet surface. The most commonly used secondary breakup model for simple hole nozzle is the RD model. Chasos et al. (2012) employed the RD model to investigate the spray atomization of injector nozzle with different biodiesel concentration. As biodiesel concentration increases, it results in a smaller spray angle and longer spray penetration. The temperature conditions and simulated sprays at high pressure were

validated with experimental data and results showed that spray penetration was slightly overpredicted and the simulated spray angle was wider than the experimental. However, simulated results showed good agreement with experiment trend. CFD simulations of the gasoline spray with the outward-opening piezoelectric injector was performed with different droplet breakup models by Wang and Zhao (2018). The injection pressure was kept constant while two different backpressures were used to assess the effectiveness of the breakup models. It is observed that the tuned RD model was robust under different backpressures and the results for spray penetration was in good agreement with the experimental results. It was found that the model parameters C_{b1} and C_{s2} affect the breakup process and spray penetration. However, these two parameters show little impact on the final value of SMD of droplets at the end of injection.

Often, break-up processes and break-up regimes of sprays cannot be described by using a single break-up model. Thus, it is essential to combine models to enhance the accuracy of prediction. Thus, KH-RT Breakup model is developed which comprises the combination of two submodels, Kelvin-Helmholtz (KH) and Rayleigh-Taylor (RT). Both breakup submodels consider the growth of instabilities on a droplet and provide expressions for their wavelength and frequency. The KHRT model was developed as a replacement for the TAB model and it is preferred at high Weber numbers (Patterson & Reitz, 1998). Park et al. (2003) investigated the prediction accuracy of KH-RT model for high-speed diesel fuel sprays and reported that the results of model agree well with the experimental results. Remarkably, Zeoli et al. (2006) implemented the KH and TAB break-up algorithms in the atomization code to investigate the breakup of droplet during the atomization. Their results indicated that at high Weber number when droplets start to breakup, small droplets are generated as result of continuous shedding from the parent droplets and this can be accurately modeled using the KH model. Weber number decreased as the droplets become smaller and it is best described by the bag break-up mechanism. At low Weber number, breakup can be more precisely represented by the TAB model. Fan et al. (2018) compared the efficiency of TAB and KH-RT models in predicting liquid jet atomization in supersonic crossflow. Model predictions were compared to experimental data and more accurate predictions of liquid penetration and droplet size distribution can be obtained with KH-RT models. The main principal difficulty in using the KH-RT breakup model is

the need of excessive fine tuning of simulation parameters to the application under consideration, reflecting the complexity of the physics (Fan et al., 2018).

Generally, primary and secondary breakup models are coupled to study the spray behaviors. Liu et al. (2016) modeled the primary and secondary atomization of kerosene from pressure swirl injector with LISA and TAB model, respectively and it was reported that the model could capture the atomization process of fuel accurately. Paredi et al. (2018) investigated the most accurate numerical set-up for primary and secondary atomization of multi-hole Gasoline Direct Injection (GDI) injectors. Their computed results were validated with data obtained experimentally for the ECN Spray G baseline condition. Spray penetrations, negative axial recirculation velocity and radial contours of the axial velocity over time were correctly predicted by the Huh and RD model. Wojdas (2010) also presented a methodology for the numerical simulations of diesel engine with Huh and RD as primary and secondary atomization model, respectively and simulated results were in an agreement with experimental results. Commonly, spray breakup models have been widely used for applications which include combustion, and industry and agricultural spraying with high pressure and less in low-pressure nozzle spray applications. The same physics of spray atomization under high-pressure applications can be used for low-pressure nozzle spray, but not much studies have been done as indicated by Fung et al. (2012). The breakup parameters must be accurately calibrated in order to estimate the spray outcomes based on the injection conditions, nozzle geometry, and fluid properties (Brulatout et al., 2016). Notably, the parameters in breakup model for low-pressure injection with small-scale spray nozzle were not studied. Thus, there is a need to fine tune the constants of breakup models of the HUH and RD model and evaluate its performance for low-pressure applications. The computational replication of this physical behavior in CFD can be achieved by adjusting the model coefficients based on experimental results.

2.6.4 Wall Impingement

Droplets can interact with each other directly through collision, creating larger droplets and changing the dynamics of the spray plume. The interaction between droplets and walls can be modeled using the Bai-Gosman (Bai et al., 2002) or the Satoh (Satoh et al., 2000) wall impingement model. Satoh model is specially developed for oil droplets in oil-

mist separators and thus, it is unsuitable for current study. In a Lagrangian framework, the Bai-Gosman model is commonly used spray impingement model for droplets and wall interaction. The outcome of the impinging droplets is the main focus of this model. The impingement regime selection is reliant on parameters which include the incident Weber number (We_I), Laplace number (La), temperature of boundary wall and the state of wall, either dry or wet. The boundaries between different regimes for the Bai-Gosman model are listed in Table 2.11. Quissek et al. (2019) implemented the Bai-Gosman model to study the critical temperature range that separates impingement regimes of the of urea water solution (UWS) droplets that results in wall wetting and regimes with thermal rebound or break-up. Hamed and Markale (2017) developed a Eulerian-Lagrangian simulation with Bai-Gosman model to study the interaction between the rain droplets and the rear-view mirror of vehicle. The simulated results showed good agreement to experimental results done at National Electric Vehicle Sweden and the fluid film thickness prediction is found to be mesh independent.

Table 2.11 Regime transition criteria for Bai-Gosman model (Bai et al., 2002)

Wall status	**Regime transition state**	**Transition criterion**
Dry	Adhesion to splash	$We_I \geq We_{cr} = 26030La^{-0.183}$
Wet	Stick to rebound	$We_I > We_{cr} = 2$
	Rebound to spread	$We_I > We_{cr} = 20$
	Spread to splash	$We_I > We_{cr} = 1320La^{-0.183}$

2.7 Concluding remarks

PSMs has the ability to promote plant growth via the solubilization and mineralization of insoluble phosphate in soil, production of plant growth regulators, siderophores and protection enzyme. PSMs need to be encapsulated prior to inoculation in order to protect PSMs from environmental stresses. Various microencapsulation techniques have been developed for microbial cells and impinging aerosol technology, a continuous process has gained the attention of researchers in recent years due to its simplicity, low operation and maintenance cost and high encapsulation efficiency. Several parameters including

alginate concentration and operating conditions affects the particle size, surface morphology, yield and encapsulation efficiency. Thus, response surface methodology is often applied to optimize these parameters. Box-Behnken Design is the most common model for optimization as it requires less runs with high efficiency. In addition, it is essential to study the cell release from alginate microbeads to ensure cells are release gradually to soil to facilitate colonization of plant roots. Among the kinetic models, Ritger-Peppas is expected to be the most suitable kinetic models for cell release from alginate microbeads. Nevertheless, optimization of parameters via extensive experiments is unfavorable and hence, CFD serves as a useful tool to predict the spray behaviors. Particularly, counter flow spray is scarcely reported in the literature. In spray modeling, Eulerian-Lagrangian framework is generally used where Huh model and Reitz-Diwakar are employed for primary and secondary atomization (Wojdas, 2010). The interaction of spray droplets with wall are usually modeled with Bai-Gosman model (Quissek et al., 2019).

CHAPTER 3

EXPERIMENTAL METHODOLOGY

In Chapter 2, critical reviews on phosphate solubilizing microorganisms, encapsulation technologies and associated numerical modeling employed by past researchers for spray modeling were discussed. This chapter focuses on the experimental methodology for current research which includes isolation and identification of PSMs, microencapsulation of PSMs via impinging aerosol method and kinetic release study of PSMs from dried alginate microbeads.

3.1 Chemical and Reagents

All chemical and reagents used in this study were of analytical grade and tabulated in Table 3.1.

Table 3.1 Chemicals and reagents used

Chemicals	**Purity and brand**	**Purpose**
D(+)-glucose	≥ 99.5 %, Merck	Culture medium
Potassium chloride (KCl)	≥ 99.5 %, Merck	Culture medium
Tryptic soy agar (TSA)	NA, Merck	Culture medium
Vanadate-molybdate reagent	NA, Merck	Phosphate estimation
Magnesium chloride hexahydrate ($MgCl_2.6H_2O$)	≥ 99 %, Merck	Culture medium
Magnesium sulphate heptahydrate ($MgSO_4.7H_2O$)	≥ 99.5 %, Merck	Culture medium

Table 3.1 (Cont') Chemicals and reagents used

Chemicals	Purity and brand	Purpose
Bromophenol blue dye	0.04 wt. % in H_2O, Merck	Isolation of PSMs
Yeast extract	NA, Merck	Culture medium
Nutrient Broth No.2	NA, Merck	Isolation of PSMs
Sodium hydroxide (NaOH)	≥ 97 %, Merck	pH adjustment
Hydrochloric acid (HCl)	37 %, Merck	pH adjustment
Potassium dihydrogen phosphate (KH_2PO_4)	≥ 99.5 %, Merck	Bacteria identification
Gram stain kit	NA, Merck	Bacteria identification
Calcium chloride	≥ 98 %, Merck	Encapsulation of PSMs
Iron (III) phosphate dihydrate ($FePO_4.2H_2O$)	29 %, Sigma Aldrich	Isolation of PSMs
Phytic acid	50 % w/w in H_2O, Sigma Aldrich	Isolation of PSMs
Aluminium phosphate ($AlPO_4$)	≥ 99.9 %, Sigma Aldrich	Isolation of PSMs and phosphate solubilization study
Ammonium sulfate ($(NH_4)_2SO_4$)	≥ 99 %, Fisher Scientific	Culture medium
Sodium alginate	NA, Fisher Scientific	Encapsulation of PSMs
Sodium citrate tribasic dihydrate	≥ 99 %, Sigma Aldrich	Cell release study
Agar	NA, Bendosen.	Isolation of PSMs
G-spin^{tm} genomic DNA extraction kit	NA, iNtRON Biotechnology, Korea	Bacteria identification

*NA= information not available

3.2 Sample Site, Collection and Characterization of Peat

Peat samples were collected during the month of October, 2017 from Paradom area (2º13'59"N, 111º47'17"E) of Sibu, Malaysia. Samples were taken from 20 cm of depth and approximately 1 kg of peat was collected and packed in sterile plastic bag. Samples

were transported to the laboratory and kept in refrigerator at 4ºC for further experiments. The moisture and organic matter content of peat were estimated by following the standard methods as described in ASTM (2014). The determination of pH were conducted by using the procedures reported by ASTM (2001).

3.3 Isolation of Phosphate Solubilizing Microorganisms (PSMs)

In order to enhance PSMs population, peat samples were enriched by the method adopted by Bardiya and Gaur (1974) and El-Tarabily and Youssef (2010). Firstly, 1 g of peat was added to 9 mL of sterile water and enriched with 5 mL of nutrient broth and various insoluble phosphate sources such as Al-P, Fe-P and phytic acid as summarized in Table 3.2. Then, these enriched samples were agitated at 130 rpm with an incubator shaker (311DS Labnet, New Jersey) at 30ºC for 7 d.

Table 3.2 Inoculum enrichment with various phosphate sources

Samples	**Enrichment**
A	No insoluble phosphate source added (Blank)
B	3 ml of 0.1 M $AlPO_4$, 3 ml of 0.1 M $FePO_4.2H_2O$ and 3 ml of 2µM phytic acids
C	3 ml of 0.1 M $AlPO_4$ and 3 ml of 0.1 M $FePO_4.2H_2O$

After 7 d, potential PSMs isolates were obtained by the serial dilution method on National Botanical Research Institute Phosphate (NBRIP) agar containing (per litre): 15 g agar, 10 g glucose, 5 g $MgCl_2.6H_2O$, 0.25 g $MgSO_4.7H_2O$, 0.2 g KCl, 0.1 g $(NH_4)_2.SO_4$ (Nautiyal, 1999) with 4 g $AlPO_4$ as the phosphate source. The pH of medium was adjusted to 4.0 by using 0.1 M HCl or 0.1 M NaOH before autoclaving at 121°C for 15 minutes (Sharma et al., 2017). Glucose was autoclaved separately to avoid caramelization. The medium was mixed well and poured into sterile petri plates. The plates were incubated in incubator at 30°C for 72 h. Experiments were done in triplicates.

As the solubilization of $AlPO_4$ did not produce halo-zone as an indication for phosphate solubilization by PSMs in this work, distinct colonies were picked and transferred to NBRIP-BPB agar where bromophenol blue (BPB) dye were added as an alternative method for insoluble phosphate solubilization indication (Gadagi et al., 2002). At pH 4.0

bromophenol dye is blue in color and it turns yellow when the pH drops to below 3. These plates were incubated (Binder BF240, Germany) at 30°C for 72 h. Potential PSMs released organic acids during solubilization and thus, colonies that turned agar plates from blue to yellow were picked and further purified in modified tryptic soy agar (TSA) consisted per litre of 2.5 g glucose, 2.5 g KH_2PO_4 and 40 g TSA and incubated at 30°C. Subsequent subcultures were done until purified isolates were obtained and these isolates were kept on modified TSA at 4°C for further study. The isolation processes were illustrated in Appendix A.

3.3.1 Prescreening on Phosphate Solubilization Potential

There were total of 16 isolates obtained from the isolation. These isolates were prescreened on their phosphate solubilization ability with $AlPO_4$ as the insoluble phosphate source. A loop of bacteria was transferred from plates to 20 ml of NBRIP broth supplemented with 2.5 g L^{-1} of KH_2PO_4 and cultivated in an incubator shaker at 37ºC and 130 rpm for 24 h. Then, 0.1 ml of cell culture (adjusted to OD 1.0 by diluting with NBRIP broth, approximately 0.5 x 10^8 CFU/ml) was inoculated into 50 ml of NBRIP broth containing 4 g L^{-1} of $AlPO_4$ and incubated at 37ºC and 130 rpm for 24 h (Walpola et al., 2012a). NBRIP broth containing PO_4^{3-} was placed into the incubator as a control without the cell culture. The samples were then centrifuged (Universal 320R, Germany) at 4000 rpm for 15 min. The obtained supernatant was analyzed for soluble phosphate concentration. Vanadate-molybdate colorimetric method was used for the quantitative estimation of soluble phosphate concentration in the supernatant (Acevedo et al., 2014). 0.25 mL of vanadate-molybdate reagent was transferred to 1 mL of supernatant and let stand for 10 min. UV-Visible spectrometer (Lambda Bio, US) was used to identify the intensity of yellow color at 400 nm. The level of phosphate concentration was estimated by using a standard graph of monopotassium phosphate, KH_2PO_4 (Refer to Appendix B). Triplicates were done for all experiments and values were expressed in mean.

3.3.2 Phosphate Solubilizing Microorganisms Characterization

Bacteria that showed the highest phosphate solubilization potential, namely A10, B02 and C11 were characterized by using gram staining method (Tiwari et al., 2009). A thin smear of bacterial isolates was prepared on a glass slide in sterile water. Air dried and heat fixed

smear was stained sequentially with crystal violet solution for 1 min, iodine solution for 1 min and decolorized by acetone–alcohol for 20 s and counterstained with safranin solution for 1 min. The slide was then observed under light microscope (Nikon Eclipse LV 100N Pol, Japan) under oil immersion at 1000x (Sharma et al., 2020). PSMs strains were identified through 16s rRNA sequencing (Anand et al., 2016). Identification of the bacterial isolates were done by inoculating pure single colony in modified NBRIP broth and grown 20 h for bacterial DNA extraction. The extraction was performed with G-spin^{TM} genomic DNA extraction kit. 16s rRNA gene was amplified by polymerase chain reaction (PCR) using forward primer 27F (5'-AGAGTTTGATCCTGGCTCAG-3') and reverse primer 1492R (5'-GGTTACCTTGTTACGACTT-3'). The PCR program (Biorad, USA) was started with initial denaturation at 94 °C for 5 min which was followed by 36 cycles of denaturation at 94°C for 60 s, annealing at 48°C for 30 s, elongation for 2 min at 72 °C and final extension at 72 °C for 7 min. After completion of the reaction, the amplified genes were gel eluted and ligated into the pGEM-T vectors as per manufacturer's instruction (Promega, USA). The sequences were generated by chain termination method using an Applied Biosystem automated sequencer. The nucleotide sequences were compared with published database sequences in the National Center for Biotechnology Information, GenBank using the megablast program (https://blast.ncbi.nlm.nih.gov/Blast.cgi). Phylogenetical analyses of 16s rRNA gene sequences were aligned using MEGA V10.0.5. The phylogenetical analysis was conducted using the Neighbor Joining Method. The confidence values of the branches were identified by using the bootstrap test (500 replications) and were shown next to the branches (Felsenstein, 1985). Evolutionary distances were calculated using the Maximum Composite Likelihood method and displayed in terms of units of the number of base substitutions per site (Tamura et al., 2011). The 16S rRNA gene sequences for A10, B02 and C11 were then deposited in GenBank (NCBI) with the accession numbers of **MK140946**, **MK140948**, and **MK140949** respectively.

3.3.3 Determination of Phosphate Solubilization Activity

NBRIP broth was modified by replacing 0.1 g L^{-1} $(NH_4)_2.SO_4$ to 2 g L^{-1} of yeast extract for further studies on their phosphate solubilization activity. Bacteria were cultured in modified NBRIP broth supplemented with KH_2PO_4 at 37ºC, 130 rpm for 24 h. Then, 0.1

ml of cell culture (adjusted to OD 1.0 by diluting with NBRIP broth, approximately 0.5 x 10^8 CFU/ml) was transferred to 50 ml of modified NBRIP broth containing 4 g L^{-1} of $AlPO_4$ at 37°C, 130 rpm for 24 h to test for the ability to solubilize insoluble phosphate. Supernatant were obtained by centrifugation and the soluble phosphate concentration were tested with vanadate-molybdate reagent. All experiments were performed in triplicates. The isolates among A10, B02 and C11 which showed the highest phosphate solubilization ability was selected for the rest of the research work.

3.3.3.1 Effect of Time on Phosphate Solubilization by Phosphate Solubilizing Microorganisms (PSMs)

Ten 150 ml Erlenmeyer flasks which consisted of 50 ml of modified NBRIP broth containing 4 g L^{-1} of $AlPO_4$ were inoculated with 0.1 ml cell culture (adjusted to OD 1.0 by diluting with NBRIP broth, approximately 0.5 x 10^8 CFU/ml) and placed into incubator shaker at 37°C and 130 rpm. Then, a flask was withdrawn at 24 h interval for 8 d and the sample was centrifuged at 4000 rpm for 15 min. The obtained supernatant was analyzed for soluble phosphate concentration using vanadate molybdate reagent. As a control, autoclaved and uninoculated modified NBRIP broth containing $AlPO_4$ was placed into the incubator. The experiments were conducted in triplicates.

3.3.3.2 Optimal Cultural Condition for Phosphate Solubilization

Optimal cultural condition for phosphate solubilization were identified by applying the one-factor-at-a-time (OFAT) method. The main aim of this optimization study is to identify the main influencing factors affecting cell growth and phosphate solubilzation. Thus, OFAT was used by investigating the effect of one variable and keeping the others unchanged. To determine the effect of carbon concentration on the phosphate solubilization, the isolate B02 were grown in the culture media containing 0 to 20 g L^{-1} of glucose. The glucose concentration that gives the highest cell growth and phosphate solubilization was selected. Then, the effect of nitrogen source was investigated by varying yeast concentration from 0 to 4 g L^{-1}. Then, the effect of $MgCl_2.6H_2O$ concentration on phosphate solubilization were studied with various concentration ranging from 0 to 10 g L^{-1}. For shaken culture in flasks, 50 ml of the medium was dispensed into 150 ml Erlenmeyer flasks followed by inoculation with 0.1 ml cell culture

(adjusted to OD 1.0 by diluting with NBRIP broth, approximately 0.5 x 10^8 CFU/ml) grown in modified NBRIP for 20 h at 37°C. Cultivations were performed at 37°C and 130 rpm for 24 h in an incubator shaker. Modified NBRIP broth containing $AlPO_4$ without cell culture served as control. The effect of KCl and $MgSO_4.7H_2O$ on phosphate solubilization were not investigated as it was reported by Park et al. (2010) that these components did not affect cell growth and phosphate solubilization.

3.4 Encapsulation of PSMs into Microbeads

3.4.1 Inoculum Preparation

B02 served as model bacteria for this study and was cultivated in tryptic soy broth (TSB). The PSMs was incubated at 37°C for 20 h at 130 rpm in an incubator rotary shaker (Bashan et al., 2002). The inoculum was harvested by centrifugation at 4000 rpm for 15 min and washed twice using saline solution (0.85 % (w/v) NaCl) (Bashan, 1986b).

3.4.2 Microbeads Formation

As shown in Figure 3.1, the production of microbeads where the encapsulated PSMs in alginate matrix was accomplished by using a impinging aerosol method developed by Bhandari (2009) where misting spray nozzles were used instead of pneumatic nozzles. The alginate solution droplets were sprayed into the encapsulation chamber and solidified upon contact with the mist of $CaCl_2$, making this a continuous process.

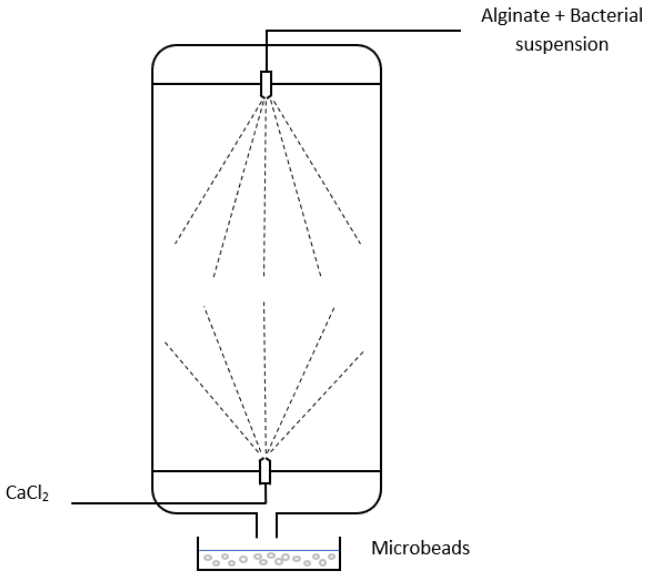

Figure 3.1 Schematic of microbead producing device

Bacterial suspension (~10^9 CFU/ml) were mixed under aseptic conditions with 2 % sodium alginate. An aerosol of bacteria-alginate suspension was injected into the top of a Plexiglas chamber (18 cm in diameter, 55 cm in height) through misting nozzles with 0.4 mm orifice size at alginate flowrate of 40 ml/min. A counter aerosol of sterile 0.1 M $CaCl_2$ was injected from the base of the chamber using a spray nozzle with 0.4 mm hole diameter at a flowrate of 30 ml/min. The microbeads was collected from the base of the encapsulation chamber (Hariyadi et al., 2010) and washed three times with saline solution (0.85 % (w/v) NaCl). Then the microbeads was separated from the suspension by centrifugation at 1500 rpm for 2 mins and rinsed three times with saline solution (Bashan et al., 2002). Dry beads were prepared by freeze drying at -40°C and 13.3 Pa (Bashan et al., 2002).

3.4.3 Optimization of Process Parameters

Often, cell viability is simultaneously affected by physicochemical characteristic of encapsulating agent and operating conditions of encapsulation process. Thus, in order to effectively identify the influence of numerous variables that will affect the response variable, RSM serves as an effective tool for optimizing the process parameters. The software Design Expert (Version 10.0.3, State-Ease Inc., Minneapolis, USA) was used for optimization by using the RSM. A total of 17 runs were generated by using Box-Behnken Design (BBD) and used to optimize the process parameters namely alginate concentration, flowrate of alginate and calcium chloride concentration for the production of microbeads with viable cells greater than ~10^9 CFU/g of dry beads. The level and code of variables considered in this study were shown in Table 3.3. The intervals for the three process variables were fixed through broad literature review and preliminary works and it will be discussed in Section 4.6.1. The experiments were conducted in triplicates and expressed as their mean. The experiments were conducted under various conditions of alginate concentration and flowrate and calcium chloride concentration as shown in Table 3.4.

Table 3.3 Level and code of variables for BBD

Variables	Symbols	Coded levels		
		-1	0	+1
Alginate flowrate (ml/min)	A	40	50	60
Concentration of alginate (%)	B	1.0	1.5	2.0
Concentration of $CaCl_2$ (M)	C	0.1	0.3	0.5

Table 3.4 BBD Matrix

Run	Alginate flowrate (ml/min)	Alginate concentration (%)	$CaCl_2$ concentration (M)
1	40	1	0.3
2	60	1	0.3
3	40	2	0.3
4	60	2	0.3
5	40	1.5	0.1
6	60	1.5	0.1
7	40	1.5	0.5
8	60	1.5	0.5
9	50	1	0.1
10	50	2	0.1
11	50	1	0.5
12	50	2	0.5
13	50	1.5	0.3
14	50	1.5	0.3
15	50	1.5	0.3
16	50	1.5	0.3
17	50	1.5	0.3

3.4.4 Enumeration of Bacteria Cells in Bead

0.1 g of wet or dried microbeads were broken down in 10 ml of sterile sodium citrate at pH 6.0 by gently shaking at room temperature for 10 min using an orbital shaker to determine the encapsulation efficiency and viable encapsulated cells in dried microbeads.

Serial dilutions were made in sterile 0.85 % (w/v) saline solution and 100 µL aliquots were plated on modified TSA agar. The PSMs were then incubated at 30°C for 24 h and the total number of released bacteria was determined by standard plate count method (Young et al., 2006). Encapsulation efficiency of PSMs and cell viability after lyophilization were determined with Equation 3.1 and 3.2 below.

$$\text{Encapsulation efficiency}(\%) = \frac{N_{ew}}{N_0} \times 100\% \tag{3.1}$$

$$\text{Cell viability}(\%) = \frac{N_{ed}}{N_0} \times 100\% \tag{3.2}$$

Where N_{ew} is the number of enumerated bacteria from wet microbeads, N_{ed} is the number of enumerated bacteria from dried microbeads and N_0 is the initial concentration of cell suspension used for microencapsulation.

3.4.5 Characterization of Microbeads

0.1 ml of alginate microbeads containing PSMs suspended in NaCl was placed under glass slide and then, examined using an optical microscope (Nikon Eclipse LV 100N Pol, Japan) under x100 and x200 magnification. Alginate sprays through nozzles was captured using a fast speed camera (FastCam Mini UX50, USA) at a frame rate of 2000 fps and shutter speed of 1/20000 sec.

3.4.6 Release Kinetics

The release kinetics of microbeads containing PSMs were studied. The dried microbeads were immersed in sterile physiological saline solution at pH 4, similar to peat pH. The cumulative amount of viable bacteria at different time intervals (M_t) were measured by the standard plate count method. Experiments were performed at room temperature for cell release analysis. Kinetic releases data were fitted into various release kinetic models as tabulated in Table 2.8.

3.4.6.1 Accuracy and prediction ability of the kinetic models

The accuracy and prediction ability of the kinetic models can be calculated by using Equation 3.3.

$$OE(\%) = \frac{100\sum_{i=1}^{N} \frac{\left|F_{cal,i} - F_{obs,i}\right|}{F_{obs,i}}}{N} \quad (3.3)$$

Where OE is overall absolute percent error, n is the number of data in each set, $F_{cal,i}$ and $F_{obs,i,}$ denote calculated fraction and observed fraction of component released at the i^{th} sample, respectively. Kinetic models with low OE best represent the kinetic release for the component.

3.5 Concluding remarks

Prior to isolation of PSMs, soil was enriched with various insoluble phosphate sources to enhance their phosphate solubilization potential. Then, isolation was done using NBRIP media with the addition of BPB dye for the identification of potential phosphate solubilizer. Potential isolates were tested under liquid media and their solubilizing potential was identified. Isolates with highest P solubilizing potential was selected for the microencapsulation using alginate via impinging aerosol method. BBD was employed to optimize various parameters which include alginate, $CaCl_2$ concentration and alginate flowrate for maximum cell viability after freeze-drying. Then, optimized alginate microbeads loaded PSMs were subjected for cell release study.

CHAPTER 4

EXPERIMENTAL RESULTS AND DISCUSSIONS

In Chapter 3, the experimental methodology for the isolation and identification of PSMs, microencapsulation of PSMs and cell release of PSMs from alginate microbeads were discussed. This chapter is the main part of the present study which discusses about the results obtained from experiments and discussion on the findings.

4.1 Peat Properties Analysis

As the solubility of Fe-P is very low in comparison with Al-P at low pH as mentioned earlier, this study aimed to identify efficient indigenous acidotolerant PSMs from peat of Sarawak that has the ability to solubilize fixed Al-P in peat. The chemical properties of the peat where the PSMs was isolated was tested and the results was tabulated in Table 4.1.

Table 4.1 Peat properties obtained in this work and past studies

Peat properties	Results in this work	Typical range of reported values
pH	3.54 ± 0.01	3.5 to 3.7 (Melling, 2016)
Organic matter	89.8 ± 0.2 %	> 65 % (Osaki & Tsuji, 2016)
Moisture content	79.8 ± 0.5 %.	36.9 to 95.5 % (Osaki et al., 2016)
Available P content	ND	60.1 to 218.3 mg kg^{-1} (Melling, 2016)

The pH and organic matter content of the peat used was identified to be 3.54 ± 0.01 and 89.8 ± 0.2 %, respectively. These results were in agreement with the findings by Melling (2016), where peat in Malaysia is found to contain organic matter content greater than 89 %

and pH ranging from 3.5 to 3.7. According to Osaki et al. (2016), soil is classified as peat when the organic matter content is greater than 65 %. The moisture content of peat used was found to be 79.8 ± 0.5 %. It has been reported that the moisture content of peats ranges from 36.9 to 95.5 % as it is largely dependent on the ground water levels and type of forest (Osaki et al., 2016). In this study, available phosphorus content in peat which is accessible for plant uptake was not determined. However, various researchers had reported on the low content of available phosphorus (P) of peat in Malaysia. Remarkably, Melling (2016) found that peat has low available P which ranged from 60.1 to 218.3 mg kg^{-1}.

4.2 Isolation of Phosphate Solubilizing Microorganisms

Enrichment culture technique is generally an isolation method intended to provide growth conditions very favorable for bacteria of interest while creating a hostile environment for competitors (Madhuri et al., 2019). As reported by Selvi et al. (2017), enrichment of soil samples with $AlPO_4$ and $FePO_4$ prior to isolation process, increase the microbial population of PSMs by 10-fold. Therefore, in current work peat samples were enriched with various insoluble phosphates sources with the aim to increase the microbial populations and to obtain competence PSMs that has potential in utilizing $AlPO_4$. A total of 16 PSMs from Sample A (namely A02, A03, A05, A06, A08, A09, A10 and A11), Sample B (namely B02, B03, B04, B05 and B06) and Sample C (namely C03, C10 and C11) were obtained from NBRIP-BPB agar. Sample B and C had lower number of isolates as these samples were treated with insoluble phosphate and thus, isolates that could not breakdown insoluble phosphate are eliminated in the process. Sample A was only enriched with nutrient broth without any insoluble phosphate therefore the microbial population is enhanced without eliminating isolates that have lower potential in utilizing insoluble phosphate. These PSMs were further tested for their phosphate solubilization potential in NBRIP broth supplemented with $AlPO_4$. Table A.2 (Appendix C) and Figure 4.1 presents the phosphate solubilization potential of PSMs for triplicates in mean.

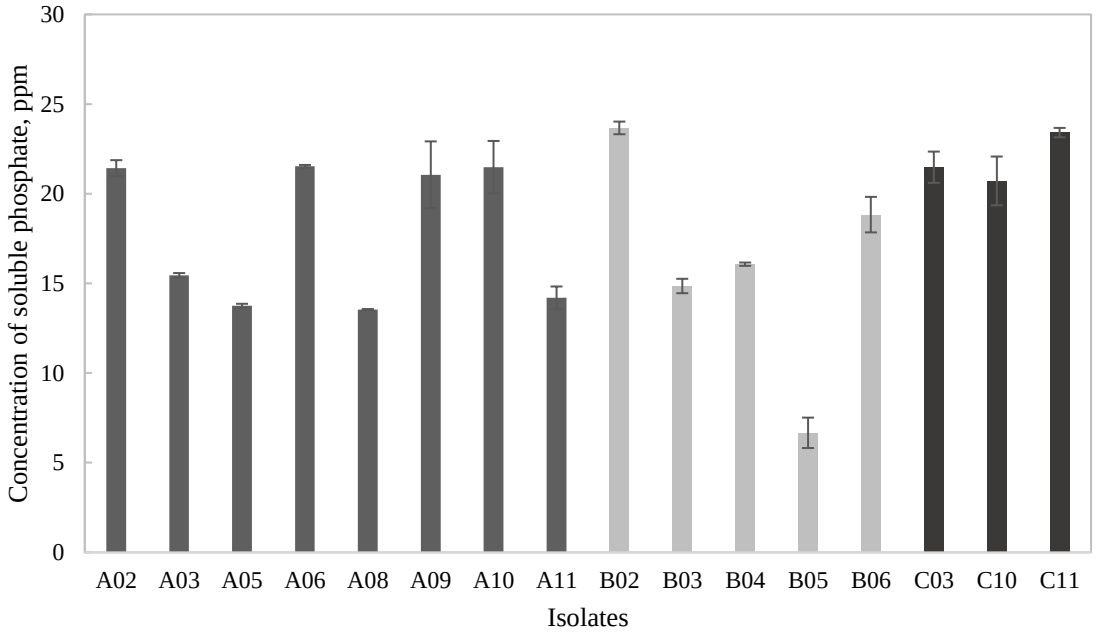

Figure 4.1 Phosphate solubilization potential of 16 PSMs from peat. Each bar represents a mean value and the error bars showed the standard deviation (n=3)

The average amount of phosphate solubilized by these 16 PSMs were in the range of 6.67 to 23.67 ppm. Figure 4.1 shows that isolate B02 had the highest phosphate solubilization potential of 23.67 ppm followed by C11 and A10, of 23.41 ppm and 21.48 ppm, respectively. On the other hand, isolates A02, A06 and A09 had similar phosphate solubilization potential when compared to isolate A10. Isolates A02 and A06 had a lower standard deviation in comparison with A10 but these bacteria were not chosen as they grow very slowly on solid medium. Besides, A09 was less preferable as it had a higher standard deviation.

4.3 Phylogenetic and DNA sequencing

The isolation was performed on NBRIP-BPB agar and purified on modified TSA agar medium. The selected isolates A10, B02 and C11 were examined for their colony morphology after 3 d of incubation at 30 °C as shown in Figure 4.2. All were spherical in shape, shining, cream colored and smooth in appearance.

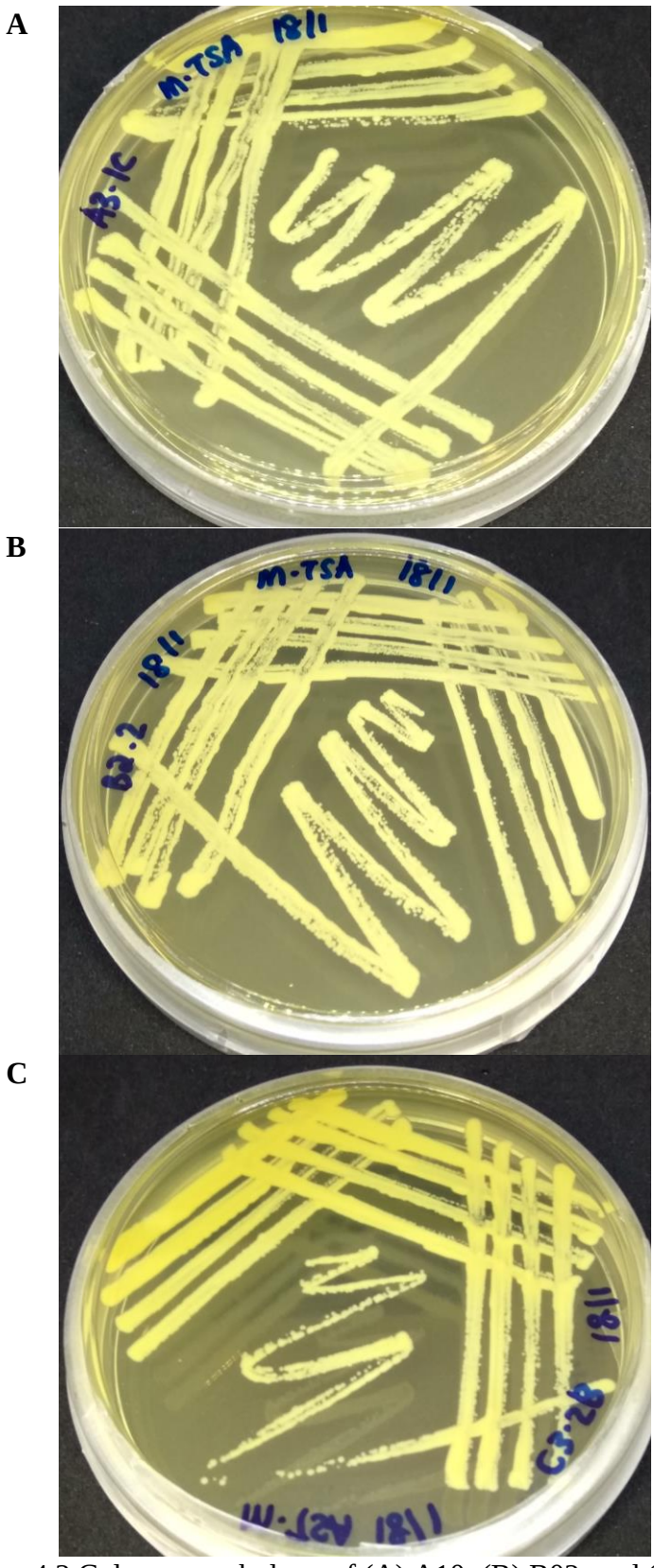

Figure 4.2 Colony morphology of (A) A10; (B) B02; and (C) C11

The gram stains for these isolates were presented in Figure 4.3, Figure 4.4, and Figure 4.5.

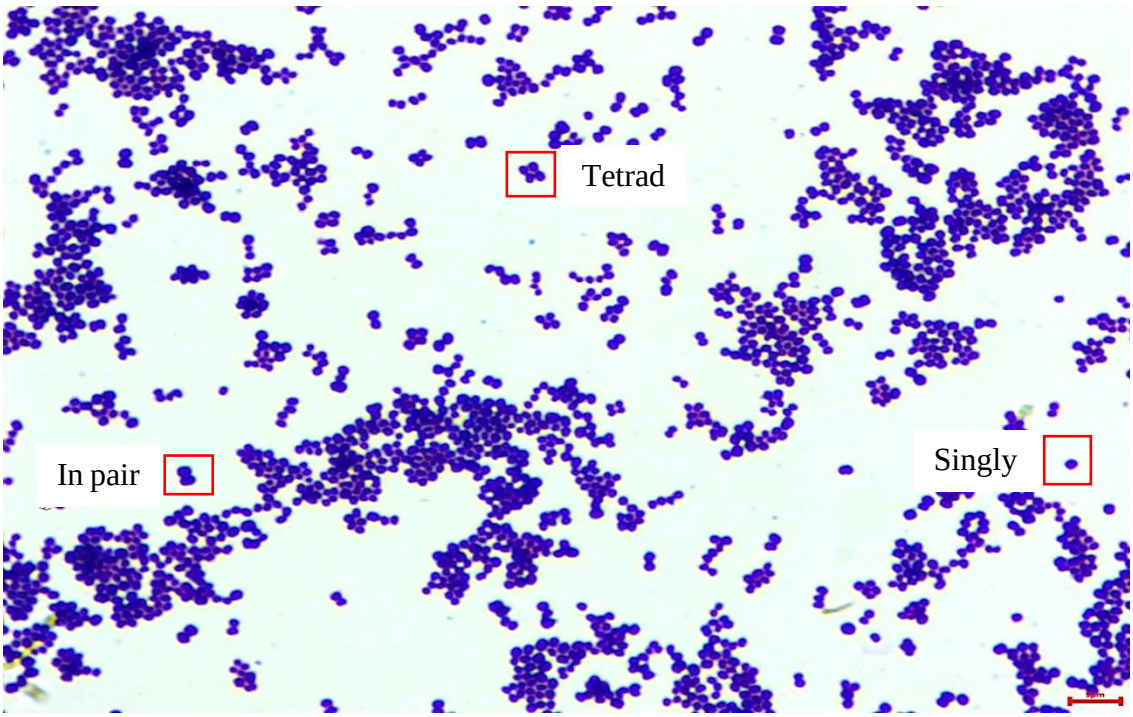

Figure 4.3 Gram stain of A10 at 5 µm scale bar with 1000x magnification

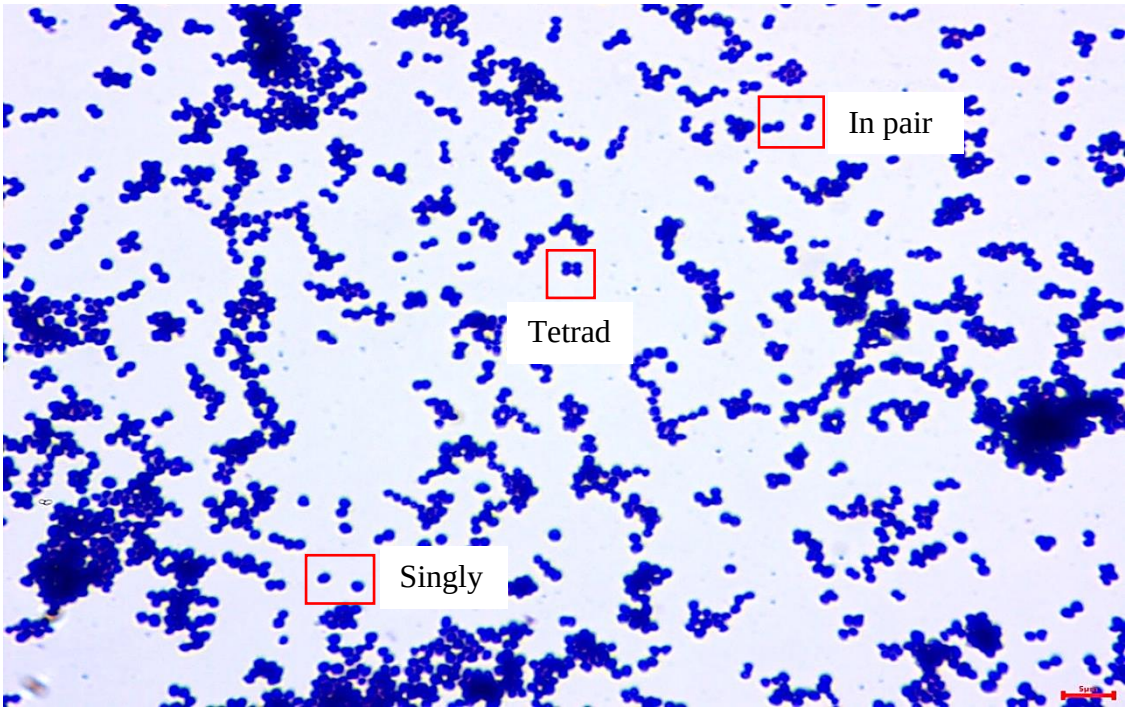

Figure 4.4 Gram stain of B02 at 5 µm scale bar with 1000x magnification

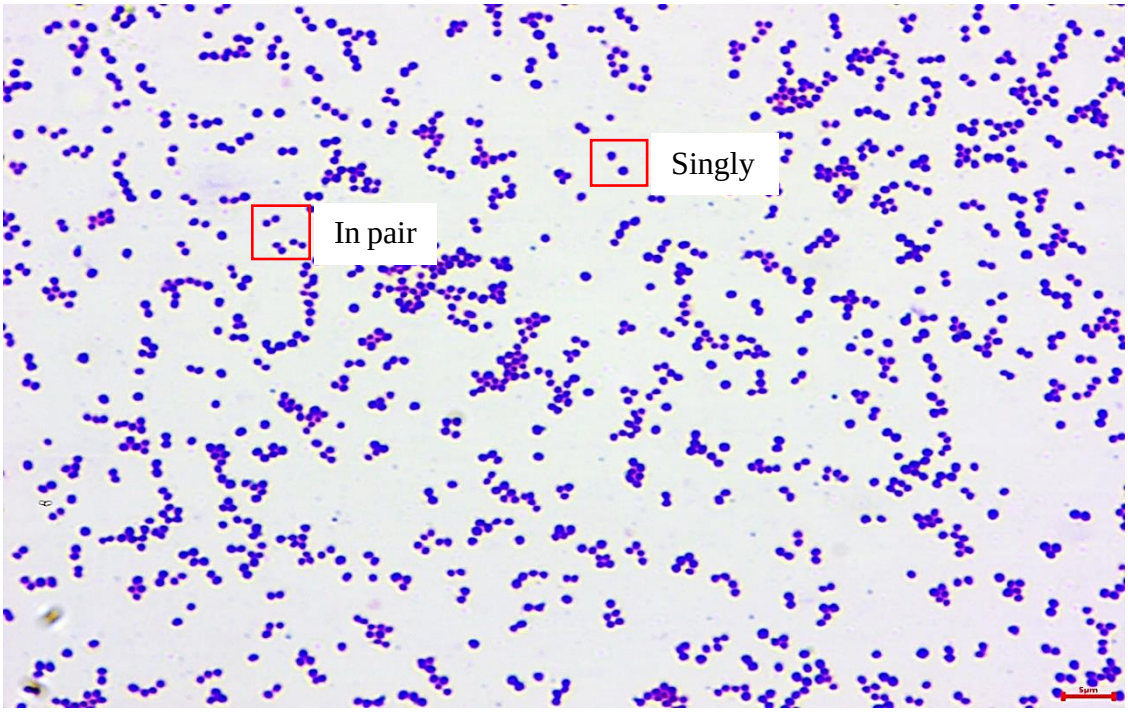

Figure 4.5 Gram stain of C11 at 5 µm scale bar with 1000x magnification

It can be seen from these gram stains that the bacteria occur singly, in pairs or tetrads with size ranging from 0.7 µm to 1.2 µm in diameter which are characteristics of *Staphylococcus sp.* (Kloos & Schleifer, 1975; Schleifer & Kloos, 1975). Nucleotide sequencing of the partial sequencing of the 16s rRNA gene of the A10, B02 and C11 isolates showed > 99 % similarity with existing species in GenBank database under the genera *Staphylococcus*. From the megablast results, isolates A10 and B02 showed 99.9 % similarity to that of *Staphylococcus haemolyticus* and C11 showed 100% similarity to *Staphylococcus cohnii*. Phylogenetic relationship of organisms is usually comparing homologous genes with other known genomes and here, the partial 16S rRNA gene sequences of the isolates were used to construct a phylogenetic tree for the identification of bacteria. Figure 4.6 shows the phylogenetic tree includes representative strains of related taxa obtained by neighbour-joining method.

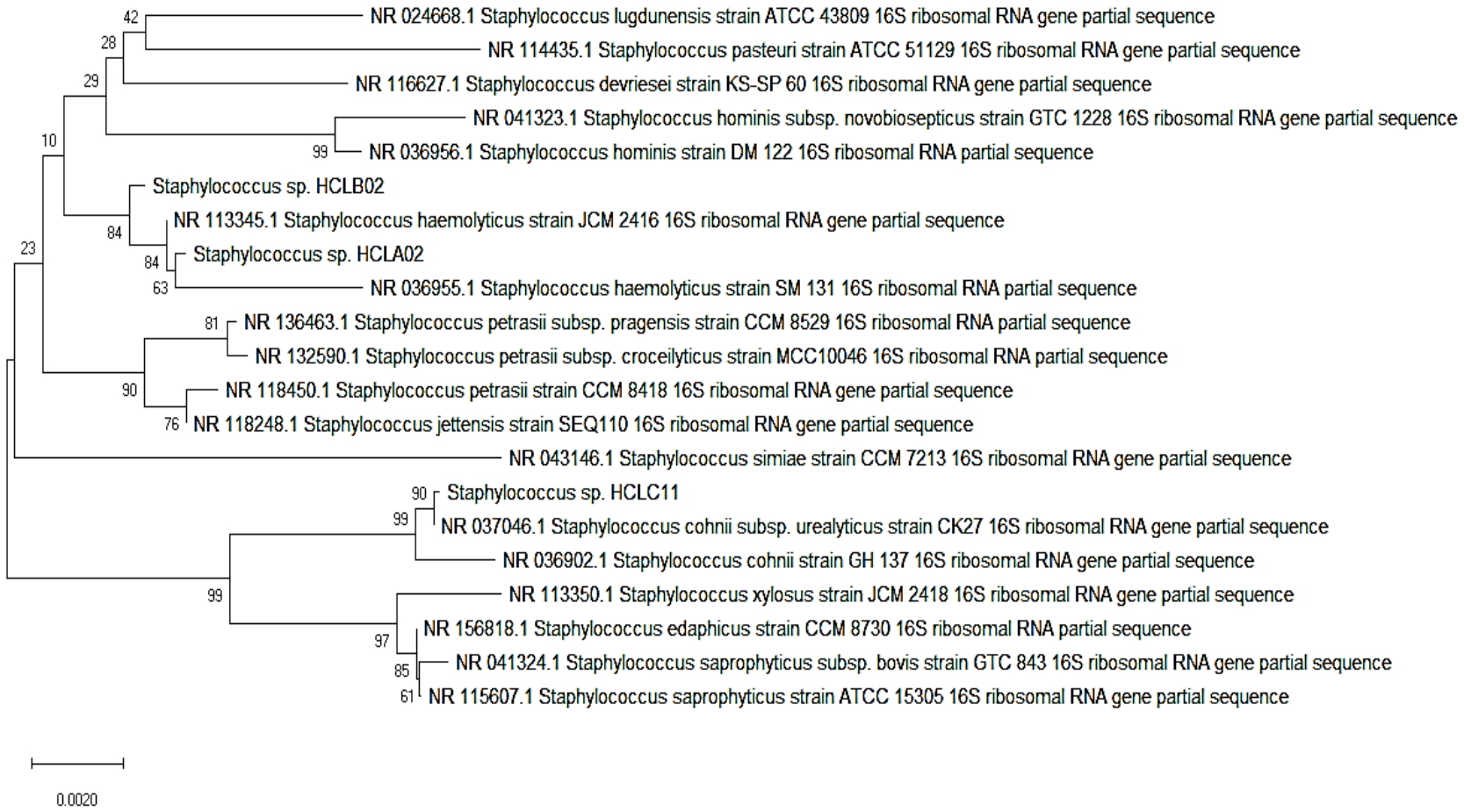

Figure 4.6 Phylogenetic tree of A10, B02 and C11

From the phylogenetic tree, it can be seen that A10 and B02 were closely related to each another, but both isolates could be of different species and/or strains as the classification of isolates to a given species requires additional phenotypic and molecular characterization. Schleifer et al. (1975) reported that *S. haemolyticus* are gram positive cocci, 0.8 to 1.3 µm in diameter and occurring predominantly in pairs and tetrads. Similarly, in this study, Figure 4.3 and Figure 4.4 show that cells were largely present in pairs or tetrads. Meanwhile, Schleifer et al. (1975) also reported that *S. cohnii* are gram positive cocci with diameter in the range of 0.5 to 1.2 µm, occurring mostly in pairs or singly. From Figure 4.5, it is very apparent that cells mostly appeared in pairs and singly with only a few tetrad cells. To conclude, isolate A10 and B02 were identified to be *S. haemolyticus* and C11, *S. cohnii* through the gram staining and 16s rRNA identification analysis. Isolates A10, B02 and C11 were registered as *S. haemolyticus* HCLA10 (**MK140946**), *S. haemolyticus* HCLB02 (**MK140948**) and *S. cohnii* HCLC11 (**MK140949**), respectively in Genbank (NCBI). Phosphate solubilization by *Staphylococcus sp.* has been reported by various researchers. Gen Fu and Xue Ping (2005) identified the capability of *Staphylococcus caprae* to solubilize tricalcium phosphate. Panda et al. (2016) isolated *Staphylococcus cohnii* and *succinus* from acidic soil and these isolates have the ability to solubilize Al-P and Fe-P. Besides, *Staphylococcus warneri* is able to solubilize tricalcium phosphate for approximately 21 to 23 % (Acevedo et al., 2014) but does not show any solubilization activity for Al-P and Fe-P. According to the authors, the weak solubilizing ability of *S. warneri* is due to the low production of gluconic acid. Highest phosphate solubilization is observed when bacteria secreted high amount of gluconic acid. This is because gluconic acid acts as chelating agent that bonds with the metal (Al or Fe) releasing the phosphate anions (Bashan et al., 2013). In recent years, the phosphate solubilization potential of *Staphylococcus haemolyticus* have been reported by various researchers such as Biswas et al. (2018), Banerjee et al. (2019) and Mushtaq et al. (2019). These authors showed that *Staphylococcus haemolyticus* has the ability to solubilize tricalcium phosphate, releasing solubilizing phosphate which promotes plant growth. Biswas et al. (2018) and Banerjee et al. (2019) showed that *Staphylococcus haemolyticus* is able to release 193.5 ± 1.5 ppm and 188.1 ± 0.05 ppm of soluble phosphate, respectively. They testified that *Staphylococcus haemolyticus* also promotes the growth

of plant through IAA, GA, ammonia and ACC deaminase production. To the best of the authors' knowledge in this work, there are no studies reported on the Al-P phosphate solubilization potential of *S. haemolyticus*. This is the first report on the ability of *S. haemolyticus* in solubilizing Al-P.

4.4 Phosphate Solubilization Potential Study

Previously, isolates A10 and B02 were identified to be closely related to *Staphylococcus haemolyticus* and it was reported that *S. haemolyticus* favors complex organic nitrogen source such as peptone or yeast extract than inorganic nitrogen source (Pandey et al., 2016). Besides, the best culture media for *S. cohnii* is nutrient broth which contains yeast and peptone as the nitrogen source (ATCC, 2018). Thus, NBRIP broth was modified by replacing ammonium sulphate with yeast as to provide a better culture medium for the bacteria growth for the determination of phosphate solubilization potential of the 3 selected isolates. In Section 4.2, when isolates were tested with NBRIP broth during prescreening, the net phosphate solubilized were in the range of 21.48 to 23.67 ppm. When the nitrogen source of culture media was replaced by yeast, the phosphate solubilization increased to 37.71 to 39.65 ppm as shown in Figure 4.7. The phosphate solubilization activity was increased by approximately 1.2 to 1.6-fold. The data on pH and amounts of soluble phosphate in medium after 24 h of incubation for *S. haemolyticus* HCLA10, *S. haemolyticus* HCLB02 and *S. cohnii* HCLC11 were presented in Table A.3 (Appendix D) and illustrated in Figure 4.7. Referring to Figure 4.7, the maximum phosphate solubilization was recorded by *S. haemolyticus* HCLB02 followed by *S. cohnii* HCLC11 and *S. haemolyticus* HCLA10 with 39.65 ppm, 37.71 ppm and 36.88 ppm, respectively. These results indicated that, culture medium that favored the growth of tested isolates gave a better phosphate solubilization capacity. Similarly, studies by Park et al. (2010) showed that when the optimal cultural conditions were used, the phosphate solubilization was approximately 1.6 fold higher. Results obtained were in agreement with the studies done by Panda et al. (2016) where *Staphylococcus* sp. were isolated from the acidic soils of Eastern Himalayan region. These isolates were tested on their solubilization activity of $AlPO_4$ and the phosphate solubilization capacity of these isolates diverse between 27 to 40 ppm.

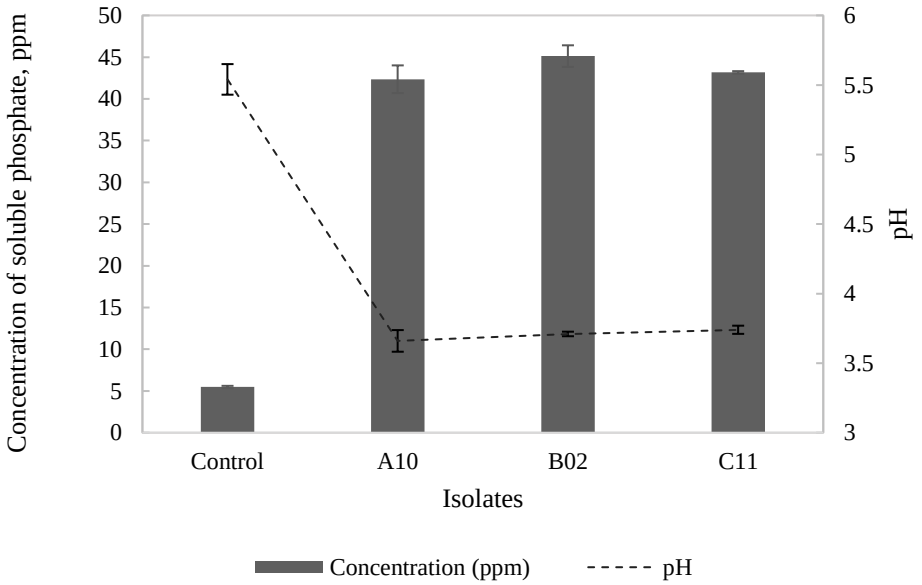

Figure 4.7 Phosphate solubilized and pH of culture medium after 24 h of incubation with $AlPO_4$ when inoculum cultured with 2.5g L^{-1} of KH_2PO_4. Each point represents a mean value and the error bars showed the standard deviation (n=3)

There are several possible phosphate solubilization mechanisms that may be involved, but the key mechanism is through the secretion of organic acids (Park et al., 2010). Referring to Figure 4.7, the solubilization of $AlPO_4$ by different isolates was accompanied by a substantial reduction in the pH of the culture medium ranged between 3.48 to 3.71 from an initial pH of 5.54 after 24 h of incubation. The drop in pH signified the release of organic acids by the isolates. According to Goldman and Green (2008), *Staphylococci* are a facultative anaerobe that grows by aerobic respiration or by fermentation, which yields principally lactic acid. Schleifer et al. (1975) also reported that *S. haemolyticus* produces mainly lactic acid from glucose. *S. haemolyticus* is also found to produce organic acids aerobically from various carbon sources such as maltose, sucrose, trehalose, glycerol, fructose, galactose, lactose, turanose, and mannitol. Barroso et al. (2006) tested the ability of lactic acid on $AlPO_4$ solubilization and approximately 14 ppm of soluble phosphate is released. Liu et al. (2012) also identified that oxalic, acetic, malic, lactic, citric and cuccinic acid produce by *Burkholderia cepacia* involves in the solubilization of Al-P. The schematic representation of chelating agents on the solubilization of Al-P was illustrated

in Figure 4.8. These organic acids act as a chelating agent, where their ligands or anions form one or more bonds with Al^{3+} ions of insoluble phosphate forming a ring structure and release the soluble phosphate (Bashan et al., 2013). The H^+ ions release from organic acids, respiration or NH_4^+ assimilation either binds with OH^- or PO_4^{3-} forming water or soluble phosphate, respectively.

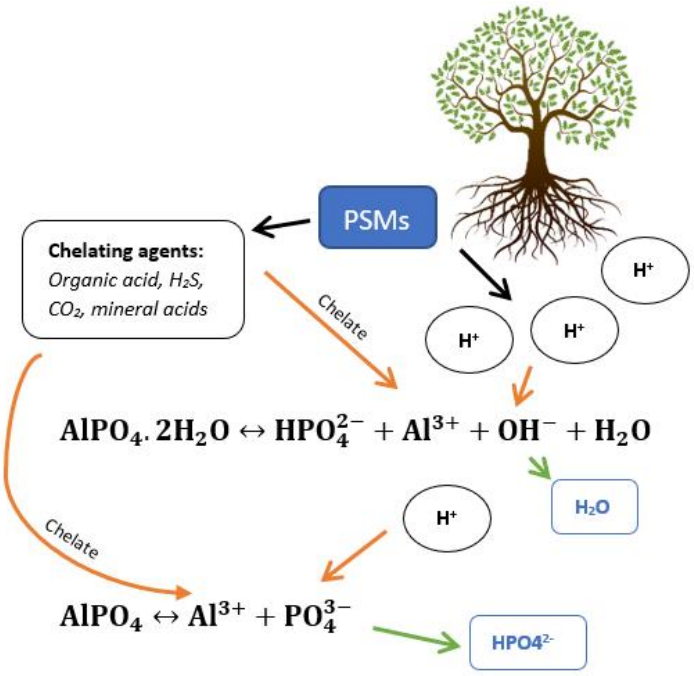

Figure 4.8 Schematic diagram of solubilization of Al-P in soil via chelation

From the phosphate solubilization estimation study, *S. haemolyticus* HCLB02 possessed the highest solubilizing potential. Therefore, *S. haemolyticus* HCLB02 was selected as the model bacteria for the remaining research works and the first objective for this research work was achieved.

S. haemolyticus HCLB02 was subjected to analysis of the changes in their phosphate solubilization activity and pH using $AlPO_4$ as the insoluble phosphate source. *S. haemolyticus* HCLB02 were assessed within a period of 8 d and the data were presented in Table A.6 (Appendix F) and the plot of concentration of phosphate solubilized against time was plotted in Figure 4.9. As shown in Figure 4.9, the concentration of soluble phosphate increased quickly between 0 to 24 h of growth and then gradually increased from day 1 to 5. Consequently, no more significant increase in soluble phosphate

concentration after 5th day. As for the pH of culture medium, the pH decreased from 5.54 to 3.78 in first 24 h and remained constant in the remaining incubation period.

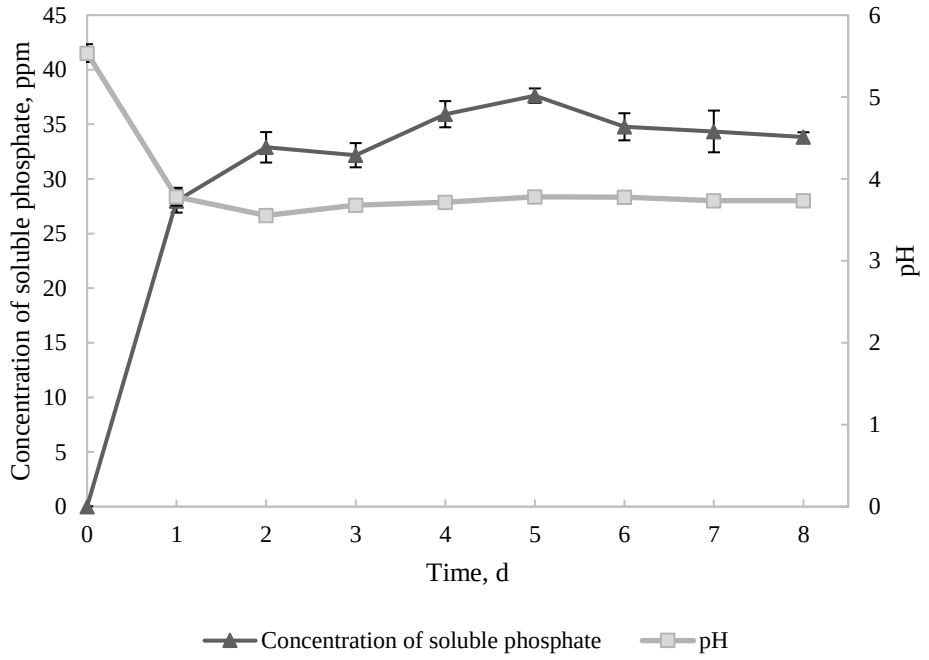

Figure 4.9 Changes in the phosphate solubilization of *S. haemolyticus* HCLB02 in modified NBRIP medium with $AlPO_4$. Each point represents a mean value and the error bars (±SD) were shown when larger than symbol (n=3)

Similar trend was reported by Acevedo et al. (2014) for isolate of the genera *Klebsiella* and Pande et al. (2017) for some isolates of the genera *Alcaligenes* and *Burkholderia*. Results obtained by Acevedo et al. (2014) showed that phosphate solubilization activity increased rapidly between 24 h to 48 h and the pH decreased from 7.0 to 4.2. Besides, the phosphate solubilization activity of isolates obtained by Pandey et al. (2016) displayed that the concentration of soluble phosphate increased slowly in the first 2 days, increased quickly from 2nd to 8th day and remained constant. While, the pH of medium gradually decreased from 7 to 3 within 8 d. Walpola et al. (2012a) revealed that pH decreased rapidly from 7 to 4 after 1 d and remained unchanged. These results confirmed that a drop in pH of culture medium led to an increase in phosphate solubilization, as the release of organic acids is one of the main mechanisms for the solubilization of insoluble phosphate. Mohamed et al. (2019) also observed that the amount of soluble P increased significantly till the 6th day, while after that there was no more changes in available P. The phosphate

solubilization activity remains constant could be due to the presence of soluble phosphate and/or excretory toxic products in culture medium inhibit further phosphate solubilization (Xiao et al., 2009; Mohamed et al., 2019). Nevertheless, some authors suggested that the decrease in phosphate solubilization may be due to the depletion of carbon source in culture medium for microbial activity and production of organic acids (Chaiharn & Lumyong, 2009).

4.5 Cultural Condition Optimization for Maximal Phosphate Solubilization

According to Park et al. (2010), glucose, yeast and $MgCl_2 \cdot 6H_2O$ affect cell growth and P solubilization. The omission of $MgSO_4 \cdot 7H_2O$ or KCl from NBRIP medium did not affect cell growth and P solubilization. Thus, the effect of glucose, yeast and $MgCl_2.6H_2O$ concentration on the cell growth and phosphate solubilization of PSMs were studied and the results were further discussed in the next few sections.

4.5.1 Effect of glucose concentration on phosphate solubilization

As reported by Nautiyal (1999), rate of P solubilization increased when glucose concentration increased due to an increase in cell growth. In current study, the optimal concentration of glucose source is vital for cell growth of *Staphylococcus sp.* for the production of the main organic acid, lactic acid (Schleifer et al., 1975). Lactic acid helps to release the bound phosphate. According to Park et al. (2010), glucose concentration greater than 25 g L^{-1} decreased the cell growth and thus, no effect on the P solubilization. In current work, concentration of glucose studied was in the range of 0 to 20 g L^{-1}. The data were presented in Table A.7 (Appendix H) and the plot of concentration of cell growth, P solubilized and pH against glucose concentration was plotted in Figure 4.10. Figure 4.10 shows that the cell growth and P solubilization were greatly enhanced with increasing amounts of glucose and reached maximum solubilization with 39.65 ppm at 10 g L^{-1}, which was approximately 253.7% increment. Further increased of glucose concentration had little effect on the cell growth and P solubilization. When the glucose concentration increased, the growth of cells increased resulting a reduction in pH. A significant reduction in the pH of the culture medium containing insoluble P suggests the secretion of organic acids by the *S. haemolyticus* HCLB02, which bind to insoluble phosphate releasing soluble phosphate.

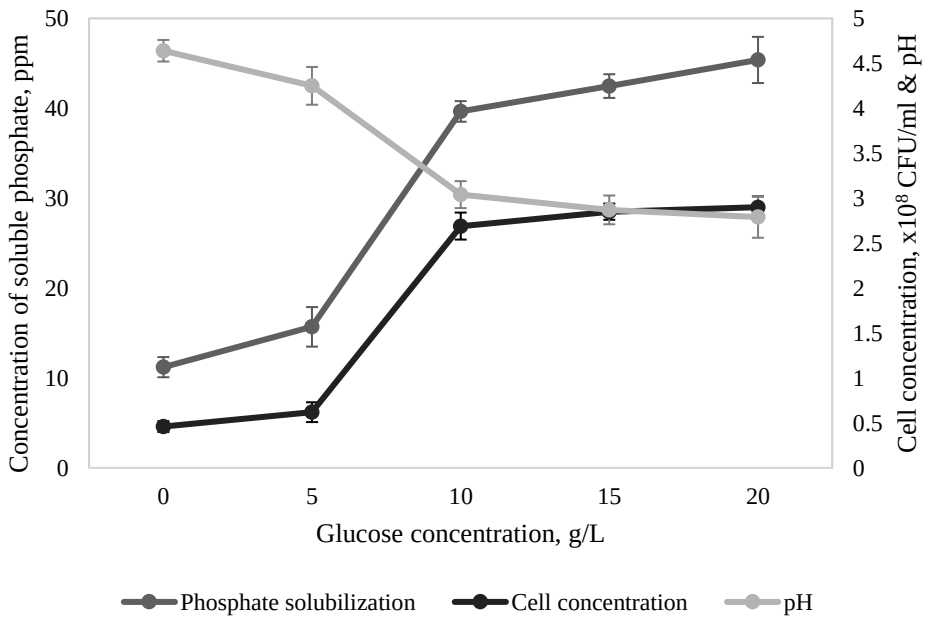

Figure 4.10 Effect of glucose concentration on phosphate solubilization for *S. haemolyticus* HCLB02, cell growth and pH of culture medium. Each point represents a mean value (n=3) and error bars (±SD) are shown when larger than symbol

Similar trends were reported by numerous researchers. Nautiyal (1999) tested the effect of glucose concentration of 5, 10 and 20 g L^{-1} on phosphate solubilization. Their results showed that when glucose concentration increased from 5 to 10 g L^{-1}, the phosphate solubilization potential of bacteria was increased by approximately 45 %, while further increase in glucose concentration only improved the phosphate solubilization activity by 18 %. Remarkably, Park et al. (2010) also reported that when the glucose concentration increased from 5 to 10 g L^{-1}, phosphate solubilization activity was enhanced by 50 % and further increase to 25 g L^{-1}, increased the solubilization by 20 %. High concentration of glucose (> 25 g L^{-1}) causes cell death and thus reduces amount of phosphate solubilized. Comparable results were also reported by Song et al. (2008) and Suleman et al. (2018) where phosphate solubilization potential increased with glucose concentration. This phenomenon can be attributed to increase energy source availability for bacteria growth and lactic acid production that involves in phosphate solubilization (Chibani et al., 2017). Lactic acid is produced by *S. haemolyticus* HCLB02 through aerobic respiration or by fermentation of glucose. These acids supply both H^+ ions and organic acid anions for

solubilization of $AlPO_4$. Thus, 10 g L^{-1} glucose concentration was selected for following experiments, keeping in mind the cost of end product.

4.5.2 Effect of yeast concentration on phosphate solubilization

As for yeast concentration, Nautiyal (1999) stated that concentration of yeast greater than 0.5 g L^{-1} caused a drop in phosphate solubilization by *Pseudomonas sp*. However, preliminary tests were carried out by using *S. haemolyticus* HCLB02 and it was found that if yeast concentration was lower than 0.5 g L^{-1}, slower growth of bacteria was observed. Therefore, it is important to determine the optimum yeast concentration for maximal cell growth. Current study employed the yeast concentration in the range of 0 to 4 g L^{-1}. The data obtained were tabulated in Table A.8 (Appendix H) and the plot of concentration of cell growth, phosphate solubilized and pH against yeast concentration was plotted in Figure 4.11.

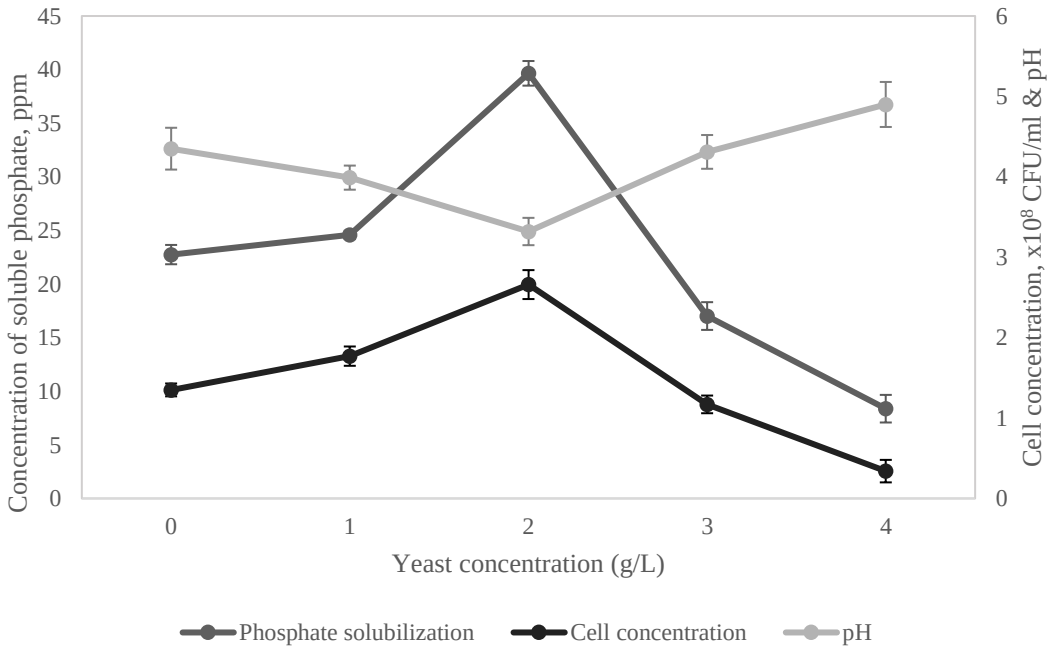

Figure 4.11 Effect of yeast concentration on phosphate solubilization for *S. haemolyticus* HCLB02, cell growth and pH of culture medium. Each point represents a mean value (n=3) and error bars (±SD) are shown when larger than symbol

Referring to Figure 4.11, cell growth of *S. haemolyticus* HCLB02 increased with yeast concentration until an optimal point. The increase in cell growth was accompanied by reduction in pH of culture medium, indicating the release of organic acids which led to

the increase in phosphate solubilization activity. At 2 g L^{-1}, the phosphate solubilization was highest with value of 39.65 ppm, an increase of 74.5% as compared with 0 g L^{-1}. Cell growth and phosphate solubilization were greatly reduced when the yeast concentration increased above 2 g L^{-1}. In addition, the cell growth and phosphate solubilization activity achieved with addition of 1 g L^{-1} yeast extract was higher than that of 3 g L^{-1}. An addition of yeast extract at a high concentration (3 g L^{-1}) does not impact as positively on cell growth and phosphate solubilization as added at a lower concentration (2 g L^{-1}). Therefore, it can be concluded that neither too little nor too much yeast extract at one time is optimal which was found to be 2 g L^{-1}.

Yeast extract contains abundant of vitamins, minerals, and amino acids, which are necessary for cell growth. During cell growth phase, the nutrients are consumed mainly for cell growth. *S. haemolyticus* HCLB02 grow by aerobic respiration or fermentation that produces lactic acid as byproduct. At high yeast concentration, the cell growth was minimal and no significant change to the pH of the culture medium as *S. haemolyticus* HCLB02 compared to control, indicating the lack of organic acids production which is the main chelating agents for the solubilization of insoluble phosphate. Hetényi et al. (2008) reported that minimal amount of yeast extract concentration is sufficient to complete lactic acid fermentation. Applying a higher concentration of yeast extract did not show significant difference in the production of lactic acid. Li et al. (2011) revealed that high level of yeast might generates inhibitory levels of amino acids which hinders cell growth. This hypothesis is supported by Kajikawa et al. (2002) where some amino acids show inhibitory effects on cell growth rate at higher concentrations but show a stimulatory effect on bacterial growth at low levels. Thus, it is essential to identify the optimal yeast concentration for the growth of *S. haemolyticus* HCLB02 and here 2 g L^{-1} is sufficient for maximum cell growth and phosphate solubilization activity.

4.5.3 Effect of magnesium chloride hexahydrate concentration on phosphate solubilization

As elucidated by Nautiyal (1999), concentration of $MgCl_2$ played an significant role in phosphate solubilization ability. According to Nautiyal (1999), $MgCl_2$ shows great synergistic effect with $MgSO_4$ on phosphate solubilization activity and their results

showed that phosphate solubilization increased with increasing $MgCl_2.6H_2O$ concentration up to 10 g L^{-1}. Based on the studies by Park et al. (2010), the optimal concentration of $MgCl_2.6H_2O$ was 4 g L^{-1}. The cell growth and P solubilization decreased with further increased in concentration. Thus, the effect of $MgCl_2.6H_2O$ concentration on cell growth and phosphate solubilization was studied in the range from 0 to 10 g L^{-1}. The data were presented in Table A.9 (Appendix H) and the plot of concentration of cell growth, phosphate solubilized and pH against $MgCl_2.6H_2O$ concentration was plotted in Figure 4.12.

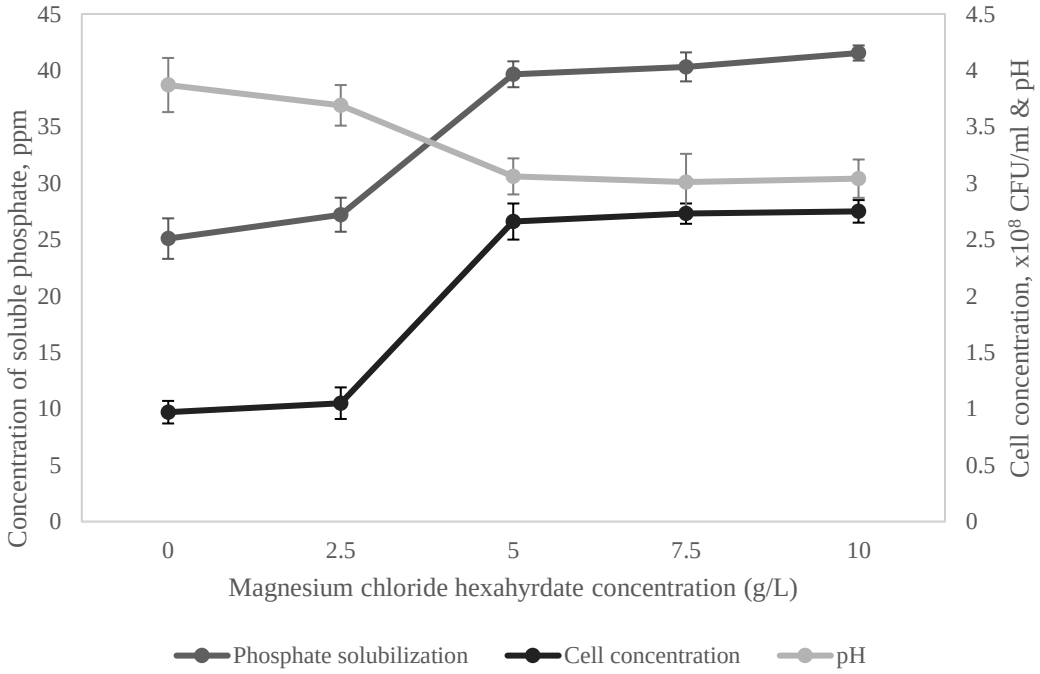

Figure 4.12 Effect of magnesium chloride hexahydrate concentration on phosphate solubilization for *S. haemolyticus* HCLB02, cell growth and pH of culture medium. Each point represents a mean value (n=3) and error bars (±SD) are shown when larger than symbol

By referring to Figure 4.12, it is apparent that increasing $MgCl_2.6H_2O$ concentration enhanced cell growth which led to higher solubilizing potential of *S. haemolyticus* HCLB02. Highest phosphate solubilization was obtained at 10 g L^{-1} with 41.54 ppm, an increase of 65.8% when compared with 0 g L^{-1}. However, further increased in $MgCl_2.6H_2O$ concentration above 5 g L^{-1} did not increased the efficacy of *S. haemolyticus* HCLB02 in solubilizing insoluble phosphate. Comparable results were obtained by

Nautiyal (1999) where further increase of $MgCl_2.6H_2O$ concentration from 5 to 10 g L^{-1} only increased the solubilization by 4 %. It is evident that phosphate solubilization activity is correlated with cell growth and pH of culture medium. At higher bacteria growth, the production of organic acids is higher and thus, the solubilization of insoluble phosphate is greater. This behavior can be well explained with the hypothesis elucidated by Christensen et al. (2017) whereby without magnesium supplementation, glucose is not fully consumed for cell growth of *Escherichia coli* prior to stationary phase. However, when magnesium is added to culture medium, the glucose is completely consumed during exponential growth which lead to higher cell numbers. In addition, $MgCl_2.6H_2O$ supplies the magnesium ions required for enzymatic replication of DNA. It can be concluded that increasing $MgCl_2.6H_2O$ concentration increases cell growth and thus, more lactic acids are produced and aids in the phosphate solubilization process and 5 g L^{-1} was found to be the optimum concentration.

4.6 Microencapsulation of phosphate solubilizing microorganisms

4.6.1 Optimization of process variable

In the present study, BBD under RSM developed by statistical software package Design-Expert (Version 10.0.3, State-Ease Inc., Minneapolis, USA) was employed to investigate the effects of the three independent variables namely alginate concentration, alginate flowrate and calcium chloride concentration on the response function and to identify the optimal conditions for highest cell viability. Therefore, for a three factor design, a total of 17 runs were carried out and their observations were fitted to the second order polynomial model as expressed in Equation 5.1.

$$Y = b_0 + b_1A + b_2B + b_3C + b_{11}A^2 + b_{22}B^2 + b_{33}C^2 + b_{12}AB + b_{13}AC + b_{23}BC \qquad (5.1)$$

Where Y is the dependent variable, A, B and C are the independent variables, b_0 is the regression coefficient at center point, b_1, b_2 and b_3 are the linear coefficient, b_{11}, b_{22} and b_{33} are the quadratic coefficient and b_{12}, b_{13} and b_{23} are the interaction coefficients between the three factors.

The level and code of variables considered in this study were shown in Table 3.3. Alginate flowrate plays an important role in microbeads size and cell viability. For impinging

aerosol method that implements the use of air atomizing nozzles, alginate flowrate used is 12 ml/min (Bhandari, 2009). This flowrate could not be used for single hole spray nozzle as the pressure is not sufficient to extrude the alginate solution through the nozzles. Thus, preliminary tests were carried out and it was found that when alginate flowrate was lower than 40 ml/min, pressure was inadequate to extrude alginate solution through nozzles to form droplets. Besides, the maximum throughput of spray nozzles in this study was found to be 63 ml/min. Thus, the effect of alginate flowrate in the interval of 40 to 60 ml/min on the cell viability were studied. In probiotic encapsulation, alginate concentration in the range of 0.75 to 2 % (w/v) is the most dominant (Chandramouli et al., 2004). As elucidated by Lotfipour et al. (2012), the use of high-concentration alginate greater than 2 % (w/v) as carrier is hard because their high viscosity obstructs their extrusion through nozzle. Furthermore, the use of low-concentration alginate lower than 1 % (w/v) is problematic. Due to their low viscosity and cross-linking site formation, it prevents the formation of uniform microbeads. Moreover, results obtained by Nami et al. (2017) indicated that the high percent of alginate is more capable to retain the survivability of cells than the low percent. Chandramouli et al. (2004) found that the viability of encapsulated bacteria increased when alginate gel concentration increased from 0.75 % to 1.8 % (w/v). There was no significant increase in viable cell numbers of capsules when the alginate gel concentration was further increased to 2 % (w/v). Thus, the effect of alginate concentration on cell viability in the range of 1 % to 2 % (w/v) were selected. The critical concentration which is the minimum concentration for gelation was estimated as 0.37 % (w/v) (Swioklo et al., 2017). In the experiments discussed here the alginate concentration was in the range from 1 % to 2 % (w/v), which is well above the critical concentration.

The ability of calcium ions in binding divalent cations and formation of microbeads under mild operating conditions makes it a widely favored method to crosslink alginates for numerous applications. The formation of calcium-alginate microbeads is achieved by the ionic interaction between Ca^{2+} ions and the carboxyl groups of the guluronic acid residues of two alginate chains (Lee & Mooney, 2012). It was reported by Hariyadi et al. (2010) that microbeads formed aggregate when prepared using 0.05 M calcium chloride solution. This is due to the low concentration of calcium ions being inadequate to fully cross link the alginate microbeads. Hence, more binding sites are accessible and induce further cross

linking and particle aggregation. Consequently, higher concentrations of calcium chloride solution of 0.1 M to 0.5 M are used as the cross linking agent, resulting in stable spherical microbeads. Thus, in this study concentration of calcium chloride solution of 0.1 to 0.5 M were used for the optimization study. Triplicate for each run was repeated and the average mean values of each run was taken as the response or dependent variables. The experiments were conducted under various conditions as shown in Table 3.4. The experiment and predicted particle size obtained from the regression equation for the 17 combinations were tabulated in Table 4.2.

Table 4.2 Design matrix in the BBD, observed response and predicted values. Each point represents a mean value and the error bars showed the standard deviation (n=3)

Run	Alginate flowrate (ml/min)	Alginate conc (%)	$CaCl_2$ conc (M)	Viability (%)		Error, %
				Experiment	Predicted	
1	40	1.0	0.3	26.03±3.17	28.53	8.76±11.07
2	60	1.0	0.3	19.07±1.85	25.08	23.97±7.38
3	40	2.0	0.3	17.33±1.59	17.39	0.40±9.14
4	60	2.0	0.3	9.19±0.89	11.81	22.22±7.54
5	40	1.5	0.1	57.14±7.92	59.43	3.85±13.33
6	60	1.5	0.1	42.54±7.33	45.85	7.21±15.99
7	40	1.5	0.5	25.59±4.62	29.78	14.10±15.51
8	60	1.5	0.5	23.34±2.82	28.38	17.78±9.94
9	50	1.0	0.1	33.13±2.66	37.09	10.66±7.17
10	50	2.0	0.1	14.89±1.67	19.40	23.24±8.61
11	50	1.0	0.5	14.83±2.26	15.42	3.87±14.65
12	50	2.0	0.5	6.67±1.12	8.24	19.09±13.59
13	50	1.5	0.3	32.28±7.36	42.02	23.17±17.52
14	50	1.5	0.3	40.80±5.64	42.02	2.90±13.42
15	50	1.5	0.3	38.27±2.24	42.02	8.93±5.33
16	50	1.5	0.3	35.36±6.56	42.02	15.84±15.61
17	50	1.5	0.3	43.88±2.56	42.02	4.43±6.09

The high percentage error for some runs were probably due to standard plate count method in cell viability determination. Standard plate count method is subjected to dilution errors, technical errors such as pipetting, plating and incubation and inaccurate counting of colonies (Sutton, 2011). A second order polynomial model was fitted to the experimental results by Design Expert software to identify the optimal condition in producing microbeads with highest cell viability. The model was illustrated as Equation 5.2.

$$\sqrt{Y} = -6.328 - 0.027A + 23.073B - 9.54C - 0.020AB + 0.101AC + 1.573BC - 7.972B^2 - 4.147C^2 \quad (5.2)$$

Where Y is cell viability (%), A is alginate flowrate (ml/min), B is alginate concentration (w/v %) and C is $CaCl_2$ concentration (M).

The significance and quality of the model were checked through the analysis of variance (ANOVA) using Fisher's statistical analysis as shown in Table 4.3. The F_{model} of 27.75 and p-value of 0.0001 which is less than 0.05 implied that the model was significant. There was only a 0.01 % chance that F value this large could occur due to noise. The significance of each coefficient was identified by the p-value which was listed in Table 4.3. The value with "Prob>*F*" less than 0.05 indicated that the model terms were significant whereas value larger than 0.1 were insignificant (Keharom et al., 2016). In this case, linear terms (A, B, C) and quadratic term (B^2) were significant model terms ($p<0.05$) whereas two-way interaction terms (AB, AC, BC) and quadratic terms (A^2, C^2) were insignificant terms. From this it was inferred that, alginate concentration, alginate flowrate and $CaCl_2$ concentration had a significant effect on cell viability. The coefficient of determination, R^2 and adjusted R^2 indicated the efficiency of the model, a value greater than 0.75 indicated fitness of the model. The R^2 and adjusted R^2 were 0.9727 and 0.9377, respectively suggesting that 97.27 % and 93.77 % variation could be accounted by the model equation. The lack-of-fit measures the failure of the model to represent data in the experimental domain at points which are not included in the regression. The non-significant value of lack of fit ($p>0.05$) revealed that the quadratic model was statistically significant for the response (Khajeh, 2011), indicating the model equation was adequate to predict the cell viability within the range of experimental variables. Adequate precision measures the signal to noise ratio and value of greater than 4 was desirable. The adequate

precision of 18.8614 indicated sufficient signal. Moreover, low value of the coefficient of variation (CV=6.63) signified that experiments were highly accurate and reliable (San Chan & Don, 2013)

Table 4.3 ANOVA Analysis for microencapsulation of PSMs

Source	**Sum of Squares**	**df**	**Mean Square**	**F-value**	**p-value**	
Model	29.13	9	3.24	27.75	0.0001	significant
A-Alginate flowrate	1.23	1	1.23	10.51	0.0142	
B-Alginate concentration	3.70	1	3.70	31.73	0.0008	
C-$CaCl_2$ concentration	6.80	1	6.80	58.26	0.0001	
AB	0.0391	1	0.0391	0.3352	0.5808	
AC	0.1639	1	0.1639	1.41	0.2745	
BC	0.0989	1	0.0989	0.8482	0.3877	
A^2	0.0007	1	0.0007	0.0056	0.9425	
B^2	16.73	1	16.73	143.38	< 0.0001	
C^2	0.1159	1	0.1159	0.9934	0.3521	
Residual	0.8166	7	0.1167			
Lack of Fit	0.2726	3	0.0909	0.6680	0.6144	not significant
Pure Error	0.5440	4	0.1360			
Cor Total	29.95	16				

R^2=0.9727, adjusted R^2=0.9377, adequate precision=18.8614, CV=6.63

The effects of process variables and their interactions on the cell viability were described by the 3D response surface plots and 2D contour plots as shown in Figure 4.13. These plots were obtained from plotting the response (cell viability) on the Z-axis against any two process variables while keeping the other variable constant at its "0" level. An elliptical or saddle nature of the contour plots indicates that the interaction between the

corresponding variables is significant whereas a circular contour of response surfaces indicates that the interaction between the corresponding variables is insignificant (Lotfi et al., 2015).

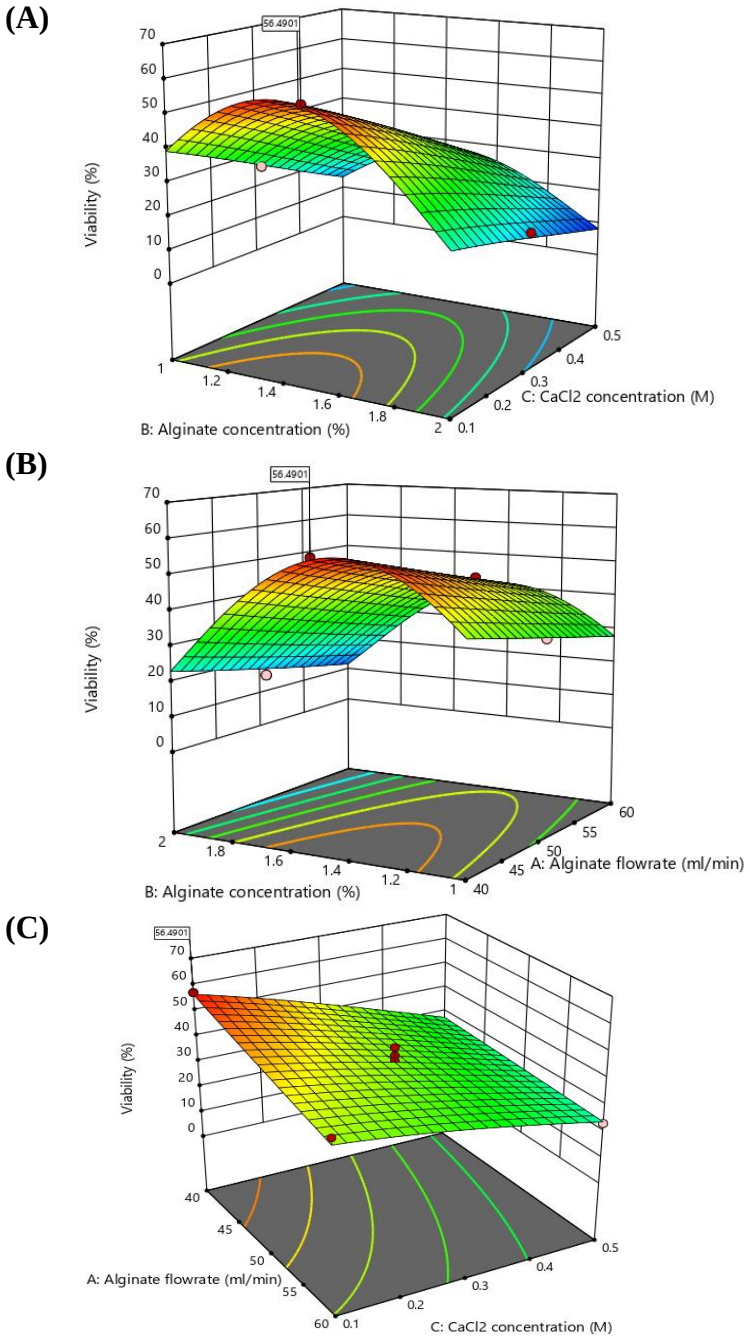

Figure 4.13 The 3D response surface of the combined effects of alginate concentration, alginate flowrate and $CaCl_2$ concentration: (A) Alginate concentration and $CaCl_2$ concentration, (B) Alginate concentration and alginate flowrate and (C) Alginate flowrate and $CaCl_2$ concentration

Figure 4.13(A) represents the response surface for alginate concentration and $CaCl_2$ concentration on the cell viability. The results revealed that cell viability gradually increased when alginate concentration increased from 1 to 1.5 % (w/v) and when $CaCl_2$ concentration decreased from 0.5 M to 0.1 M. A further increase in alginate concentration caused the cell viability to drop significantly. Figure 4.13(B) shows the response surface for alginate concentration and alginate flowrate. From the graph, it is evident that cell viability increased slightly when alginate flowrate reduced from 60 ml/min to 40 ml/min and highest cell viability was obtained at 1.5 % (w/v) alginate concentration. Figure 4.13(C) displays the response surface for alginate flowrate and $CaCl_2$ concentration. The results obtained showed that highest cell viability was obtained at lower alginate flowrate and $CaCl_2$ concentration. From these response surface graphs, it can be seen that a change in alginate concentration, alginate flowrate and $CaCl_2$ concentration affect the cell viability. Hence, the highest cell viability at 56.37 % was predicted by solving the model at optimum condition of 40 ml/min alginate flowrate, 1.5 % (w/v) alginate concentration, and 0.1 M $CaCl_2$ concentration.

From Figure 4.13(A), when the alginate concentration increased from 1 % to 1.5 % (w/v), cell viability was enhanced by 17 % reaching maximum point, however further increased in alginate concentration caused the cell viability to drop by approximately 34 %. Similar results were reported by Cao et al. (2012) and Yu et al. (2013) where the cells survival in 2 % and 4 % alginate solution were studied. It was seen that cell viability was greater in 2 % alginate microbeads as compared to 4 %. Besides, Bajaj et al. (2010) studied the effect of alginate concentration on the survival of *Lactobacillus fermentum* and their results also showed that cell viability increased with increasing alginate concentration and decreased when alginate concentration increased over 3 %. Lopes et al. (2017) also investigated the effect of alginate concentration on the cell viability in the range of 1 % to 5 % and their results showed that higher viable cell counts were obtained at lower alginate concentrations. This can be explained by the hypothesis enlighten by Wright et al. (2012) whereby increasing the concentration of sodium alginate, decreases the pore size which might affect the mass transfer properties of the gel and results in lower cell survival. Cell viability improves as gel internal pore size increases. This is because high porosity promotes the inflow of oxygen and nutrients and the outflow of metabolites and waste

products from microbeads. Ning et al. (2016) suggested that in the microencapsulation process when the cell suspensions are extruded through the nozzle tip, cells are subjected to shear force which causes cell damage. The intensity of shear force applied to the cells is determined by the dispensing pressure and the properties of the suspension. Lange et al. (2001) reviewed that some morphological variations and reduced resistance to freezing have been observed for some fungi and bacteria. They confirmed that the tensile strength of walls or membranes confers rigidity of the cells and thus tolerance to shear stress. Their results showed that *E.coli*, a Gram negative bacteria with thin peptidoglycan layer has lower resistant to shear stress than *S. cerevisiae* which has a relatively thick cell wall made of glucan and mannan. Cell damage causes by shear force occurs when the forces applied to the cells exceeds their tolerance limits to shear stress (Ning et al., 2016). The shear stress increases with alginate concentration which suggests the alginate solution becomes more viscous as the alginate concentration increases. Ning et al. (2016) results showed that the cell worsened as the shear stress increased. Cells were damaged by 4.89 ± 0.89 %, 5.21 ± 0.74 %, 10.73 ± 0.80 % and 21.36 ± 2.39 % at 1.0 %, 1.5 %, 2.0 % and 2.5 % alginate solution, respectively. Similarly, Yu et al. (2013) noticed visible drop in cell viability when alginate concentration increased from 2 % to 6 %. This may suggest that an increase in alginate concentration follows by an increase in viscosity, generates higher shear stress at the interface between the nozzle and the suspension, resulting in higher cell death. Besides, increasing flowrate of alginate also increases the dispensing pressure. Referring to Figure 4.13(B), when the alginate flowrate increased from 40 ml/min to 60 ml/min, the cell viability reduced by at least 15 %. This is due to the mechanical stresses applied to the cells during extrusion through nozzles. Li et al. (2010) and Yan et al. (2010) investigated the influence of process-induced mechanical force on cell damage or survival. Their results showed that increasing applied dispensing pressure increased mechanical stresses which reduced cell viability. Similarly, Yu et al. (2013) also reported that average cell viability significantly decreases with increasing alginate dispensing pressure.

From Figure 4.13(C), it can be seen that when $CaCl_2$ concentration increased from 0.1 M to 0.5 M, the cell viability was reduced by approximately 18 %. Similar trend was reported by Chandramouli et al. (2004) where increasing the $CaCl_2$ concentration beyond 0.1 M during encapsulation did not improve the capsules efficacy in protecting the viable cell.

The Ca^{2+} ions act as a connective bridge to bound with two alginate chains during the formation of calcium alginate microbeads. Thus, an increase in the Ca^{2+} concentration results in a stronger, thicker and more compact alginate shells (Liu et al., 2019b). However, Liu et al. (2019b) found that an increase in $CaCl_2$ concentration did not significantly affect the average diameter and strength of microbeads. Similarly, Swioklo et al. (2017) studied the effect of calcium concentrations on the gel structure and mechanical strength. Their results indicated that pore size and strength of bead is practically independent of calcium concentrations. Notably, at high Ca^{2+} concentrations, calcium crystals were observed inside pores implying calcium salt precipitation during drying. Cao et al. (2012) studied the effect of calcium ions on cell survival and proliferation as high content of calcium ions involved in crosslinking process. As observed, cells viability was higher when treated with 0.1 M $CaCl_2$ concentration when compared with 0.5 M and 1 M. The damage and cell loss are mainly instigated by osmosis effect. Depending on the seriousness of cell damage, cells can either recover from damage via self-repair mechanism or remain to be dysfunctional till cell death. Thus, 0.1 M $CaCl_2$ concentration was selected to minimize cell death. This concentration were deemed appropriate following structural and mechanical characterization and have been previously established to be suitable in alginate-based systems (Swioklo et al., 2017). In order to validate the optimization results and to verify the model developed, triplicates were conducted with the optimized conditions and the result were tabulated in Table 4.4. It can be seen that the cell viability was 54.71 % with only 2.95 % percentage error between experimental and predicted results.

Table 4.4 Validation of experimental model. Each point represents a mean value and the error bars showed the standard deviation (n=3)

Alginate flowrate (ml/min)	**Alginate conc (%)**	**$CaCl_2$ conc (M)**	**Viability (%)**		**Error %**
			Experiment	**Predicted**	
40	1.5	0.1	54.71±4.58	56.37	2.95±2.24

4.6.2 Size, morphology and encapsulated cell numbers of alginate microbeads

The size of the alginate beads is mainly controlled by regulating the formation of the droplet (Andersen et al., 2015). In this regard, the impinging aerosol method gains the attention of researchers as this method involves exposing droplets of alginate solution to $CaCl_2$ mist which results in efficient contact of the droplet surface with salt (Ca^{2+}) solution, producing alginate microbeads. This method produces small microbeads and retain its shape as it prevents deformation of the droplet due to impact with a liquid surface in a receiver bath containing cross linking solution. Blank and PSMs loaded alginate microbeads were produced with 1.5 % alginate concentration, 40 ml/min alginate flowrate and 0.1 M $CaCl_2$. Their size and morphology were visualized by light microscopy as shown in Figure 4.14 and Figure 4.15.

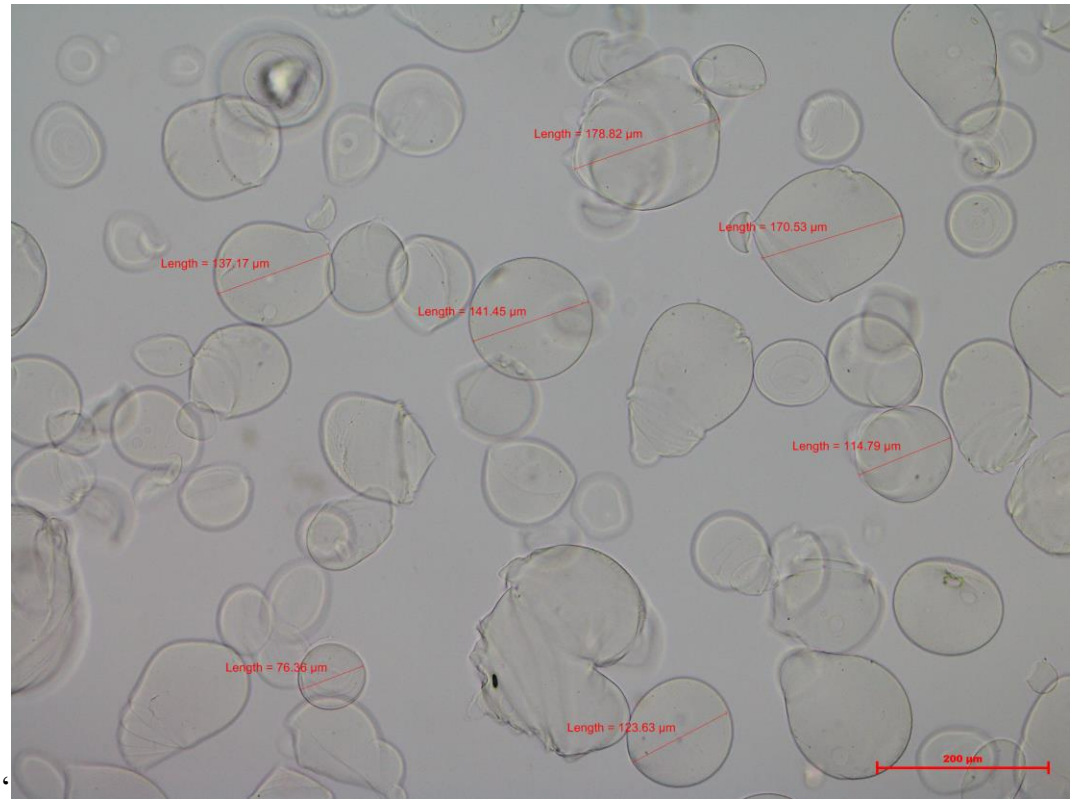

Figure 4.14 Optical micrographs of blank alginate microbeads produced at 1.5 % alginate concentration, 40 ml/min and 0.1 M $CaCl_2$ viewed under 200 µm scale bar

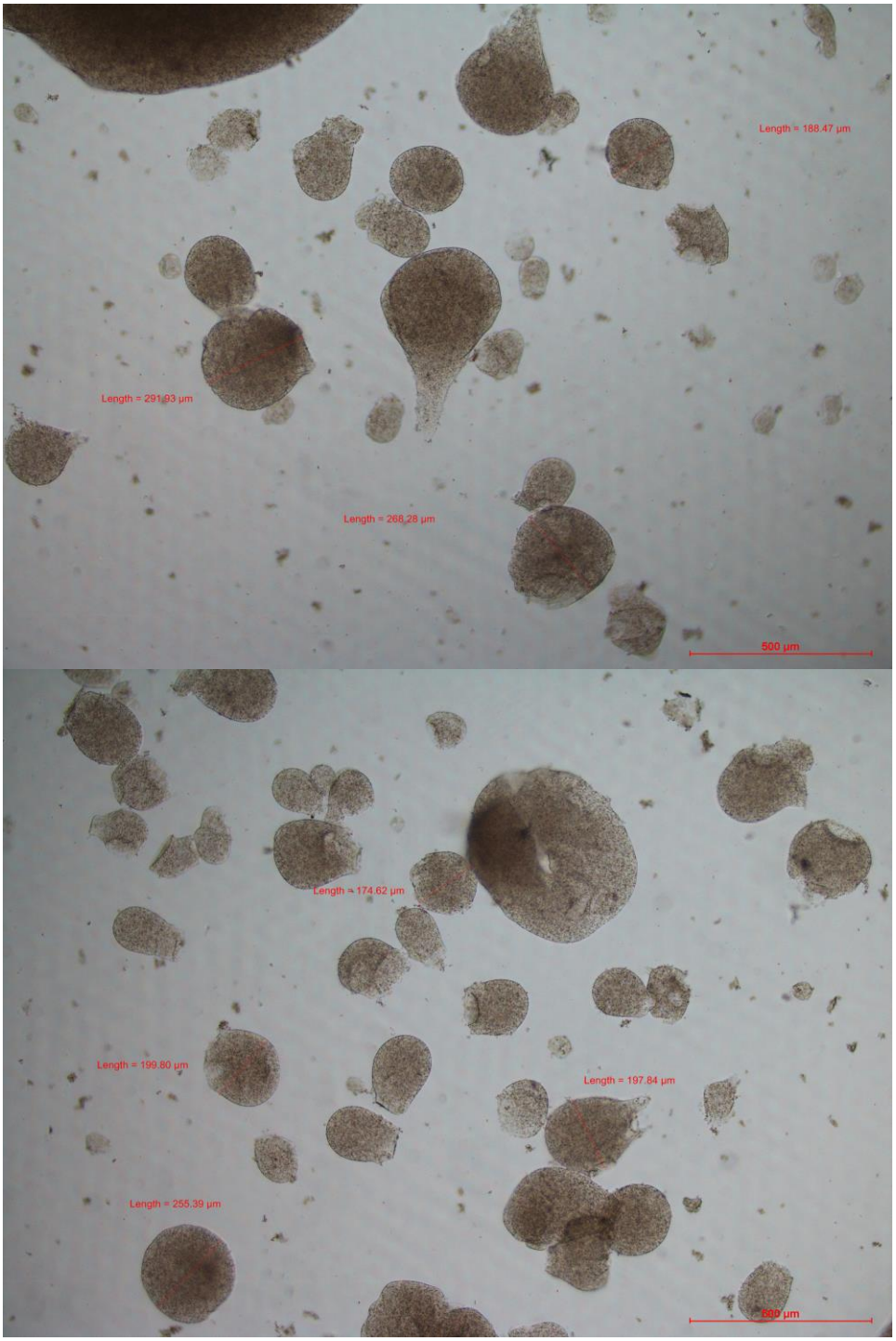

Figure 4.15 Optical micrographs of alginate microbeads containing PSMs produced at 1.5 % alginate concentration, 40 ml/min and 0.1 M $CaCl_2$ viewed at 500 µm

Both the blank and the alginate microbeads containing PSMs were spherical in shape. Blank alginate microbeads without PSMs were generally in the size range of 70 to 250 µm whereas alginate microbeads containing the PSMs in the range of 100 to 350 µm with

a mean size of 236.87 ± 12.25 μm were readily produced. Bead size is one of the most important parameters of alginate microbeads as microbial inoculant. The bead itself must be large enough to immobilize a reasonable number of the cells (Andersen et al., 2015) while small enough to provide high oxygen concentrations at the center of the microbeads (Ogbonna et al., 1991). This is to ensure cells encapsulated in the beads remain viable during storage and to ensure they are adequately released from the beads following introduction to the soil. In a 2-mm bead, active aerobic cells may be found to a depth of only 50–200 μm into the bead, so about 80 % of the volume of contain inactive or even dead cells (Chen and Humphrey 1988). Thus, aerobic PSMs will be stressed in a macrobead formulation.

In the encapsulation process, the transfer of oxygen from the medium to immobilized cells involves three main steps which include the diffusion through the stagnant liquid film surrounding the gel bead, diffusion through the gel matrix and finally, diffusion through the cell wall. Diffusional resistance to oxygen flow exerted by the cell wall may be important but this is a biological parameter which is difficult to control. Thus, the most practical method of increasing liquid-cell oxygen transfer in encapsulation system is by improving diffusion through the matrix. An effective method of increasing oxygenation of immobilized cells is to reduce the mean distance of diffusion in the matrix and this can be achieved by using beads of small diameters (Ogbonna et al., 1991). Limitation in diffusions within large beads reduces cellular metabolism and causes the lack of supply of essential substances to the center of beads which may results in cell death. Liffourrena et al. (2018) reported that survival of bacteria can be increased by reducing bead size. Moreover, smaller beads are less fragile than larger beads and have higher surface to volume ratio which permits good preservation of the entrapped bacteria (Robitaille et al., 1999). Similarly, Gryshkov et al. (2014) also agreed with the above statements where smaller alginate beads are desirable in cell culture. This is because smaller alginate beads, increases the surface-to-volume ratio which improves survival of cells due to better nutritional, oxygen supply and heat transfer. Liffourrena et al. (2018) apprehended that the root colonization of *A. thaliana* by *P. putida* A cells obtained with Ca-alginate perlite-microbeads was superior when compared with Ca-alginate-beads. This is due to the smaller size of the Ca-alginate perlite-microbeads. Thus, it is essential to produce small

size alginate microbeads containing PSMs as microbial inoculant to ensure high cell viability and allow a better root colonization.

Figure 4.16 shows the optical micrographs of alginate microbeads containing PSMs produced at 1.5 % alginate concentration, 40 ml/min and 0.1 M $CaCl_2$ at 100 µm scale bar. From the figures, an even distribution of PSMs throughout gelling alginate beads can be observed. Swioklo et al. (2017) reported that if alginate solutions are too concentrated, the increase in viscosity may affect the even distribution of cells throughout the microbeads. Besides, it also increases the shear stress imposed on cells during distribution and extrusion, causing cell death. Thus, high cell viability was expected from the wet microbeads prior to freeze-drying.

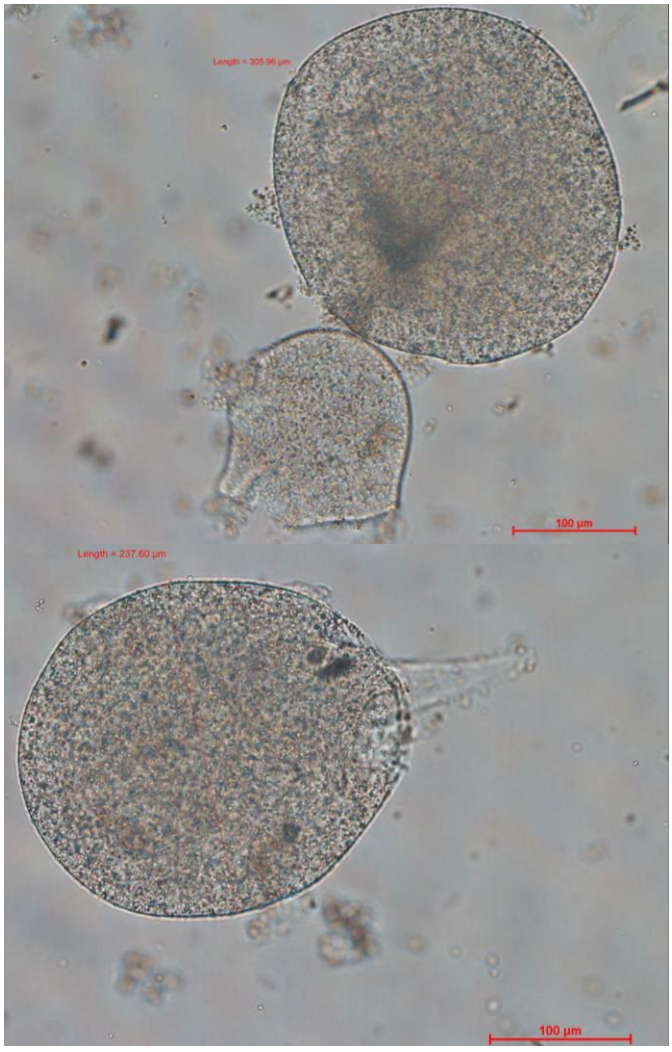

Figure 4.16 Optical micrographs of alginate microbeads containing PSMs produced at 1.5 % alginate concentration, 40 ml/min and 0.1 M $CaCl_2$ at 100 µm scale bar

There are studies that clearly show the relationship between number of bacteria applied on plants and crop yields (Bernabeu et al., 2018). Generally, inoculant quality standards require the minimum amount of 10^7 to 10^9 colony forming units per gram of beads (CFU/g) or per milliliter of formulation (CFU/mL) (Malusá & Vassilev, 2014) to ensure positive response on plant inoculation. In China, depending on the kind of bacteria utilised for the production of the biofertilizer, the amount of living cells differs. For PSMs, the amount of viable cells ranges between > 0.5-1.5×10^9 CFU/mL or > 0.1-0.3×10^9 CFU/g, for liquid and solid products, respectively (Suh et al., 2006). As for India, the minimum count of viable cells is 5 × 10^7 CFU/g of solid carrier, or 1×10^8 CFU/ml of liquid carrier (Malusá et al., 2014). In this study, the cell suspensions used for encapsulation contained ~1.0×10^9 CFU/mL and the number of cells encapsulated in alginate microbeads using the impinging aerosol method was in the range of 0.97 to 0.98×10^9 CFU/g of wet microbeads. Thus, a very high cell loading was observed with encapsulation efficiency of at least 97 %. Isailović et al. (2013) reported the increase of alginate viscosity induced higher encapsulation efficiency as it has more concentrated network, create less pores and the surrounding membrane is thicker. Porous structure of lower alginate concentration permits facile diffuse of encapsulated compounds to an external solution, causing lower encapsulation efficiency. Ćujić et al. (2016) also achieved a higher actual load of encapsulated polyphenols for formulations with medium viscosity alginate in comparison with low viscosity alginate. Wet PSMs loaded alginate microbeads were subjected to lyophilization in order to obtain dry microbeads. Dried alginate microbeads were found to contain approximately 0.54 × 10^9 CFU/g of dried microbeads, indicating cell viability of 54 %. Bashan et al. (2002) produced dry inoculant containing *A. brasilense* loaded with >10^9 CFU/g beads. Inoculation of *A. brasilense* encapsulated in the alginate microbeads on wheat and tomato plants significantly increased plant height and the dry weight of both shoots and roots. Schoebitz et al. (2013a) encapsulated bacteria concentration of 2.72 x 10^9 CFU/g and 2.17 x 10^9 CFU/g for *P. fluorescens* and *Serratia sp.* respectively. Plant growth promotion was demonstrated by the improved of P uptake and growth of shoot length. Thus, it can be hypothesized that the produced dried microbeads containing PSMs with >10^9 CFU/g beads is sufficient to obtain a plant response. Herein, the third objective of this study was achieved by obtaining alginate

microbeads containing PSMs with mean size of 250 μm and cell concentration of 0.54 × 10^9 CFU/g of dried microbeads.

4.7 Kinetic release of bacteria from microbeads

As reported by Zohar Perez et al. (2002), the immobilization of PSMs into polymer matrix is beneficial over direct soil inoculation. The key aim of encapsulation of PSMs is to protect them from harsh soil environment, lessen microbial competition and release them gradually to facilitate colonization of plant roots. Hence, it is essential to study the kinetic release of PSMs from alginate microbeads in order to understand its capability in root colonization (Young et al., 2006). The cell release from dried alginate microbeads was performed at pH 4.0 to mimic pH of peat for 4 h and the cumulative release profile was shown in Figure 4.17.

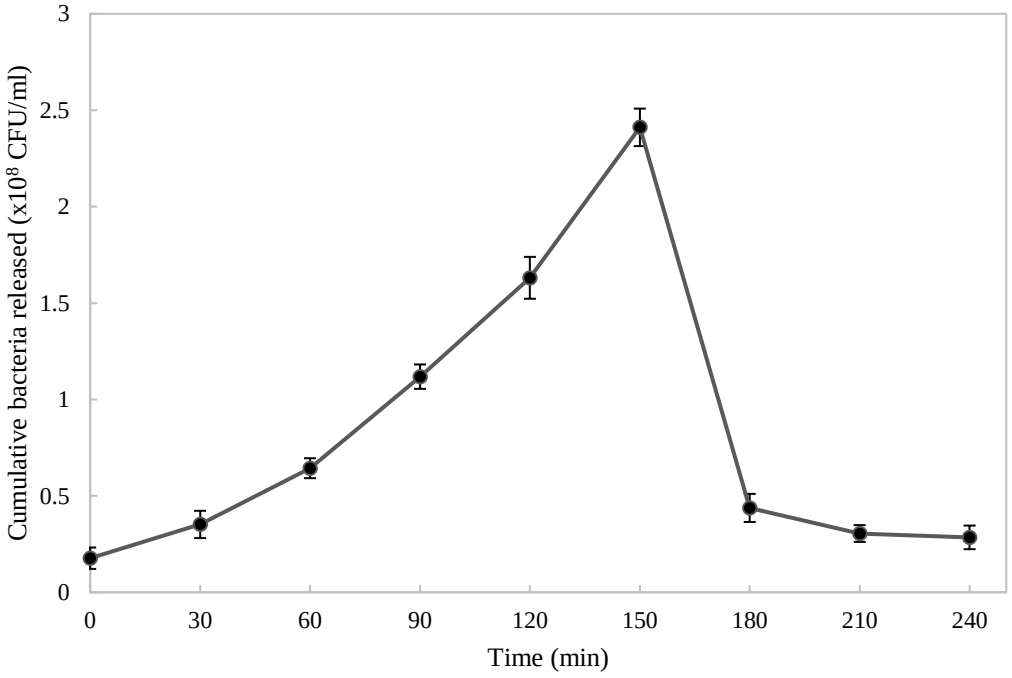

Figure 4.17 Cumulative *S. haemolyticus HCLB02 released* from microbeads at pH 4.0. Each point represents a mean value (n=3) and error bars (±SD) are shown when larger than symbol

Referring to Figure 4.17, number of bacteria released were maximum at 150 min signifying that microbeads were completely broken within the time frame and entire load

of PSMs were released from microbeads. Note that the initial concentration of PSMs in dried microbeads was 0.54×10^9 CFU/g and the maximum number of bacteria released at 150 min was 0.24×10^9 CFU/g which was about 44.44% of initial concentration. The lower number of bacteria obtained may be due to the death of starving bacteria in saline solution or the low pH of medium could have killed the bacteria released (Paramithiotis et al., 2006). The PSMs released from microbeads was evaluated kinetically using various notable kinetic models such as zero order, first order, Higuchi, Ritger-Peppas, and Weibull. The coefficient of determination (R^2) and overall error (OE) percent values of these models were evaluated to study the fitness of the model to represent the release kinetics from nanoparticles as tabulated in Table 4.5 and the curve fittings were attached in Appendix I.

Table 4.5 Kinetic models used in analyzing the release and their corresponding constants, R^2 and overall means percent error (OE). Each point represents a mean value and the error bars showed the standard deviation (n=3)

	Zero order	**First order**	**Higuchi**	**Ritger Peppas**	**Weibull**
K_i	0.0026±0.0001	0.003±0.000	0.029±0.0000	0.001±0.001	-
C_i	-	0.030±0.039	-0.038±0.009	-	-
n	-	-	-	1.186±0.083	-
a	-	-	-	-	1568.7±539.6
b	-	-	-	-	1.314±0.084
R^2	0.949±0.001	0.915±0.001	0.761±0.001	0.983±0.010	0.974±0.012
OE (%)	34.38±4.70	47.92±6.04	72.61±10.07	7.99±0.41	10.00±1.20

Subscription i represents, 0 for zero order, 1 for first order, H for Higuchi and R for Ritger Peppas

It can be seen that Ritger Peppas model has the highest R^2 value of 0.983 followed by Weibull and zero order models with R^2 value of 0.974 and 0.949, respectively. Likewise, Barzegar-Jalali et al. (2008) reported that OE lesser than 10 % is the criteria for the general model for kinetic study. In this case, only 2 models had OE lesser than 10 % and Ritger Peppas had the lowest OE of 7.99 %, followed by Weibull with 10 %. Based on R^2 and

OE, Ritger Peppas was considered as the kinetic model that best represented the release data of PSMs from alginate microbeads in this study. The cell release mechanism in swelling-controlled bacterial release can be elucidated well using the Ritger–Peppas model, in which the release exponent "n" differs in accordance with the release mechanism. Data acquired from the kinetic release studies in 150 min for the initial portion ($M_t/M_\infty \leq 60$) were fitted into Ritger Peppas's model. The value of release exponent 'n' obtained was 1.186 (n>0.89), indicating the mechanism of cell release from the alginate microbeads followed the main Case II release mechanism with skeleton corrosion mechanism (Wu et al., 2014). The release of PSMs occurs as it diffuses out when the microbeads swell by absorbing water. With the expansion of the microbeads, the calcium alginate matrix was also partially dissolved, releasing the bacteria as shown in Figure 4.18. As time increases, the released amount becomes more significant. Singh et al. (2009) and Wu et al. (2014) studied the release kinetics of cells from alginate beads and reported a similar diffusion mechanism.

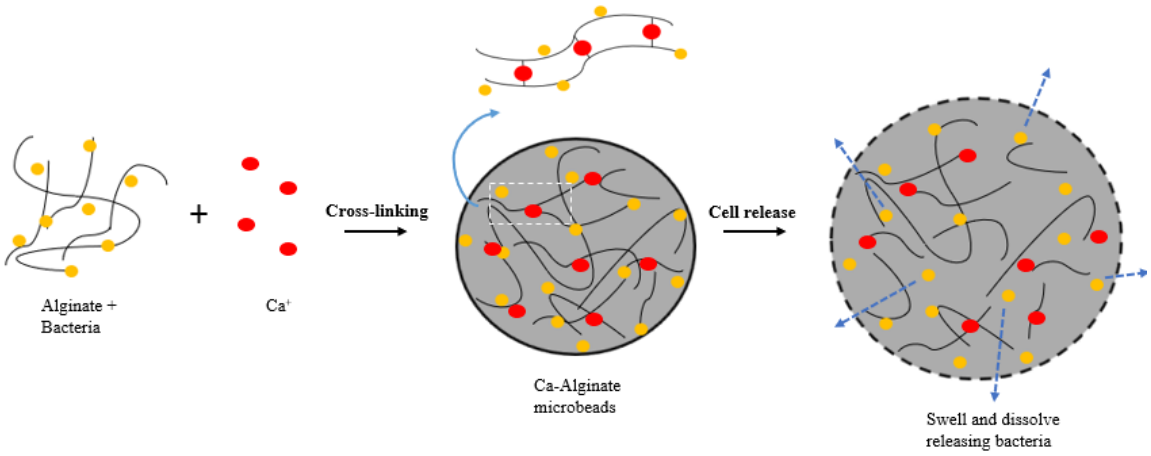

Figure 4.18 Schematic representation of cell release from alginate microbeads

Figure 4.19 was plotted based on the constants parameters evaluated from the fitting of 5 kinetic models as tabulated in Table 4.5.

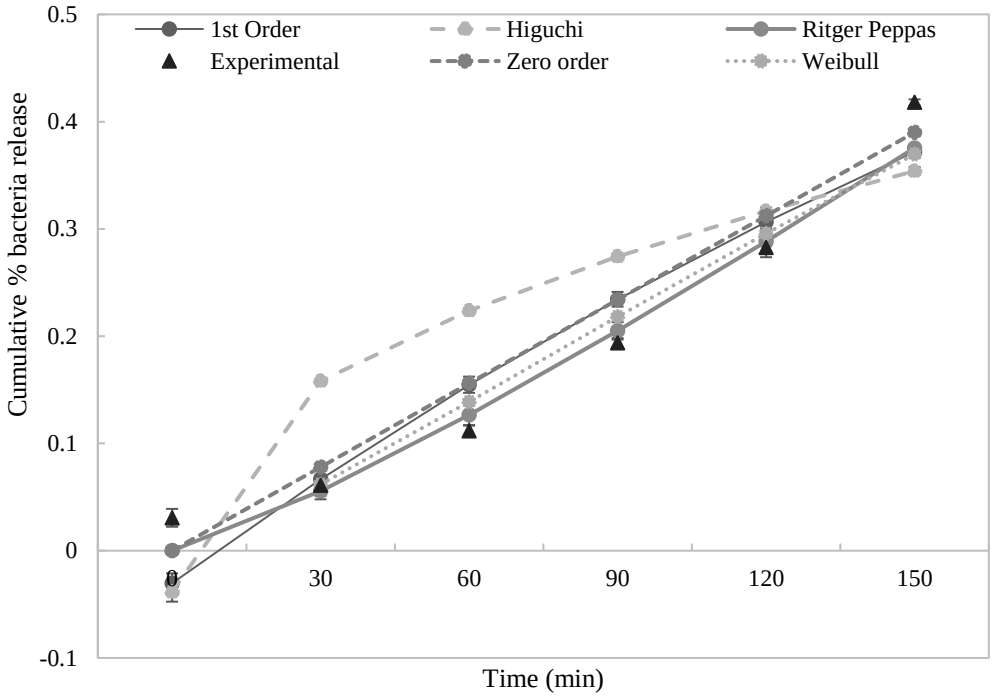

Figure 4.19 Cumulative % cell release vs time for experimental, zero order, first order, Higuchi, Ritger peppas and Weibull models

By referring to Figure 4.19, it can be seen that Ritger Peppas model had similar trend as experimental cell release data. From the results, it is evident that bacteria cells were not released gradually from the dried microbeads and further improvement is required to enhance the control release properties of the microbeads. Some recommendations were suggested in Chapter 7. Similar results was obtained by Li et al. (2016), where they found alginate microbeads without perlite as filling material could not be used as inoculants due to their low stability. Within 12 h, the microbeads were completed disintegrated releasing all entrapped cells. The release of cells entrapped in a polymer, occur only after water penetrates the network to swell the polymer, followed by diffusion along the aqueous pathways to the surface of the beads. Alginate beads are structured as a loose network filled with a large amount of water (Schoebitz et al., 2013a), thus without the addition of filler cells release easily through beads once it swell up. The pores between cross-linked alginate chains can be filled with the addition of filler such as starch, perlite, kaolin, skim milk, talc and humic acid (Schoebitz et al., 2013b). The addition of filler improves the

integrity and strength of beads structure and gives better mechanical resistance and allowing for a progressive release of cells into the soil as illustrated in Figure 4.20 (Liu et al., 2019a).

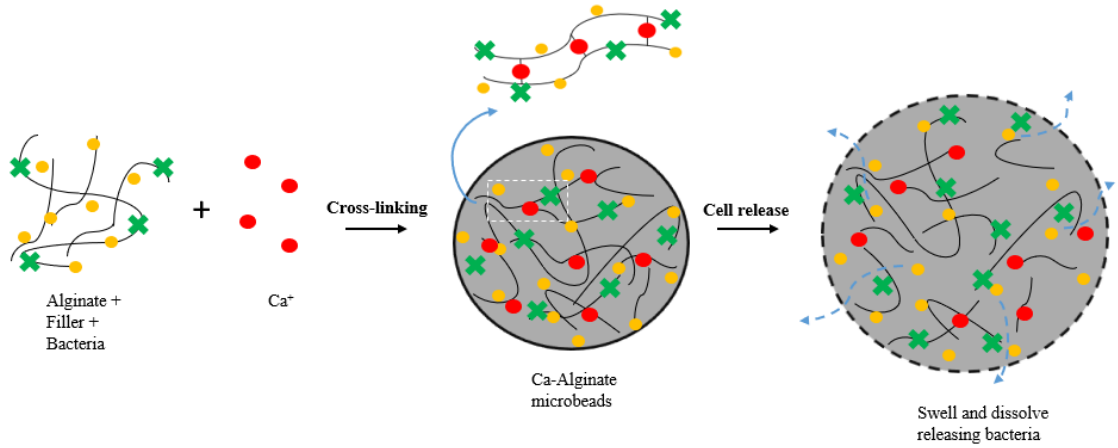

Figure 4.20 Schematic representation of cell release from alginate microbeads with filler

Singh et al. (2009) studied the release of thiram from the starch-alginate-beads and their results showed that the cumulative release of thiram from the beads occurred in very controlled and sustained manner. The rate of release of fungicide from the beads prepared with 3 % starch contents up to 204 h has been observed. Feng et al. (2019) also developed a starch–alginate-kaolin based formulations encapsulation of non-toxigenic *Aspergillus flavus* spores. As the release of spores from the beads was in a controlled and sustained manner, the feasibility of the formulation as a controlled release substance was demonstrated.

4.8 Concluding remarks

Staphylococcus haemolyticus was isolated from peat and possessed the ability to solubilize Al-P releasing soluble phosphate for plant uptake. Then, the optimal cultural condition for maximum phosphate solubilization was identified to be 10 g/L of glucose, 2 g/L of yeast and 5 g/L $MgCl_2.6H_2O$ as it stimulated the highest cell growth. Cell growth is correlated with the production of organic acids, a chelating agent in solubilizing insoluble phosphate. Then, *Staphylococcus haemolyticus* was microencapsulated using the impinging aerosol method. The alginate concentration, alginate flowrate and calcium chloride concentration that yielded the highest cell viability were identified as 1.5 % (w/v), 40 ml/min and 0.1 M $CaCl_2$. It was observed that high alginate concentration and flowrate

had a lower cell viability due to the shear stresses applied to the cells during extrusion process. Alginate microbeads with mean size of 250 μm and PSMs concentration of 0.54 × 10^9 CFU/g of dried microbeads was obtained. Nevertheless, PSMs were not released in a very controlled and sustained manner and thus, concluded that the produced alginate microbeads require further studies to improve the control release of PSMs from alginate microbeads before it can be used as a microbial inoculant.

CHAPTER 5

MODELING METHODOLOGY

In Chapter 4, the results obtained for isolation and microencapsulation of PSMs were discussed. This chapter describes the modeling methodology for the impinging aerosols. The models include the Eulerian-Lagrangian framework to solve the continuous and discrete phases, Huh and Reitz-Diwakar as the spray atomization models and Bai-Gosman model for the wall impingement.

5.1 Computational domain, assumptions, and limitation of the model

The computational domain of the model is depicted in Figure 5.1. The model was developed based on the lab-scaled impinging aerosol spray device as shown in Figure 3.1.

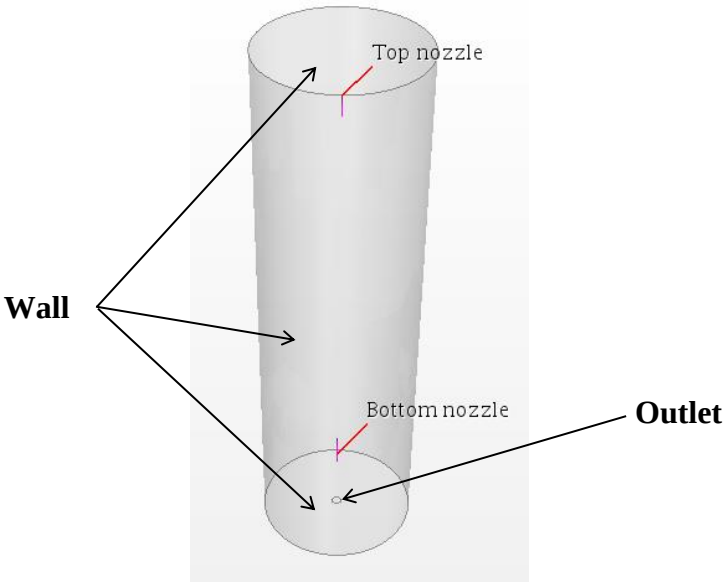

Figure 5.1 Computational domain of the CFD model and injectors

The model consists of a vertical cylinder with 17.5 cm in diameter and 55 cm in height. Both ends of the cylinder were equipped with an injector nozzle. Bacteria encapsulated alginate and calcium chloride were injected from the top and bottom nozzles respectively, into the air-filled cylinder. An outlet was generated at the bottom of the cylinder to ensure mass continuity of the domain. In this model, the addition of bacterial suspension to alginate was assumed to have negligible effect on the properties of alginate. The simulation was also assumed to be in isothermal condition. Supposedly, alginate droplets form solidified microbeads upon contact with $CaCl_2$ mists. However, due to software limitation, the formation of solidified alginate microbeads upon impingement with $CaCl_2$ could not be modeled. Thus, the SMD of microbeads was assumed to be equal to the size of alginate droplets. This assumption was based on the study by Liu et al. (2019b) where $CaCl_2$ concentration did not significantly affect the diameter of microbeads.

5.2 Governing equations

For the present study, Eulerian-Lagrangian framework was selected and simulated using the commercial software STAR-CCM+ (ver 14.02). The surrounding air was chosen as the continuous phase and alginate or $CaCl_2$ as the discrete phase. The main governing equations for the continuous fluid phase and discrete aerosol phase solved during the simulations were provided in the following sections.

5.2.1 Modeling of continuous phase

The motion of the continuum gas phase is governed by the Reynolds-Averaged Navier–Stokes equations assuming the gas to be an incompressible fluid and constant properties as expressed in Equation 5.1 and 5.2 (Alfonsi, 2009), using Einstein's notation.

$$\frac{\partial \overline{u_i}}{\partial_{x_j}} = 0 \tag{5.1}$$

$$\frac{\partial \overline{\rho u_i}}{\partial t} + \frac{\overline{u_j}\partial \overline{\rho u_i}}{\partial x_j} = \frac{\partial}{\partial x_j}\left[-\frac{\partial \overline{p}\delta_{ij}}{\partial x_i} + \mu\left(\frac{\partial \overline{u_i}}{\partial_{x_j}} + \frac{\partial \overline{u_j}}{\partial x_i} \right) - \tau_{ij} \right] \tag{5.2}$$

where $\overline{u_i}$ is the average fluid velocity, ρ is the fluid density, p is the pressure, μ is the dynamic viscosity and τ_{ij} is the Reynolds-stress term. τ_{ij} is defined as Equation 5.3.

$$\tau_{ij} = \rho\overline{u_i' u_j'} \tag{5.3}$$

As a result of Reynolds-averaging, τ_{ij} appeared and need to be modeled by using a turbulence model. In this thesis work, the realizable k−ε turbulence model was used. It is a two-equation model based on the Boussinesq assumption, with transport equations for turbulent kinetic energy, k and its dissipation rate, ε. Boussinesq assumption introduces a turbulent viscosity, μ_t to characterize the transport and dissipation of energy at the small turbulent scales. The assumption is that the Reynolds stresses can be related to the mean strain tensors as Equation 5.4. This hypothesis is the base of most turbulence models.

$$-\rho\overline{u_i' u_j'} = 2\mu_t S_{ij} - \frac{2}{3}\rho k\delta_{ij} = \mu_t\left(\frac{\partial U_i}{\partial x_j} + \frac{\partial U_j}{\partial x_i}\right) - \frac{2}{3}\,\rho k\delta_{ij} \tag{5.4}$$

The realizable k−ε turbulence model was employed with a two-layer shear driven wall-treatment and a second order upwind convection term. It is known to predict swirling flows and the spreading rate of jet streams more accurately, which is important when modeling spray nozzles. The transport of turbulent kinetic energy, k is formulated as Equation 5.5.

$$\frac{\partial k}{\partial t} + \overline{u}_j\frac{\partial k}{\partial x_j} = v_t\left[\left(\frac{\partial u_i}{\partial x_j} + \frac{\partial u_j}{\partial x_i}\right)\left(\frac{\partial u_i}{\partial x_j}\right)\right] - \varepsilon + \frac{\partial}{\partial x_j}\left[\left(v + \frac{v_t}{\sigma_k}\right)\left(\frac{\partial k}{\partial x_j}\right)\right] \tag{5.5}$$

where the first term is the local change of k in time, the second term represents the change due to convection, the third term is production of k due to velocity gradient of the mean flow and the last two terms represents dissipation and diffusion of k.

The realizable model introduces a new transport equation for the turbulent dissipation rate ε. This is formulated as Equation 5.6.

$$\frac{\partial \varepsilon}{\partial t} + \overline{u}_j\frac{\partial \varepsilon}{\partial x_j} = \frac{\partial}{\partial x_j}\left[\left(v + \frac{v_t}{\sigma_\varepsilon}\right)\left(\frac{\partial \varepsilon}{\partial x_j}\right)\right] + C_{\varepsilon 1}s_\varepsilon - C_{\varepsilon 2}\frac{\varepsilon}{k + \sqrt{v\varepsilon}} \tag{5.6}$$

where the terms represent local rate of change of dissipation followed by convection, diffusion production and dissipation. The kinematic eddy viscosity v_t is defined as Equation 5.7.

$$v_t = C_\mu\frac{k^2}{\varepsilon} \tag{5.7}$$

where the important model parameter C_μ is expressed as a function of the mean flow and turbulence properties. The expression is formulated as Equation 5.8.

$$C_\mu = \frac{1}{A_0 + A_s U \frac{k}{\varepsilon}} \tag{5.8}$$

5.3 Modeling of dispersed phase

Dispersed phase is tracked using Lagrangian framework where the tracking is carried out by forming a set of ordinary differential equations in time for each droplet, consisting of equations for position, velocity, temperature and mass. These equations are then integrated to calculate the behavior of the droplet as they traverse the flow domain. The governing equation for the motion of liquid droplets is as Equation 5.9 (Khatami et al., 2013).

$$\frac{du_p}{dt} = \frac{18\mu}{\rho_p D_p^2} \frac{C_D Re_p}{24} \left(u - u_p\right) + \frac{g\left(\rho_p - \rho\right)}{\rho_p} + \frac{1}{2}\frac{\rho}{\rho_p}\frac{d}{dt}\left(u - u_p\right) \tag{5.9}$$

where u is the fluid phase velocity, u_p is the droplet velocity, ρ_p is the density of the droplet, D_p is the droplet diameter, C_D is the drag coefficient and Re_p is the droplet relative Reynolds number as expressed in Equation 5.10.

$$Re_p = \frac{\rho\left|u_p - u\right| D_p}{\mu} \tag{5.10}$$

The first term on the right-hand side of Equation 5.9 is the drag force per unit droplet mass, the second is the buoyancy force due to gravity, and the third is the virtual mass force which is the force required to accelerate the fluid surrounding the particle. The virtual mass force is negligible since the density of air is much less than the droplet density.

A number of correlations have been established for the drag coefficient, C_D, for the Euler–Lagrangian model. The Schiller–Maumann correlation has been used in this study because the Reynolds number range considered is less than 1000. The drag coefficient is calculated according to the Schiller (1933) drag model as expressed in Equation 5.11.

$$C_D = \frac{24}{Re_p}\left(1 + 0.15 Re_p^{0.687}\right) \tag{5.111}$$

5.3.1 Primary droplet breakup

Huh and Gosman (1991) published a model of turbulence-induced atomization for full-cone sprays. The turbulent length scale (L_t) and turbulent time scale (τ_t) are assumed to be the dominant parameters about atomization process. L_t and τ_t can be expressed as Equation 5.12 and 5.13 (Lucchini et al., 2010).

$$L_t = C_\mu^{0.75} \cdot \frac{K_{avg}^{\frac{3}{2}}}{\varepsilon_{avg}} \tag{5.12}$$

$$\tau_t = C_\mu^{0.75} \cdot \frac{K_{avg}}{\varepsilon_{avg}} \tag{5.13}$$

where K_{avg} and ε_{avg} represent the liquid jet average turbulent kinetic energy and its dissipation rate at nozzle exit, respectively and $C\mu = 0.09$.

The droplets break up with a characteristic atomization length scale L_A and time scale τ_A. The characteristic atomization length is proportional to the L_t which can be expressed as Equation 5.14 (Dos Santos & Le Moyne, 2011).

$$L_A = C_1 L_t = C_2 L_w \tag{5.14}$$

where L_w is the wavelength of surface instability determined by turbulence, C_1= 2 and C_2= 0.5. The characteristic atomization time scale τ_A can be calculated under the assumption that the time scale of atomization is a linear combination of the turbulence time scale τ_t and the wave growth time scale τ_w as shown in Equation 5.15.

$$\tau_A = C_3 \tau_t + C_4 \tau_w = \tau_{spn} + \tau_{exp} \tag{5.15}$$

where C_3 = 1.0 and C_4 = 1.5. τ_{spn} and τ_{exp} indicate spontaneous wave growth time and exponential growth time (Dos Santos et al., 2011).

The wave growth timescale is approximated by neglecting the surface tension and viscous effects and expressed as Equation 5.16.

$$\tau_w = \frac{L_w}{U} \sqrt{\frac{\rho_l}{\rho}} \tag{5.16}$$

Where ρ is the density of the continuous phase, ρ_l is the liquid density and U is spray velocity.

The liquid jet can be represented in the form of computational parcels (blobs) with breakup rate proportional to the ratio of the atomization length over the time scale as shown in Equation 5.17 (Adapco, 2016).

$$\frac{dD_d}{dt} = -\frac{2L_A}{\tau_A K_A} \tag{5.17}$$

Where D_d is the diameter of the parent droplet and K_A is a model constant to control the break-up rate with default value of 0.1.

The spray semi-cone angle, β is calculated from Equation 5.18 (Paredi et al., 2018).

$$\tan(\beta) = \frac{L_A / \tau_A}{U} \tag{5.18}$$

where τ_A is the breakup time. β determines the upper limit of the initial radial droplet velocity component. The estimation of initial velocity for each droplet is based on the assumption of equal probability of velocity direction within a spray cone. The components of droplet velocity v_d are calculated as Equation 5.19 (Adapco, 2016).

$$v_{d,x} = v_d \sin(\beta_d)\cos(\alpha_d) \tag{5.19}$$

$$v_{d,y} = v_d \sin(\beta_d)\sin(\alpha_d)$$

$$v_{d,z} = v_d \cos(\beta_d)$$

Where β_d and α_d are randomized angles that are given by $\beta_d = X_{r,1}\beta$ and $\alpha_d = 2\pi X_{r,2}$ where $X_{r,1}$ and $X_{r,2}$ are random numbers in the range [0, 1].

5.3.2 Secondary Droplet Breakup

In the Reitz-Diwakar (RD) model, there are two regimes controlling the breakup process of the droplets which include bag and stripping breakup. In the bag breakup regime, the nonuniform pressure field around the droplet leads to the disintegration of the droplet when its surface tension forces are overcome. In the stripping breakup regime, the liquid is sheared or stripped from the droplet surface. The breakup rate of the droplet for each regime can be calculated by Equation 5.20 (Kaario et al., 2014).

$$\frac{dD_p}{dt} = \frac{D_s - D_p}{\tau_b} \tag{5.20}$$

where D_s is the stable diameter and τ_b is the breakup time-scale. Both D_s and τ_b depend on the active breakup regime.

In the bag breakup regime, the instability is determined by the Weber number (We_p) as expressed in Equation 5.21 (Wang et al., 2018).

$$We_p = \frac{\rho \left| u - u_p \right|^2 D_p}{\sigma_p} \geq We_{crit} \tag{5.21}$$

Where u is the velocity of the continuum, u_p is the relative velocity of the droplet in the continuum, σ_p is the surface tension of droplet and We_{crit} is the critical Weber number of bag breakup regime value of 0.1.

The characteristic breakup time-scale for bag breakup regime is expressed as Equation 5.22 (Wang et al., 2018).

$$\tau_b = \frac{C_{b2} D_p}{4} \sqrt{\frac{\rho_p D_p}{\sigma_p}} \tag{5.22}$$

Where $C_{b2} = \pi$.

The criterion for the onset of stripping breakup regime is described as Equation 5.23.

$$\frac{We_p}{\sqrt{Re_p}} \geq C_{s1} \tag{5.23}$$

Where C_{s1} is a coefficient with the value of 0.5 and C_{s2} is in the range of 2-20.

The characteristic breakup time-scale for the stripping breakup regime is shown as Equation 5.24 (Wang et al., 2018).

$$\tau_b = \frac{C_{s2}}{2} \sqrt{\frac{\rho_p}{\rho}} \frac{D_p}{\left| u - u_p \right|} \tag{5.24}$$

5.3.3 Droplet size distribution

One of the main characteristics of spray atomization is the droplet size distribution. The Rosin–Rammler distribution method presents the most probable droplet size and a spread parameter to characterize the droplet size distribution. The Rosin–Rammler distribution can be expressed as Equation 5.25 (Bebe et al., 2017).

$$1 - Q = e^{\left(-\left(\frac{D_p}{X} \right)^q \right)} \tag{5.25}$$

where Q is the volume fraction of the droplets with a diameter smaller than D_p, X is the mean size of droplets for which Q equals 0.6321 and q is the droplet size spread parameter with default value of 3.5.

5.3.4 Collision and Coalescence

The outcome of a collision is coalescence or bouncing according to the O'Rourke algorithm. Collision outcomes are described by collision Weber number (We_{co}) and drop size ratio (γ) expressed as Equation 5.26 and Equation 5.27 (Adapco, 2016).

$$We_{co} = \frac{\rho\left(\left|u_1 - u_2\right|\right)^2 \left(\frac{1}{2}\right)\left(r_1 + r_2\right)}{\sigma_p} \tag{5.26}$$

where u_1 and u_2 are the velocities of the colliding drops, and r_1 and r_2 are their corresponding radii.

$$\gamma = \frac{r_2}{r_1} \quad , \; r_2 > r_1 \tag{5.27}$$

Generally, coalescence happens if the droplets collide head-on and bounces if the collision is oblique. There is a critical offset which is a function of the collisional Weber number and the relative radii of the droplets defined by the critical collision parameter b_{crit} according to Equation 5.28 (Khatami et al., 2013).

$$b_{crit} = \left(r_2 - r_1\right)\sqrt{\min\left(1.0, \frac{2.4f}{We_{co}}\right)} \tag{5.28}$$

Where f is a function of γ defined as Equation 5.29.

$$f\left(\gamma\right) = \gamma^3 - 2.4\gamma^2 + 2.7\gamma \tag{5.29}$$

The value of the actual collision parameter, b, is expressed as Equation 5.30.

$$b = \left(r_1 + r_2\right)\sqrt{Y} \tag{5.30}$$

where Y is a random number between 0 and 1. The calculated b is compared to b_{crit} and if $b < b_{crit}$ we can assume that the result of collision is coalescence. Otherwise, the droplets bounce and each one has a new velocity and direction based on conservation of momentum and energy.

5.4 Wall Impingement

In the simulation, the Bai-Gosman wall impingement model was coupled with droplet breakup. Depending on the Weber and Laplace numbers for the droplets, the Bai-Gosman model simulates a wide range of behaviors of particles impacting walls such as sticking, rebounding, spreading and splashing. The choice of regime for a given impingement event is made using three parameters, i.e. the incident Weber number, Laplace number and wall state (wet or dry). Incident Weber number (We_I) is expressed as Equation 5.31 and Laplace number as Equation 5.32 (Ashkezari et al., 2014).

$$We_I = \frac{\rho_p v_{r,n}^2 D_p}{\sigma_p} \tag{5.31}$$

in which $v_{r,n} = \left(v_p - v_w\right) n_w$ is the normal component of the particle velocity relative to the wall and n_w is the unit vector normal to the boundary.

$$La = \frac{\rho_p \sigma_p D_p}{\mu_p^2} \tag{5.32}$$

Where μ_p is the dynamic viscosity of droplet.

5.5 Fluid film thickness

Droplet impingement, where droplets are carried along in the gas, impinges on surfaces to form a liquid layer, governs the film mass conservation according to Equation 5.33 (Adapco, 2016). Equation 5.33 is used to calculate the film thickness h_f.

$$\frac{\partial}{\partial t}\int_V \rho_f dV + \int_A \rho_f v_f \; da = \int_V \frac{S_u}{h_f} dV \tag{5.33}$$

where ρ_f is the film density, v_f is the film velocity, and the subscript f denotes the fluid film values. The quantity S_u is the mass source/sink per unit area from droplet impingement. It is specific in the sense that the volume V and the surface A are functions of the film thickness and its spatial distribution.

The momentum conservation equation is expressed in Equation 5.34 (Adapco, 2016).

$$\frac{\partial}{\partial t}\int_V \rho_f v_f dV + \int_A \rho_f v_f \otimes vf\, da = \int_A (T_f\ da - \int_A p_f\ da + \int_V \left(f_b + \frac{s_m}{h_f} \right) dV \tag{5.34}$$

where s_m is the momentum source corresponding to the mass source S_u, p_f is the pressure, f_b is the body force such as gravity and the form drag force and T_f is the viscous stress tensor within the film.

5.6 Boundary and initial conditions

The model was assumed to be filled with air at room temperature and the initial fluid film on the wall was set as zero thickness. The operating conditions and physical properties of alginate, $CaCl_2$ and air were tabulated in Table 5.1. The outlet of cylinder was set to atmospheric pressure of 101.325 kPa.

Table 5.1 Operating parameters and physical properties of alginate, $CaCl_2$ and air (Nunamaker et al., 2011; Al-Damook et al., 2016; Chloride)

Properties	**Value**
Top Nozzle – Alginate (1.5 %), low viscosity	
Density	1007 kg/m^3
Surface Tension	0.055 N/m
Dynamic viscosity	0.08 Pa.s
Flowrate	40 ml/min
Nozzle diameter	0.4 mm
Bottom Nozzle – 0.1 M Calcium chloride	
Density	1006.5 kg/m^3
Surface Tension	0.073 N/m
Dynamic viscosity	0.00103 Pa.s
Flowrate	30 ml/min
Nozzle diameter	0.4 mm
Air, continuum phase	
Density	1.184 kg/m^3
Dynamic viscosity	1.849 x 10^{-5} Pa.s

5.7 Solution procedures and model validation

The governing equations were solved using first order, implicit unsteady and segregated flow solver with a time-step of 10^{-4} s. Figure 5.2 shows the algorithms for segregated flow solver. The convergence criteria of the model was set to be 10^{-4}. For each time-step, 5 inner iterations were specified for each time step. The simulation was run for 0.5 s to study the spray behaviors.

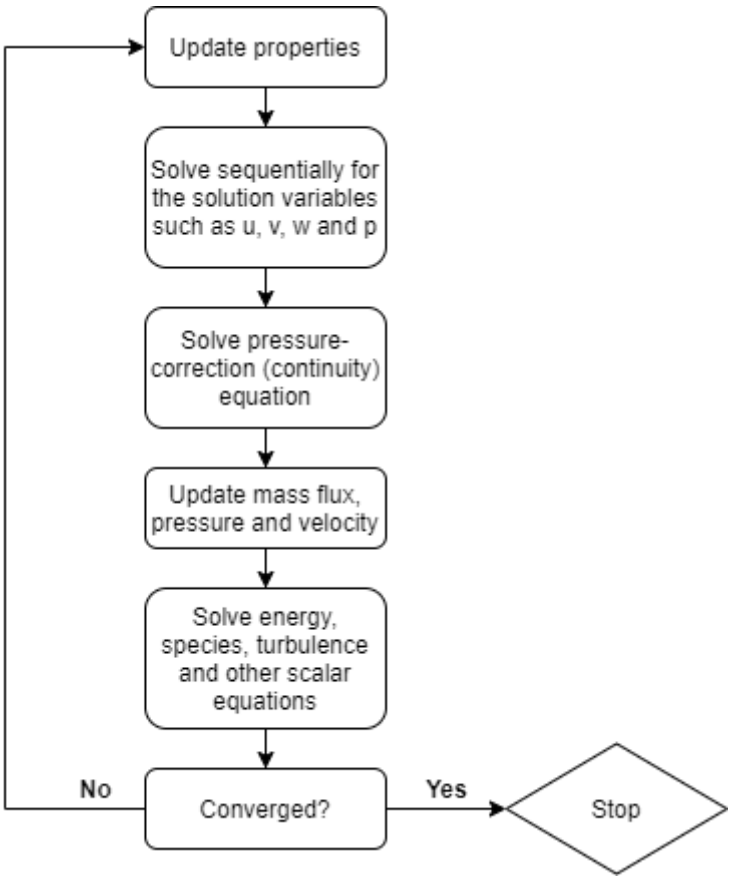

Figure 5.2 The segregated flow solver algorithms

The computational domain was meshed using quadrilateral meshes on the cross-section of the cylinder. The meshes were extruded along the length of the cylinder. Figure 5.3 shows the resulting meshes of the domain. A grid independency test was performed to ensure that the model was free from discretization errors. The model was validated by comparing the Sauter mean diameter of droplets and spray angle obtained experimentally and numerically at alginate flowrate of 40 ml/min, 50 ml/min and 60 ml/min.

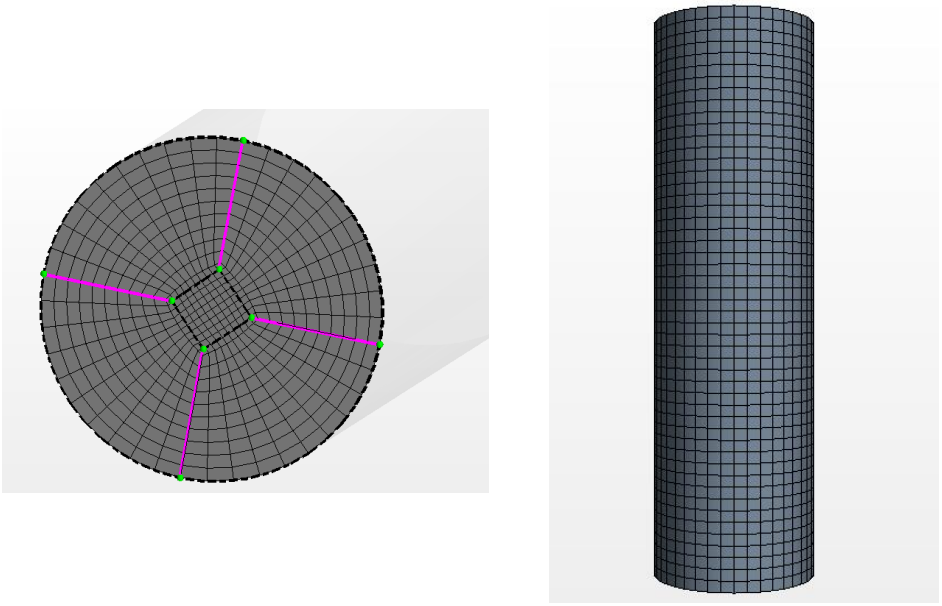

Figure 5.3 Mesh distribution on (A) cross-section; (B) along the length of the cylinder

5.8 Concluding remarks

This project was based on the assumption that the atomization of alginate and calcium chloride in still air can be modeled using an Eulerian-Lagrangian framework where the surrounding air was treated as a continuum with the flow-field solved by the Navier–Stokes equations and the spray atomization was tracked using Lagrangian framework. The primary and secondary breakup of alginate and $CaCl_2$ through nozzles were modeled using Huh and Reitz-Diwakar models, respectively. Then, the wall impingement of spray droplets was modeled using the Bai-Gosman model. The simulated results were validated with experimental results and the models were subjected for parametric studies. Various scenarios such as the effect of nozzle orifice size, alginate concentration, size of encapsulation chamber and parameters of breakup models on the spray angle, droplet size and wetting of wall were investigated. The next chapter discusses the results from the numerical modeling.

CHAPTER 6

SIMULATION RESULTS AND VALIDATION

In Chapter 5, the modeling methodology for spray atomization modeling were discussed. This chapter describes the model validation and simulation findings.

6.1 Mesh independency

Since the region of primary concern in this study is the central region of the chamber spray, the grid was built with smaller quadrilateral mesh in the central region followed with a coarse quadrilateral to the wall as shown in Figure 5.3. The mesh was refined at the central region to capture the details of the spray behaviors near nozzles. Grid independency tests were done based on nozzle orifice size of 0.4 mm and alginate flowrate of 40 ml/min. The mesh settings resulted in an overall computational cell count of 180, 000 to 570, 000 cells. The alginate droplet size distribution from top nozzle were observed at different number of cell count and the results were plotted in Figure 6.1. Frequency percentage is defined as the number of frequency in the category divided by the total number of frequency and multiplying by 100 % Referring to Figure 6.1, it can be seen that coarse mesh of 180, 000 cells and 270, 000 cells underestimated and overvalued the frequency percentage for droplet size below 255 µm and in between 255 µm to 270 µm, respectively. This showed that coarse meshes were unable to accurately predict the particles Sauter Mean Diameter (SMD) values. While, when the cell count increased from 389, 000 to 570, 000 cells, no significant difference was observed in the frequency percentage, indicating that further refinement in mesh would not substantially affect the SMD value. In addition, it was found that the spray angle were not influenced by grid size significantly with further grid refinement. Thus, 389, 000 cells were selected for the rest of the studies.

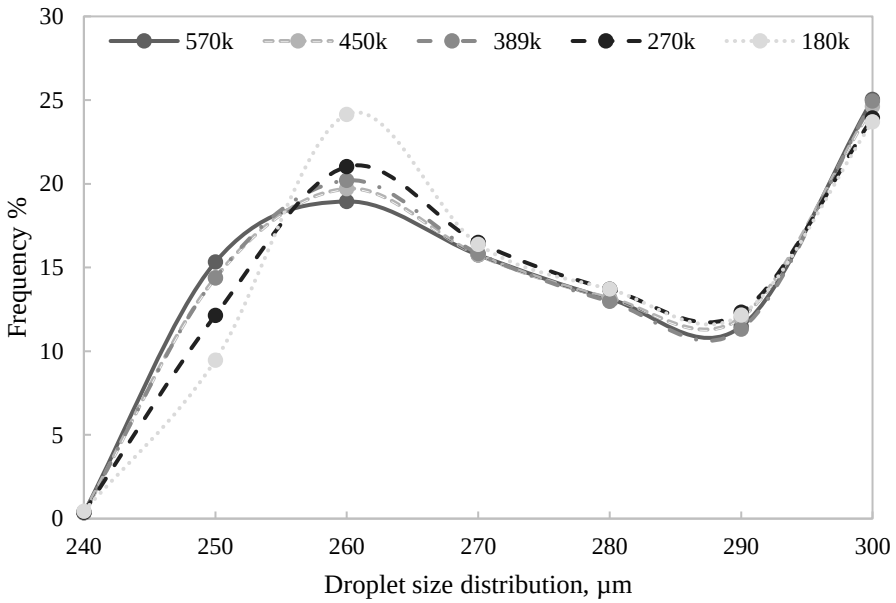

Figure 6.1 Simulation results of the mesh independence test in terms of the alginate droplets size distribution

6.2 Model validation and comparison with experimental data

During the spray process, flowrate is related to the thickness of the liquid sheet and the size of droplets. A higher flowrate is prone to form thinner liquid sheet (longer spray breakup length), a wider spray angle and smaller droplets (Zhang et al., 2017). CFD model was developed to study the spray behaviors and the numerical results were validated with experimental results. Experimental procedures have been carried out to investigate the effects of alginate flowrate of 40 ml/min, 50 ml/min and 60 ml/min on the spray angle and SMD at an alginate concentration of 1.5 % (w/v) and 0.4 mm orifice diameter. Spray angle was obtained by adapting the method reported by Ahmed et al. (2009) where a tangent to the tip of the nozzle at its centerline was drawn and the intersection points of this tangent with the edges of the sheet were determined as shown in Figure 6.2. Then, two tangents to the liquid sheet were drawn from the two intersection points. The angle between the two tangent lines to the sheet is defined as the spray angle. The spray angle analysis for experiments and CFD results at different flowrate were carried out by using ImageJ software as shown in Figure 6.3 to Figure 6.5.

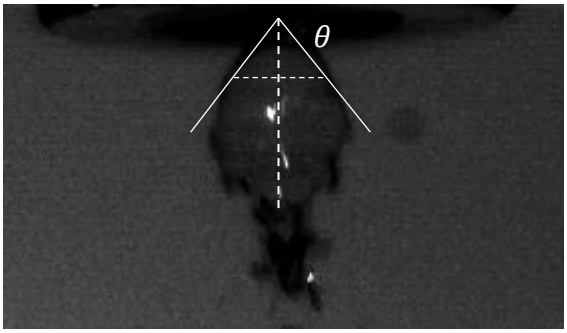

Figure 6.2 Definition of spray angle

(A)

(B)

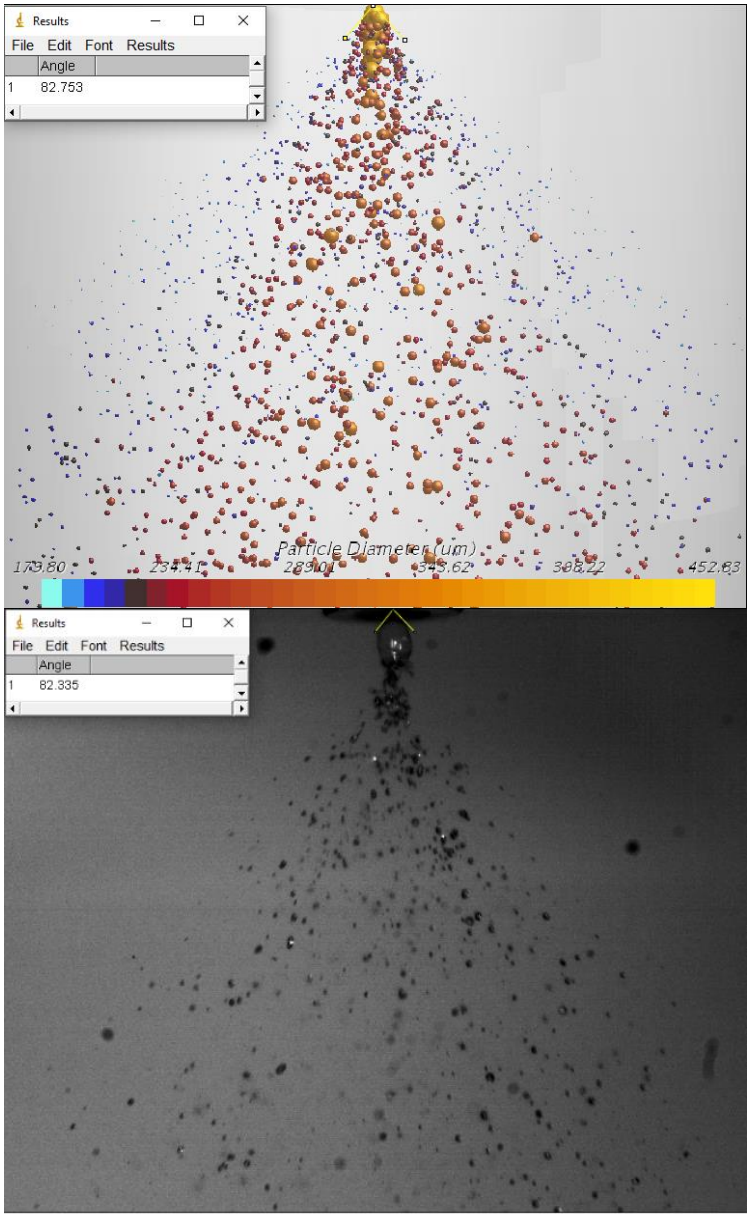

Figure 6.3 Alginate breakup of 1.5 % alginate concentration at 40 ml/min (A) simulation (B) experiment with 0.4 mm nozzle diameter

(A)

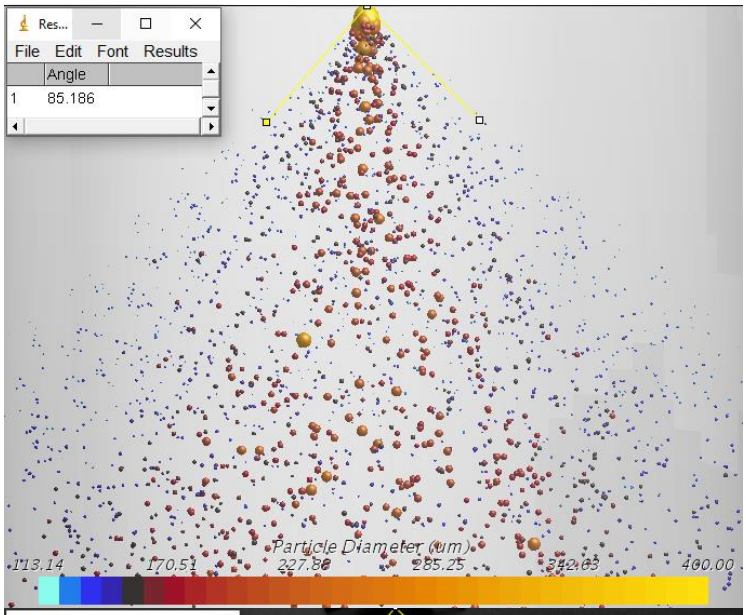

(B)

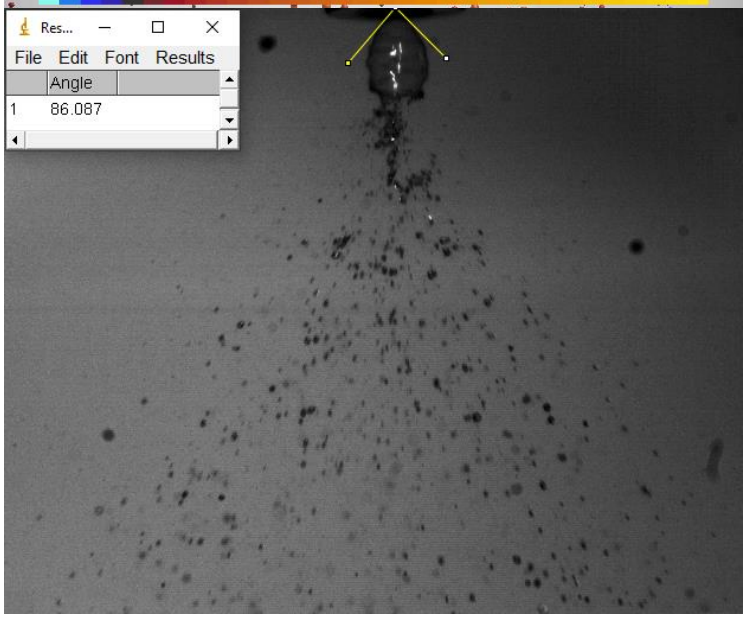

Figure 6.4 Alginate breakup of 1.5 % alginate concentration at 50 ml/min (A) simulation (B) experiment with 0.4 mm nozzle diameter

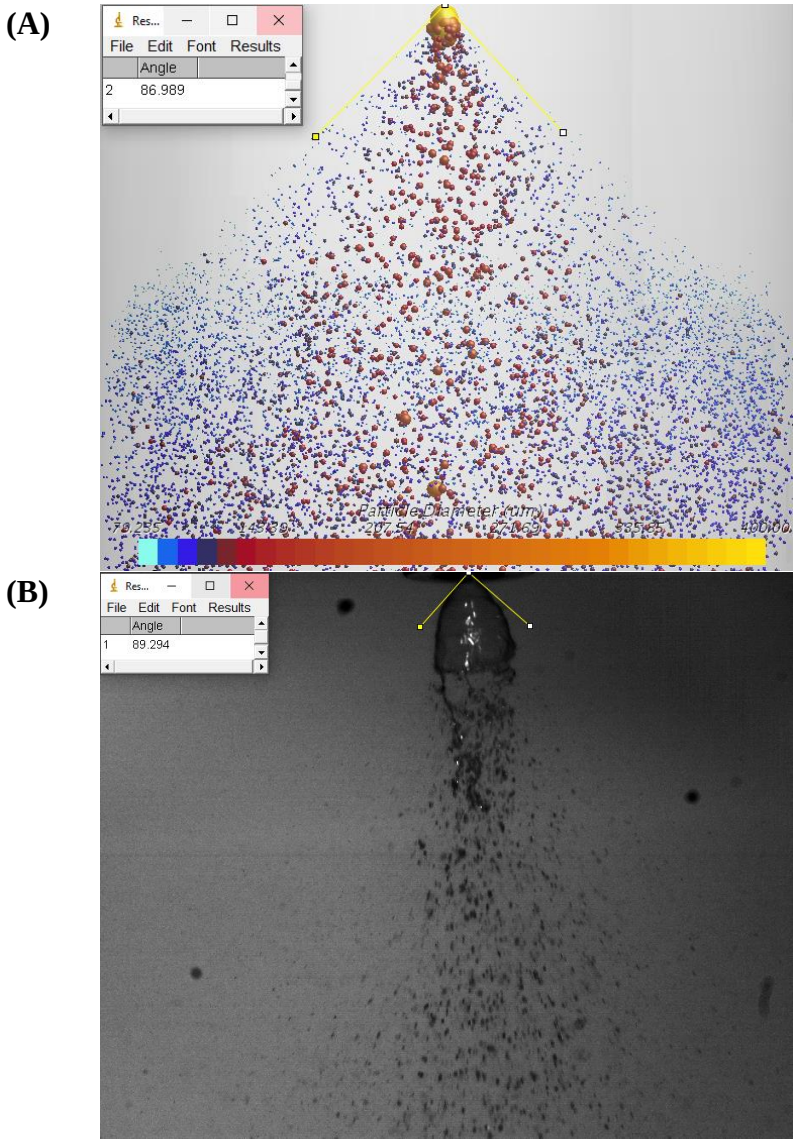

Figure 6.5 Alginate breakup of 1.5 % alginate concentration at 60 ml/min (A) simulation (B) experiment with 0.4 mm nozzle diameter

The spray angle versus different alginate flowrate were plotted in Figure 6.6. Based on the plot, spray angle increased with alginate flowrate. Spray angle at 40 ml/min, 50 ml/min and 60 ml/min flowrate for experiment was 82.3 ± 2.1°, 86.1 ± 1.7° and 89.3 ± 1.9° whereas for CFD, spray angle obtained was 82.8°, 85.2° and 87.0°, respectively. The percentage error between simulated and experimental results were 0.61 %, 1.05 % and 2.58 % for 40 ml/min, 50 ml/min and 60 ml/min, respectively. The CFD results of spray angle for alginate atomization obtained showed a good agreement when compared with experimental results.

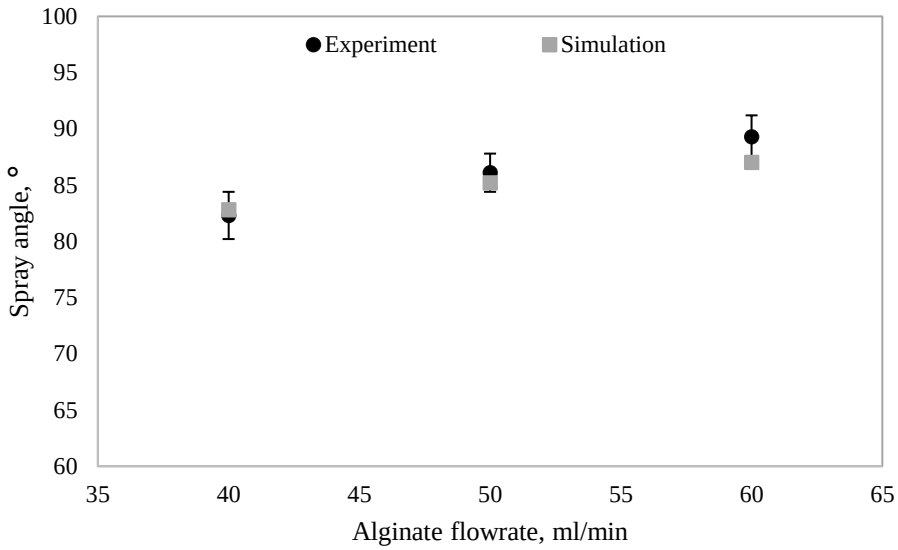

Figure 6.6 Spray angle at different flowrate for experiment and simulation with 1.5 % alginate concentration and orifice size of 0.4 mm. Each point represents a mean value and the error bars showed the standard deviation (n=3)

Spray angle increases with alginate flowrate can be associated with the spray breakup length. From Figure 6.7 to Figure 6.9, the spray breakup length as labelled L_{bu} were observed to increase with flowrate. The spray breakup length was not captured in CFD results as it is impossible to quantify these values with Lagrangian computation. A longer spray breakup length indicates that the spatial extent of the primary atomization region is longer and results in a longer time to break up into droplets (Isa et al., 2019).

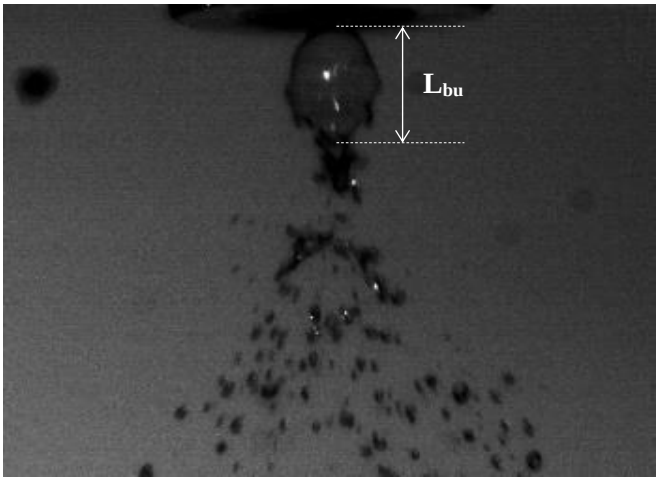

Figure 6.7 Length breakup at 40 ml/min, 1.5 % alginate concentration and 0.4 mm orifice size

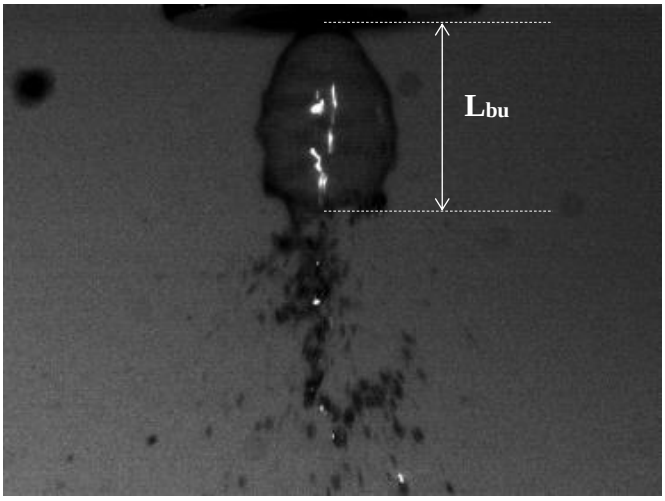

Figure 6.8 Length breakup at 50 ml/min, 1.5 % alginate concentration and 0.4 mm orifice size

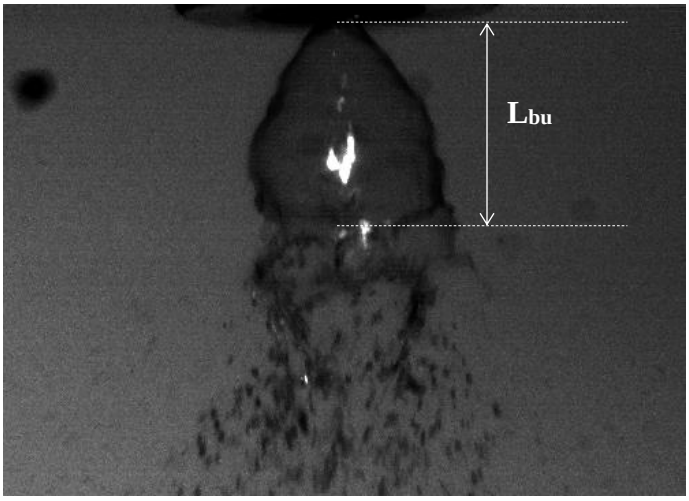

Figure 6.9 Length breakup at 60 ml/min, 1.5 % alginate concentration and 0.4 mm orifice size

With increasing flowrate, droplets formed near nozzles tip are expected to have higher Weber number as shown in Figure 6.10. At 40 ml/min, 50 ml/min and 60 ml/min, the Weber number of droplets were found to be 0.205, 0.255 and 0.384, respectively. Thus, it can be concluded that greater Weber numbers leads to a greater spray breakup length. Similar result was obtained by Ahmed et al. (2009) where breakup length is found to be linearly proportional to the Weber number. A longer breakup length results in a wider spray angle (Wang et al., 2015).

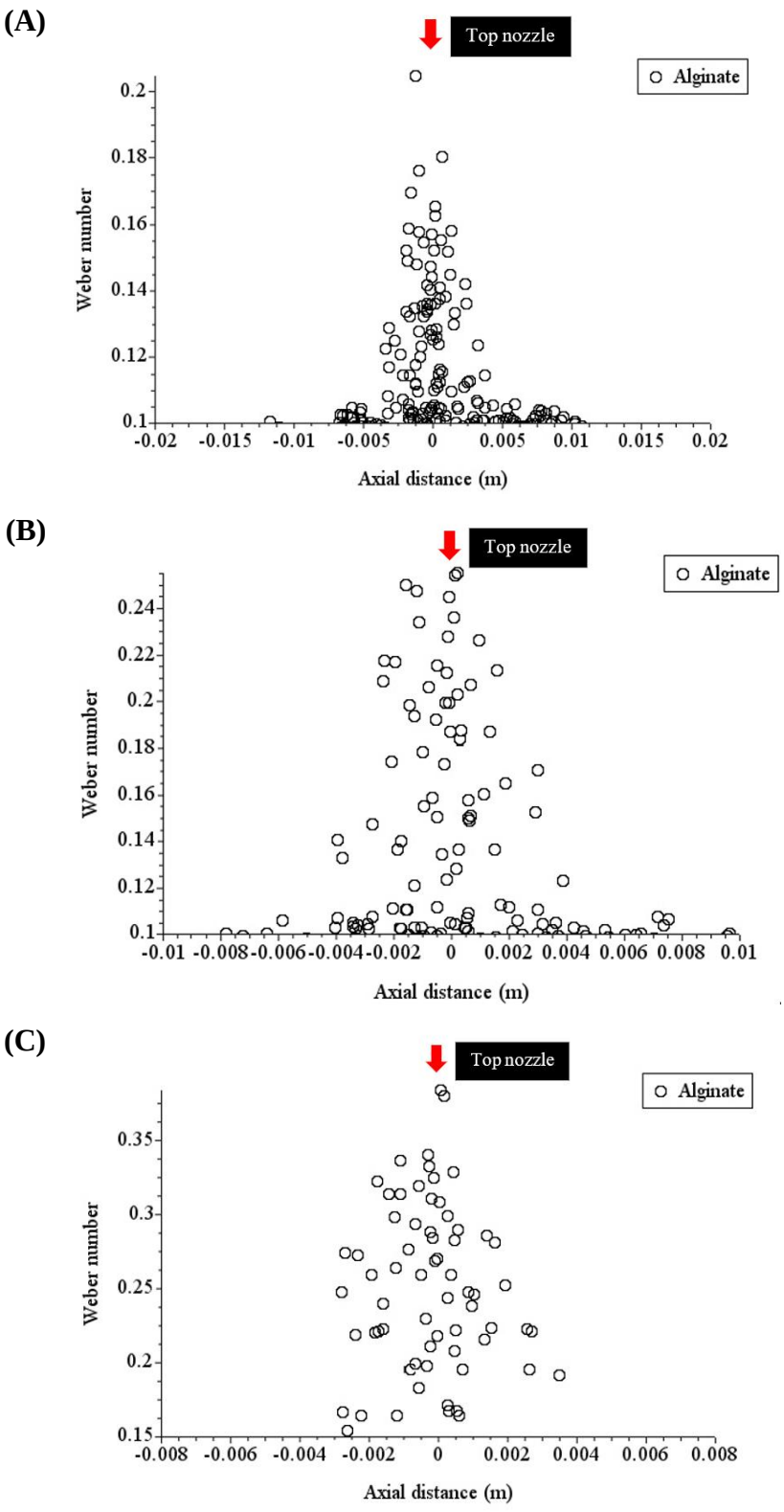

Figure 6.10 Weber number of droplets from nozzle (A) 40 ml/min, (B) 50 ml/min, and (C) 60 ml/min with 1.5 % alginate concentration and 0.4 mm orifice size

The optical micrographs of PSMs loaded alginate microbeads produced under 1.5 % (w/v) alginate concentration, 0.4 mm orifice size and 0.1 M $CaCl_2$ concentration with different flowrate were shown in Figure 6.11 to Figure 6.13. These micrographs were analyzed with ImageJ software to identify the droplets size distribution and used to calculate the SMD.

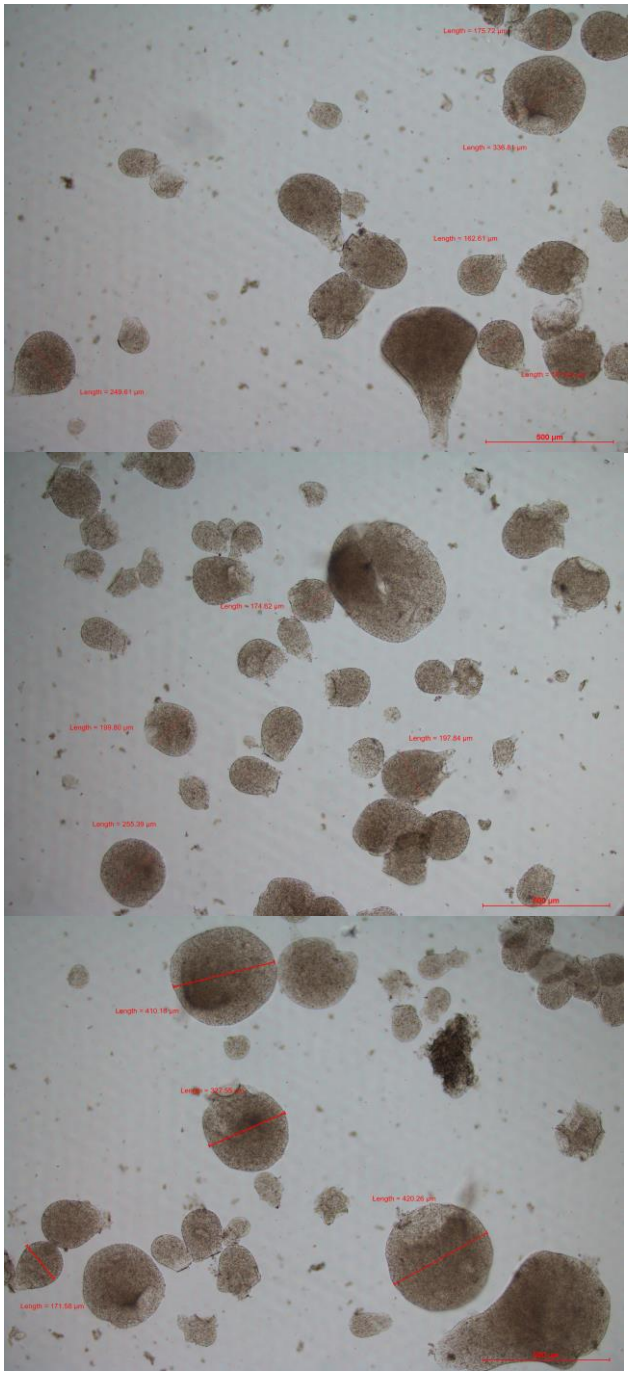

Figure 6.11 Optical micrographs of PSMs loaded alginate microbeads produced under 1.5 % alginate, 0.1 M $CaCl_2$ concentration and 0.4 mm orifice size at 40 ml/min alginate flowrate

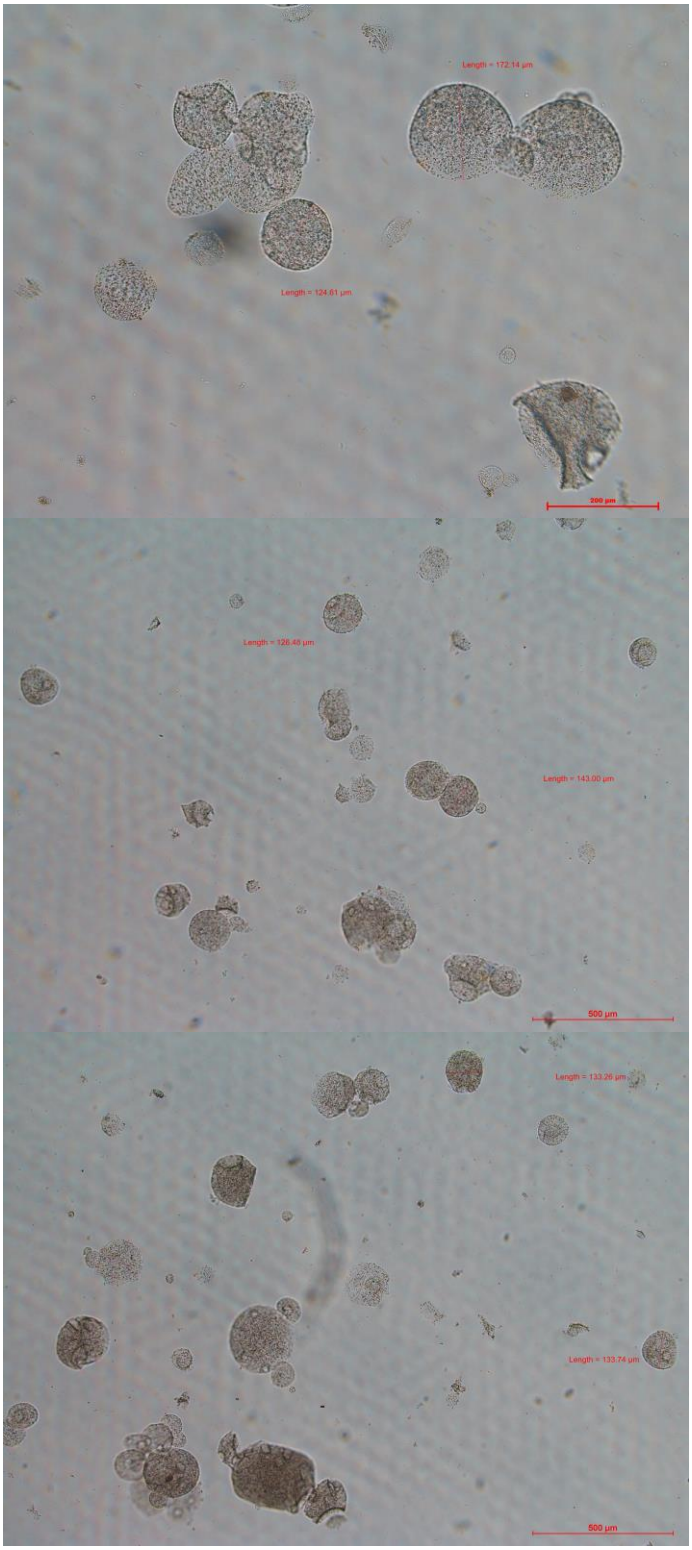

Figure 6.12 Optical micrographs of PSMs loaded alginate microbeads produced under 1.5 % alginate, 0.1 M $CaCl_2$ concentration and 0.4 mm orifice size at 50 ml/min alginate flowrate

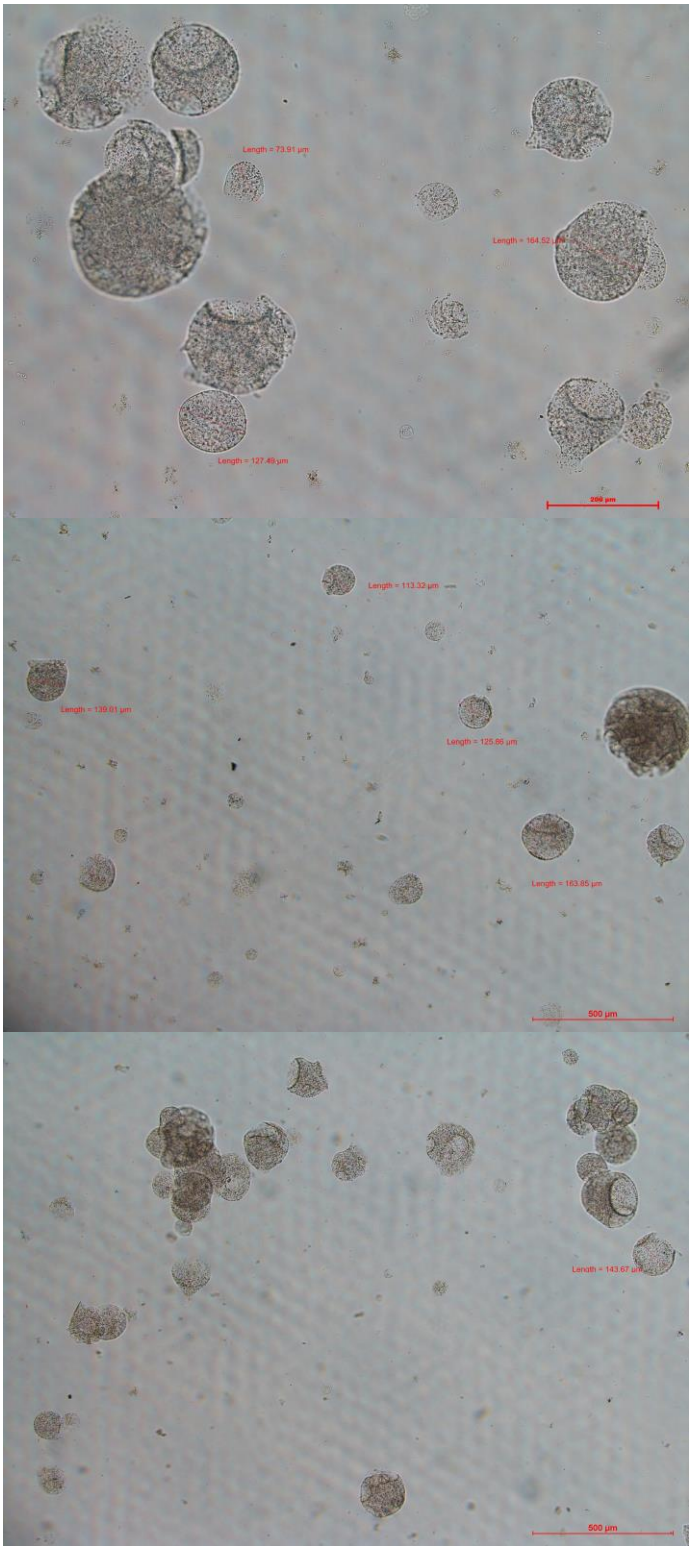

Figure 6.13 Optical micrograph of PSMs loaded alginate microbeads produced under 1.5 % alginate, 0.1 M $CaCl_2$ concentration and 0.4 mm orifice size at 60 ml/min alginate flowrate

Meanwhile, the simulated alginate droplets size distribution produced under different alginate flowrate were plotted in Figure 6.14. Referring to Figure 6.14, it can be observed that wider droplet size distribution was obtained with higher flowrate.

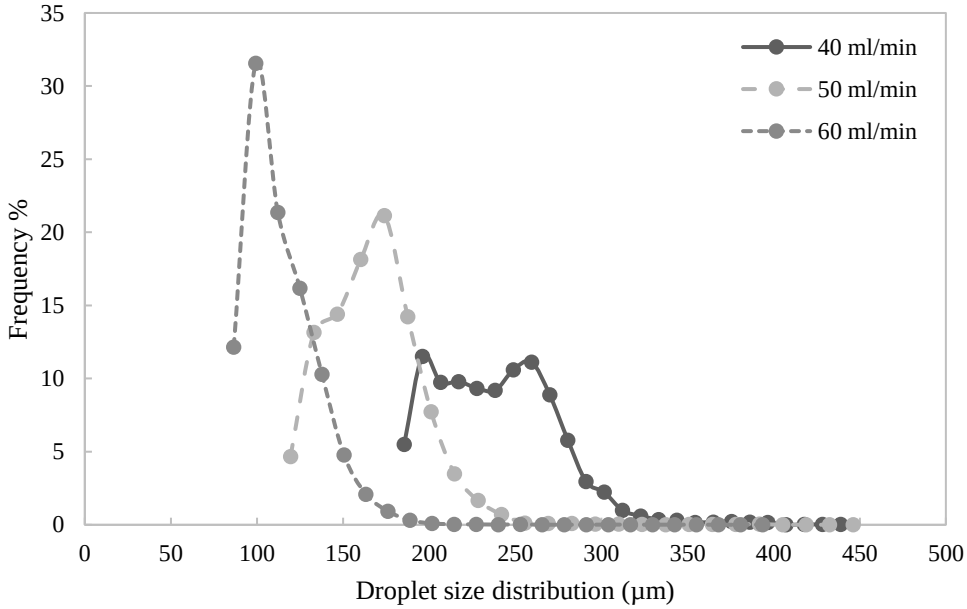

Figure 6.14 Droplet size distribution for alginate flowrate 40 ml /min, 50 ml/min and 60 ml/min with 1.5 % alginate concentration and 0.4 mm orifice size

The frequency and droplets size obtained experimentally and numerically were used to calculate the SMD value using Equation 6.1.

$$\mathrm{SMD} = \frac{\sum n_i d_i^3}{\sum n_i d_i^2} \tag{6.1}$$

Where n is frequency and d is the droplet diameter

The SMD value were plotted in Figure 6.15 and it shows that the SMD values decreased with increased flowrate. SMD of microbeads for 40 ml/min, 50 ml/min and 60 ml/min obtained for experiment were 236.87 ± 12.25 µm, 162.3 ± 9.62 µm and 137.2 ± 8.95 µm, respectively and 251.0 µm, 177.9 µm, and 123.7 µm, correspondingly for simulation. The percentage error between simulated and experimental results were 5.97 %, 9.61 % and 9.82 % for 40 ml/min, 50 ml/min and 60 ml/min, respectively. Here, it can be concluded that the SMD results between experimental and simulation were found to be in a good agreement.

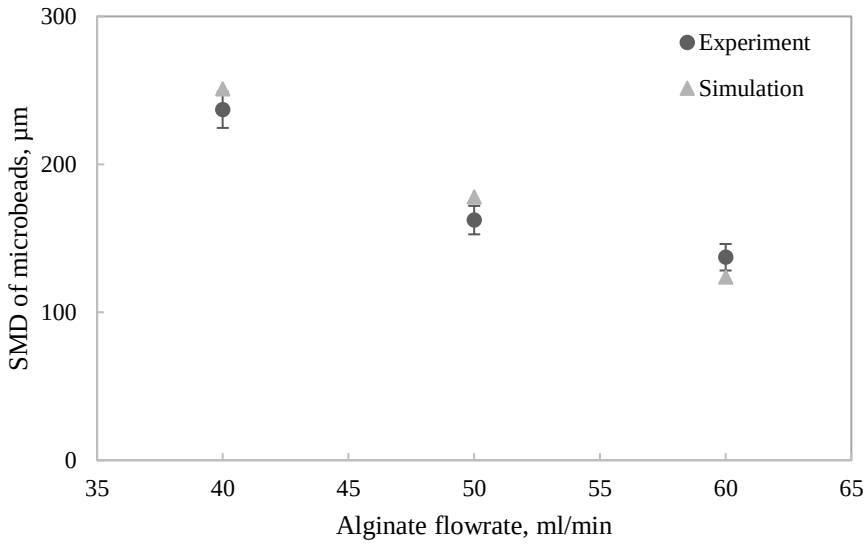

Figure 6.15 SMD of droplets at different flowrate for experiment and simulation with 1.5 % alginate concentration and 0.4 mm orifice size. Each point represents a mean value and the error bars showed the standard deviation (n=3)

The estimation of SMD of the droplets after the primary breakup is generally correlated with droplets Weber number. It is well understood that there is an inverse relationship between Weber number and SMD (Wu et al., 1992; Brennen & Brennen, 2005). Figure 6.16 shows the correlation between Weber number and SMD for current study. From the graph fitting, a semi-empirical formula expressed as Equation 6.2 was obtained.

$$SMD = 60.515\ We_p^{-0.811} \tag{6.2}$$

Referring to Figure 6.16, the lower R^2 value of 0.854 was obtained and this can be associated with the wide droplets size distribution resulted from spray atomization, which caused difficulty in identifying the SMD experimentally. Besides, the percentage error of this correlation was determined to be 8.01 %. Thus, it can be suggested that in future studies more experimental results under different flowrate should be taken to improve the correlation between SMD and Weber number. As shown in Equation 5.21, the droplet exit velocity from nozzle can be calculated with Equation 6.3.

$$u_p = \frac{\dot{m}}{\rho_p A} \tag{6.3}$$

Where A is the nozzle area and $\dot{m}$ is the mass flowrate.

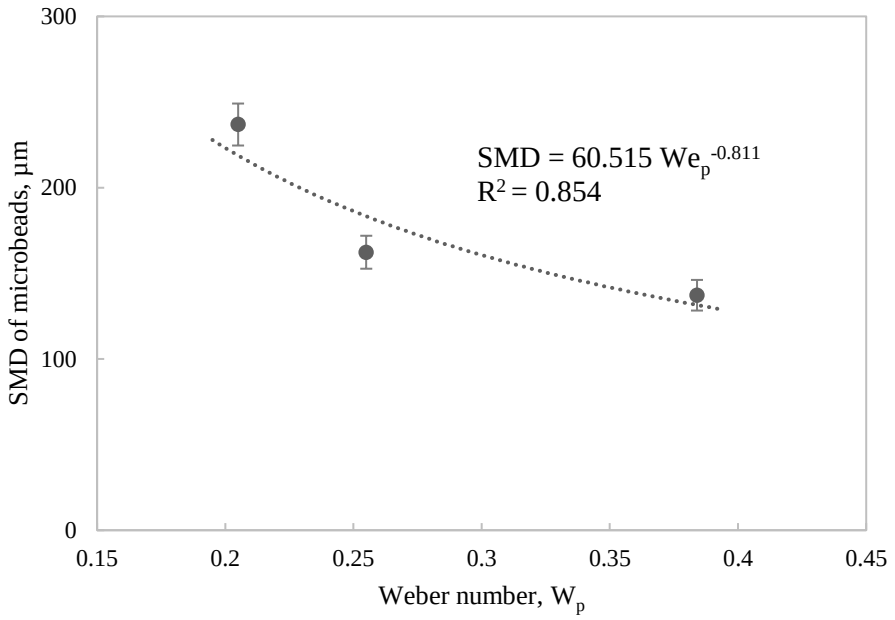

Figure 6.16 Influence of droplets Weber number on SMD. Each point represents a mean value and the error bars showed the standard deviation (n=3)

From Equation 6.2, it can be observed that SMD is highly dependent on the Weber number of the droplets. When the density of droplet and nozzle diameter are kept constant, the droplet exit velocity from nozzle is directly proportional to flowrate based on Equation 6.3. Referring to Figure 6.17, Figure 6.18 and Figure 6.19, the exit velocity of droplets from nozzle was 5.3 m/s, 6.62 m/s and 7.84 m/s at 40 ml/min, 50 ml/min and 60 ml/min, respectively.

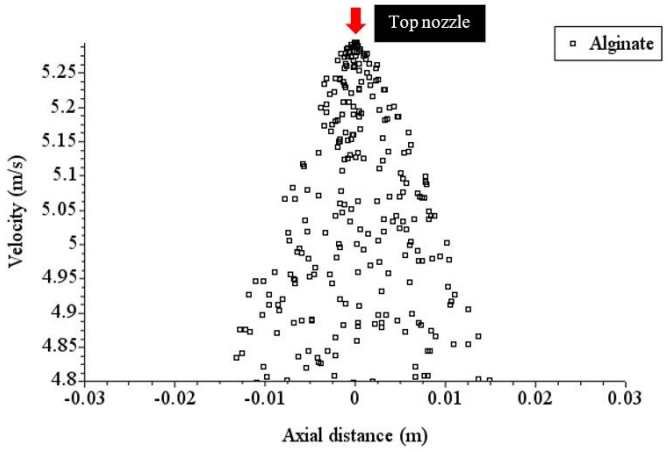

Figure 6.17 Simulated droplet velocity at 40 ml/min with 1.5 % alginate concentration and 0.4 mm orifice size

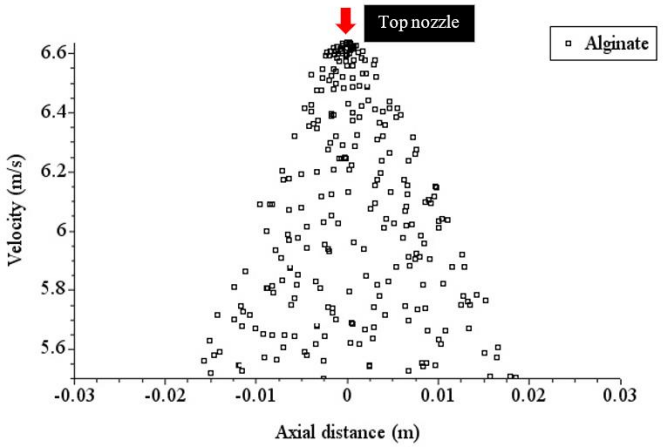

Figure 6.18 Simulated droplet velocity at 50 ml/min with 1.5 % alginate concentration and 0.4 mm orifice size

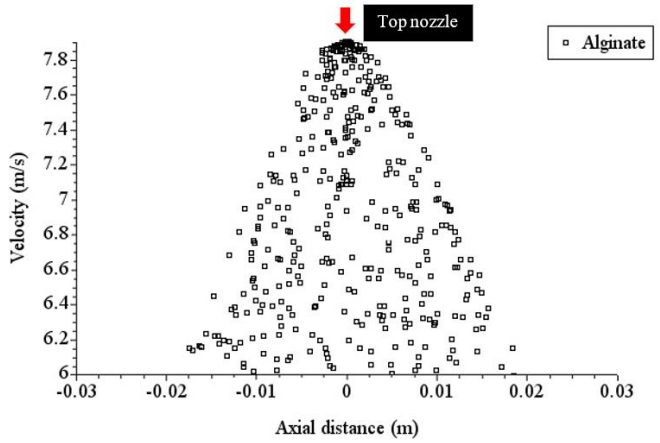

Figure 6.19 Simulated droplet velocity at 60 ml/min with 1.5 % alginate concentration and 0.4 mm orifice size

Therefore, an increase in flowrate results in a greater Weber number. Since SMD is inversely proportional to Weber number, an increase in Weber number leads to a smaller SMD value. As discussed earlier, spray breakup length increases with flowrate. Longer spray breakup length will have thinner liquid sheet as shown in Figure 6.20.

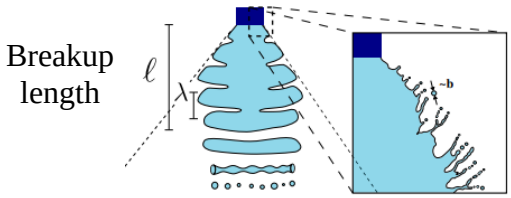

Figure 6.20 Schematic representation of the breakup mechanism (Kooij et al., 2018). Reproduced under Creative Commons licenses

Sprays with longer breakup length produces smaller droplets (Arvidsson et al., 2011; Wang et al., 2015) because droplet sizes are mostly close to the thickness of the sheet from which they are formed (Hilz & Vermeer, 2013). Thickness of sheets decreases along with the central line due to centrifugal force and the sheets break up into droplets. To conclude, spray angle increases and SMD decreases with flowrate. Similar results was obtained by Isa et al. (2019) where the SMD values of ethanol atomization decreased when flowrate increased. This is because the liquid is discharged from the nozzle at a higher velocity which promotes a finer spray (Lefebvre & McDonell, 2017).

Fluid film formation on chamber wall with different alginate flowrate was also studied as shown in Figure 6.21. A thicker fluid film formation indicates that the alginate droplets tend to stick on the wall, resulting product loss which is unfavorable for the production of microbeads.

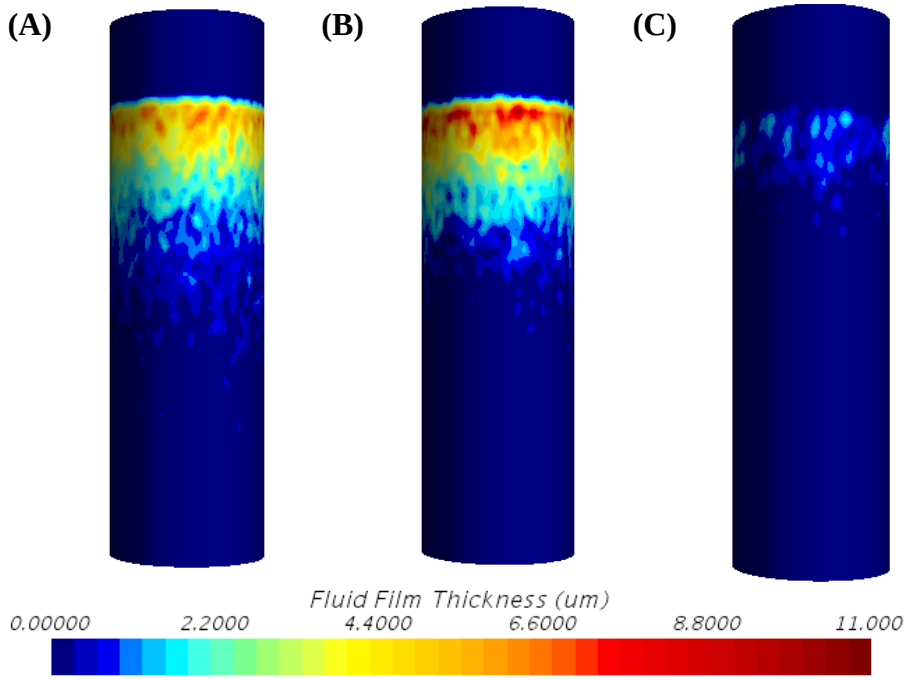

Figure 6.21 Film thickness of alginate to chamber wall (A) 40 ml/min; (B) 50 ml/min and (C) 60 ml/min with 1.5 % alginate concentration and 0.4 mm orifice size at 0.5 s

It can be seen at 50 ml/min the fluid film thickness was thicker when compared with 40 ml/min. This is because as flowrate increases, spray angle increases and results in wall wetting. However, at 60 ml/min, when the spray angle was wider, film thickness was thinner and this is might be due to the low velocity of droplets associated with the small

droplets size (Figure 6.5). The speed at which a droplet falls when released into still air is strongly related to its diameter (Nuyttens et al., 2009). Smaller droplets having less momentum penetrates slower and less deep and this lessen the formation of fluid film at chamber wall (Wojdas, 2010).

Well distributed spray is the main aim for impinging aerosol method. This method involves formation of mist of the cross-linking agent which is the $CaCl_2$ solution in a spray chamber. The alginate solution droplets are then sprayed into the chamber and solidified upon impinging with the $CaCl_2$ mist. It can be hypothesized that a good droplets distribution of sprays allows efficient impingement of alginate droplets with $CaCl_2$ mists and promotes the formation of gelled microbeads with narrow size distribution. The droplets distribution of sprays of alginate and $CaCl_2$ mists at 40 ml/min, 50 ml/min and 60 ml/min of alginate flowrate at 0.5 s physical time were shown in Figure 6.22, Figure 6.23 and Figure 6.24, respectively.

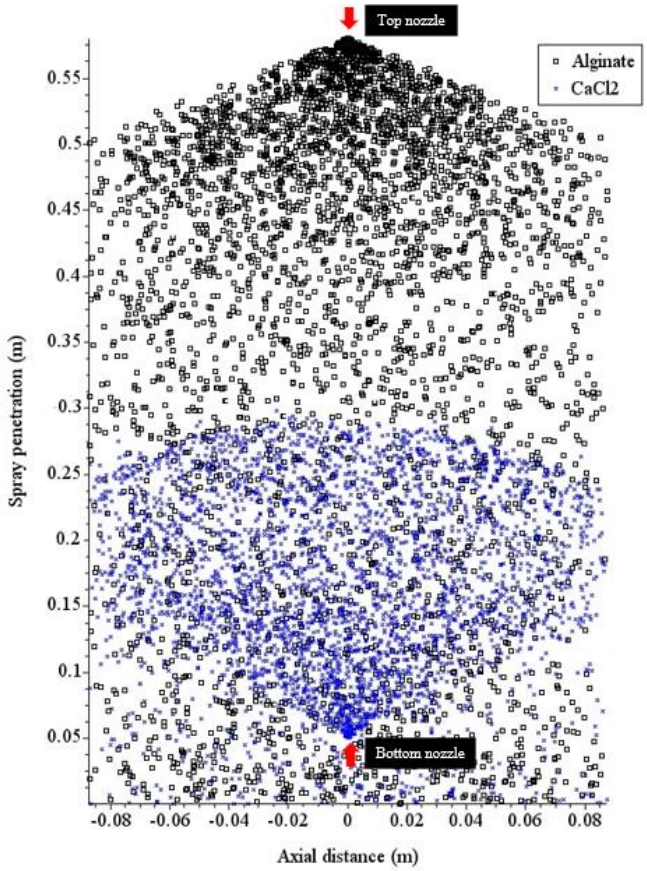

Figure 6.22 Droplets distribution of sprays of alginate and $CaCl_2$ at 40 ml/min of alginate flowrate, 1.5 % alginate concentration and 0.4 mm orifice size at 0.5 s

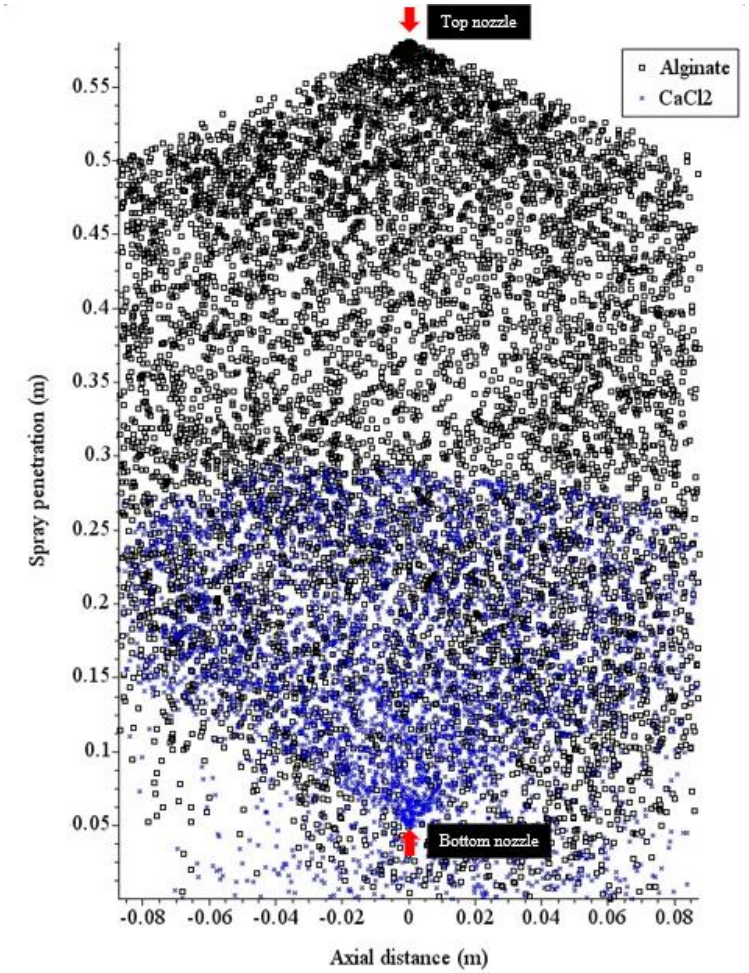

Figure 6.23 Droplets distribution of sprays of alginate and $CaCl_2$ at 50 ml/min of alginate flowrate, 1.5 % alginate concentration and 0.4 mm orifice size at 0.5 s

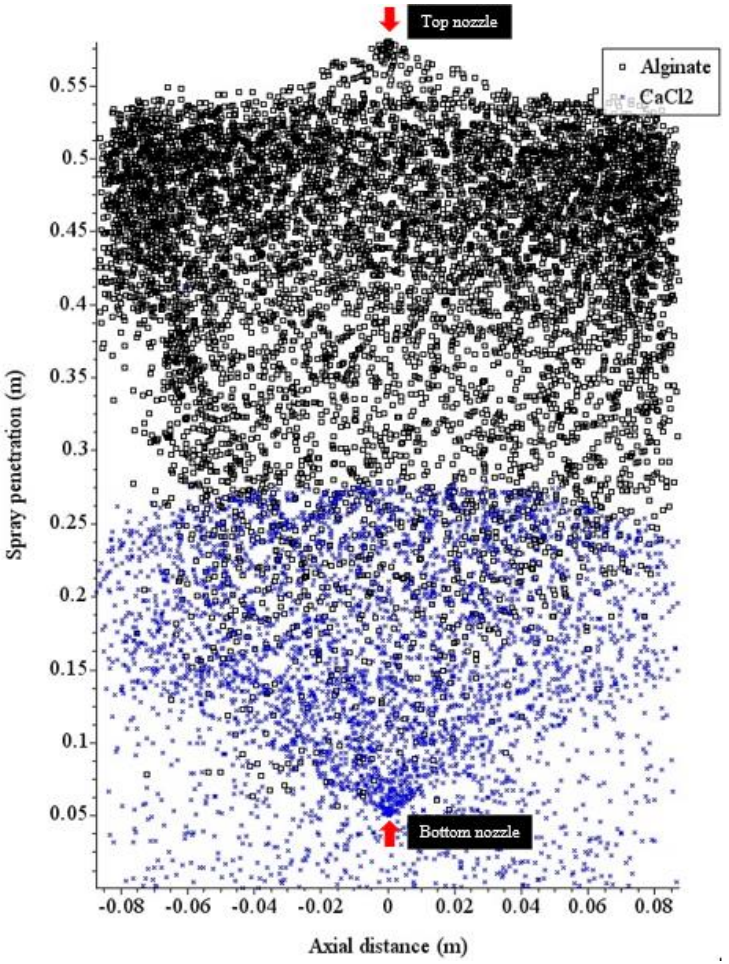

Figure 6.24 Droplets distribution of sprays of alginate and $CaCl_2$ at 60 ml/min of alginate flowrate, 1.5 % alginate concentration and 0.4 mm orifice size at 0.5 s

From Figure 6.22, it can be seen that the at 40 ml/min flowrate, alginate droplets were well dispersed within the $CaCl_2$ mists, indicating a great opportunity for alginate droplets to impinge with $CaCl_2$ mists, forming gelled beads. Besides, there was more space between alginate droplets indicating less chance of collision and coalescence. As for 50 ml/min (Figure 6.23), alginate droplets were also well distributed within the cross linking mists but the sprays were dense signifying that more collisions between alginate droplets which might results in formation of larger microbeads. Larger microbeads in the encapsulation of microbials is unfavorable as it would not be able to provide sufficient oxygen to the center region of microbeads resulting in low cell viability. At 60 ml/min (Figure 6.24), it is evident that the alginate sprays were not well spread within the $CaCl_2$ mists. This is associated with the fact that at high flowrate, small droplets size is produced which have less energy and travel less far. This causes lower likelihood of impingement between alginate droplets and $CaCl_2$ mists. By considering spray distribution and fluid film formation, alginate flowrate of 40 ml/min is deemed suitable for the application of impinging aerosol method in microbial encapsulation. Lower fluid film formation and well-distributed sprays ensure higher yield of products.

6.3 Model with collision and without collision

The sensitivity to collisions was evaluated by comparing the results for simulations with and without the NTC collision model. As expected, the particle size distribution is different when toggling the collision model as shown in Figure 6.25. Modeling of collisions resulted in increased frequency of larger particle size and wider particle size distribution most likely due to collisions between neighboring droplets. Modeling of droplet collisions have a significant effect on diameter distribution for dense sprays. As mentioned earlier, increasing in alginate flowrate results in a denser spray. From the simulation results, the total number of collisions for 40 ml/min, 50 ml/min and 60 ml/min was 4124, 7994 and 37901, respectively. As sprays become denser the total number of collisions between droplets increased significantly. Thus, to accurately predict the SMD value of sprays it is essential to activate the collisions model.

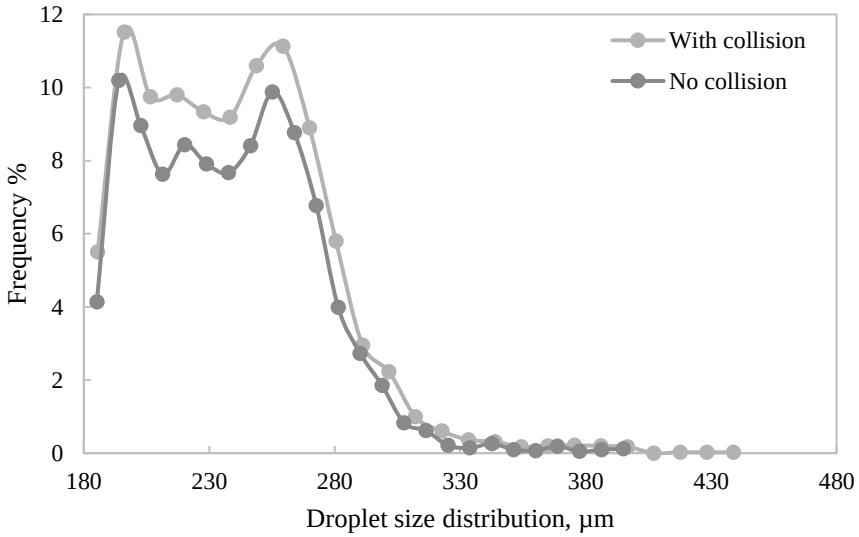

Figure 6.25 With and without NTC collision model at 40 ml/min, 1.5 % alginate concentration and 0.4 mm orifice size

6.4 Parametric studies

Three scenarios were investigated with the validated CFD model: (i) change in alginate concentration, (ii) change in nozzle orifice size and (iii) fine tuning of the Huh and Reitz-Diwakar break parameters which include K_A, c_4, and c_{b1} on spray outcomes.

6.4.1 Effect of alginate concentration on spray behaviors

The CFD model was used to study the effect of alginate concentration on spray behaviors such as the spray angle, SMD value, fluid film formation and droplets distribution of sprays of alginate and $CaCl_2$. Alginate concentration in the range of 1 to 2.5 % (w/v) were tested. The density, surface tension and dynamic viscosity at different alginate concentration were obtained from literature and tabulated in Table 6.1.

Table 6.1 Physical properties of alginate at different concentration (Del Gaudio et al., 2005)

Alginate concentration (%)	**1**	**1.5 (Default)**	**2.0**	**2.5**
Density, kg/m^3	1004	1007	1010	1012
Surface Tension, N/m	0.051	0.055	0.059	0.062
Dynamic viscosity, Pa.s	0.042	0.080	0.160	0.353

Figure 6.26 shows the droplet size distribution of alginate sprays at different flowrate. It can be observed that at 2.5 % alginate concentration, size distribution was more heavily weighted towards larger particles. Alginate concentration of 1 % to 2 % produced a smaller particle size distribution with particle size range within 160 to 400 µm. The frequency and droplets size were used to determine the SMD value by using Equation 6.1.

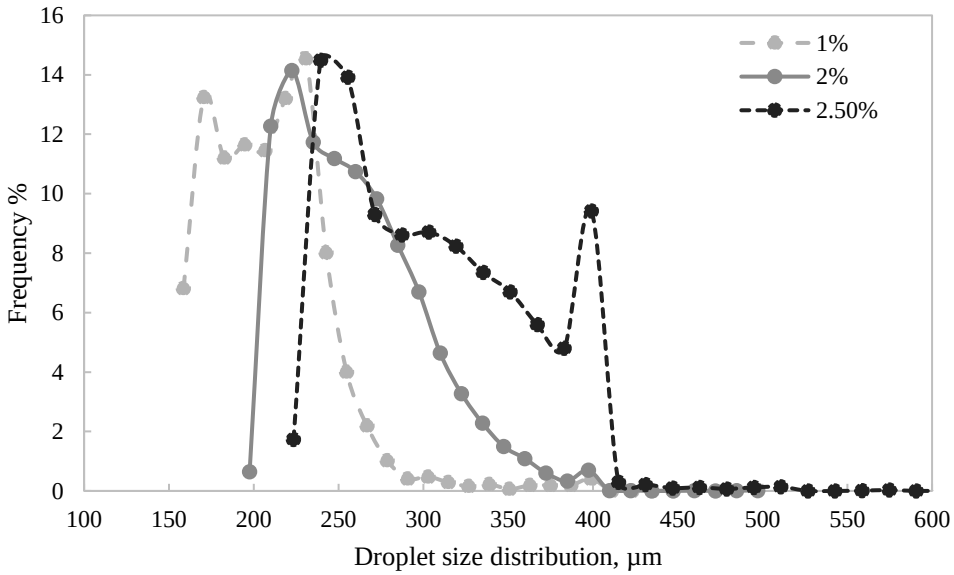

Figure 6.26 Droplet size distribution at different alginate concentration with 40 ml/min of alginate flowrate and 0.4 mm orifice size

The simulated spray angle at different flowrate were analyzed using ImageJ software as shown in Figure 6.27 to Figure 6.29.

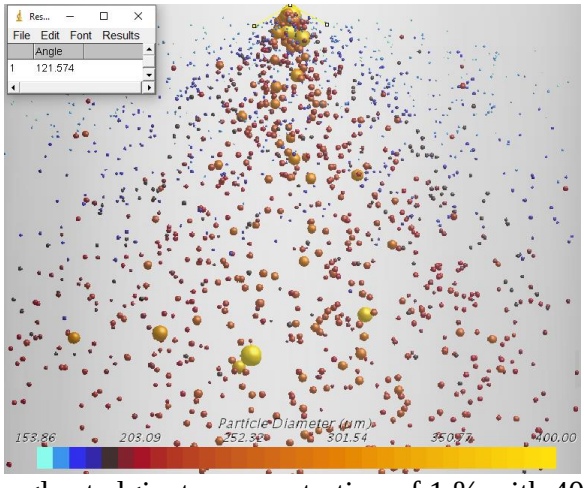

Figure 6.27 Spray angle at alginate concentration of 1 % with 40 ml/min of alginate flowrate and 0.4 mm orifice size

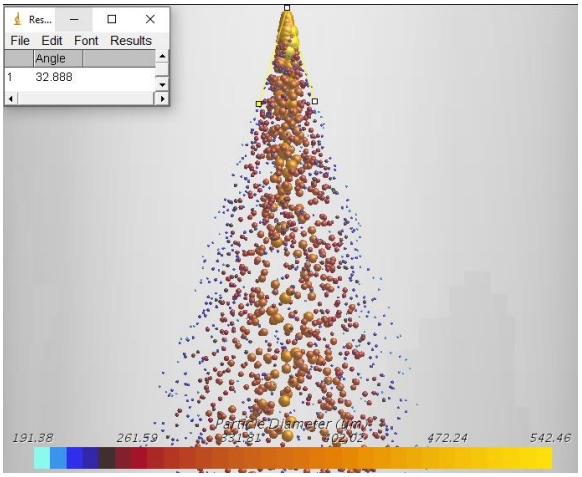

Figure 6.28 Spray angle at alginate concentration of 2 % with 40 ml/min of alginate flowrate and 0.4 mm orifice size

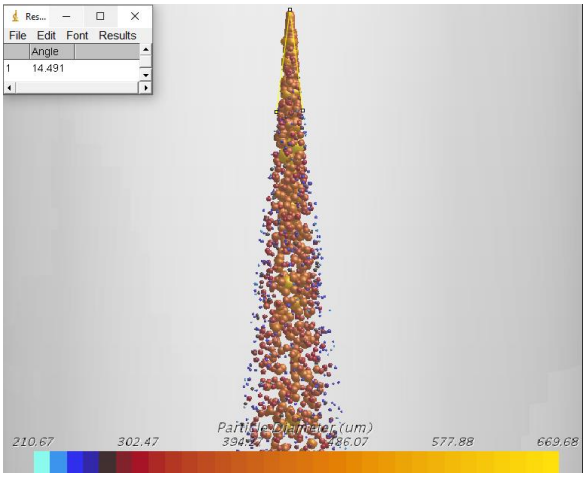

Figure 6.29 Spray angle at alginate concentration of 2.5 % with 40 ml/min of alginate flowrate and 0.4 mm orifice size

The SMD and spray angle of sprays at different alginate concentration were plotted in Figure 6.30. Based on Figure 6.30, when alginate concentration increased, the spray angle decreased. At alginate concentration of 1 %, the spray angle and SMD were 121.1° and 224.4 µm, respectively. By increasing the concentration to 1.5 %, 2 % and 2.5 %, the spray angle decreased to 82.8°, 32.9° and 14.5°, respectively while SMD increased to 251.0 µm, 273.7 µm and 327.1 µm, individually. These trends can be linked with the increasing viscosity and surface tension of alginate when concentration increases as shown in Table 6.1.

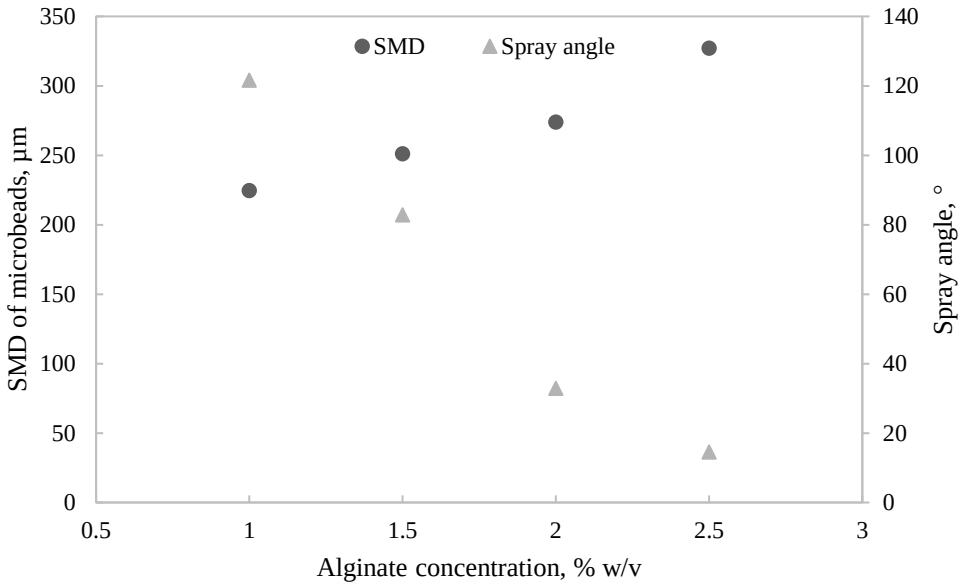

Figure 6.30 SMD and spray angle at different alginate concentration with 40 ml/min of alginate flowrate and 0.4 mm orifice size

When the alginate concentration increases from 1 % to 2.5 %, the surface tension increases from 0.05 N/m to 0.062 N/m and viscosity increases significantly from 0.042 Pa.s to 0.353 Pa.s. The cause of the decrease in spray angle with increasing viscosity is due to an increase in surface shear on the nozzles. At higher liquid viscosity, wall shear stress increases which retards the flow (Ahmed et al., 2009). This effect is relatively small for fluids with viscosities below 0.01 Pa.s but becomes more pronounced with higher viscosity.

Furthermore, when concentration increases, viscosity increases which reduces the Reynolds number of droplets exiting nozzle as shown in Equation 5.10. From the simulations, the Reynolds number at 1 %, 1.5 %, 2 % and 2.5 % was 133.96, 129.58, 115.15 and 111.35, accordingly. At 1 % alginate concentration, low viscosity leads to large Reynolds number and thus, the liquid sheet is thin, perturbed, and unstable with significant surface waves as shown in Figure 6.31(A). However, increasing the concentration to 1.5 % increases the viscosity which results in lower Reynolds number and thus, the sheet becomes thick and stable as illustrated in Figure 6.31(B). The liquid viscosity damps the surface waves and limits the spreading of the liquid sheet and therefore reduces the spray angle (Ahmed et al., 2009).

(A) 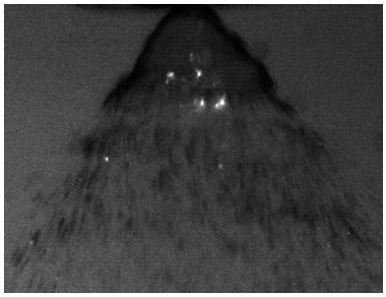 **(B)** 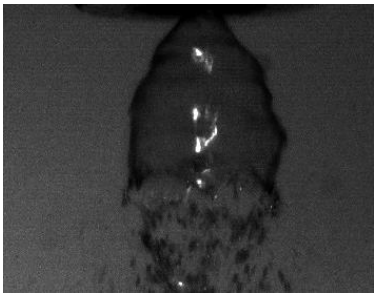

Figure 6.31 Liquid sheet at (A) 1 % alginate concentration and (B) 1.5 % alginate concentration with 40 ml/min of alginate flowrate and 0.4 mm orifice size

In addition, the simulated exit velocity of droplets from nozzle was found to be 5.30 m/s, 5.29 m/s, 5.28 m/s and 5.27 m/s at 1 %, 1.5 %, 2 % and 2.5 %, respectively. At high alginate concentration, the viscous force hinders the discharge of alginate from nozzle and results in more friction loss in the nozzle, and hence a lower velocity outside of the nozzle and causes a smaller spray angle. Similar trend was obtained by Chang and Farrell (1997), Davanlou et al. (2015) and Zhang et al. (2018) where sprays of high viscosity liquid had smaller spray angles when compared with low viscosity liquid. Moreover, Figure 6.30 also shows that when alginate concentration decreased, the spray angle increased significantly. This can be described by the fact that when alginate concentration decreases, the surface tension decreases. The reduction of surface tension leads to earlier sheet breakup due to an increase in the growth rate of the most unstable modes. An earlier sheet breakup indicates that the primary breakup occurs earlier which results in a smaller diameter of mother droplets and breaks into smaller child droplets (Davanlou et al., 2015). The smaller droplet size with lower surface tensions at the same spatial location leads to substantial centrifugal dispersion due to lower inertia leading to a wider spray cone angle (Butler Ellis et al., 2001). Similar result was reported by Kang et al. (2018), where an increased in liquid viscosity and surface tension suppressed the breakup and atomization of the conical liquid film. Besides, larger spray angle produces smaller droplets as there is more space to distribute the droplets and so there is less chance of collision and coalescence and a greater opportunity to atomize. The fluid film formation was also studied for different alginate concentration. These results were presented in Figure 6.32. From Figure 6.32(A), it can be observed that when alginate concentration was 1 %, liquid film formed were thicker than 1.5 % (Figure 6.21(A)). When the alginate concentration

increased to 2 % (Figure 6.32(B)) the film thickness significantly reduced. Figure 6.32(C) shows that there was no fluid film formation on wall for 2.5 % alginate concentration.

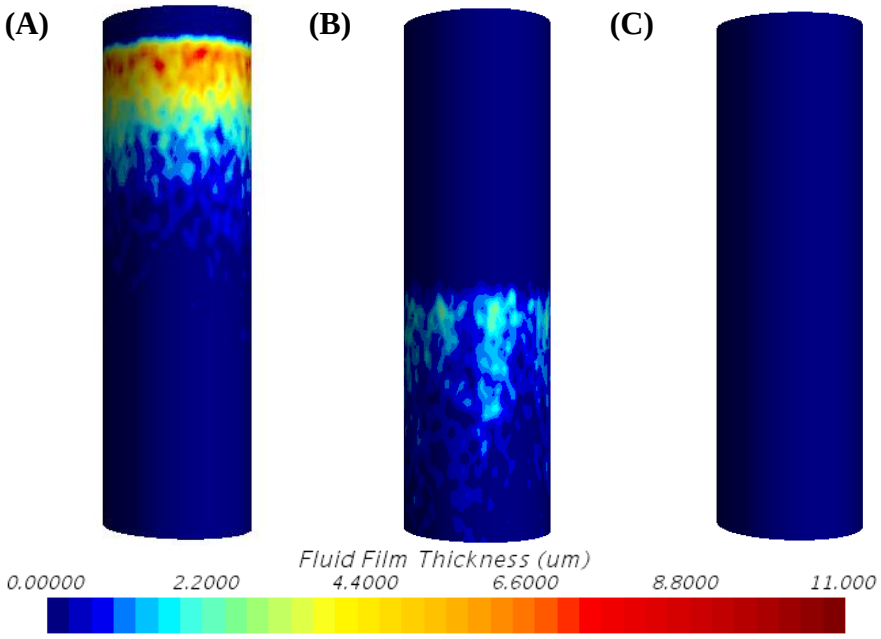

Figure 6.32 Film thickness of alginate at chamber wall at alginate concentration of (A) 1 % (B) 2 % and (C) 2.5 % with 40 ml/min flowrate and 0.4 mm orifice size at 0.5 s

The droplets distribution of alginate sprays at different alginate concentration were also studied and the results were presented in Figure 6.33, Figure 6.34 and Figure 6.35. From Figure 6.33, the alginate sprays at 1 % were too widely dispersed in the $CaCl_2$ mists. Less alginate droplets were available for the cross-linking with $CaCl_2$ as most of it were impinged on the wall. For 2 % alginate concentration (Figure 6.34), the spray distribution is very evenly distributed within the $CaCl_2$ mists and it is comparable with 1.5 % (Figure 6.22), indicating that the collision efficiency between alginate droplets and $CaCl_2$ is high. As for 2.5 % concentration (Figure 6.35), the spray distribution was more heavily dispersed in the center and alginate droplets were closely packed. This spray pattern is unfavorable as it increases the chance of agglomeration of alginate microbeads. Based on the spray distribution and fluid film formation, low alginate concentration of 1 % is undesirable due to thick fluid film formation and poor alginate spray distribution within mists. These issues could result in low production of microbeads and product loss. Remarkably, 2 % alginate concentration is the most appropriate due to its uniform droplets distribution and lower fluid film formation which assure high throughput.

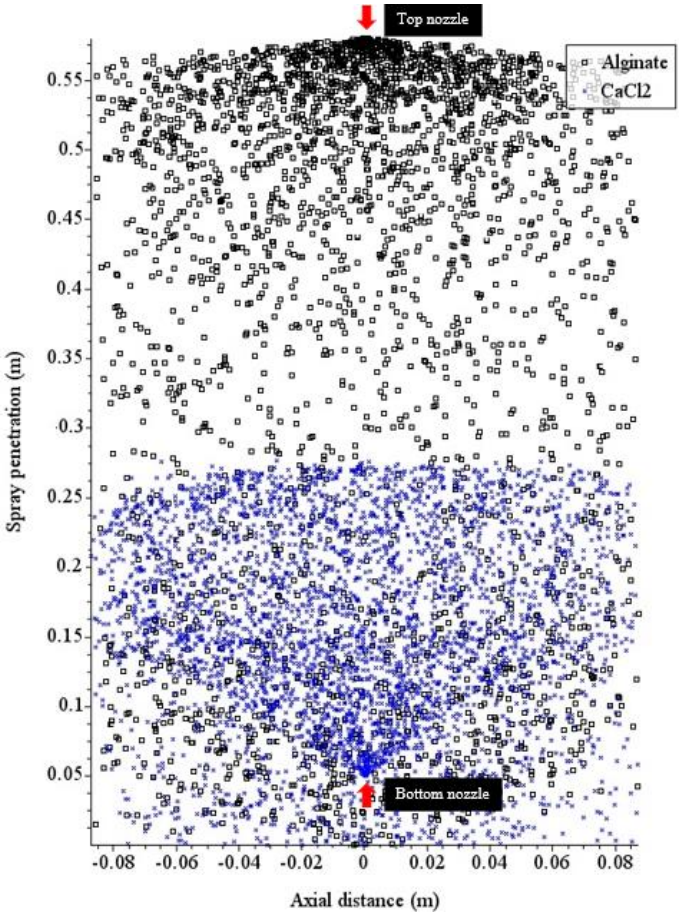

Figure 6.33 Droplets distribution at 1 % alginate concentration with 40 ml/min flowrate and 0.4 mm orifice size at 0.5 s

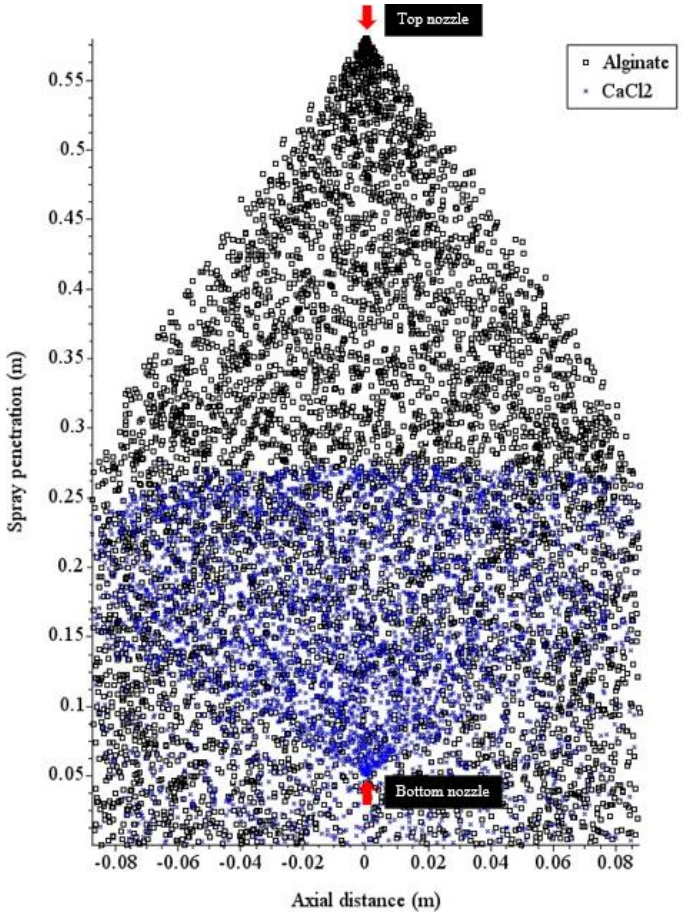

Figure 6.34 Droplets distribution at 2 % alginate concentration with 40 ml/min flowrate and 0.4 mm orifice size at 0.5 s

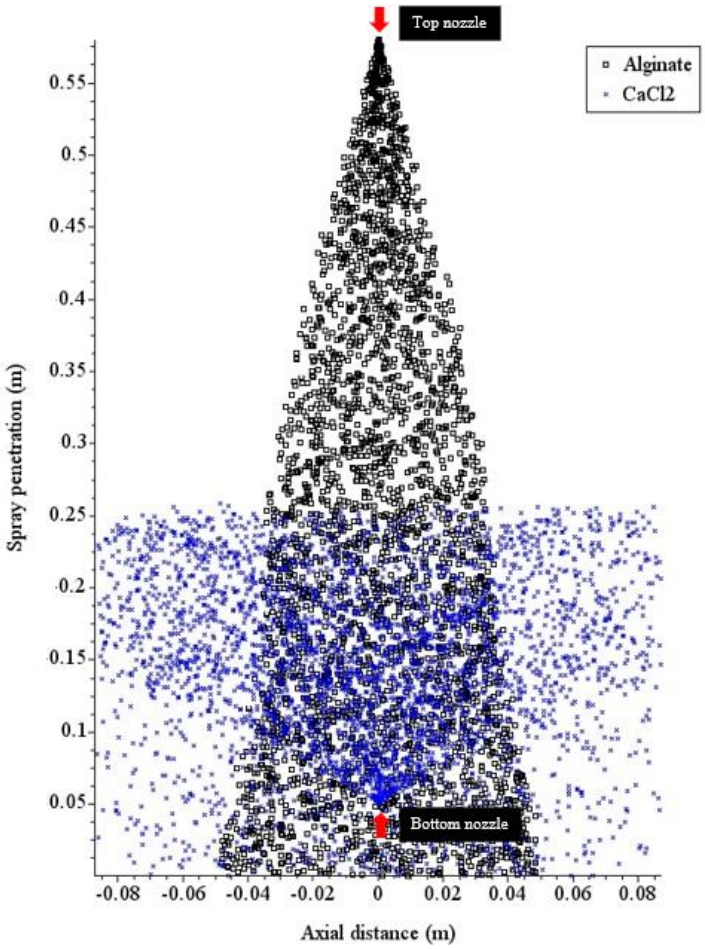

Figure 6.35 Droplets distribution at 2.5 % alginate concentration with 40 ml/min flowrate and 0.4 mm orifice size at 0.5 s

6.5 Effect of nozzle orifice size on spray behaviors

Besides, the effect of nozzle orifice size on spray behaviors was also studied. The effect of orifice size on droplets' SMD and spray angle was studied within the range of 0.2 mm to 0.50 mm while alginate concentration and flowrate were kept constant at 1.5 % (w/v) and 40 ml/min, respectively. Figure 6.36 shows the droplet size distribution at different orifice size. The droplet size distribution was wider with greater orifice size. The frequency and size of droplets were used to calculate the SMD under different orifice size. Meanwhile, Figure 6.37 to Figure 6.39 show the simulated spray angle under various orifice size. The spray angle was determined by using the ImageJ software.

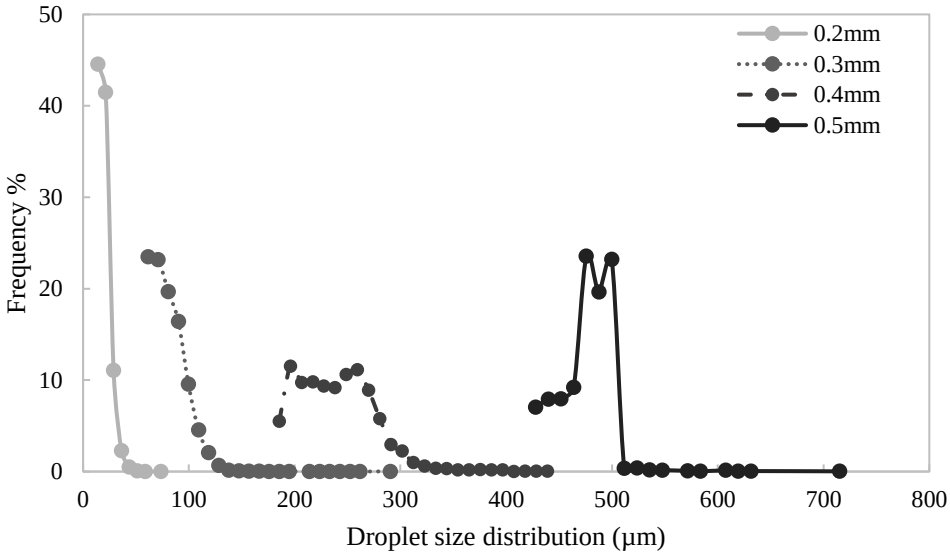

Figure 6.36 Particle size distribution at different nozzle size at 40 ml/min alginate flowrate and 1.5 % of alginate concentration

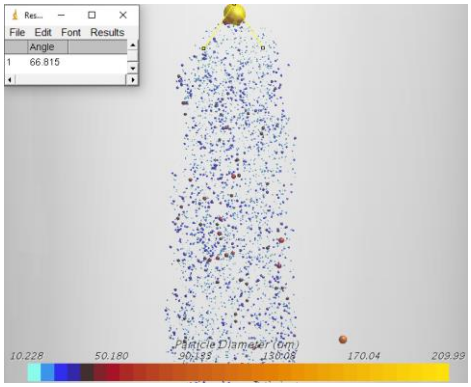

Figure 6.37 Spray angle with 0.20 mm nozzle orifice size at 40 ml/min alginate flowrate and 1.5 % alginate concentration

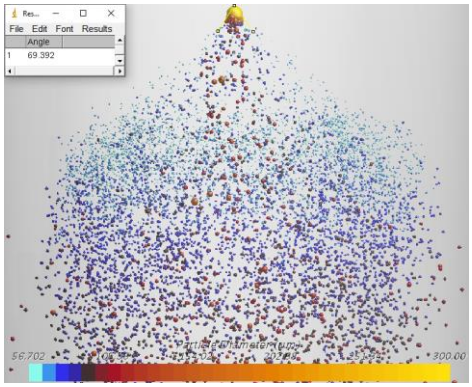

Figure 6.38 Spray angle with 0.30 mm nozzle orifice size at 40 ml/min alginate flowrate and 1.5 % alginate concentration

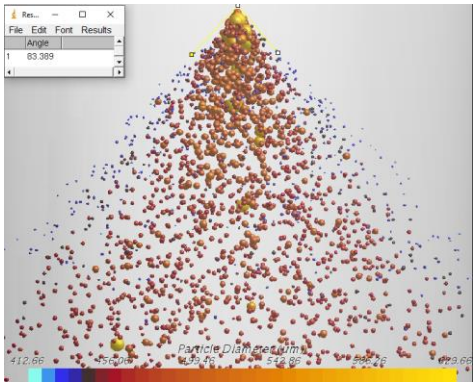

Figure 6.39 Spray angle with 0.50 mm nozzle orifice size at 40 ml/min alginate flowrate and 1.5 % alginate concentration

The calculated SMD and spray angle were plotted against orifice size in Figure 6.40.

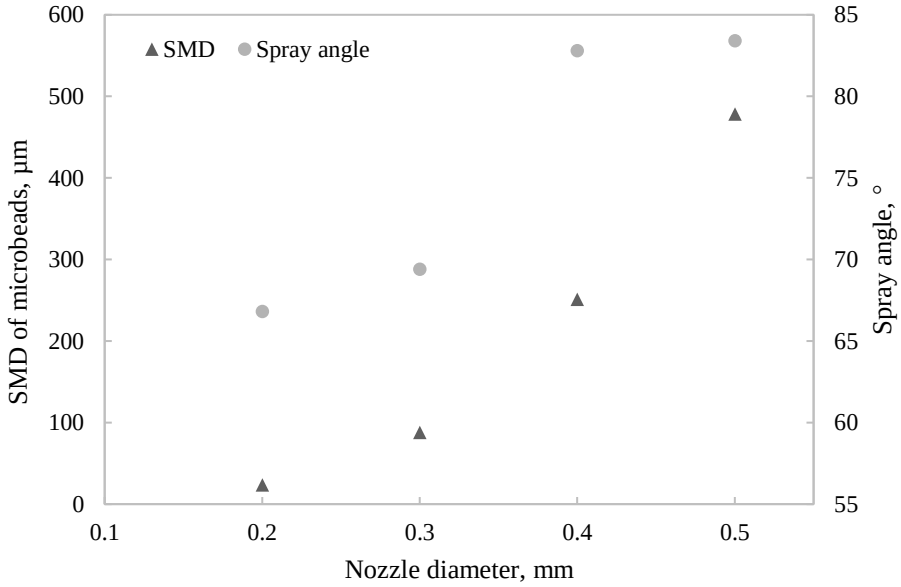

Figure 6.40 SMD and spray angle at different nozzle diameter at 40 ml/min alginate flowrate and 1.5 % of alginate concentration

Referring to Figure 6.40, it is evident that smaller orifice size produced smaller droplets size and spray angle. When nozzle orifice size was 0.2 mm and 0.3 mm the SMD of 23.4 µm, and 87.8 µm were obtained, accordingly. However, when nozzle orifice size was 0.4 mm and 0.5 mm, the SMD value was larger with droplets size of 251.0 µm and 478.2 µm, respectively. Nozzle with larger orifice diameter produces longer liquid film which increase the resistance of spray to disintegrate earlier and results in a greater droplets size. According to the simulation results, at 0.2 mm, 0.3 mm, 0.4 mm and 0.5 mm, the droplets

exit velocity was 21.2 m/s, 9.41 m/s, 5.29 m/s, 3.39 m/s, respectively. The velocity of droplets reduced significantly with orifice size. As the liquid velocity decreases and the aerodynamic effect on the liquid sheet reduces and results in a greater droplet size and spray angle (Zhang et al., 2017). This trend is in agreement with results obtained by various researchers. Ahmed et al. (2009), Chu et al. (2008) and Hussein et al. (2012) observed that an increase in orifice diameter increases the spray angle and SMD. Moreover, the fluid film formation at different orifice size were studied and the results were presented in Figure 6.41.

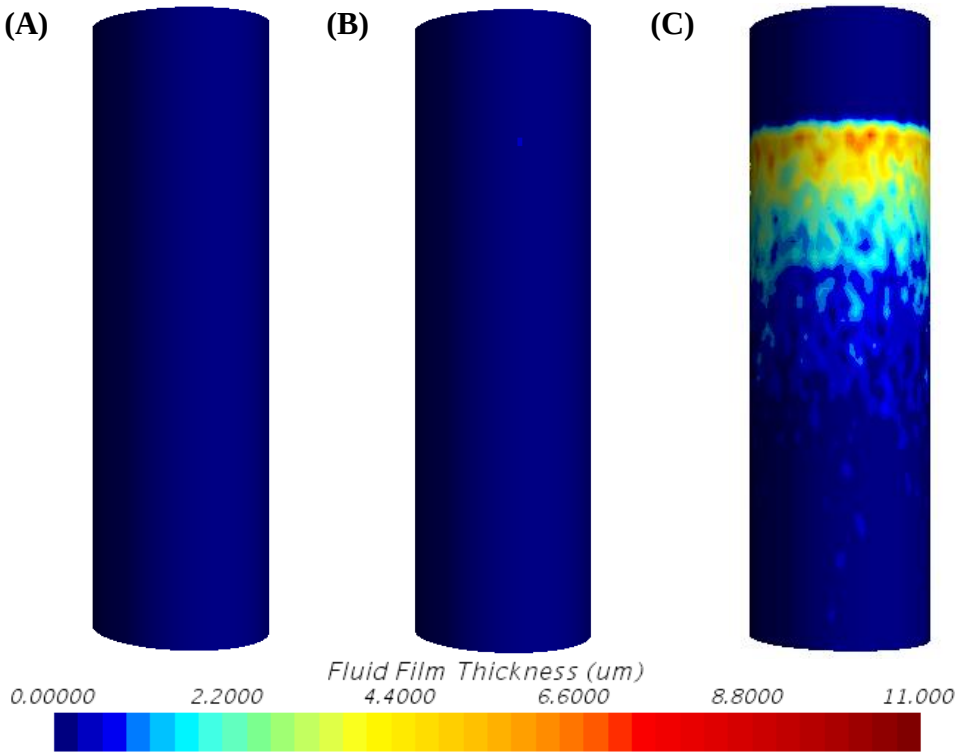

Figure 6.41 Film thickness of alginate at chamber wall at nozzle size of (A) 0.20mm, (B) 0.30 mm and (C) 0.50mm at 40 ml/min alginate flowrate and 1.5 % of alginate concentration at 0.5 s

Based on Figure 6.41 when the nozzles size was and 0.2 mm, no fluid film formed on the wall due to small spray angle. However, spray angle increased with 0.30 mm nozzle orifice size and some fluid film formation can be observed as shown in Figure 6.41(A). By comparing Figure 6.41(B), the fluid film formation for 0.5 mm orifice diameter and Figure 6.21(A) for 0.4 mm, it is remarkable that even though nozzles size of 0.5 mm had a wider

spray angle than 0.4 mm, its fluid film thickness was thinner. This is probably due to the lower exit liquid velocity at larger orifice size and thus, the droplets travel less far in the radial direction. Figure 6.42 to Figure 6.44 show the droplets distribution of sprays of alginate at different orifice size with 40 ml/min alginate flowrate, 1.5 % alginate concentration at 0.5 s.

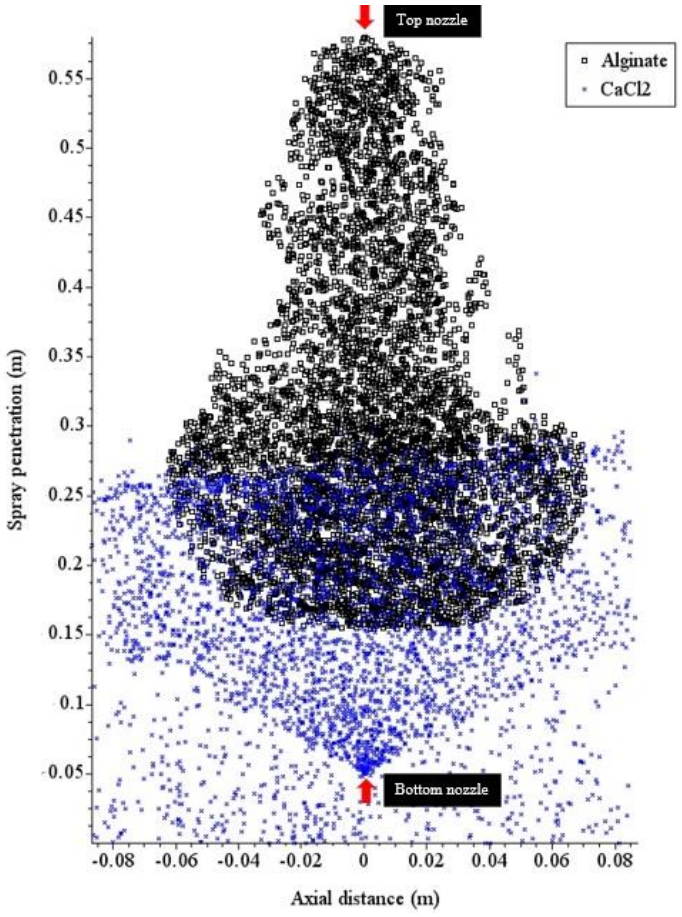

Figure 6.42 Spray distribution of alginate and $CaCl_2$ at 0.20 mm nozzle orifice size at 40 ml/min alginate flowrate and 1.5 % of alginate concentration at 0.5 s

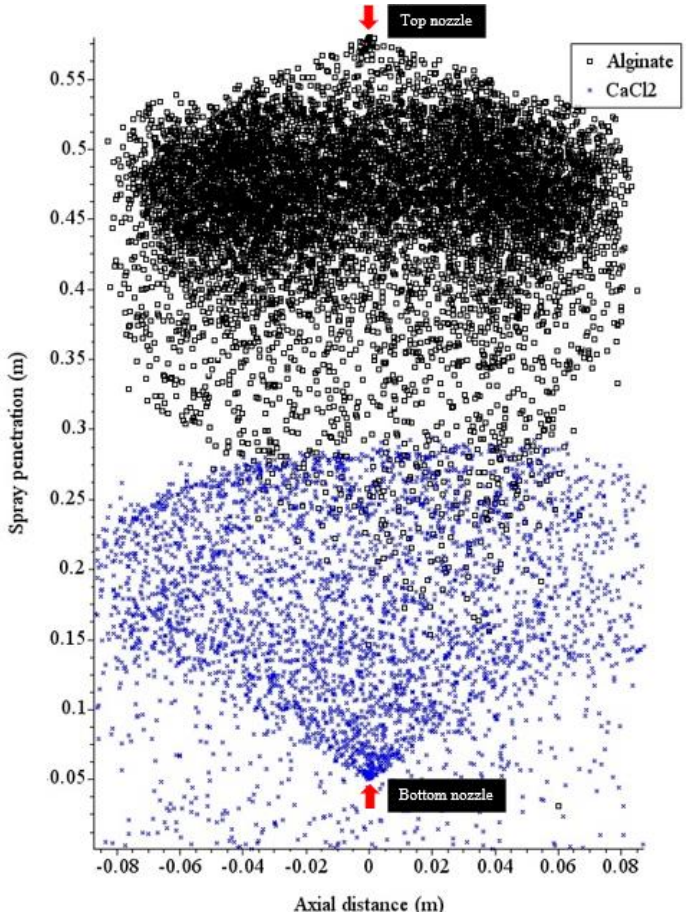

Figure 6.43 Spray distribution of alginate and $CaCl_2$ at 0.30 mm nozzle orifice size at 40 ml/min alginate flowrate and 1.5 % of alginate concentration at 0.5 s

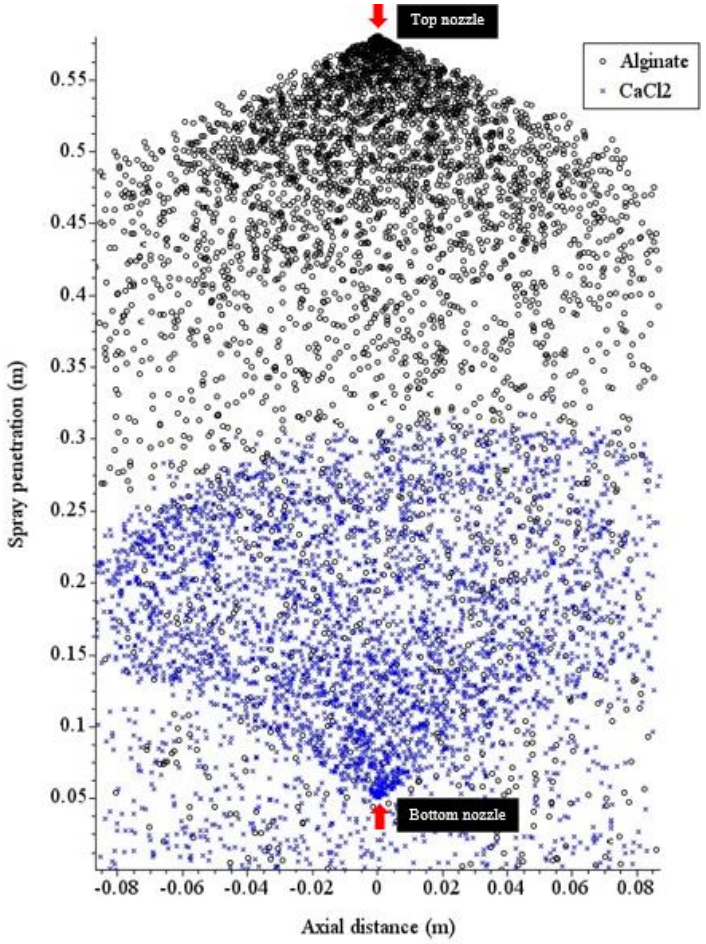

Figure 6.44 Spray distribution of alginate and $CaCl_2$ at 0.50 mm nozzle orifice size at 40 ml/min alginate flowrate and 1.5 % of alginate concentration at 0.5 s

At 0.2 mm orifice size, irregular spray pattern was observed possibly due to the small droplets formed. The sprays remain airborne and drift away from their initial trajectory because of their light weight and small size. As reported by Sampath (2005), aerodynamic forces have a significant effect on the trajectories of the small droplets. At 0.3 mm orifice size, the droplets were heavily dispersed at the top of the chamber. This is because tiny droplets have no energy of their own and move with the air mass they are released into. In still air, the droplets fraction tends to stay aloft and concentrated. These results showed that orifice size of 0.2 mm and 0.3 mm are unsuitable in the application of impinging aerosol due to their poor droplets distribution. At 0.5 mm, the alginate spray is well-distributed. Thus, it can be hypothesized nozzle orifice size of 0.4 or 0.5 mm seems appropriate in the impinging aerosol application.

6.6 Spray Model Tuning

As presented in Chapter 5, the primary and secondary breakup models can be altered through the physical phenomena, such as breakup rate, the unstable droplet lifetime or atomization time scale. These phenomena can be controlled by some coefficients, which appear in the equations describing the models and which are accessible through the commercial code interface. Thus, current study aimed to study the effect in altering the parameters on spray behaviours. Concerning the modeling of the primary atomization, as shown in Equation 5.17, the breakup rate, K_A is responsible for diameters' speed decrease. From Equation 5.15 which describes $\tau_{A,}$ it can be seen that the atomization can be prolonged (droplets fragmentation slows down) or shortened (faster breakup) by changing the parameters C_3 and C_4. As reported by Wojdas (2010) the growth of C_3 and C_4 would have the same effect on the bresakup rate, thus this study focused on the effect of C_4, time scale caused by the KH wave growth mechanism (Baumgarten, 2006). Various constants' values were chosen in order to study the effects of the droplets' breakup rate, K_A and the atomization time scale, $C_{4.}$ By increasing $K_{A,}$ the breakup rate is expected to decrease and so longer atomization. The growth of C_4 would act on the droplets size, as well as on the spray angle. The secondary breakup phenomenon can be also affected by modifying the equations of unstable droplet lifetime, for bag and/or stripping breakup regime. As this study involved low pressure sprays, only bag breakup mode is expected. From Equation 5.22, C_{b2} define the unstable state duration of a droplet before fragmentation in the bag

breakup regime. The general trend linked by decreasing the constants C_{b2} will result in an earlier atomization and an associated momentum loss, thus decreasing spray penetration length (Brulatout et al., 2016).

K_A is a parameter which controls the droplets size of sprays. The droplets size of the global spray is primarily controlled by the mother parcels of the Huh model which are responsible for emulating the liquid core. At lower value of K_A, the atomization proceeds faster due to the faster growths of stripped mass, and consequently, the Huh breakup produces mother droplets with lesser mass and as a consequence with smaller diameters. Figure 6.45 shows the droplets size distribution at different K_A value.

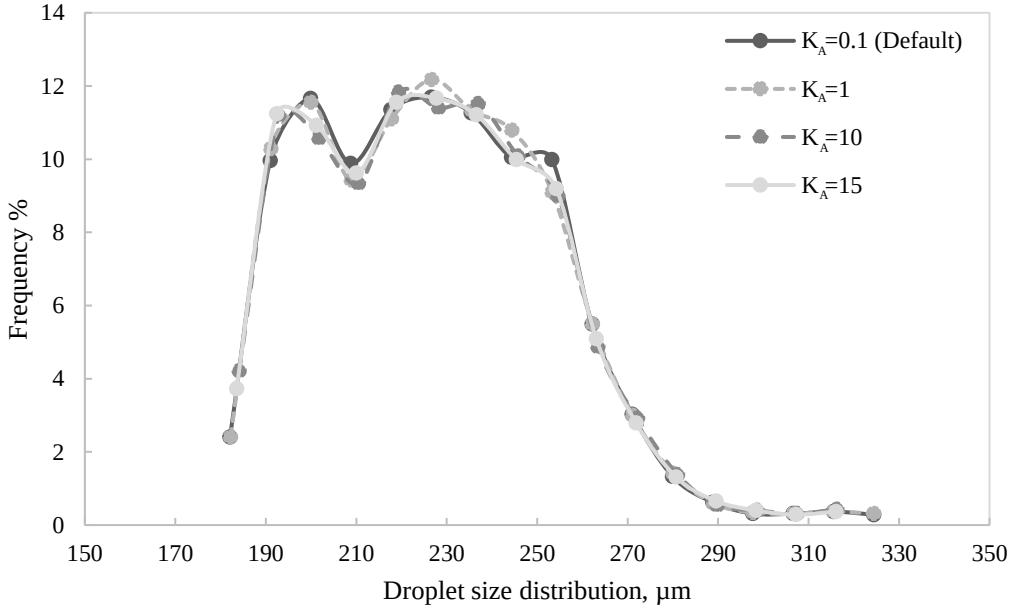

Figure 6.45 Size distribution of droplets at different K_A value, alginate flowrate of 40 ml/min, 1.5 % alginate concentration and 0.4 mm orifice size

Referring to Figure 6.45, when K_A increased from default value of 0.1 up to 15, there was no visible effect on the size distribution of droplets. The spray angle and spray penetration length with different K_A value were studied and the results were illustrated in Figure 6.46. It can be observed that the spray angle and spray penetration length were almost insensible to the increase of the K_A, a parameter responsible for the diameter decrease speed. Similar results was reported by Wojdas (2010), where an increase in K_A had negligible effect in spray penetration length.

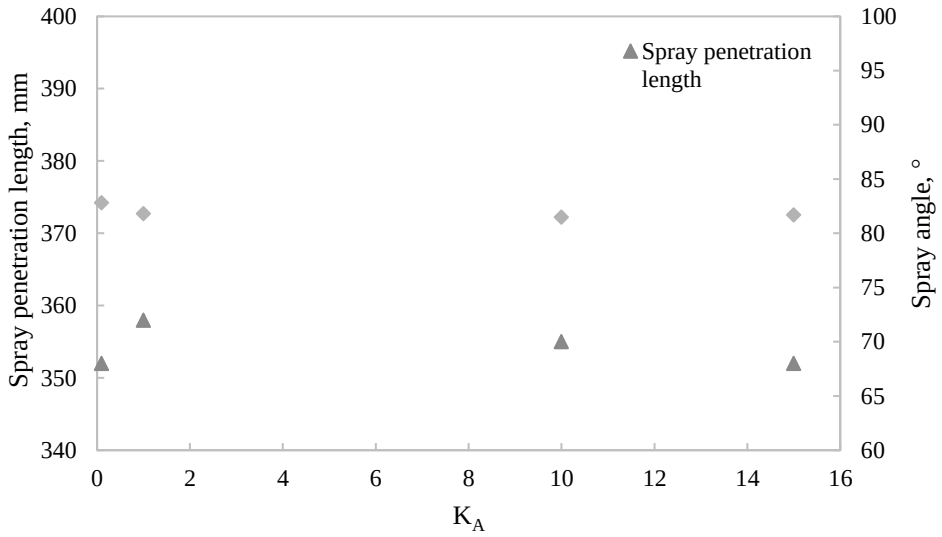

Figure 6.46 Effect of K_A on spray angle and spray penetration, alginate flowrate of 40 ml/min, 1.5 % alginate concentration and 0.4 mm orifice size

As for the studies of the atomization time scale parameter, this study focused on the C_4 parameter to simulate jet behaviour for slower and faster primary breakup. Slower primary breakup was achieved by increasing the C_4 above default value of 1.5, whereas faster primary breakup was accomplished by reducing C_4 below 1.5. The droplet size distribution at different C_4 value was plotted in Figure 6.47.

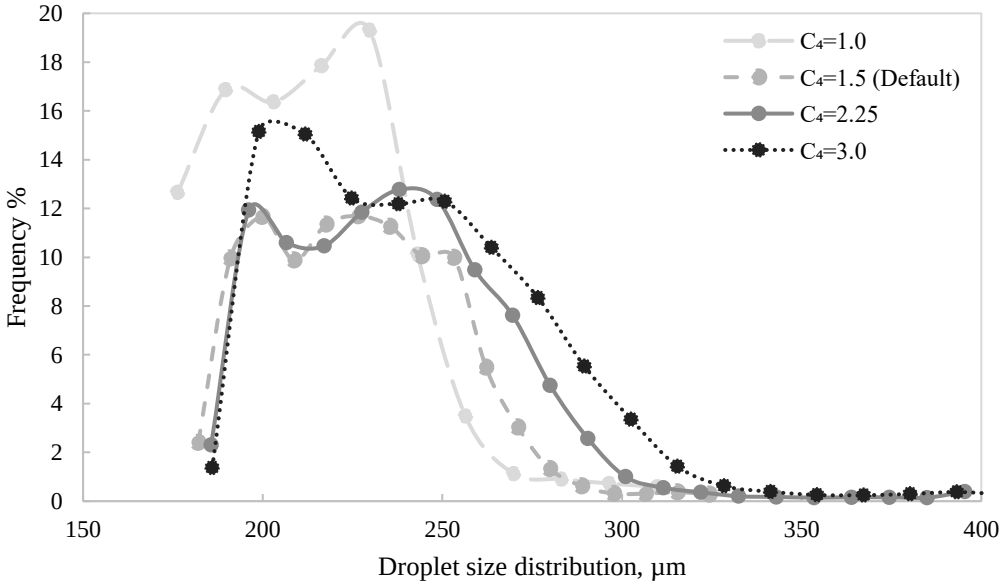

Figure 6.47 Size distribution of droplets at different C_4 value, alginate flowrate of 40 ml/min, 1.5 % alginate concentration and 0.4 mm orifice size

Referring to Figure 6.47, When C_4 increased above 1.5, it can be observed that wider droplet distribution was obtained and more droplets with greater size was produced. Thus, it can be hypothesized that an increase in C_4 value leads to an increase in SMD value. When primary breakup is slower, the breakup generates larger parents droplets and which results in child droplets with larger diameters due to later breakups which suffer from the turbulence decay (Aguerre et al., 2019). The spray angle and spray penetration length results for various C_4 values were presented in Figure 6.48.

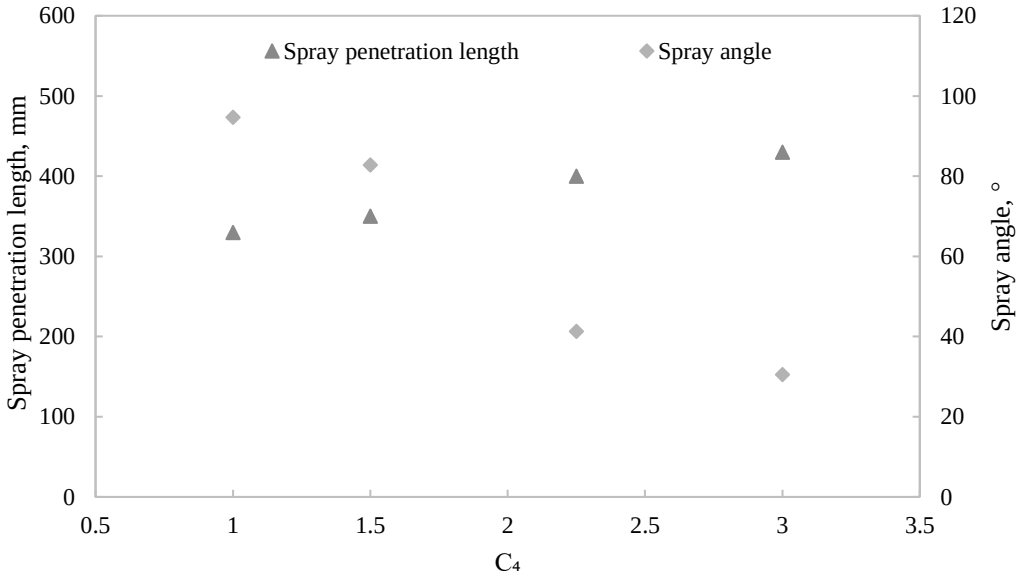

Figure 6.48 Effect of C_4 on spray angle and spray penetration, alginate flowrate of 40 ml/min, 1.5 % alginate concentration and 0.4 mm orifice size

Based on Figure 6.48, it can be detected that such a C_4 has an important influence on the simulated spray penetration length and spray angle. This behaviour can be explained by the fact that the atomization time scale, τ_A, affects not only the breakup rate but also the shape of the simulated jet (semi-cone angle), as indicated in the Equation 5.18. Once τ_A increases by increasing C_4, the droplets follow more radial directions (spray cone angle increase), the liquid penetration shortens (Wojdas, 2010). In addition, when spray angle decreases, the sprays become denser and droplet collision occurs frequently in dense sprays (Hou & Schmidt, 2006). As reported by Finotello et al. (2017) and Wu et al. (2020), the droplet size is significantly affected by the collision dynamics. Larger droplets tend to form when coalescence happens.

The physical phenomena of the secondary breakup duration can be controlled by the constant C_{b2}. Increasing this parameter leads to the unstable droplet lifetime extension, in other words, slower breakup of the secondary droplets. Figure 6.49 shows the droplet size distribution with different C_{b2} values.

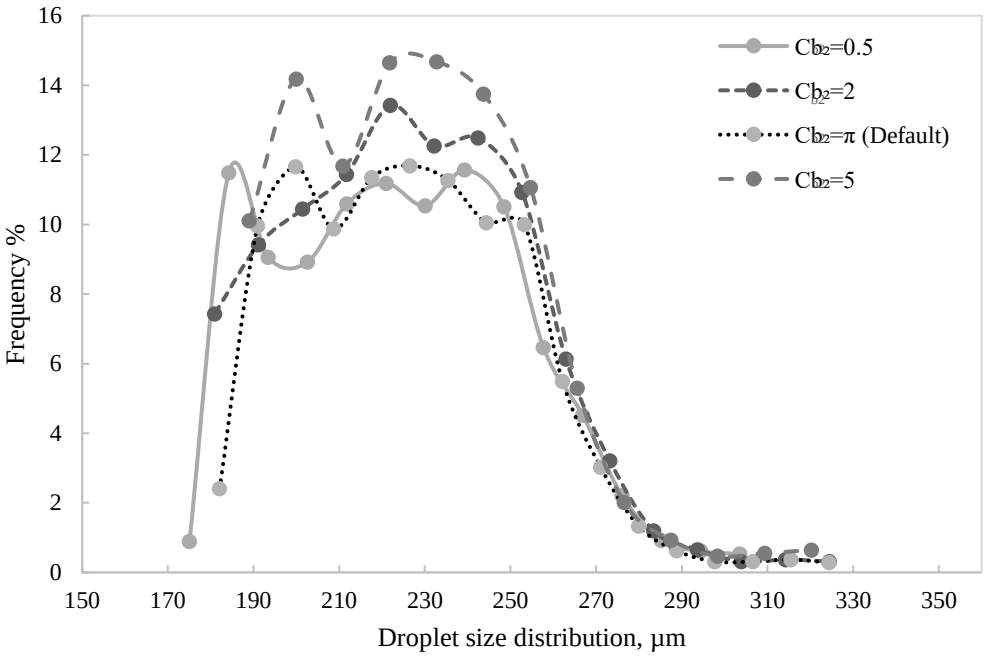

Figure 6.49 Size distribution of droplets at different c_{b2} value, alginate flowrate of 40 ml/min, 1.5 % alginate concentration and 0.4 mm orifice size

As presented in Figure 6.49, the obtained results confirmed the theory where greater C_{b2} value (C_{b2}=5) prolonged unstable droplet lifetime, the size of droplet decreases slower which leads to a greater droplets size. When C_{b2}=π, the smallest droplets size obtained was 182µm, whereas when C_{b2} was 5, 189 µm were produced. At C_{b2} of 0.5 and 2, smallest droplets size obtained was 175 µm and 180 µm, correspondingly. By decreasing the value of C_{b2}, it accelerates the breakup process and faster fragmentation could be achieved. As shown in Figure 6.50 with unstable droplet lifetime diminishing (lower C_{b2} value), the spray penetration length decreased, which is the direct result of smaller droplets diameters having less momentum. Nevertheless, by altering the value of C_{b2} did not affect the spray angle and spray penetration length is only slightly affected.

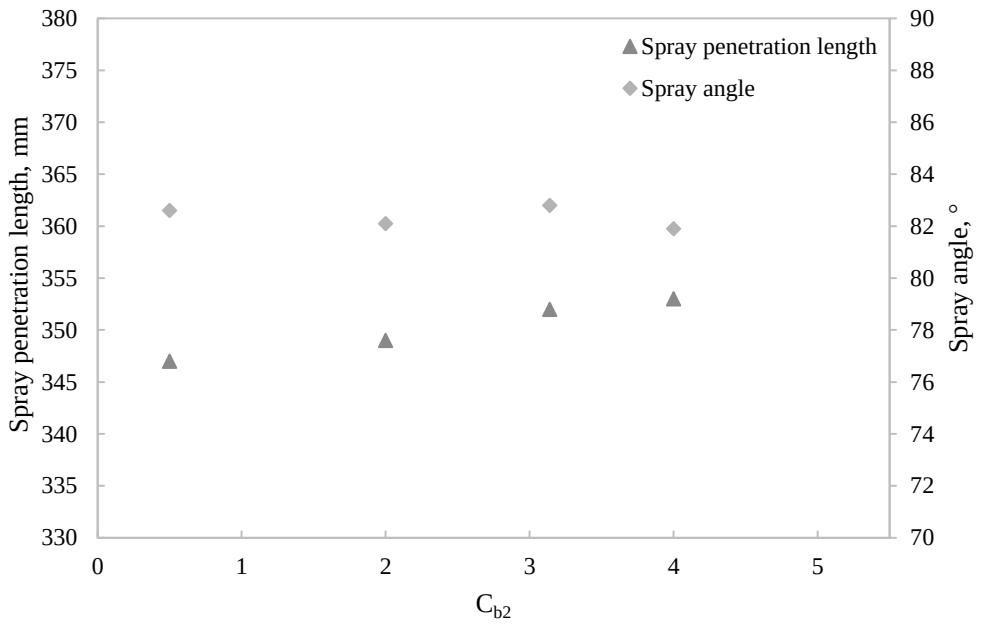

Figure 6.50 Effect of C_{b2} on spray angle and spray penetration, alginate flowrate of 40 ml/min, 1.5 % alginate concentration and 0.4 mm orifice size

In summary, valuable findings regarding effect of parameters of Huh and Reitz-Diwakar on spray outcomes were determined. It was observed that at low pressure sprays application, K_A has negligible effect on spray behaviors. While, C_4 has a greater effect on droplets size, spray penetration length and spray angle. Slight tuning of the value of C_{b2} significantly affects the diameter of the droplets resulting from the secondary atomization. Remarkably, C_4 and C_{b2} can be used to fine tune the validated model based on the experimental results in the future research works under different operating conditions. Satisfactory results in terms of spray outcomes can be achieved if proper tuning is adopted.

6.7 Concluding remarks

Experiments results with different alginate flowrate were used to validate the simulation results obtained and then the validated model was used for parametric studies. Some of the key findings are:

1. Spray angle increased and SMD decreased with increasing flowrate. Good agreement was obtained for SMD and spray angles between experiments and simulations. Well-distributed droplets distribution of alginate sprays within $CaCl_2$ mists was observed at alginate flowrate of 40 ml/min.

2. By increasing the alginate concentration, spray angle was reduced and SMD was larger. Alginate concentration of 2 % was found to be the most suitable concentration to be used in impinging aerosol application due to its uniform spray distribution and minimal fluid film formation.
3. An increase in nozzle orifice size caused the spray angle and SMD to increase. Orifice size of 0.4 mm and 0.5 mm were found to be appropriate for the impinging aerosol techniques due to its desirable SMD of alginate droplets. The alginate sprays were well dispersed within the $CaCl_2$ mists which allows high encapsulation efficiency.

Besides, the parameters in primary and secondary breakup that involve in breakup rate and atomization time were studied. The main purpose of sensitivity analysis is to provide insight on which parameter is important for break up mechanism and allows future researches to pay more attention to carry out experiments to determine better prediction of the parameters. Some of the findings include:

1. Breakup rate, K_A had negligible influence on droplets size, spray penetration length and angle.
2. The atomization time scale, C_4 changes affect mainly the droplets size distribution, spray cone angle and spray penetration length.
3. Secondary breakup can be modified through the variation in the duration of the droplets' breakup, C_{b2}. Results shown that C_{b2} had desirable effect on droplets size but very slight influence on the spray length penetration and negligible effect on spray angle.

CHAPTER 7

CONCLUSION AND RECOMMENDATION

This chapter represents a conclusion to the work achieved in this doctoral dissertation. The main findings and contributions are highlighted and follows by recommendations of potential future works.

7.1 Conclusion

The first objective of the present work is to identify the native PSMs that possess the ability to solubilize fixed phosphate in soil. Isolation of PSMs from peat was done as it was reported by various researchers that PSMs isolated from stressed environment would have the tendency to solubilize more phosphate that PSMs isolated from mild condition environment. Peat is very acidic and thus it can be hypothesized that PSMs obtained from peat would be able to survive the high acidity and compete with the native microflora. Isolation from peat ensures that the PSMs isolated is suitable to be used as microbial inoculant for acid-soil based agriculture. The findings showed that *Staphylococcus sp.* isolated from tropical peat has the capability to solubilize insoluble phosphate. When tested in modified NBRIP broth, *Staphylococcus haemolyticus* HCLB02 had the highest phosphate solubilization potential. The culture medium with glucose, yeast and magnesium chloride hexahydrate concentration of 10 g/L, 2 g/L and 5 g/L, respectively gave the highest phosphate solubilization activity of 39.65 ppm. This can be associated with the cell growth of *Staphylococcus haemolyticus* HCLB02. At optimized culture medium, cell growth is highest and thus, more organic acids are produced. These organic acids act as chelating agent and form stable complexes with Al^{3+} ions releasing soluble

phosphate for plant uptake. To the best of the authors' knowledge in this work, this is the first report on the $AlPO_4$ solubilization ability of *S. haemolyticus*.

Microencapsulation is a useful method in enhancing the survival of PSMs in harsh soil environment after inoculation. However, conventional extrusion method is a batch process and limit the process scale up. Thus, the feasibility of a continuous impinging aerosol method to encapsulate cells was demonstrated in this study. Alginate microbeads in a range of 100 to 300 μm in size, encapsulating *S. haemolyticus* as active ingredient were produced by a novel technique involving dual aerosols of alginate solution and $CaCl_2$ cross linking solution. Cell viability of dried microbeads was optimized by varying three parameters namely alginate flowrate, alginate concentration and $CaCl_2$ concentration and the optimized conditions were found to 40 ml/min of alginate flowrate, 1.5 % (w/v) alginate concentration and 0.1 M $CaCl_2$. The results obtained showed that cell viability was approximately 54 % after lyophilization with 0.54×10^9 CFU/g of dried microbeads. It is believed that the cell concentration of dried beads obtained is sufficient to obtain positive response from plants as various researchers have been reporting that minimum count of viable cells of 10^7 to 10^9 CFU/g is required. The cell release of PSMs from dried microbeads was investigated and it was found that cell release followed the main Case II release mechanism with skeleton corrosion mechanism. Microbeads swell by absorbing water follows by partial disintegration of matrix and thus, releasing the bacteria.

Generally, the microencapsulation of PSMs by using the impinging aerosol method can be controlled by altering the physical properties of solutions, operating conditions and type of nozzles. These parameters can be adjusted to control the spray outcomes which include droplets' distribution, spray angle, droplets size and fluid film formation on encapsulation chamber wall. However, it is impracticable to test these parameters experimentally as it is time consuming and unsustainable. Hence, CFD model with Eulerian-Lagrangian framework was developed to predict the spray outcomes. Huh model and Reitz-Diwakar were employed for primary and secondary atomization, respectively. The impingement of spray droplets on wall was modeled with Bai-Gosman model. The numerical results showed good agreement when validated with against experimental results. Based on the spray distribution and fluid film formation, alginate flowrate of 40

ml/min seems to be appropriate for the application of impinging aerosol method in microbial encapsulation due to its lower fluid film formation and well-distributed sprays when compared with 50 ml/min and 60 ml/min. The validated model was then used to investigate the effects of alginate concentration and nozzle orifice size on spray behaviors. Based on the results obtained for SMD, spray distribution and fluid film formation, it was observed that alginate concentration of 2 % and orifice size in the range of 0.4 mm to 0.5 mm are suitable for the production of alginate microbeads. At 40 ml/min with 2 % of alginate concentration and orifice size of 0.4 mm or 0.5 mm, well-dispersed sprays and desirable SMD of microbeads can be achieved. The primary and secondary breakup phenomena was also investigated by adjusting the parameters such as K_A, C_4 and C_{b2}. Results showed that breakup rate, K_A has negligible effect on the droplets size while the time scale parameter, C_4 and unstable droplet lifetime, C_{b2} have significant effect on the droplets diameter. These parameters can be used to fine tune the model based on experimental results in the future works.

The key findings and novel contributions of this works are summarized below:

1. *Staphylococcus haemolyticus* HCLB02 isolated from peat possesses the ability to solubilize insoluble fixed phosphate. It can be hypothesized that *S. haemolyticus* HCLB02 is suitable to be used as microbial inoculant in the acid or peat-based agriculture.

2. The production of PSMs-loaded alginate microbeads by employing the impinging aerosol method is feasible. Under optimized operating conditions, microbeads with average particle size of 250 µm can be obtained with high cell viability. It seems that there is a great potential for this method to be used in the mass production of PSMs-loaded alginate microbeads as microbial inoculant.

3. The validated CFD model could be used to predict the spray outcomes in impinging aerosol application. The droplets' distribution profiles give insight on the mixing of alginate droplets and $CaCl_2$ mists. High efficiency of encapsulation is expected when alginate droplets is well-distributed within the $CaCl_2$ mists.

7.2 Future Research Directions

The following recommendations are made for future studies to advance the development of *Staphylococcus haemolyticus* as microbial inoculants in acid-soil based agriculture.

Experiments:

1. The type and amount of organic acids produced by *Staphylococcus haemolyticus* should be identified and quantified.
2. Before *Staphylococcus haemolyticus* could be recommended as biofertilizers, pot culture experiments as well as field conditions should be carried out to study their plant growth promoting potential.
3. Additional results should be taken to reduce the error from standard plate count method when determine the cell viability for microencapsulation.
4. Additional improvement needs to be done in terms of bacterial survival after lyophilization. Fillers that serve as a carbon source to bacteria such as starch, skim milk, chitosan or humic acid could be mixed with alginate solution during encapsulation process in order to improve cell survival.
5. Improvement in terms of the control release of PSMs from the microbeads at acidic soil should be carried out. The mechanical stability of the beads is largely influenced by the properties of the support material. Biopolymer such as chitosan can be used to coat the alginate microbeads to improve the cell release.
6. As *Staphylococcus haemolyticus* is an opportunistic pathogen that is well-known for its highly antibiotic-resistant phenotype, additional researches must be done before industrial application. Firstly, the threat posed by *Staphylococcus haemolyticus* in soil towards animal and human health must be assessed. Secondly, proper management procedures to be taken in order to prevent these microbial inoculants from entering any source of drinking water or food. The application should also be timed to avoid spreading during heavy rainfall which may lead to run off and leaching of nutrients into water resources where they become pollutants. Lastly, identify the minimal dose (application rate) needed for bacterial colonization of plants to prevent excessive application which might cause toxicity to livestock consuming the crops.

7. The effect of nozzles distance on encapsulation efficiency and cell viability could be further explore.

Simulations:

1. Laser diffraction (LD) and phase doppler particle analysis (PDPA) techniques should be used to characterize the droplet size near the point of liquid atomization or breakup in order to obtain accurate predictions of sprays. By employing these techniques, droplets size distribution profiles could be obtained, and this can be used to fine-tune the breakup parameters in order to obtain a more precise results.
2. Different breakup models such as TAB or KHRT breakup model on spray atomization could be studied to identify the best breakup model that explains the spray behaviors.
3. Film thickness could be measured and spray distribution profiles under different alginate flowrate should be captured to further improve and supports the model validation.
4. More experimental results at different alginate flowrate could be obtained to improve the correlation between SMD and Weber number. More samples should be taken for the determination of SMD experimentally.

REFERENCES

Acevedo, E., Galindo-Castañeda, T., Prada, F., Navia, M., & Romero, H. M. (2014). Phosphate-solubilizing microorganisms associated with the rhizosphere of oil palm (*Elaeis guineensis Jacq*.) in Colombia. *Applied soil ecology, 80*, 26-33. doi:https://doi.org/10.1016/j.apsoil.2014.03.011

Adapco, C. (2016). STAR-CCM+ User Guide Version 13.04.

Adesemoye, A., Torbert, H., & Kloepper, J. (2009). Plant growth-promoting rhizobacteria allow reduced application rates of chemical fertilizers. *Microbial ecology, 58*(4), 921-929.

Afzal, A., & Bano, A. (2008). Rhizobium and phosphate solubilizing bacteria improve the yield and phosphorus uptake in wheat (*Triticum aestivum*). *Int J Agric Biol, 10*(1), 85-88.

Aguerre, H. J., & Nigro, N. M. (2019). Implementation and validation of a Lagrangian spray model using experimental data of the ECN Spray G injector. *Computers & Fluids, 190*, 30-48.

Ahmed, M., Ashgriz, N., & Tran, H. (2009). Break-up length and spreading angle of liquid sheets formed by splash plate nozzles. *Journal of fluids engineering, 131*(1).

Ahmed, N., & Shahab, S. (2011). Phosphate solubilization: their mechanism genetics and application. *Int. J. Microbiol, 9*, 4408-4412.

Al-Damook, A., Summers, J., Kapur, N., & Thompson, H. (2016). Effect of temperature-dependent air properties on the accuracy of numerical simulations of thermal airflows over pinned heat sinks: Elsevier.

Alfonsi, G. (2009). Reynolds-averaged Navier–Stokes equations for turbulence modeling. *Applied Mechanics Reviews, 62*(4).

Alkhedhair, A., Jahn, I., Gurgenci, H., Guan, Z., He, S., & Lu, Y. (2016). Numerical simulation of water spray in natural draft dry cooling towers with a new nozzle representation approach. *Applied Thermal Engineering, 98*, 924-935.

Alori, E. T., Glick, B. R., & Babalola, O. O. (2017). Microbial Phosphorus Solubilization and Its Potential for Use in Sustainable Agriculture. *Frontiers in Microbiology, 8*.

Anand, K., Kumari, B., & Mallick, M. (2016). Phosphate solubilizing microbes: an effective and alternative approach as biofertilizers. *International Journal of Pharmacy and Pharmaceutical Sciences, 8*, 37-40.

Andersen, T., Auk-Emblem, P., & Dornish, M. (2015). 3D cell culture in alginate hydrogels. *Microarrays, 4*(2), 133-161.

Anzuay, M. S., Ciancio, M. G. R., Luduena, L. M., Angelini, J. G., Barros, G., Pastor, N., et al. (2017). Growth promotion of peanut *(Arachis hypogaea L.)* and maize *(Zea mays L.)* plants by single and mixed cultures of efficient phosphate solubilizing bacteria that are tolerant to abiotic stress and pesticides. *Microbiological Research, 199*, 98-109. doi:https://doi.org/10.1016/j.micres.2017.03.006

Arshad, M., Javaid, A., Manzoor, M., Hina, K., Ali, M. A., & Ahmed, I. (2019). Isolation and identification of chromium-tolerant bacterial strains and their potential to promote plant growth. Paper presented at the E3S Web of Conferences.

Arvidsson, T., Bergström, L., & Kreuger, J. (2011). Spray drift as influenced by meteorological and technical factors. *Pest management science, 67*(5), 586-598.

Ashkezari, A. Z., Forouzan, H., Masoomi, S. K., & Divsalar, K. (2014). Investigation of Different of Spray-Wall Impingement on Performance and Emissions in DI Diesel Engines. *International Journal of Engineering Innovations and Research, 3*(4), 567.

ASTM. (2001). D4972-95a, Standard Test Method for pH of Soils. West Conshocken, PA: ASTM International.

ASTM. (2014). D2974-14 Standard Test Methods for Moisture, Ash, and Organic Matter of Peat and Other Organic Soils *American Society of Testing and Materials*. West Conshohocken, PA: ASTM International.

ATCC, A. T. C. C. (2018). *Staphylococcus cohnii*. https://www.atcc.org/~/ps/29974.ashx

Backer, R., Rokem, J. S., Ilangumaran, G., Lamont, J., Praslickova, D., Ricci, E., et al. (2018). Plant Growth-Promoting Rhizobacteria: Context, Mechanisms of Action, and Roadmap to Commercialization of Biostimulants for Sustainable Agriculture. *Frontiers in Plant Science, 9*(1473). doi:10.3389/fpls.2018.01473

Bai, C., Rusche, H., & Gosman, A. (2002). Modeling of gasoline spray impingement. *Atomization and Sprays, 12*(1-3).

Bajaj, P. R., Survase, S. A., Bule, M. V., & Singhal, R. S. (2010). Studies on viability of *Lactobacillus fermentum* by microencapsulation using extrusion spheronization. *Food Biotechnology, 24*(2), 150-164.

Banerjee, A., Biswas, J. K., Pant, D., Sarkar, B., Chaudhuri, P., Rai, M., et al. (2019). Enteric bacteria from the earthworm *(Metaphire posthuma)* promote plant growth and remediate toxic trace elements. *Journal of environmental management, 250*, 109530.

Bardiya, M., & Gaur, A. (1974). Isolation and screening of microorganisms dissolving low-grade rock phosphate. *Folia Microbiologica, 19*(5), 386-389.

Barroso, C. B., Pereira, G. T., & Nahas, E. (2006). Solubilization of CaHPO4 and AlPO4 by *Aspergillus niger* in culture media with different carbon and nitrogen sources. *Brazilian Journal of Microbiology, 37*(4), 434-438.

Barzegar-Jalali, M., Adibkia, K., Valizadeh, H., Siahi-Shadbad, M. R., & Nokhodchi, A. (2008). Kinetic analysis of drug release from nanoparticles. *Journal of Pharmacy & Pharmaceutical Sciences, 11*(1), 167-177.

Bashan, Y. (1986a). Alginate beads as synthetic inoculant carriers for slow release of bacteria that affect plant growth. *Applied and Environmental Microbiology, 51*(5), 1089-1098.

Bashan, Y. (1986b). Significance of timing and level of inoculation with rhizosphere bacteria on wheat plants. *Soil Biology and Biochemistry, 18*(3), 297-301.

Bashan, Y. (1998). Inoculants of plant growth-promoting bacteria for use in agriculture. *Biotechnology advances, 16*(4), 729-770.

Bashan, Y., de-Bashan, L. E., Prabhu, S., & Hernandez, J.-P. (2014). Advances in plant growth-promoting bacterial inoculant technology: formulations and practical perspectives (1998–2013). *Plant and Soil, 378*(1-2), 1-33.

Bashan, Y., Hernandez, J.-P., Leyva, L. A., & Bacilio, M. (2002). Alginate microbeads as inoculant carriers for plant growth-promoting bacteria. *Biology and Fertility of Soils, 35*(5), 359-368.

Bashan, Y., Kamnev, A., & de-Bashan, L. (2013). Tricalcium phosphate is inappropriate as a universal selection factor for isolating and testing phosphate-solubilizing bacteria that enhance plant growth: A proposal for an alternative procedure. *Biology and Fertility of Soils, 49*, 465-469. doi:https://doi.org/10.1007/s00374-012-0737-7

Baumgarten, C. (2006). Mixture formation in internal combustion engines: Springer Science & Business Media.

Bebe, J. E., & Andersen, K. S. (2017). Validation of a CFD Spray Model Based on Spray Nozzle Characteristics.

Behera, B., Yadav, H., Singh, S., Mishra, R., Sethi, B., Dutta, S., et al. (2017). Phosphate solubilization and acid phosphatase activity of *Serratia* sp. isolated from mangrove soil of Mahanadi river delta, Odisha, India. *Journal of Genetic Engineering and Biotechnology, 15*(1), 169-178.

Behjat, Y., Shahhosseini, S., & Marvast, M. A. (2010). Modeling gas oil spray coalescence and vaporization in gas solid riser reactor. *International communications in heat and mass transfer, 37*(7), 935-943.

Bernabeu, P. R., Garcia, S. S., López, A. C., Vio, S. A., Carrasco, N., Boiardi, J. L., et al. (2018). Assessment of bacterial inoculant formulated with *Paraburkholderia tropica* to enhance wheat productivity. *World Journal of Microbiology and biotechnology, 34*(6), 81.

Bhai, R. S. (2020). Preservation and long-term storage of *Trichoderma* spp. by sodium alginate encapsulation. *Journal of Plantation Crops*, 36-44.

Bhandari, B. (2009). Device and method for preparing microparticles: Google Patents.

Bhushani, J. A., & Anandharamakrishnan, C. (2014). Electrospinning and electrospraying techniques: Potential food based applications. *Trends in food science & technology, 38*(1), 21-33.

Biswas, J. K., Banerjee, A., Rai, M., Naidu, R., Biswas, B., Vithanage, M., et al. (2018). Potential application of selected metal resistant phosphate solubilizing bacteria

isolated from the gut of earthworm *(Metaphire posthuma)* in plant growth promotion. *Geoderma, 330*, 117-124.

Bode, M., Falkenstein, T., Le Chenadec, V., Kang, S., Pitsch, H., Arima, T., et al. (2015). A new Euler/Lagrange approach for multiphase simulations of a multi-hole GDI injector.

Bojórquez-Quintal, E., Escalante-Magaña, C., Echevarría-Machado, I., & Martínez-Estévez, M. (2017). Aluminum, a friend or foe of higher plants in acid soils. *Frontiers in Plant Science, 8*, 1767.

Bononi, L., Chiaramonte, J. B., Pansa, C. C., Moitinho, M. A., & Melo, I. S. (2020). Phosphorus-solubilizing *Trichoderma* spp. from Amazon soils improve soybean plant growth. *Scientific Reports, 10*(1), 1-13.

Bosnea, L. A., Moschakis, T., & Biliaderis, C. G. (2014). Complex coacervation as a novel microencapsulation technique to improve viability of probiotics under different stresses. *Food and bioprocess technology, 7*(10), 2767-2781.

Bouwman, L., Goldewijk, K. K., Van Der Hoek, K. W., Beusen, A. H., Van Vuuren, D. P., Willems, J., et al. (2013). Exploring global changes in nitrogen and phosphorus cycles in agriculture induced by livestock production over the 1900–2050 period. *Proceedings of the National Academy of Sciences, 110*(52), 20882-20887.

Brennen, C. E., & Brennen, C. E. (2005). Fundamentals of multiphase flow: Cambridge university press.

Brulatout, J., Garnier, F., Mounaïm-Rousselle, C., & Seers, P. (2016). Calibration strategy of diesel-fuel spray atomization models using a design of experiment method. *International Journal of Engine Research, 17*(7), 713-731.

Brusiani, F., Bianchi, G. M., Falfari, S., Onorati, A., Lucchini, T., & Di Gioia, R. (2014). Influence of cylindrical, k, and ks diesel nozzle shape on the injector internal flow field and on the emerging spray characteristics.

Burey, P., Bhandari, B., Howes, T., & Gidley, M. (2008). Hydrocolloid gel particles: formation, characterization, and application. *Critical reviews in food science and nutrition, 48*(5), 361-377.

Burgain, J., Gaiani, C., Linder, M., & Scher, J. (2011). Encapsulation of probiotic living cells: From laboratory scale to industrial applications. *Journal of Food Engineering, 104*(4), 467-483.

Bustamante, M., Villarroel, M., Rubilar, M., & Shene, C. (2015). *Lactobacillus acidophilus* La-05 encapsulated by spray drying: Effect of mucilage and protein from flaxseed *(Linum usitatissimum L.). LWT - Food Science and Technology, 62*(2), 1162-1168. doi:https://doi.org/10.1016/j.lwt.2015.02.017

Butler Ellis, M. C., Tuck, C. R., & Miller, P. C. H. (2001). How surface tension of surfactant solutions influences the characteristics of sprays produced by hydraulic nozzles used for pesticide application. *Colloids and Surfaces A: Physicochemical and Engineering Aspects, 180*(3), 267-276. doi:https://doi.org/10.1016/S0927-7757(00)00776-7

Cai, M., Wang, S., & Liang, H.-h. (2012). Optimization of ultrasound-assisted ultrafiltration of *Radix astragalus* extracts with hollow fiber membrane using response surface methodology. *Separation and Purification Technology, 100*, 74-81. doi:https://doi.org/10.1016/j.seppur.2012.09.002

Cai, S., Zhao, M., Fang, Y., Nishinari, K., Phillips, G. O., & Jiang, F. (2014). Microencapsulation of *Lactobacillus acidophilus* CGMCC1. 2686 via emulsification/internal gelation of alginate using Ca-EDTA and CaCO3 as calcium sources. *Food hydrocolloids, 39*, 295-300.

Campos, D. C., Acevedo, F., Morales, E., Aravena, J., Amiard, V., Jorquera, M. A., et al. (2014). Microencapsulation by spray drying of nitrogen-fixing bacteria associated with lupin nodules. *World Journal of Microbiology and biotechnology, 30*(9), 2371-2378.

Cao, N., Chen, X., & Schreyer, D. (2012). Influence of calcium ions on cell survival and proliferation in the context of an alginate hydrogel. *ISRN Chemical Engineering, 2012*.

Chaiharn, M., & Lumyong, S. (2009). Phosphate solubilization potential and stress tolerance of rhizobacteria from rice soil in Northern Thailand. *World Journal of Microbiology and biotechnology, 25*(2), 305-314.

Chan, E.-S., Lim, T.-K., Voo, W.-P., Pogaku, R., Tey, B. T., & Zhang, Z. (2011). Effect of formulation of alginate beads on their mechanical behavior and stiffness. *Particuology, 9*(3), 228-234.

Chandramouli, V., Kailasapathy, K., Peiris, P., & Jones, M. (2004). An improved method of microencapsulation and its evaluation to protect *Lactobacillus* spp. in simulated gastric conditions. *Journal of microbiological methods, 56*(1), 27-35.

Chang, C. T., & Farrell, P. V. (1997). A Study on the Effects of Fuel Viscosity and Nozzle Geometry on High Injection Pressure Diesel Spray Characteristics. *SAE Transactions, 106*, 558-567.

Chapman, Z. (2020). Using Computational Fluid Dynamics To Accurately Model Agricultural Spray Nozzles.

Chasos, C., Christodoulou, C., & Karagiorgis, G. (2012). CFD simulations of multi-hole Diesel injector nozzle flow and sprays for various biodiesel blends. Paper presented at the Proceedings of 12th Triennial International Conference on Liquid Atomization and Spray Systems (ICLASS'12).

Chávarri, M., Marañón, I., & Villarán, M. C. (2012). Encapsulation technology to protect probiotic bacteria Probiotics: IntechOpen.

Chawngthu, L., Hnamte, R., & Lalfakzuala, R. (2020). Isolation and Characterization of Rhizospheric Phosphate Solubilizing Bacteria from Wetland Paddy Field of Mizoram, India. *Geomicrobiology Journal, 37*(4), 366-375.

Chen, H., Ma, D., Li, Y., Liu, Y., & Wang, Y. (2016). Optimization the process of microencapsulation of *Bifidobacterium bifidum* BB01 by Box-Behnken design. *Acta Universitatis Cibiniensis. Series E: Food Technology, 20*(2), 17-28.

Chen, K.-N., Chen, C.-Y., Lin, Y.-C., & Chen, M.-J. (2013). Formulation of a novel antagonistic bacterium based biopesticide for fungal disease control using microencapsulation techniques. *Journal of Agricultural Science, 5*(3), 153.

Chen, Y., Rekha, P., Arun, A., Shen, F., Lai, W.-A., & Young, C. (2006). Phosphate solubilizing bacteria from subtropical soil and their tricalcium phosphate solubilizing abilities. *Applied soil ecology, 34*(1), 33-41.

Chhetri, T. K., Subedee, B. R., & Pant, B. (2019). Isolation, Identification and Production of Encapsulated *Bradyrhizobium japonicum* and Study on their Viability. *Nepal Journal of Biotechnology, 7*(1), 39-49.

Chibani, H. R., Bellahcene, M., Bouznad, A., Djibaoui, R., & Hamoum, H. (2017). Optimization of inorganic phosphate solubilization by *Pseudomonas fluorescens* and *Bacillus* sp. isolated from wheat rhizospheric soil.

Ching, S. H., Bansal, N., & Bhandari, B. (2017). Alginate gel particles–A review of production techniques and physical properties. *Critical reviews in food science and nutrition, 57*(6), 1133-1152.

Chloride, C. (2020). A Guide to Physical Properties: Occidental Chemical Corporation.

Cho, J.-C., & Tiedje, J. M. (2000). Biogeography and degree of endemicity of fluorescent *Pseudomonas* strains in soil. *Applied and Environmental Microbiology, 66*(12), 5448-5456. doi:https://doi.org/10.1128/AEM.66.12.5448-5456.2000

Chowdhury, R. B., Moore, G. A., Weatherley, A. J., & Arora, M. (2017). Key sustainability challenges for the global phosphorus resource, their implications for global food security, and options for mitigation. *Journal of Cleaner Production, 140*, 945-963. doi:https://doi.org/10.1016/j.jclepro.2016.07.012

Christensen, D. G., Orr, J. S., Rao, C. V., & Wolfe, A. J. (2017). Increasing growth yield and decreasing acetylation in *Escherichia coli* by optimizing the carbon-to-magnesium ratio in peptide-based media. *Appl. Environ. Microbiol., 83*(6), e03034-03016.

Chryssakis, C., Driscoll, K., Sick, V., & Assanis, D. (2002). Validation of an enhanced liquid sheet atomisation model against quantitative laser diagnostic measurements. *Zaragoza, 9*, 11.

Chu, C.-C., Chou, S.-F., Lin, H.-I., & Liann, Y.-H. (2008). An experimental investigation of swirl atomizer sprays. *Heat and Mass Transfer, 45*(1), 11-22.

Collavino, M. M., Sansberro, P. A., Mroginski, L. A., & Aguilar, O. M. (2010). Comparison of in vitro solubilization activity of diverse phosphate-solubilizing bacteria native to acid soil and their ability to promote *Phaseolus vulgaris* growth. *Biology and Fertility of Soils, 46*(7), 727-738.

Collazo, J., Porteiro, J., Patiño, D., Miguez, J. L., Granada, E., & Moran, J. (2009). Simulation and experimental validation of a methanol burner. *Fuel, 88*(2), 326-334.

Costa, P., & Sousa Lobo, J. M. (2001). Modeling and comparison of dissolution profiles. *European Journal of Pharmaceutical Sciences, 13*(2), 123-133. doi:http://dx.doi.org/10.1016/S0928-0987(01)00095-1

Ćujić, N., Trifković, K., Bugarski, B., Ibrić, S., Pljevljakušić, D., & Šavikin, K. (2016). Chokeberry *(Aronia melanocarpa L.)* extract loaded in alginate and alginate/inulin system. *Industrial crops and products, 86*, 120-131.

Davanlou, A., Lee, J. D., Basu, S., & Kumar, R. (2015). Effect of viscosity and surface tension on breakup and coalescence of bicomponent sprays. *Chemical Engineering Science, 131*, 243-255.

Del Gaudio, P., Colombo, P., Colombo, G., Russo, P., & Sonvico, F. (2005). Mechanisms of formation and disintegration of alginate beads obtained by prilling. *International journal of pharmaceutics, 302*(1-2), 1-9.

Demitri, C., Lamanna, L., De Benedetto, E., Damiano, F., Stella Cappello, M., Siculella, L., et al. (2017). Encapsulation of *Lactobacillus kefiri* in alginate microbeads using a double novel aerosol technique (Vol. 77).

DID. (2017). Peat Swamp Development. from Department of Irrigation and Drainage Sarawak http://www.did.sarawak.gov.my/modules/web/pages.php?lang=en&mod=webpage&sub=page&id=97&menu_id=0&sub_id=117

Dinkecha, K. (2019). Effects of Soil Acidity on Plant Nutrient Availability and Lime Requirement in Welmera Woreda, Oromia Region, Ethiopia.

Đorđević, V., Balanč, B., Belščak-Cvitanović, A., Lević, S., Trifković, K., Kalušević, A., et al. (2015). Trends in encapsulation technologies for delivery of food bioactive compounds. *Food Engineering Reviews, 7*(4), 452-490.

Dos Santos, F., & Le Moyne, L. (2011). Spray atomization models in engine applications, from correlations to direct numerical simulations. *Oil & Gas Science and Technology–Revue d'IFP Energies nouvelles, 66*(5), 801-822.

Duangkhamchan, W., Ronsse, F., Depypere, F., Dewettinck, K., & Pieters, J. (2012). CFD study of droplet atomisation using a binary nozzle in fluidised bed coating. *Chemical Engineering Science, 68*(1), 555-566.

Ebrahimi-Najafabadi, H., Leardi, R., & Jalali-Heravi, M. (2014). Experimental design in analytical chemistry—part I: theory. *Journal of AOAC International, 97*(1), 3-11.

Ejim, C., Rahman, M., Amirfazli, A., & Fleck, B. (2010). Effects of liquid viscosity and surface tension on atomization in two-phase, gas/liquid fluid coker nozzles. *Fuel, 89*(8), 1872-1882.

El-Tarabily, K. A., & Youssef, T. (2010). Enhancement of morphological, anatomical and physiological characteristics of seedlings of the mangrove *Avicennia marina* inoculated with a native phosphate-solubilizing isolate of *Oceanobacillus picturae* under greenhouse conditions. *Plant and Soil, 332*(1), 147-162. doi:https://doi.org/10.1007/s11104-010-0280-y

Etesami, H., & Alikhani, H. A. (2016). Co-inoculation with endophytic and rhizosphere bacteria allows reduced application rates of N-fertilizer for rice plant. *Rhizosphere, 2*, 5-12. doi:http://dx.doi.org/10.1016/j.rhisph.2016.09.003

Fan, X., Wang, J., Zhao, F., Li, J., & Yang, T. (2018). Eulerian–Lagrangian method for liquid jet atomization in supersonic crossflow using statistical injection model. *Advances in Mechanical Engineering, 10*(2), 1687814018761295.

Fang, Z., & Bhandari, B. (2012). Spray drying, freeze drying and related processes for food ingredient and nutraceutical encapsulation *Encapsulation technologies and delivery systems for food ingredients and nutraceuticals* (pp. 73-109): Elsevier.

Fauchais, P. L., Heberlein, J. V. R., & Boulos, M. I. (2014). *Thermal Spray Fundamentals: From Powder to Part*: Springer US.

Felsenstein, J. (1985). Confidence limits on phylogenies: an approach using the bootstrap. *Evolution, 39*(4), 783-791. doi:https://doi.org/10.1111/j.1558-5646.1985.tb00420.x.

Feng, J., Dou, J., Wu, Z., Yin, D., & Wu, W. (2019). Controlled release of biological control agents for preventing aflatoxin contamination from starch–alginate beads. *Molecules, 24*(10), 1858.

Finotello, G., Kooiman, R. F., Padding, J. T., Buist, K. A., Jongsma, A., Innings, F., et al. (2017). The dynamics of milk droplet–droplet collisions. *Experiments in Fluids, 59*(1), 17. doi:10.1007/s00348-017-2471-2

Fitriatin, B. N., Yuniarti, A., Turmuktini, T., & Ruswandi, F. K. (2014). The effect of phosphate solubilizing microbe producing growth regulators on soil phosphate, growth and yield of maize and fertilizer efficiency on Ultisol. *Eurasian Journal of Soil Science, 3*(2), 101.

Fogliati, M., Fontana, D., Garbero, M., Vanni, M., Baldi, G., & Donde, R. (2006). CFD simulation of paint deposition in an air spray process. *JCT research, 3*(2), 117-125.

Frakolaki, G., Giannou, V., Kekos, D., & Tzia, C. (2020). A review of the microencapsulation techniques for the incorporation of probiotic bacteria in functional foods. *Critical reviews in food science and nutrition*, 1-22. doi:10.1080/10408398.2020.1761773

Fraser, T. D., Lynch, D. H., Gaiero, J., Khosla, K., & Dunfield, K. E. (2017). Quantification of bacterial non-specific acid (phoC) and alkaline (phoD) phosphatase genes in bulk and rhizosphere soil from organically managed soybean fields. *Applied soil ecology, 111*, 48-56. doi:https://doi.org/10.1016/j.apsoil.2016.11.013

Fung, M. C., Inthavong, K., Yang, W., & Tu, J. (2012). CFD modeling of spray atomization for a nasal spray device. *Aerosol Science and Technology, 46*(11), 1219-1226.

Fuster, D., Bagué, A., Boeck, T., Le Moyne, L., Leboissetier, A., Popinet, S., et al. (2009). Simulation of primary atomization with an octree adaptive mesh refinement and VOF method. *International Journal of Multiphase Flow, 35*(6), 550-565.

Gadagi, R. S., & Sa, T. (2002). New isolation method for microorganisms solulbilizing iron and aluminum phosphates using dyes. *Soil science and plant nutrition, 48*(4), 615-618. doi:https://doi.org/10.1080/00380768.2002.10409246

Gaonkar, A. G., Vasisht, N., Khare, A. R., & Sobel, R. (2014). Microencapsulation in the Food Industry: A Practical Implementation Guide: Elsevier Science.

García-Fraile, P., Menéndez, E., & Rivas, R. (2015). Role of bacterial biofertilizers in agriculture and forestry. *AIMS Bioengineering*, *2*(3), 183.

Gavtash, B., Versteeg, H., Hargrave, G., Lewis, D., Church, T., & Brambilla, G. (2014). Linear Instability Sheet Atomisation (LISA) Model to Predict Droplet Size Issued from a pMDI.

Gen Fu, W., & Xue Ping, Z. (2005). Characterization of phosphorus-releasing bacteria in a small eutrophic shallow lake, Eastern China. *Water research*, *39*(19), 4623-4632.

Ghorani, B., & Tucker, N. (2015). Fundamentals of electrospinning as a novel delivery vehicle for bioactive compounds in food nanotechnology. *Food hydrocolloids*, *51*, 227-240.

Ghosh, S., Mukherjee, P., Pati, P., Roychowdhury, R., Roy, A., & Roy, M. (2015). Isolation and Characterization of Mercury Resistant Bacteria from Fly Ash Sample of Mejia Thermal Power Plant, W. B, India for Application in Bioremediation and Phytoremediation.

Gibaldi, M., & Feldman, S. (1967). Establishment of sink conditions in dissolution rate determinations. Theoretical considerations and application to nondisintegrating dosage forms. *Journal of pharmaceutical sciences*, *56*(10), 1238-1242.

Gilbert, N. (2009). The disappearing nutrient: phosphate-based fertilizers have helped spur agricultural gains in the past century, but the world may soon run out of them. Natasha Gilbert investigates the potential phosphate crisis. *Nature*, *461*(7265), 716-719.

Glendinning, J. (2000). Australian soil fertility manual: CSIRO Pub.

Goldman, E., & Green, L. H. (2008). Practical Handbook of Microbiology: CRC Press.

Goldstein, A. H. (1994). Involvement of the quinoprotein glucose dehydrogenase in the solubilization of exogenous phosphates by gram-negative bacteria. *Phosphate in microorganisms: cellular and molecular biology. ASM Press, Washington, DC*, 197-203.

Gonzalez, L. E., & Bashan, Y. (2000). Increased growth of the microalga *chlorella vulgaris* when coimmobilized and cocultured in alginate beads with the plant-

growth-promoting bacterium *Azospirillum brasilense*. *Applied and Environmental Microbiology, 66*(4), 1527-1531.

Gotor-Vila, A., Usall, J., Torres, R., Solsona, C., & Teixidó, N. (2017). Biocontrol products based on *Bacillus amyloliquefaciens* CPA-8 using fluid-bed spray-drying process to control postharvest brown rot in stone fruit. *LWT - Food Science and Technology, 82*, 274-282. doi:https://doi.org/10.1016/j.lwt.2017.04.034

Gouin, S. (2004). Microencapsulation: Industrial appraisal of existing technologies and trends. *Trends in food science & technology, 15*(7), 330-347.

Gryshkov, O., Pogozhykh, D., Hofmann, N., Pogozhykh, O., Mueller, T., & Glasmacher, B. (2014). Encapsulating non-human primate multipotent stromal cells in alginate via high voltage for cell-based therapies and cryopreservation. *PLOS ONE, 9*(9), e107911.

Gupta, R., Singal, R., Shankar, A., Kuhad, R. C., & Saxena, R. K. (1994). A modified plate assay for screening phosphate solubilizing microorganisms. *The Journal of General and Applied Microbiology, 40*(3), 255-260. doi:https://doi.org/10.2323/jgam.40.255

Habchi, C. (2011). The energy Spectrum Analogy Breakup (SAB) model for the numerical simulation of sprays. *Atomization and Sprays, 21*(12).

Hamed, H. E., & Markale, I. (2017). Eulerian-Lagrangian Modeling of contamination on exterior of a NEVS Vehicle.

Hariyadi, D. M., Lin, S. C.-Y., Wang, Y., Bostrom, T., Turner, M. S., Bhandari, B., et al. (2010). Diffusion loading and drug delivery characteristics of alginate gel microparticles produced by a novel impinging aerosols method. *Journal of drug targeting, 18*(10), 831-841.

Hariyadi, D. M., Wang, Y., Lin, S. C.-Y., Bostrom, T., Bhandari, B., & Coombes, A. G. (2012). Novel alginate gel microspheres produced by impinging aerosols for oral delivery of proteins. *Journal of microencapsulation, 29*(3), 250-261.

He, S.-M., Luo, Y., Hove-Jensen, B., & Zechel, D. L. (2009). A fluorescent substrate for carbon–phosphorus lyase: Towards the pathway for organophosphonate

metabolism in bacteria. *Bioorganic & Medicinal Chemistry Letters, 19*(20), 5954-5957. doi:https://doi.org/10.1016/j.bmcl.2009.08.035

He, Y., Wu, Z., Tu, L., Han, Y., Zhang, G., & Li, C. (2015). Encapsulation and characterization of slow-release microbial fertilizer from the composites of bentonite and alginate. *Applied Clay Science, 109*, 68-75.

He, Y., Wu, Z., Ye, B.-C., Wang, J., Guan, X., & Zhang, J. (2016). Viability evaluation of alginate-encapsulated *Pseudomonas putida* Rs-198 under simulated salt-stress conditions and its effect on cotton growth. *European journal of soil biology, 75*, 135-141. doi:http://dx.doi.org/10.1016/j.ejsobi.2016.05.002

Hede, P. D., Bach, P., & Jensen, A. D. (2008). Two-fluid spray atomisation and pneumatic nozzles for fluid bed coating/agglomeration purposes: A review. *Chemical Engineering Science, 63*(14), 3821-3842.

Her, J.-Y., Kim, M. S., & Lee, K.-G. (2015). Preparation of probiotic powder by the spray freeze-drying method. *Journal of Food Engineering, 150*, 70-74. doi:https://doi.org/10.1016/j.jfoodeng.2014.10.029

Hetényi, K., Németh, Á., & Sevella, B. (2008). Examination of medium supplementation for lactic acid fermentation. *Hungarian Journal of Industry and Chemistry, 36*(1-2).

Hilz, E., & Vermeer, A. W. P. (2013). Spray drift review: The extent to which a formulation can contribute to spray drift reduction. *Crop Protection, 44*, 75-83. doi:https://doi.org/10.1016/j.cropro.2012.10.020

Hou, S., & Schmidt, D. P. (2006). Adaptive collision meshing and satellite droplet formation in spray simulations. *International Journal of Multiphase Flow, 32*(8), 935-956.

Hove-Jensen, B., Zechel, D. L., & Jochimsen, B. (2014). Utilization of Glyphosate as Phosphate Source: Biochemistry and Genetics of Bacterial Carbon-Phosphorus Lyase. *Microbiology and Molecular Biology Reviews, 78*(1), 176. doi:10.1128/MMBR.00040-13

Huh, K., & Gosman, A. (1991). A Phenomenological model of diesel spray atomization [C] Proceedings of the International Conference of Multi-Phase Flows. *Tsukuba, Japan*.

Hussain, Z., Khan, M. A., Iqbal, F., Raffi, M., & Hafeez, F. Y. (2019). Electrospun Microbial-Encapsulated Composite-Based Plasticized Seed Coat for Rhizosphere Stabilization and Sustainable Production of Canola *(Brassica napus L.). Journal of Agricultural and Food Chemistry, 67*(18), 5085-5095. doi:10.1021/acs.jafc.8b06505

Hussein, A., Hafiz, M., Rashid, H., Halim, A., Wisnoe, W., & Kasolang, S. (2012). Characteristics of hollow cone swirl spray at various nozzle orifice diameters. *Jurnal Teknologi, 58*(2).

Hynes, R. K., Chumala, P. B., Hupka, D., & Peng, G. (2010). A complex coacervate formulation for delivery of *Colletotrichum truncatum* 00-003B1. *Weed technology, 24*(2), 185-192.

Ikoyi, I., Fowler, A., & Schmalenberger, A. (2018). One-time phosphate fertilizer application to grassland columns modifies the soil microbiota and limits its role in ecosystem services. *Science of the Total Environment, 630*, 849-858.

Illmer, P., Barbato, A., & Schinner, F. (1995). Solubilization of hardly-soluble AlPO4 with P-solubilizing microorganisms. *Soil Biology and Biochemistry, 27*(3), 265-270.

Iqbal Hussain, M., Naeem Asghar, H., Javed Akhtar, M., & Arshad, M. (2013). Impact of phosphate solubilizing bacteria on growth and yield of maize. *Soil & Environment, 32*(1).

Isa, K. M., Osman, K., Yahya, A., Ghaffar, Z. A., Abdul, A. H., & Hamid, S. K. (2019). Studies on the Spray Characteristics of Pressure-Swirl Atomizers for Automatic Hand Sanitizer Application.

Isailović, B., Djordjević, V., Nedović, V., & Bugarski, B. (2013). Liposome-in-alginate systems for encapsulation of natural antioxidants. Paper presented at the Inside Food Symposium.

Istina, I. N., Widiastuti, H., Joy, B., & Antralina, M. (2015). Phosphate-solubilizing microbe from saprists peat soil and their potency to enhance oil palm growth and p uptake. *Procedia Food Science, 3*, 426-435. doi:https://doi.org/10.1016/j.profoo.2015.01.047

John, R. P., Tyagi, R., Brar, S., Surampalli, R., & Prévost, D. (2011). Bio-encapsulation of microbial cells for targeted agricultural delivery. *Critical reviews in biotechnology, 31*(3), 211-226.

Julin, T., Vaari, J., Hostikka, S., & Paajanen, A. (2014). Modeling and Simulation of High Pressure Water Mist Systems. *Fire Technology, 50*. doi:10.1007/s10694-013-0335-8

Kaario, O., Sarjovaara, T., Ranta, O., Hulkkonen, T., Keskinen, K., Larmi, M., et al. (2014). Comparing Breakup Models in a Novel High Injection Pressure SCR System using Polyhedral Meshing.

Kajikawa, H., Mitsumori, M., & Ohmomo, S. (2002). Stimulatory and Inhibitory Effects of Protein Amino Acids on Growth Rate and Efficiency of Mixed Ruminal Bacteria. *Journal of Dairy Science, 85*(8), 2015-2022. doi:https://doi.org/10.3168/jds.S0022-0302(02)74278-1

Kalayu, G. (2019). Phosphate solubilizing microorganisms: promising approach as biofertilizers. *International Journal of Agronomy, 2019*.

Kalsi, H. K., Singh, R., Dhaliwal, H. S., & Kumar, V. (2016). Phytases from *Enterobacter* and *Serratia* species with desirable characteristics for food and feed applications. *3 Biotech, 6*(1), 64. doi:10.1007/s13205-016-0378-x

Kang, Z., Wang, Z.-g., Li, Q., & Cheng, P. (2018). Review on pressure swirl injector in liquid rocket engine. *Acta Astronautica, 145*, 174-198.

Keharom, S., Mahachai, R., & Chanthai, S. (2016). The optimization study of α-amylase activity based on central composite design-response surface methodology by dinitrosalicylic acid method. *International Food Research Journal, 23*(1).

Khajeh, M. (2011). Response surface modelling of lead pre-concentration from food samples by miniaturised homogenous liquid–liquid solvent extraction: Box–Behnken design. *Food chemistry, 129*(4), 1832-1838.

Khalil, K. A., Mustafa, S., Mohammad, R., Ariff, A. B., Ahmad, S. A., Dahalan, F. A., et al. (2019). Encapsulation of *Bifidobacterium pseudocatenulatum* Strain G4 within Bovine Gelatin-Genipin-Sodium Alginate Combinations: Optimisation Approach Using Face Central Composition Design-Response Surface Methodology (FCCD-RSM). *International Journal of Microbiology, 2019*.

Khan, M. S., Ahmad, E., Zaidi, A., & Oves, M. (2013). Functional aspect of phosphate-solubilizing bacteria: importance in crop production *Bacteria in agrobiology: Crop productivity* (pp. 237-263): Springer.

Khan, M. S., Zaidi, A., & Ahmad, E. (2014). Mechanism of phosphate solubilization and physiological functions of phosphate-solubilizing microorganisms *Phosphate Solubilizing Microorganisms* (pp. 31-62): Springer.

Khan, M. S., Zaidi, A., & Wani, P. A. (2009). Role of phosphate solubilizing microorganisms in sustainable agriculture-a review *Sustainable agriculture* (pp. 551-570): Springer.

Khatami, S. N., Ilegbusi, O., & Trakhtenberg, L. (2013). Modeling of aerosol spray characteristics for synthesis of sensor thin film from solution. *Applied Mathematical Modelling, 37*(9), 6389-6399.

Kim, B. J., Park, T., Park, S. Y., Han, S. W., Lee, H. S., Kim, Y. G., et al. (2015). Control of microbial growth in alginate/polydopamine core/shell microbeads. *Chemistry–An Asian Journal, 10*(10), 2130-2133.

Kim, J. U., Kim, B., Shahbaz, H. M., Lee, S. H., Park, D., & Park, J. (2017). Encapsulation of probiotic *Lactobacillus acidophilus* by ionic gelation with electrostatic extrusion for enhancement of survival under simulated gastric conditions and during refrigerated storage. *International Journal of Food Science & Technology, 52*(2), 519-530.

Kirk, J. L., Beaudette, L. A., Hart, M., Moutoglis, P., Klironomos, J. N., Lee, H., et al. (2004). Methods of studying soil microbial diversity. *Journal of microbiological methods, 58*(2), 169-188.

Kloos, W. E., & Schleifer, K. H. (1975). Isolation and Characterization of *Staphylococci* from Human Skin II. Descriptions of Four New Species: *Staphylococcus warneri, Staphylococcus capitis, Staphylococcus hominis,* and *Staphylococcus simulans*. *International Journal of Systematic and Evolutionary Microbiology, 25*(1), 62-79. doi:https://doi.org/10.1099/00207713-25-1-62

Kolli, R., Asi, E., Apuhtin, V., Kauer, K., & Szajdak, L. (2010). Chemical properties of surface peat on forest land in Estonia. *Mires & Peat, 6*.

Kononen, M., Jauhiainen, J., Laiho, R., Kusin, K., & Vasander, H. (2015). Physical and chemical properties of tropical peat under stabilised land uses. *Mires and Peat, 16*(8), 1-13.

Kooij, S., Sijs, R., Denn, M. M., Villermaux, E., & Bonn, D. (2018). What determines the drop size in sprays? *Physical Review X, 8*(3), 031019.

Korsmeyer, R. W., Gurny, R., Doelker, E., Buri, P., & Peppas, N. A. (1983). Mechanisms of solute release from porous hydrophilic polymers. *International journal of pharmaceutics, 15*(1), 25-35.

Krasaekoopt, W., Bhandari, B., & Deeth, H. (2003). Evaluation of encapsulation techniques of probiotics for yoghurt. *International Dairy Journal, 13*(1), 3-13.

Krell, V., Jakobs-Schoenwandt, D., Vidal, S., & Patel, A. V. (2018). Encapsulation of *Metarhizium brunneum* enhances endophytism in tomato plants. *Biological Control, 116*, 62-73.

Kuhad, R. C., Singh, S., Lata, & Singh, A. (2011). Phosphate-Solubilizing Microorganisms. In A. Singh, N. Parmar, & R. C. Kuhad (Eds.), *Bioaugmentation, Biostimulation and Biocontrol* (pp. 65-84). Berlin, Heidelberg: Springer Berlin Heidelberg.

Kumar, V., Singh, P., Jorquera, M. A., Sangwan, P., Kumar, P., Verma, A., et al. (2013). Isolation of phytase-producing bacteria from Himalayan soils and their effect on growth and phosphorus uptake of Indian mustard (Brassica juncea). *World Journal of Microbiology and biotechnology, 29*(8), 1361-1369.

Lan, S.-F., Kehinde, T., Zhang, X., Khajotia, S., Schmidtke, D. W., & Starly, B. (2013). Controlled release of metronidazole from composite poly-ε-caprolactone/alginate (PCL/alginate) rings for dental implants. *Dental Materials, 29*(6), 656-665. doi:https://doi.org/10.1016/j.dental.2013.03.014

Lange, H., Taillandier, P., & Riba, J. P. (2001). Effect of high shear stress on microbial viability. *Journal of Chemical Technology and Biotechnology, 76*, 501-505. doi:10.1002/jctb.401

Lavanya, G., Sahu, P., & Brahmaprakash, G. P. (2015). Effect of fluid bed dried formulation in comparison with lignite formulation of microbial consortium on

finger millet *(Eleucine coracana Gaertn.)*. *Journal of Pure and Applied Microbiology, 9*, 193-199.

Lee, B. B., Bhandari, B. R., & Howes, T. (2016). Air Extrusion System for Ionotropic Alginate Microgel Particle Formation: A Review. *Chemical Engineering & Technology, 39*(12), 2355-2369.

Lee, K. Y., & Mooney, D. J. (2012). Alginate: properties and biomedical applications. *Progress in polymer science, 37*(1), 106-126. doi:10.1016/j.progpolymsci.2011.06.003

Lefebvre, A. H., & McDonell, V. G. (2017). *Atomization and Sprays*: CRC Press.

Li, M., Liao, X., Zhang, D., Du, G., & Chen, J. (2011). Yeast Extract Promotes Cell Growth and Induces Production of Polyvinyl Alcohol-Degrading Enzymes. *Enzyme Research, 2011*, 179819. doi:10.4061/2011/179819

Li, M., Rouaud, O., & Poncelet, D. (2008). Microencapsulation by solvent evaporation: State of the art for process engineering approaches. *International journal of pharmaceutics, 363*(1-2), 26-39.

Li, M., Tian, X., Zhu, N., Schreyer, D. J., & Chen, X. (2010). Modeling process-induced cell damage in the biodispensing process. *Tissue Engineering Part C: Methods, 16*(3), 533-542.

Li, M., Tshabalala, M. A., & Buschle-Diller, G. (2016). Formulation and characterization of polysaccharide beads for controlled release of plant growth regulators. *Journal of Materials Science, 51*(9), 4609-4617.

Li, X., Du, J., Wang, L., Fan, J., & Peng, X. (2019). Effects of different nozzle materials on atomization results via CFD simulation. *Chinese Journal of Chemical Engineering*.

Li, Y., Liu, X., Hao, T., & Chen, S. (2017). Colonization and maize growth promotion induced by phosphate solubilizing bacterial isolates. *International journal of molecular sciences, 18*(7), 1253. doi:https://doi.org/10.3390/ijms18071253

Librán, C. M., Castro, S., & Lagaron, J. M. (2017). Encapsulation by electrospray coating atomization of probiotic strains. *Innovative Food Science & Emerging Technologies, 39*, 216-222. doi:https://doi.org/10.1016/j.ifset.2016.12.013

Liffourrena, A. S., & Lucchesi, G. I. (2018). Alginate-perlite encapsulated *Pseudomonas putida A* (ATCC 12633) cells: Preparation, characterization and potential use as plant inoculants. *Journal of Biotechnology, 278*, 28-33. doi:https://doi.org/10.1016/j.jbiotec.2018.04.019

Liu, H., Cui, S. W., Chen, M., li, Y., Liang, R., Xu, F., et al. (2019a). Protective approaches and mechanisms of microencapsulation to the survival of probiotic bacteria during processing, storage and gastrointestinal digestion: A review. *Critical reviews in food science and nutrition, 59*(17), 2863-2878. doi:10.1080/10408398.2017.1377684

Liu, R.-C., Le, J.-L., Song, W.-Y., & Yang, S.-H. (2016). LISA model for simulation of liquid sheet breakup in swirl injection. Paper presented at the Material Science And Environmental Engineering: The Proceedings of 2016 International Workshop on Material Science and Environmental Engineering (IWMSEE2016).

Liu, W., He, Y., Zhang, K., Fan, J., & Cao, H. (2012). Isolation, identification and characterization of a strain of phosphate-solubilizing bacteria from red soil. *Wei sheng wu xue bao= Acta microbiologica Sinica, 52*(3), 326-333.

Liu, X., Huo, J.-L., Li, T.-T., Peng, H.-K., Lin, J.-H., & Lou, C.-W. (2019b). Investigation of the shear thickening fluid encapsulation in an orifice coagulation bath. *Polymers, 11*(3), 519.

Lopes, S., Bueno, L., AGUIAR JÚNIOR, F. D., & Finkler, C. (2017). Preparation and characterization of alginate and gelatin microcapsules containing *Lactobacillus rhamnosus*. *Anais da academia brasileira de ciências, 89*(3), 1601-1613.

López Córdoba, A., Deladino, L., & Martino, M. (2013). Effect of starch filler on calcium-alginate hydrogels loaded with yerba mate antioxidants. *Carbohydrate Polymers, 95*(1), 315-323. doi:https://doi.org/10.1016/j.carbpol.2013.03.019

Lotfi, D., Anissa, M., Hafsa, B., Djamila, B., Ihdene, Z., yelda Bakos, P., et al. (2015). Optimization of hydrolysis degradation of neurotoxic pesticide methylparathion using a response surface methodology (RSM).

Lotfipour, F., Mirzaeei, S., & Maghsoodi, M. (2012). Preparation and characterization of alginate and psyllium beads containing *Lactobacillus acidophilus*. *The Scientific World Journal, 2012*.

Lucchini, T., D'Errico, G., Ettorre, D., Brusiani, F., Bianchi, G. M., Montanaro, A., et al. (2010). Experimental and numerical investigation of high-pressure diesel sprays with multiple injections at engine conditions.

Ma, X., Wang, X., Cheng, J., Nie, X., Yu, X., Zhao, Y., et al. (2015). Microencapsulation of *Bacillus subtilis* B99-2 and its biocontrol efficiency against *Rhizoctonia solani* in tomato. *Biological Control, 90*, 34-41. doi:https://doi.org/10.1016/j.biocontrol.2015.05.013

Maciel, G. M., Chaves, K. S., Grosso, C. R. F., & Gigante, M. L. (2014). Microencapsulation of *Lactobacillus acidophilus* La-5 by spray-drying using sweet whey and skim milk as encapsulating materials. *Journal of Dairy Science, 97*(4), 1991-1998. doi:https://doi.org/10.3168/jds.2013-7463

Madhuri, R. J., Saraswathi, M., Gowthami, K., Bhargavi, M., Divya, Y., & Deepika, V. (2019). Chapter 19 - Recent Approaches in the Production of Novel Enzymes From Environmental Samples by Enrichment Culture and Metagenomic Approach. In V. Buddolla (Ed.), *Recent Developments in Applied Microbiology and Biochemistry* (pp. 251-262): Academic Press.

Maes, N., Dam, N., Somers, B., Lucchini, T., D'Errico, G., & Hardy, G. (2016). Experimental and numerical analyses of liquid and spray penetration under heavy-duty diesel engine conditions. *SAE International Journal of Fuels and Lubricants, 9*(1), 108-124.

Maheshwari, D. K., Saraf, M., & Aeron, A. (2013). Bacteria in agrobiology: Crop productivity. Berlin, Heidelberg: Springer.

Malakar, J., Nayak, A. K., Pal, D., & Jana, P. (2014). Potato starch-blended alginate beads for prolonged release of tolbutamide: Development by statistical optimization and in vitro characterization. *Asian Journal of Pharmaceutics (AJP): Free full text articles from Asian J Pharm, 7*(1).

Malusá, E., & Vassilev, N. (2014). A contribution to set a legal framework for biofertilisers. *Applied microbiology and biotechnology, 98*(15), 6599-6607.

Mandato, S., Rondet, E., Delaplace, G., Barkouti, A., Galet, L., Accart, P., et al. (2012). Liquids' atomization with two different nozzles: Modeling of the effects of some

processing and formulation conditions by dimensional analysis. *Powder technology, 224*, 323-330.

Marques da Silva, T., Jacob Lopes, E., Codevilla, C. F., Cichoski, A. J., Flores, É. M. d. M., Motta, M. H., et al. (2018). Development and characterization of microcapsules containing *Bifidobacterium Bb-12* produced by complex coacervation followed by freeze drying. *LWT, 90*, 412-417. doi:https://doi.org/10.1016/j.lwt.2017.12.057

Martín, M. J., Lara-Villoslada, F., Ruiz, M. A., & Morales, M. E. (2015). Microencapsulation of bacteria: A review of different technologies and their impact on the probiotic effects. *Innovative Food Science & Emerging Technologies, 27*, 15-25.

Martins, S., Sarmento, B., Souto, E. B., & Ferreira, D. C. (2007). Insulin-loaded alginate microspheres for oral delivery–effect of polysaccharide reinforcement on physicochemical properties and release profile. *Carbohydrate Polymers, 69*(4), 725-731.

Mauriello, G., Aponte, M., Andolfi, R., Moschetti, G., & Villani, F. (1999). Spray-drying of bacteriocin-producing lactic acid bacteria. *Journal of food protection, 62*(7), 773-777.

Melling, L. (2016). Peatland in Malaysia. In M. Osaki & N. Tsuji (Eds.), Tropical Peatland Ecosystems (pp. 59-73). Japan, Tokyo: Springer.

Merbach, W., Fankem, H., & Deubel, A. (2009). Influence of rhizosphere bacteria of African oil palm *(Elaeis guineensis)* on calcium, iron, and aluminum phosphate in vitro mobilization. Paper presented at the International symposium “Root Research and Applications.

Metson, G. S., Bennett, E. M., & Elser, J. J. (2012). The role of diet in phosphorus demand. *Environmental Research Letters, 7*(4), 044043.

Mezhericher, M., Levy, A., & Borde, I. (2010). Spray drying modelling based on advanced droplet drying kinetics. *Chemical Engineering and Processing: Process Intensification, 49*(11), 1205-1213.

Mohamed, A. E., Nessim, M. G., Ibrahim Abou-el-seoud, I., Darwish, K. M., & Shamseldin, A. (2019). Isolation and selection of highly effective phosphate

solubilizing bacterial strains to promote wheat growth in Egyptian calcareous soils. *Bulletin of the National Research Centre, 43*(1), 1-13.

Mujumdar, A. S. (2014). Handbook of Industrial Drying: CRC Press.

Mushtaq, S., Shafiq, M., Ashraf, T., Haider, M., Ashfaq, M., & Ali, M. (2019). Characterization of plant growth promoting activities of bacterial endophytes and their antibacterial potential isolated from citrus. *J. Anim. Plant Sci, 29*, 978-991.

Nag, A., & Das, S. (2013). Improving ambient temperature stability of probiotics with stress adaptation and fluidized bed drying. *Journal of functional foods, 5*(1), 170-177.

Nami, Y., Haghshenas, B., & Yari Khosroushahi, A. (2017). Effect of psyllium and gum Arabic biopolymers on the survival rate and storage stability in yogurt of *Enterococcus durans* IW 3 encapsulated in alginate. *Food science & nutrition, 5*(3), 554-563.

Naturalfog. (2020). Misting Nozzles. Retrieved from https://www.naturalfog.com/NFN-type-10-24unc2A.html

Nautiyal, C. S. (1999). An efficient microbiological growth medium for screening phosphate solubilizing microorganisms. *FEMS microbiology Letters, 170*(1), 265-270. doi:https://doi.org/10.1111/j.1574-6968.1999.tb13383.x

Nayak, A. K., Pal, D., & Santra, K. (2016). Swelling and drug release behavior of metformin HCl-loaded tamarind seed polysaccharide-alginate beads. *International Journal of Biological Macromolecules, 82*, 1023-1027. doi:https://doi.org/10.1016/j.ijbiomac.2015.10.027

Ning, L., Guillemot, A., Zhao, J., Kipouros, G., & Chen, X. (2016). Influence of Flow Behavior of Alginate–Cell Suspensions on Cell Viability and Proliferation. *Tissue Engineering Part C: Methods, 22*(7), 652-662.

Noppakundilograt, S., Piboon, P., Graisuwan, W., Nuisin, R., & Kiatkamjornwong, S. (2015). Encapsulated eucalyptus oil in ionically cross-linked alginate microcapsules and its controlled release. *Carbohydrate Polymers, 131*, 23-33.

Nunamaker, E. A., Otto, K. J., & Kipke, D. R. (2011). Investigation of the material properties of alginate for the development of hydrogel repair of dura mater. *Journal of the Mechanical Behavior of Biomedical Materials, 4*(1), 16-33.

Nuyttens, D., Schampheleire, M., Verboven, P., Brusselman, E., & Dekeyser, D. (2009). Droplet Size and Velocity Characteristics of Agricultural Sprays. *Transactions of the Asabe, 52*, 1471-1480. doi:10.13031/2013.29127

O'Driscoll, C., Rodgers, M., O'Connor, M., Asam, Z.-u.-Z., de Eyto, E., Poole, R., et al. (2011). A Potential Solution to Mitigate Phosphorus Release Following Clearfelling in Peatland Forest Catchments. *Water, Air, & Soil Pollution, 221*(1), 1-11. doi:https://doi.org/10.1007/s11270-011-0764-2

Ogbonna, J. C., Matsumura, M., & Kataoka, H. (1991). Effective oxygenation of immobilized cells through reduction in bead diameters: a review. *Process biochemistry, 26*(2), 109-121.

Omar, W., Aziz, N. A., Mohammed, A. T., Harun, M. H., & Din, A. K. (2010). Mapping of oil palm cultivation on peatland in Malaysia. *MPOB Informafion Series*.

Omar, Z., Qiang, K., Mohd, S., & Rosly, N. (2016). CFD Simulation of Aerial Crop Spraying. *IOP Conference Series: Materials Science and Engineering, 160*, 012028. doi:10.1088/1757-899X/160/1/012028

Organization, F. a. A. (2017). The future of food and agriculture - Trends and challenges. Retrieved from http://www.fao.org/3/a-i6583e.pdf

Orhan, F. (2016). Alleviation of salt stress by halotolerant and halophilic plant growth-promoting bacteria in wheat *(Triticum aestivum)*. *Brazilian Journal of Microbiology, 47*(3), 621-627.

Orhan, F., & Gulluce, M. (2015). Isolation and characterization of salt-tolerant bacterial strains in salt-affected soils of Erzurum, Turkey. *Geomicrobiology Journal, 32*(6), 521-529.

Osaki, M., & Tsuji, N. (2016). Tropical peatland ecosystems: Springer.

Osorio, N. W. (2011). Effectiveness of phosphate solubilizing microorganism in increasing plant phosphate uptake and growth in tropical soils *Bacteria in agrobiology: plant nutrient management* (pp. 65-80): Springer.

Paavilainen, E., & Paivanen, J. (2013). Peatland Forestry: Ecology and Principles. Berlin, Heidelberg: Springer

Panda, B., Rahman, H., & Panda, J. (2016). Phosphate solubilizing bacteria from the acidic soils of Eastern Himalayan region and their antagonistic effect on fungal

pathogens. *Rhizosphere, 2,* 62-71. doi:https://doi.org/10.1016/j.rhisph.2016.08.001

Pande, A., Pandey, P., Mehra, S., Singh, M., & Kaushik, S. (2017). Phenotypic and genotypic characterization of phosphate solubilizing bacteria and their efficiency on the growth of maize. *Journal of Genetic Engineering and Biotechnology, 15*(2), 379-391.

Pandey, A., Negi, S., & Soccol, C. R. (2016). Current Developments in Biotechnology and Bioengineering: Production, Isolation and Purification of Industrial Products: Elsevier Science.

Paramithiotis, S., Melissari, I., & Drosinos, E. H. (2006). In vitro assessment of properties associated with the survival through the gastro-intestinal tract of staphylococci isolated from traditional sausage fermentation. *Food microbiology, 23*(7), 663-671.

Paredi, D., Lucchini, T., D'Errico, G., Onorati, A., Montanaro, A., Allocca, L., et al. (2018). Combined Experimental and Numerical Investigation of the ECN Spray G under Different Engine-Like Conditions.

Paredi, D., Lucchini, T., D'Errico, G., Onorati, A., Pickett, L., & Lacey, J. (2020). Validation of a comprehensive computational fluid dynamics methodology to predict the direct injection process of gasoline sprays using Spray G experimental data. *International Journal of Engine Research, 21*(1), 199-216.

Park, K.-H., Lee, O.-M., Jung, H.-I., Jeong, J.-H., Jeon, Y.-D., Hwang, D.-Y., et al. (2010). Rapid solubilization of insoluble phosphate by a novel environmental stress-tolerant *Burkholderia vietnamiensis* M6 isolated from ginseng rhizospheric soil. *Applied microbiology and biotechnology, 86*(3), 947-955. doi:https://doi.org/10.1007/s00253-009-2388-7

Park, S. W., Kim, H. J., & Lee, C. S. (2003). Investigation of atomization characteristics and prediction accuracy of hybrid models for high-speed diesel fuel sprays.

Parnell, J. J., Berka, R., Young, H. A., Sturino, J. M., Kang, Y., Barnhart, D. M., et al. (2016). From the Lab to the Farm: An Industrial Perspective of Plant Beneficial Microorganisms. *Frontiers in Plant Science, 7*(1110). doi:https://doi.org/10.3389/fpls.2016.01110

Patterson, M. A., & Reitz, R. D. (1998). Modeling the effects of fuel spray characteristics on diesel engine combustion and emission. *SAE Transactions*, 27-43.

Paul, D. R. (2011). Elaborations on the Higuchi model for drug delivery. *International journal of pharmaceutics, 418*(1), 13-17. doi:https://doi.org/10.1016/j.ijpharm.2010.10.037

Paulo, F., & Santos, L. (2017). Design of experiments for microencapsulation applications: A review. *Materials Science and Engineering: C, 77*, 1327-1340.

Pengnoo, A., Hashidoko, Y., Onthong, J., Gimsanguan, S., Sae-ong, M., Shinano, T., et al. (2007). Screening of phosphate-solubilizing microorganisms in rhizosphere and rhizoplane of adverse soil-adapting plants in Southern Thailand. *Tropics, 16*(1), 1-7. doi:https://doi.org/10.3759/tropics.16.1

Persson, T. (2013). Eulerian-Lagrangian Modeling of Multicomponent Spray for Aseptic Treatment of Carton Bottles in the Food Process and Packaging Industry.

Pikovskaya, R. (1948). Mobilization of phosphorus in soil in connection with vital activity of some microbial species. *Mikrobiologiya, 17*(362), 362-370.

Pimentel, R., Dechamplain, A., Kretschmer, D., Stowe, R., Harris, P., & Kurbatskii, K. (2006). Improved Atomization Model for CFD Codes. *1*.

Pinto, S. S., Fritzen-Freire, C. B., Benedetti, S., Murakami, F. S., Petrus, J. C. C., Prudêncio, E. S., et al. (2015). Potential use of whey concentrate and prebiotics as carrier agents to protect *Bifidobacterium*-BB-12 microencapsulated by spray drying. *Food Research International, 67*, 400-408. doi:https://doi.org/10.1016/j.foodres.2014.11.038

Quintal Martínez, J. P., Ruiz Ruiz, J. C., & Segura Campos, M. R. (2018). Release Kinetic Studies of *Stevia rebaudiana* Extract Capsules from Sodium Alginate and Inulin by Ionotropic Gelation. *Advances in Materials Science and Engineering, 2018*.

Quissek, M., Lauer, T., García-Afonso, O., & Fowles, S. (2019). Identification of film breakup for a liquid urea-water-solution and application to CFD.

Ragavan, M. L., & Das, N. (2018). Process optimization for microencapsulation of probiotic yeasts. *Frontiers in Biology*, *13*(3), 197-207.

Rahman, Z. A., Gikonyo, E., Silek, B., Goh, K., & Soltangheisi, A. (2014). Evaluation of phosphate rock sources and rate of application on oil palm yield grown on peat soils of Sarawak, Malaysia. *Journal of Agronomy, 13*(1), 12-22. doi:https://doi.org/10.3923/ja.2014.12.22.

Rajam, R., & Anandharamakrishnan, C. (2015). Spray freeze drying method for microencapsulation of *Lactobacillus plantarum*. *Journal of Food Engineering, 166*, 95-103. doi:https://doi.org/10.1016/j.jfoodeng.2015.05.029

Ratanavaraporn, J., Chuma, N., Kanokpanont, S., & Damrongsakkul, S. (2019). Beads fabricated from alginate, hyaluronic acid, and gelatin using ionic crosslinking and layer-by-layer coating techniques for controlled release of gentamicin. *Journal of Applied Polymer Science, 136*(1), 46893.

Rathore, S., Desai, P. M., Liew, C. V., Chan, L. W., & Heng, P. W. S. (2013). Microencapsulation of microbial cells. *Journal of Food Engineering, 116*(2), 369-381.

Reitz, R. D., & Diwakar, R. (1986). Effect of drop breakup on fuel sprays. *SAE Transactions*, 218-227.

Robitaille, R., Pariseau, J. F., Leblond, F. A., Lamoureux, M., Lepage, Y., & Hallé, J. P. (1999). Studies on small (< 350 μm) alginate-poly-L-lysine microcapsules. III. Biocompatibility of smaller versus standard microcapsules. *Journal of Biomedical Materials Research: An Official Journal of The Society for Biomaterials, The Japanese Society for Biomaterials, and The Australian Society for Biomaterials and the Korean Society for Biomaterials, 44*(1), 116-120.

Rodriguez, H., & Fraga, R. (1999). Phosphate solubilizing bacteria and their role in plant growth promotion. *Biotechnology advances, 17*(4), 319-339. doi:https://doi.org/10.1016/S0734-9750(99)00014-2

Rodriguez, H., Fraga, R., Gonzalez, T., & Bashan, Y. (2006). Genetics of phosphate solubilization and its potential applications for improving plant growth-promoting bacteria. *Plant and Soil, 287*(1), 15-21. doi:https://doi.org/10.1007/978-1-4020-5765-6_2

Sahu, P., Lavanya, G., & Brahmaprakash, G. P. (2013). Fluid Bed Dried Microbial Inoculants Formulation with Improved Survival and Reduced Contamination Level. *33*, 81-94.

Sahu, P., Lavanya, G., Gupta, A., & Brahmaprakash, G. P. (2016). Fluid Bed dried microbial consortium for enhanced plant growth: A step towards next generation bio formulation. *Vegetos- An International Journal of Plant Research, 29*, 6. doi:10.5958/2229-4473.2016.00093.8

Salinas, C., Vasco, D. A., & Moraga, N. O. (2013). Two-dimensional non-Newtonian injection molding with a new control volume FEM/volume of fluid method. *International Journal for Numerical Methods in Fluids, 71*(12), 1509-1523.

Sampath, M. K. (2005). *Computational Study of Large Droplet Breakup in the Vicinity of an Airfoil*.

San Chan, Y., & Don, M. M. (2013). Optimization of process variables for the synthesis of silver nanoparticles by *Pycnoporus sanguineus* using statistical experimental design. *Journal of the Korean Society for Applied Biological Chemistry, 56*(1), 11-20.

Santos, C. H. B., do Nascimento, F. C., Lobo, L. L. B., Martins, A. B. G., de Almeida Teixeira, G. H., & Rigobelo, E. C. (2020). Effect of encapsulated plant growth promoting microorganisms on soil biochemical parameters and development of fruit tree seedlings. *Australian Journal of Crop Science, 14*(3), 3006-3014.

Satoh, K., Kawai, T., Ishikawa, M., & Matsuoka, T. (2000). Development of method for predicting efficiency of oil mist separators.

Satyaprakash, M., Nikitha, T., Reddi, E., Sadhana, B., & Vani, S. S. (2017). Phosphorous and phosphate solubilising bacteria and their role in plant nutrition. *Int. J. Curr. Microbiol. App. Sci*, *6*(4), 2133-2144.

Schiller, L. (1933). Über die grundlegenden Berechnungen bei der Schwerkraftaufbereitung. *Z. Vereines Deutscher Inge., 77*, 318-321.

Schleifer, K. H., & Kloos, W. E. (1975). Isolation and characterization of *Staphylococci* from human skin I. Amended descriptions of *Staphylococcus epidermidis* and *Staphylococcus saprophyticus* and descriptions of three new species: *Staphylococcus cohnii*, *Staphylococcus haemolyticus*, and *Staphylococcus*

xylosus. *International Journal of Systematic and Evolutionary Microbiology, 25*(1), 50-61. doi:https://doi.org/10.1099/00207713-25-1-50

Schmidt, D. P., Nouar, I., Senecal, P., Rutland, J., Martin, J., Reitz, R. D., et al. (1999). Pressure-swirl atomization in the near field. *SAE Transactions*, 471-484.

Schoebitz, M., & Belchí, M. D. L. (2016). Encapsulation techniques for plant growth-promoting rhizobacteria *Bioformulations: for sustainable agriculture* (pp. 251-265): Springer.

Schoebitz, M., Ceballos, C., & Ciamp, L. (2013a). Effect of immobilized phosphate solubilizing bacteria on wheat growth and phosphate uptake. *Journal of soil science and plant nutrition, 13*(1), 1-10.

Schoebitz, M., López, M. D., & Roldán, A. (2013b). Bioencapsulation of microbial inoculants for better soil–plant fertilization. A review. *Agronomy for Sustainable Development, 33*(4), 751-765.

Schoebitz, M., Osman, J., & Ciampi, L. (2013c). Effect of immobilized Serratia sp. by spray-drying technology on plant growth and phosphate uptake. *Chilean Journal of Agricultural & Animal Sciences, Ex Agro-Ciencia, 29*(2), 111-119.

Scholz, R. W., Ulrich, A. E., Eilittä, M., & Roy, A. (2013). Sustainable use of phosphorus: a finite resource. *Science of the Total Environment, 461*, 799-803.

Schutyser, M. A., Perdana, J., & Boom, R. M. (2012). Single droplet drying for optimal spray drying of enzymes and probiotics. *Trends in food science & technology, 27*(2), 73-82.

Selim, H. M. (2015). Phosphate in Soils: Interaction with Micronutrients, Radionuclides and Heavy Metals: CRC Press.

Selvakumar, G., Mohan, M., Kundu, S., Gupta, A., Joshi, P., Nazim, S., et al. (2008). Cold tolerance and plant growth promotion potential of *Serratia marcescens* strain SRM (MTCC 8708) isolated from flowers of summer squash *(Cucurbita pepo)*. *Letters in applied microbiology, 46*(2), 171-175.

Selvi, K., Paul, J., Vijaya, V., & Saraswathi, K. (2017). Analyzing the efficacy of phosphate solubilizing microorganisms by enrichment culture techniques. *Biochemistry and Molecular Biology Journal, 3*(1), 1-7. doi:https://doi.org/10.21767/2471-8084.100029

Semyonov, D., Ramon, O., Kaplun, Z., Levin-Brener, L., Gurevich, N., & Shimoni, E. (2010). Microencapsulation of *Lactobacillus paracasei* by spray freeze drying. *Food Research International, 43*(1), 193-202. doi:https://doi.org/10.1016/j.foodres.2009.09.028

Senecal, P., Schmidt, D. P., Nouar, I., Rutland, C. J., Reitz, R. D., & Corradini, M. (1999). Modeling high-speed viscous liquid sheet atomization. *International Journal of Multiphase Flow, 25*(6-7), 1073-1097.

Shamekhi, F., Shuhaimi, M., Ariff, A., & Manap, Y. A. (2013). Cell viability of microencapsulated *Bifidobacterium animalis* subsp. lactis under freeze-drying, storage and gastrointestinal tract simulation conditions. *Folia Microbiologica, 58*(2), 91-101.

Sharma, S., Acharya, J., Banjara, M. R., Ghimire, P., & Singh, A. (2020). Comparison of acridine orange fluorescent microscopy and gram stain light microscopy for the rapid detection of bacteria in cerebrospinal fluid. *BMC Research Notes, 13*(1), 29. doi:10.1186/s13104-020-4895-7

Sharma, S., Kumar, V., & Tripathi, R. B. (2017). Isolation of phosphate solubilizing microorganism (PSMs) from soil. *Journal of microbiology and Biotechnology Research, 1*(2), 90-95.

Sharma, S., Sayyed, R. Z., Trivedi, M. H., & Gobi, T. A. (2013). Phosphate solubilizing microbes: sustainable approach for managing phosphorus deficiency in agricultural soils. *SpringerPlus, 2*(1), 587. doi:https://doi.org/10.1186/2193-1801-2-587

Shu, G., He, Y., Chen, L., Song, Y., Meng, J., & Chen, H. (2018). Microencapsulation of *Bifidobacterium bifidum* BB01 by xanthan–chitosan: preparation and its stability in pure milk. *Artificial Cells, Nanomedicine, and Biotechnology, 46*(sup1), 588-596.

Singh, A., Parmar, N., & Kuhad, R. C. (2011). Bioaugmentation, Biostimulation and Biocontrol. Berlin, Heidelberg: Springer

Singh, B., Sharma, D., & Gupta, A. (2009). A study towards release dynamics of thiram fungicide from starch–alginate beads to control environmental and health hazards. *Journal of hazardous materials, 161*(1), 208-216.

Singh, P., Kumar, V., & Agrawal, S. (2014). Evaluation of Phytase Producing Bacteria for Their Plant Growth Promoting Activities. *International Journal of Microbiology, 2014*, 426483. doi:10.1155/2014/426483

Sirignano, W. A. (2010). Fluid dynamics and transport of droplets and sprays: Cambridge university press.

Situmorang, E. C., Prameswara, A., Sinthya, H. C., Toruan-Mathius, N., & Liwang, T. (2015). Indigenous Phosphate Solubilizing Bacteria from Peat Soil for an Eco-friendly Biofertilizer in Oil Palm Plantation. *KnE Energy, 1*(1), 65-72. doi:https://dx.doi.org/10.18502/ken.v1i1.324

Sohail, A., Turner, M. S., Coombes, A., & Bhandari, B. (2013). The viability of *Lactobacillus rhamnosus* GG and *Lactobacillus acidophilus* NCFM following double encapsulation in alginate and maltodextrin. *Food and bioprocess technology, 6*(10), 2763-2769.

Sohail, A., Turner, M. S., Coombes, A., Bostrom, T., & Bhandari, B. (2011). Survivability of probiotics encapsulated in alginate gel microbeads using a novel impinging aerosols method. *International Journal of Food Microbiology, 145*(1), 162-168.

Sohail, A., Turner, M. S., Prabawati, E. K., Coombes, A. G., & Bhandari, B. (2012). Evaluation of *Lactobacillus rhamnosus* GG and *Lactobacillus acidophilus* NCFM encapsulated using a novel impinging aerosol method in fruit food products. *International Journal of Food Microbiology, 157*(2), 162-166.

Song, O.-R., Lee, S.-J., Lee, Y.-S., Lee, S.-C., Kim, K.-K., & Choi, Y.-L. (2008). Solubilization of insoluble inorganic phosphate by *Burkholderia cepacia* DA23 isolated from cultivated soil. *Brazilian Journal of Microbiology, 39*(1), 151-156.

Sousa, S. M., de Oliveira, C. A., Andrade, D. L., de Carvalho, C. G., Ribeiro, V. P., Pastina, M. M., et al. (2020). Tropical *Bacillus* Strains Inoculation Enhances Maize Root Surface Area, Dry Weight, Nutrient Uptake and Grain Yield.

Souza, A. S., Santos, W. N. L. d., & Ferreira, S. L. C. (2005). Application of Box–Behnken design in the optimisation of an on-line pre-concentration system using knotted reactor for cadmium determination by flame atomic absorption spectrometry.

Spaepen, S., & Vanderleyden, J. (2011). Auxin and plant-microbe interactions. *Cold Spring Harbor perspectives in biology, 3*(4), a001438.

Spaepen, S., Vanderleyden, J., & Remans, R. (2007). Indole-3-acetic acid in microbial and microorganism-plant signaling. *FEMS microbiology reviews, 31*(4), 425-448.

Stähle, P., Gaukel, V., & Schuchmann, H. P. (2017). Comparison of an Effervescent Nozzle and a Proposed Air-Core-Liquid-Ring (ACLR) Nozzle for Atomization of Viscous Food Liquids at Low Air Consumption. *Journal of Food Process Engineering, 40*(1), e12268. doi:10.1111/jfpe.12268

Stephens, J., & Rask, H. (2000). Inoculant production and formulation. *Field Crops Research, 65*(2), 249-258.

Storm, C., & Joos, F. (2019). Comparison of secondary breakup models for droplet-laden compressor flows. *International Journal of Multiphase Flow, 116*, 125-136. doi:https://doi.org/10.1016/j.ijmultiphaseflow.2019.04.005

Story, S., & Brigmon, R. L. (2017). Influence of triethyl phosphate on phosphatase activity in shooting range soil: Isolation of a zinc-resistant bacterium with an acid phosphatase. *Ecotoxicology and Environmental Safety, 137*, 165-171. doi:https://doi.org/10.1016/j.ecoenv.2016.12.003

Suh, J., Jiarong, P., & Toan, P. (2006). Quality control of biofertilizers. Paper presented at the Biofertilizers Manual. Forum for Nuclear Cooperation in Asia. Japan.

Sulandjari, Sakya, A. T., Syamsiyah, J., & Panji, D. (2019). The application of amendments to increase nutrients absorption of *Petiveria aleaceae L*. (Singawalang) in peat soils. *IOP Conference Series: Earth and Environmental Science, 250*, 012017. doi:10.1088/1755-1315/250/1/012017

Suleman, M., Yasmin, S., Rasul, M., Yahya, M., Atta, B. M., & Mirza, M. S. (2018). Phosphate solubilizing bacteria with glucose dehydrogenase gene for phosphorus uptake and beneficial effects on wheat. *PLOS ONE, 13*(9).

Sutejo, Y., Saggaff, A., Rahayu, W., & Hanafiah. (2017). Physical and chemical characteristics of fibrous peat. Paper presented at the AIP Conference Proceedings.

Sutton, S. (2011). Accuracy of plate counts. *Journal of validation technology, 17*(3), 42-46.

Swioklo, S., Ding, P., Pacek, A. W., & Connon, C. J. (2017). Process parameters for the high-scale production of alginate-encapsulated stem cells for storage and distribution throughout the cell therapy supply chain. *Process biochemistry, 59*, 289-296.

Szczech, M., & Maciorowski, R. (2016). Microencapsulation technique with organic additives for biocontrol agents. *Journal of Horticultural Research, 24*(1), 111-122.

Tamura, K., Peterson, D., Peterson, N., Stecher, G., Nei, M., & Kumar, S. (2011). MEGA5: molecular evolutionary genetics analysis using maximum likelihood, evolutionary distance, and maximum parsimony methods. *Molecular biology and evolution, 28*(10), 2731-2739. doi:https://doi.org/10.1093/molbev/msr121.

Tanner, F. X. (1997). Liquid jet atomization and droplet breakup modeling of non-evaporating diesel fuel sprays. *SAE Transactions*, 127-140.

Taurian, T., Anzuay, M. S., Angelini, J. G., Tonelli, M. L., Ludueña, L., Pena, D., et al. (2010). Phosphate-solubilizing peanut associated bacteria: screening for plant growth-promoting activities. *Plant and Soil, 329*(1), 421-431. doi:https://doi.org/10.1007/s11104-009-0168-x

Taylor, G. (1963). The shape and acceleration of a drop in a high speed air stream. The Scientific Papers of GI Taylor, Vol III, Edition GK Batchelor: University Press, Cambridge.

Teng, Z., Shao, W., Zhang, K., Huo, Y., & Li, M. (2019). Characterization of phosphate solubilizing bacteria isolated from heavy metal contaminated soils and their potential for lead immobilization. *Journal of environmental management, 231*, 189-197. doi:https://doi.org/10.1016/j.jenvman.2018.10.012

Timilsena, Y. P., Akanbi, T. O., Khalid, N., Adhikari, B., & Barrow, C. J. (2019). Complex coacervation: Principles, mechanisms and applications in microencapsulation. *International Journal of Biological Macromolecules, 121*, 1276-1286. doi:https://doi.org/10.1016/j.ijbiomac.2018.10.144

Tiwari, R., Hoondal, G., & Tewari, R. (2009). Laboratory techniques in microbiology and biotechnology. Chandigarh, India: Abhishek Publications.

Tomar, G., Fuster, D., Zaleski, S., & Popinet, S. (2010). Multiscale simulations of primary atomization. *Computers & Fluids, 39*(10), 1864-1874.

Trabelsi, I., Bejar, W., Ayadi, D., Chouayekh, H., Kammoun, R., Bejar, S., et al. (2013). Encapsulation in alginate and alginate coated-chitosan improved the survival of newly probiotic in oxgall and gastric juice. *International Journal of Biological Macromolecules, 61*, 36-42.

Trivedi, P., Pandey, A., & Palni, L. M. S. (2005). Carrier-based preparations of plant growth-promoting bacterial inoculants suitable for use in cooler regions. *World Journal of Microbiology and biotechnology, 21*(6-7), 941-945.

Tu, L., He, Y., Yang, H., Wu, Z., & Yi, L. (2015). Preparation and characterization of alginate–gelatin microencapsulated *Bacillus subtilis* SL-13 by emulsification/internal gelation. *Journal of Biomaterials Science, Polymer Edition, 26*(12), 735-749.

Vejan, P., Abdullah, R., Khadiran, T., Ismail, S., & Nasrulhaq Boyce, A. (2016). Role of plant growth promoting rhizobacteria in agricultural sustainability—a review. *Molecules, 21*(5), 573.

Vemmer, M., & Patel, A. V. (2013). Review of encapsulation methods suitable for microbial biological control agents. *Biological Control, 67*(3), 380-389.

Venegas Mendez, J. (2013). An approach to power efficiency determination in the solar energy systems using central composite design and Box-Behnken design.

Verma, P., Yadav, A. N., Kumar, V., Singh, D. P., & Saxena, A. K. (2017). Beneficial plant-microbes interactions: biodiversity of microbes from diverse extreme environments and its impact for crop improvement *Plant-microbe interactions in agro-ecological perspectives* (pp. 543-580): Springer.

Viveganandan, G., & Jauhri, K. (2000). Growth and survival of phosphate-solubilizing bacteria in calcium alginate. *Microbiological Research, 155*(3), 205-207.

Vyas, P., & Gulati, A. (2009). Organic acid production in vitro and plant growth promotion in maize under controlled environment by phosphate-solubilizing fluorescent *Pseudomonas*. *BMC microbiology, 9*(1), 174.

Walpola, B. C., Song, J.-S., Keum, M.-J., & Yoon, M.-H. (2012a). Evaluation of phosphate solubilizing potential of three *Burkholderia* species isolated from green house soils. *Korean Journal of Soil Science and Fertilizer, 45*(4), 602-609. doi:http://dx.doi.org/10.7745/KJSSF.2012.45.4.602

Walpola, B. C., Song, J.-S., & Yoon, M.-H. (2012b). Assessment of Plant Growth Promoting Activities of Phosphorus Solubilizing Bacteria. *Korean Journal of Soil Science and Fertilizer, 45*(1), 66-73. doi:https://doi.org/10.7745/KJSSF.2012.45.1.066

Wang, S., Dorr, G., Khashehchi, M., & He, X. (2015). Performance of selected agricultural spray nozzles using particle image velocimetry. *Journal of Agricultural Science and Technology, 17*(3), 601-613.

Wang, X., & Zhao, H. (2018). Numerical simulation of the gasoline spray with an outward-opening piezoelectric injector: a comparative study of different breakup models.

Wang, X., Zhu, C., & Ahluwalia, R. (2004). Numerical simulation of evaporating spray jets in concurrent gas–solids pipe flows. *Powder technology, 140*(1-2), 56-67.

Wirunpan, M., Savedboworn, W., & Wanchaitanawong, P. (2016). Survival and shelf life of *Lactobacillus lactis* 1464 in shrimp feed pellet after fluidized bed drying. *Agriculture and Natural Resources, 50*(1), 1-7. doi:https://doi.org/10.1016/j.anres.2016.01.001

Wojdas, O. (2010). Numerical simulations for diesel engine development. Doc'INSA-INSA de Lyon.

Wongkanya, R., Chuysinuan, P., Pengsuk, C., Techasakul, S., Lirdprapamongkol, K., Svasti, J., et al. (2017). Electrospinning of alginate/soy protein isolated nanofibers and their release characteristics for biomedical applications. *Journal of Science: Advanced Materials and Devices, 2*(3), 309-316. doi:https://doi.org/10.1016/j.jsamd.2017.05.010

Wright, B., Cave, R. A., Cook, J. P., Khutoryanskiy, V. V., Mi, S., Chen, B., et al. (2012). Enhanced viability of corneal epithelial cells for efficient transport/storage using a structurally modified calcium alginate hydrogel. *Regenerative medicine, 7*(3), 295-307.

Wu, J., Xu, J., & Wang, H. (2020). Numerical simulation of aerosol dynamics in an impinging jet with microdroplet coalescence. *Aerosol Science and Technology*(just-accepted), 1-22.

Wu, L., Yick, K.-l., Ng, S.-p., & Yip, J. (2012a). Application of the Box–Behnken design to the optimization of process parameters in foam cup molding. *Expert Systems with Applications, 39*(9), 8059-8065. doi:https://doi.org/10.1016/j.eswa.2012.01.137

Wu, P.-K., Tseng, L.-K., & Faeth, G. (1992). Primary breakup in gas/liquid mixing layers for turbulent liquids. *Atomization and Sprays, 2*(3).

Wu, Z., Guo, L., Qin, S., & Li, C. (2012b). Encapsulation of *R. planticola* Rs-2 from alginate-starch-bentonite and its controlled release and swelling behavior under simulated soil conditions. *Journal of industrial microbiology & biotechnology, 39*(2), 317-327.

Wu, Z., He, Y., Chen, L., Han, Y., & Li, C. (2014). Characterization of *Raoultella planticola* Rs-2 microcapsule prepared with a blend of alginate and starch and its release behavior. *Carbohydrate Polymers, 110*, 259-267. doi:http://dx.doi.org/10.1016/j.carbpol.2014.04.011

Wu, Z., Zhao, Y., Kaleem, I., & Li, C. (2011). Preparation of calcium–alginate microcapsuled microbial fertilizer coating *Klebsiella oxytoca* Rs-5 and its performance under salinity stress. *European journal of soil biology, 47*(2), 152-159.

Wyciszkiewicz, M., Saeid, A., Chojnacka, K., & Górecki, H. (2015). Production of phosphate biofertilizers from bones by phosphate-solubilizing bacteria *Bacillus megaterium*. *Open Chemistry, 13*(1).

Xiao, C., Chi, R., He, H., Qiu, G., Wang, D., & Zhang, W. (2009). Isolation of phosphate-solubilizing fungi from phosphate mines and their effect on wheat seedling growth. *Applied biochemistry and biotechnology, 159*(2), 330-342.

Yadav, S., Kaushik, R., Saxena, A. K., & Arora, D. K. (2011). Diversity and phylogeny of plant growth-promoting bacilli from moderately acidic soil. *Journal of Basic Microbiology, 51*(1), 98-106.

Yadav, S., Yadav, S., Kaushik, R., Saxena, A. K., & Arora, D. K. (2014). Genetic and functional diversity of fluorescent *Pseudomonas* from rhizospheric soils of wheat crop. *Journal of Basic Microbiology, 54*(5), 425-437.

Yan, K. C., Nair, K., & Sun, W. (2010). Three dimensional multi-scale modelling and analysis of cell damage in cell-encapsulated alginate constructs. *Journal of biomechanics, 43*(6), 1031-1038.

Young, C.-C., Rekha, P., Lai, W.-A., & Arun, A. (2006). Encapsulation of plant growth-promoting bacteria in alginate beads enriched with humic acid. *Biotechnology and bioengineering, 95*(1), 76-83.

Yu, Y., Zhang, Y., Martin, J. A., & Ozbolat, I. T. (2013). Evaluation of cell viability and functionality in vessel-like bioprintable cell-laden tubular channels. *Journal of biomechanical engineering, 135*(9).

Zaeim, D., Sarabi-Jamab, M., Ghorani, B., Kadkhodaee, R., & Tromp, R. H. (2017). Electrospray assisted fabrication of hydrogel microcapsules by single- and double-stage procedures for encapsulation of probiotics. *Food and Bioproducts Processing, 102*, 250-259. doi:https://doi.org/10.1016/j.fbp.2017.01.004

Zeoli, N., & Gu, S. (2006). Numerical modelling of droplet break-up for gas atomisation. *Computational Materials Science, 38*(2), 282-292. doi:https://doi.org/10.1016/j.commatsci.2006.02.012

Zhang, T., Dong, B., Chen, X., Qiu, Z., Jiang, R., & Li, W. (2017). Spray characteristics of pressure-swirl nozzles at different nozzle diameters. *Applied Thermal Engineering, 121*, 984-991. doi:https://doi.org/10.1016/j.applthermaleng.2017.04.089

Zhang, T., Dong, B., Zhou, X., Guan, L., Li, W., & Zhou, S. (2018). Experimental Study of Spray Characteristics of Kerosene-Ethanol Blends from a Pressure-Swirl Nozzle. *International Journal of Aerospace Engineering, 2018*, 2894908. doi:10.1155/2018/2894908

Zhao, M., Wang, Y., Huang, X., Gaenzle, M., Wu, Z., Nishinari, K., et al. (2018). Ambient storage of microencapsulated Lactobacillus plantarum ST-III by complex coacervation of type-A gelatin and gum arabic. *Food Funct, 9*(2), 1000-1008. doi:10.1039/c7fo01802a

Zhu, F., Qu, L., Hong, X., & Sun, X. (2011). Isolation and Characterization of a Phosphate-Solubilizing Halophilic Bacterium *Kushneria* sp. YCWA18 from Daqiao Saltern on the Coast of Yellow Sea of China. *Evidence-Based Complementary and Alternative Medicine, 2011,* 615032. doi:10.1155/2011/615032

Zohar Perez, C., Ritte, E., Chernin, L., Chet, I., & Nussinovitch, A. (2002). Preservation of Chitinolytic Pantoae agglomerans in a Viable Form by Cellular Dried Alginate-Based Carriers. *Biotechnology progress, 18*(6), 1133-1140.

APPENDIX

Appendix A Isolation Process

Isolation of phosphate solubilizing microorganisms were done on NBRIP and NBRIP-BPB agar and pure isolates were obtained by sub-culturing on modified TSA. The isolation process for Sample A was as follow:

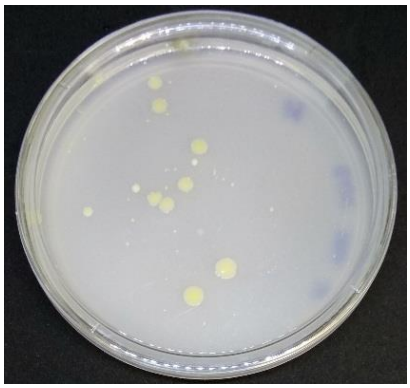

0.1 ml of sample were spread on NBRIP agar and incubated at 30ºC for 5 d

Distinct colonies were picked and transferred to NBRIP-BPB agar

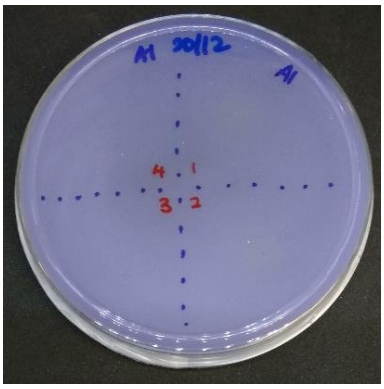

Incubated at 30ºC for 3 d

Colonies that turned dye to yellow were further purified with modified TSA until pure isolates were obtained. Pure isolates were kept in refrigerator at 4ºC

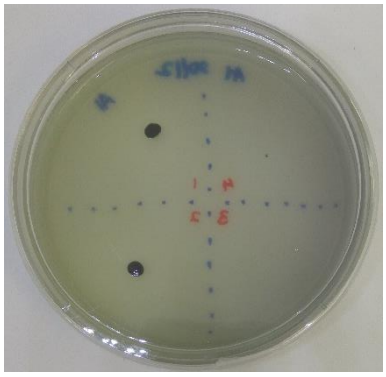

Appendix B Preparation of Phosphate Calibration Curve

Phosphate calibration curve was prepared by using standard phosphate solution KH_2PO_4 (150 mg PO_4^- /L) as the stock solution. The calibration curve was prepared in the range of 0 to 30 ppm of PO_4^-. The absorbance was taken at wavelength of 400 nm using UV-Visible spectrometer. The results were tabulated as follow in Table A.1. Plot of absorbance against phosphate concentration was shown in Figure A.1.

Table A.1 Phosphate calibration curve. Each point represents a mean value and the error bars showed the standard deviation (n=3)

Concentration, ppm	**Stock solution, ml**	**NBRIP solution, ml**	**Vanadate molybdate reagent, ml**	**Distilled water, ml**	**Absorbance**
0	0	3	1	1	0
7.5	0.25	3	1	0.75	0.32±0.01
15	0.5	3	1	0.5	0.60±0.02
22.5	0.75	3	1	0.25	0.91±0.03
30	1	3	1	0	1.20±0.02

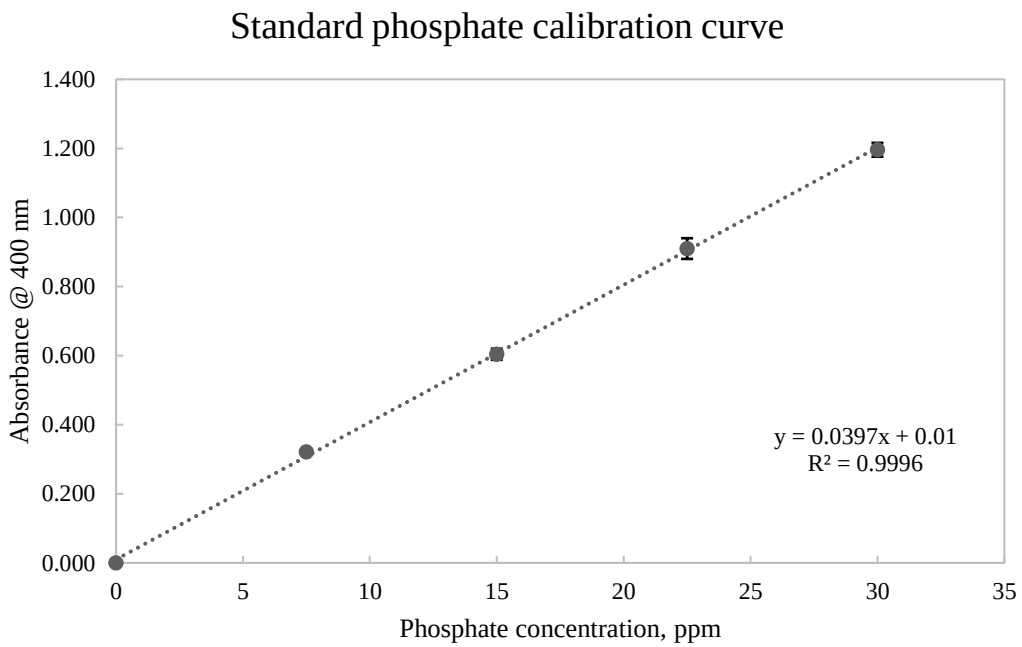

Figure A.1 Plot of absorbance against phosphate concentration. Each point represents a mean value (n=3) and error bars (±SD) are shown when larger than symbol

From the plot, the r-squared of the standard phosphate calibration curve was determined to be 0.9996 with equation of y=0.0397x+0.01, where y is the absorbance measure at wavelength of 400 nm and x is the soluble phosphate concentration in ppm. This equation was used to identify the amount of soluble phosphate in supernatant throughout the studies.

Appendix C Data on Preliminary Test of Phosphate Solubilization Potential of Isolated Bacteria

16 isolates were obtained and tested for their phosphate solubilization ability in NBRIP broth supplemented with $AlPO_4$ as the insoluble phosphate source. The results were expressed in mean for triplicates and tabulated in Table A.*2*.

Table A.2 Preliminary test on the phosphate solubilization potential of 16 isolates. Each point represents a mean value and the error bars showed the standard deviation (n=3)

	Absorbance @ 400 nm	**Phosphate solubilized, ppm**	**Net phosphate solubilized, ppm**
Control	0.23±0.01	5.47±0.14	0.00
A02	1.08±0.02	26.90±0.59	21.43±0.45
A03	0.84±0.01	20.92±0.27	15.45±0.13
A05	0.77±0.01	19.22±0.26	13.75±0.11
A06	1.08±0.01	26.90±0.22	21.42±0.08
A08	0.77±0.01	19.01±0.11	13.54±0.03
A09	1.06±0.08	26.53±2.00	21.06±1.86
A10	1.08±0.06	26.95±1.61	21.48±1.46
A11	0.79±0.03	19.67±0.78	14.19±0.63
B02	1.17±0.02	29.14±0.50	23.67±0.35
B03	0.82±0.02	20.33±0.55	14.85±0.40
B04	0.87±0.01	21.55±0.24	16.07±0.09
B05	0.49±0.04	12.14±0.99	6.67±0.85
B06	0.98±0.05	24.31±1.13	18.83±0.99
C03	1.08±0.04	26.95±1.01	21.48±0.87
C10	1.05±0.06	26.19±1.50	20.71±1.36
C11	1.16±0.02	28.88±0.40	23.41±0.26

** A denotes samples enriched with nutrient broth; B denotes samples enriched with Al-P, Fe-P and phytate; C denotes samples enriched with Al-P and Fe-P before isolation process.*

Appendix D Data on Determination of Isolates A10, B02 and C11

The 3 isolates from preliminary tests that showed highest phosphate solubilization potential were selected and tested in modified NBRIP. Besides, the effect of addition of soluble during inoculum preparation were studied. The results of triplicates were expressed in average and shown in Table A.3.

Table A.3 Comparison on soluble P concentration and pH when cell culture grown with KH_2PO_4 prior to testing using modified NBRIP broth. Each point represents a mean value and the error bars showed the standard deviation (n=3)

	Absorbance	**Phosphate solubilized, ppm**	**Net phosphate solubilized, ppm**	**pH of medium**
Control	0.11±0.01	5.47±0.14	0.000	5.54±0.11
A10	0.88±0.04	44.04±1.78	38.56±1.64	3.66±0.08
B02	0.91±0.03	45.13±1.29	39.65±1.15	3.71±0.02
C11	0.67±0.03	33.31±1.43	27.83±1.29	3.74±0.03

Appendix E Preparation of Growth Curve for Bacteria, *S. haemolyticus* HCLB02

A loop of *S. haemolyticus* HCLB02 was transferred from modified TSA plates to 20 ml of modified NBRIP broth containing per litre: 10 g glucose, 5 g $MgCl_2.6H_2O$, 0.25g $MgSO_4$. $7H_2O$, 0.2 g KCl, 2 g yeast extract (Nautiyal, 1999) supplemented with 2.5 g soluble phosphate, KH_2PO_4 and grown at 37ºC, 130 rpm for 24 h. Then, 1 ml of cell culture (adjusted to OD 1.0 by diluting with NBRIP broth, approximately 0.5 x 10^8 CFU/ml) was transferred into 50 ml of fresh modified NBRIP broth and incubated at 37ºC for 24 h at 130 rpm. Samples were removed at intervals and the OD were recorded. Experiments were in performed in triplicate and the data were tabulated in Table A.4.

Table A.4 Optical density of *S. haemolyticus* HCLB02 over period of 24h. Each point represents a mean value and the error bars showed the standard deviation (n=3)

Time (h)	OD_{600}	Time (h)	OD_{600}
0	0.04±0.02	10	3.09±0.18
2	0.03±0.02	11	4.48±0.14
4	0.08±0.01	12	4.70±0.14
5	0.14±0.02	13	5.08±0.21
6	0.26±0.01	16	6.40±0.01
7	0.62±0.03	20	6.20±0.22
8	1.29±0.01	24	5.89±0.09
9	2.33±0.13		

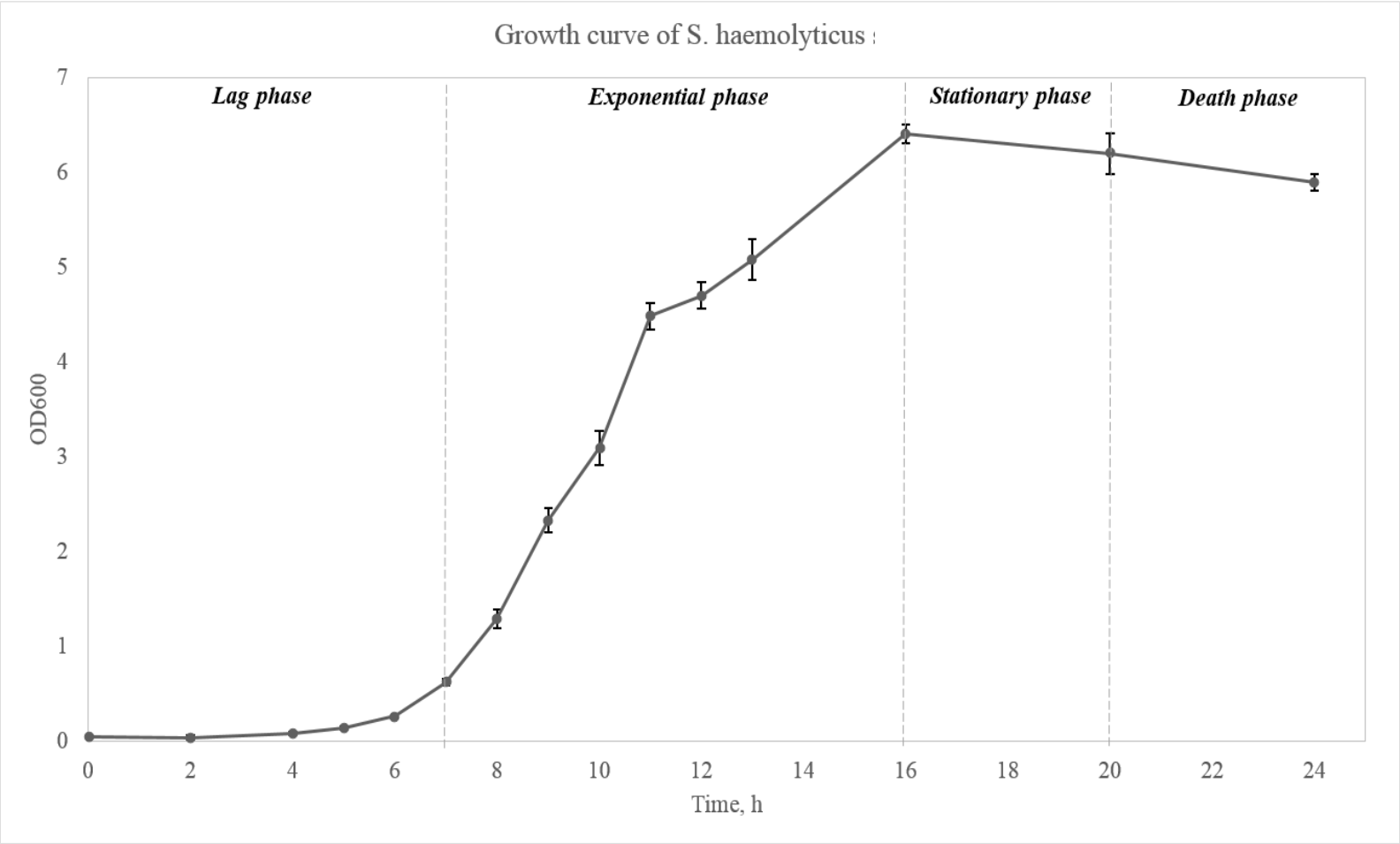

Figure A.2 Growth curve for *S. haemolyticus* HCLB02. Each point represents a mean value (n=3) and error bars (±SD) are shown when larger than symbol

Figure A.2 shows the growth curve of *S. haemolyticus* HCLB02 over period of 24 h. From the curve, at 0 – 7 h it was in the lag phase where there was only small increase in cell numbers. At this phase, cells were adjusting to its new environment and started to synthesize ribosomal RNA and enzymes for replication. The cells increased slowly initially and approaching an exponential growth rate at 7 – 16 h. At exponential phase, cells doubled at a constant, exponential rate. It entered the stationary phase at 16 h to 18 h and at this phase, growth rate and death rate were equal as nutrients were depleted and accumulated carbon dioxide and wastes caused the pH of medium to drop. Eventually, the cells entered the death phase after 20 h. Here, the death rate was greater than growth rate caused the cells number to decrease. Based on the growth curve, B02 entered stationary phase between 16 – 20 h. Thus, inoculum in this research works was prepared by culturing bacteria for 20 h at 37ºC.

The specific growth rate of *S. haemolyticus* can be determined with following equations:

$$\frac{dX}{dt} = uX \text{ , where u= specific growth rate } (h^{-1})$$

Rearranging it,

$$\frac{dX}{X} = u\ dt$$

Integrate it,

$$\ln X = u\,t + C, \text{ where } C = \ln X_0$$

$$\ln X = u\,t + \ln X_0$$

Note that, specific growth rate, u is the slope of the straight line at exponential phase. Straight line of exponential phase was presented in Figure A.3. The specific growth rate was found to be 0.9035 h^{-1}.

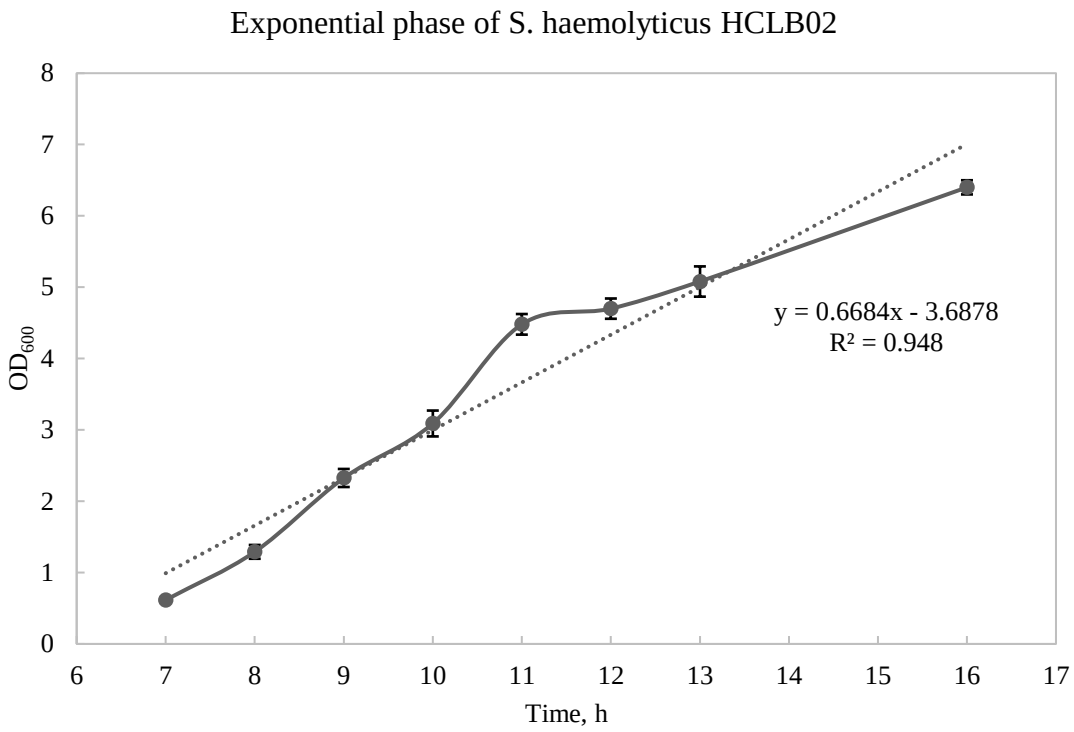

Figure A.3 Exponential phase for *S. haemolyticus* HCLB02. Each point represents a mean value (n=3) and error bars (±SD) are shown when larger than symbol

Appendix F Data on Changes in Phosphate Solubilization and pH of *S. haemolyticus* HCLB02

The changes in phosphate solubilization and pH of culture medium by *S. haemolyticus* HCLB02 were studied for a period of 8 d. Results were tabulated in Table A.5.

Table A.5 Changes in the phosphate solubilization and pH of S. haemolyticus *HCLB02*. Each point represents a mean value and the error bars showed the standard deviation (n=3)

Time, d	Absorbance @ 400nm	Net concentration of soluble phosphate, ppm	pH
0	0	0	5.54±0.11
1	0.67±0.02	27.98±1.06	3.78±0.11
2	0.77±0.03	32.90±1.39	3.56±0.05
3	0.76±0.02	32.18±1.11	3.68±0.02
4	0.83±0.02	35.93±1.20	3.72±0.04
5	0.87±0.01	37.62±0.67	3.78±0.06
6	0.81±0.03	34.78±1.24	3.78±0.04
7	0.80±0.04	34.35±1.91	3.73±0.03
8	0.79±0.01	33.84±0.44	3.74±0.05

Appendix G 16s rRNA Sequencing of A10, B02 and C11

A10 - *Staphylococcus haemolyticus* HCLA10 (MK140946)

CAGACAAGGAGCTTGCTCCTTTGACGTTAGCGGCGGACGGGTGAGTAACAC
GTGGGTAACCTACCTATAAGACTGGGATAACTTCGGGAAACCGGAGCTAAT
ACCGGATAATATTTCGAACCGCATGGTTCGATAGTGAAAGATGGTTTTGCTA
TCACTTATAGATGGACCCGCGCCGTATTAGCTAGTTGGTAAGGTAACGGCTT
ACCAAGGCGACGATACGTAGCCGACCTGAGAGGGTGATCGGCCACACTGGA
ACTGAGACACGGTCCAGACTCCTACGGGAGGCAGCAGTAGGGAATCTTCCG
CAATGGGCGAAAGCCTGACGGAGCAACGCCGCGTGAGTGATGAAGGTCTTC
GGATCGTAAAACTCTGTTATTAGGGAAGAACATACGTGTAAGTAACTATGCA
CGTCTTGACGGTACCTAATCAGAAAGCCACGGCTAACTACGTGCCAGCAGCC
GCGGTAATACGTAGGTGGCAAGCGTTATCCGGAATTATTGGGCGTAAAGCG
CGCGTAGGCGGTTTTTTAAGTCTGATGTGAAAGCCCACGGCTCAACCGTGGA
GGGTCATTGGAAACTGGAAAACTTGAGTGCAGAAGAGGAAAGTGGAATTCC
ATGTGTAGCGGTGAAATGCGCAGAGATATGGAGGAACACCAGTGGCGAAGG
CGACTTTCTGGTCTGTAACTGACGCTGATGTGCGAAAGCGTGGGGATCAAAC
AGGATTAGATACCCTGGTAGTCCACGCCGTAAACGATGAGTGCTAAGTGTTA
GGGGGTTTCCGCCCCTTAGTGCTGCAGCTAACGCATTAAGCACTCCGCCTGG
GGAGTACGACCGCAAGGTTGAAACTCAAAGGAATTGACGGGGACCCGCACA
AGCGGTGGAGCATGTGGTTTAATTCGAAGCAACGCGAAGAACCTTACCAAA
TCTTGACATCCTTTGACAACTCTAGAGATAGAGCCTTCCCCTTCGGGGGACA
AAGTGACAGGTGGTGCATGGTTGTCGTCAGCTCGTGTCGTGAGATGTTGGGT
TAAGTCCCGCAACGAGCGCAACCCTTAAGCTTAGTTGCCATCATTAAGTTGG
GCACTCTAAGTTGACTGCCGGTGACAAACCGGAGGAAGGTGGGGATGACGT
CAAATCATCATGCCCCTTATGATTTGGGCTACACACGTGCTACAATGGACAA
TACAAAGGGCAGCGAAACCGCGAGGTCAAGCAAATCCCATAAAGTTGTTCT
CAGTTCGGATTGTAGTCTGCAACTCGACTACATGAAGCTGGAATCGCTAGTA
ATCGTAGATCAGCATGCTACGGTGAATACGTTCCCGGGTCTTGTACACACCG
CCCGTCACACCACGAGAGTTTGTAACACCCGAAGCCGGTGGAGTAA

B02 - *Staphylococcus haemolyticus* HCLB02 (MK140948)

AAGGAGCTTGCTCCTTTGACGTTAGCGGCGGACGGGTGAGTAACACGTGGG
TAACCTACCTATAAGACTGGGATAACTTCGGGAAACCGGAGCTAATACCGG
ATAATATTTCGAACCGCATGGTTCGATAGTGAAAGATGGTTTTGCTATCACT
TATAGATGGACCCGCGCCGTATTAGCTAGTTGGTAAGGTAACGGCTTACCAA
GGCGACGATACGTAGCCGACCTGAGAGGGTGATCGGCCACACTGGAACTGA
GACACGGTCCAGACTCCTACGGGAGGCAGCAGTAGGGAATCTTCCGCAATG
GGCGAAAGCCTGACGGAGCAACGCCGCGTGAGTGATGAAGGTCTTCGGATC
GTAAAACTCTGTTATTAGGGAAGAACATACGTGTAAGTAACTGTGCACGTCT
TGACGGTACCTAATCAGAAAGCCACGGCTAACTACGTGCCAGCAGCCGCGG
TAATACGTAGGTGGCAAGCGTTATCCGGAATTATTGGGCGTAAAGCGCGCGT
AGGCGGTTTTTTAAGTCTGATGTGAAAGCCCACGGCTCAACCGTGGAGGGTC
ATTGGAAACTGGAAAACTTGAGTGCAGAAGAGGAAAGTGGAATTCCATGTG
TAGCGGTGAAATGCGCAGAGATATGGAGGAACACCAGTGGCGAAGGCGACT
TTCTGGTCTGTAACTGACGCTGATGTGCGAAAGCGTGGGGATCAAACAGGAT
TAGATACCCTGGTAGTCCACGCCGTAAACGATGAGTGCTAAGTGTTAGGGG
GTTTCCGCCCCTTAGTGCTGCAGCTAACGCATTAAGCACTCCGCCTGGGGAG
TACGACCGCAAGGTTGAAACTCAAAGGAATTGACGGGGACCCGCACAAGCG
GTGGAGCATGTGGTTTAATTCGAAGCAACGCGAAGAACCTTACCAAATCTTG
ACATCCTTTGACAACTCTAGAGATAGAGCTTTCCCCTTCGGGGGACAAAGTG
ACAGGTGGTGCATGGTTGTCGTCAGCTCGTGTCGTGAGATGTTGGGTTAAGT
CCCGCAACGAGCGCAACCCTTAAGCTTAGTTGCCATCATTAAGTTGGGCACT
CTAAGTTGACTGCCGGTGACAAACCGGAGGAAGGTGGGGATGACGTCAAAT
CATCATGCCCCTTATGATTTGGGCTACACACGTGCTACAATGGACAATACAA
AGGGCAGCGAAACCGCGAGGTCAAGCAAATCCCATAAAGTTGTTCTCAGTT
CGGATTGTAGTCTGCAACTCGACTACATGAAGCTGGAATCGCTAGTAATCGT
AGATCAGCATGCTACGGTGAATACGTTCCCGGGTCTTGTACACACCGCCCGT
CACACCACGAGAGTTTGTAACACCCGAAGCCGGTGGAG

C11 – *Staphylococcus cohnii* HCLC11 (MK140949)

TTTGACGTTAGCGGCGGACGGGTGAGTAACACGTGGGTAACCTACCTATAA
GACTGGAATAACTCCGGGAAACCGGGGCTAATGCCGGATAACATTTAGAAC
CGCATGGTTCTAAAGTGAAAGATGGTTTTGCTATCACTTATAGATGGACCCG
CGCCGTATTAGCTAGTTGGTAAGGTAACGGCTTACCAAGGCAACGATACGTA
GCCGACCTGAGAGGGTGATCGGCCACACTGGAACTGAGACACGGTCCAGAC
TCCTACGGGAGGCAGCAGTAGGGAATCTTCCGCAATGGGCGAAAGCCTGAC
GGAGCAACGCCGCGTGAGTGATGAAGGTCTTCGGATCGTAAAACTCTGTTAT
TAGGGAAGAACAAATGTGTAAGTAACTGTGCACGTCTTGACGGTACCTAATC
AGAAAGCCACGGCTAACTACGTGCCAGCAGCCGCGGTAATACGTAGGTGGC
AAGCGTTATCCGGAATTATTGGGCGTAAAGCGCGCGTAGGCGGTTTCTTAAG
TCTGATGTGAAAGCCCACGGCTCAACCGTGGAGGGTCATTGGAAACTGGGA
AACTTGAGTGCAGAAGAGGAAAGTGGAATTCCATGTGTAGCGGTGAAATGC
GCAGAGATATGGAGGAACACCAGTGGCGAAGGCGACTTTCTGGTCTGTAAC
TGACGCTGATGTGCGAAAGCGTGGGGATCAAACAGGATTAGATACCCTGGT
AGTCCACGCCGTAAACGATGAGTGCTAAGTGTTAGGGGGTTTCCGCCCCTTA
GTGCTGCAGCTAACGCATTAAGCACTCCGCCTGGGGAGTACGACCGCAAGG
TTGAAACTCAAAGGAATTGACGGGGACCCGCACAAGCGGTGGAGCATGTGG
TTTAATTCGAAGCAACGCGAAGAACCTTACCAAATCTTGACATCCTTTGACA
ACTCTAGAGATAGAGCCTTCCCCTTCGGGGGACAAAGTGACAGGTGGTGCA
TGGTTGTCGTCAGCTCGTGTCGTGAGATGTTGGGTTAAGTCCCGCAACGAGC
GCAACCCTTAAGCTTAGTTGCCAGCATTAAGTTGGGCACTCTAAGTTGACTG
CCGGTGACAAACCGGAGGAAGGTGGGGATGACGTCAAATCATCATGCCCCT
TATGATTTGGGCTACACACGTGCTACAATGGACAATACAAAGGGCAGCTAA
ACCGCGAGGTCATGCAAATCCCATAAAGTTGTTCTCAGTTCGGATTGTAGTC
TGCAACTCGACTACATGAAGCTGGAATCGCTAGTAATCGTAGATCAGCATGC
TACGGTGAATACGTTCCCGGGTCTTGTACACACCGCCCGTCACACCA

Appendix H Data on Cultural Condition Optimization for Maximal Phosphate Solubilization

H.1 Data on effect of glucose concentration on phosphate solubilization of *S. haemolyticus* HCLB02

The effect of glucose concentration on the phosphate solubilization ability of *S. haemolyticus* HCLB02 were studied in the range of 0 g L^{-1} to 20 g L^{-1}. Results were tabulated in Table A.6.

Table A.6 Effect of glucose concentration on the phosphate solubilization and cell growth of S. haemolyticus *HCLB02*. Each point represents a mean value and the error bars showed the standard deviation (n=3)

Glucose concentration (g/L)	**Absorbance (P-solubilized) @ 400nm**	**Absorbance (Control) @ 400nm**	**Net concentration of soluble phosphate, ppm**	**Cell concentration (x10^8 CFU/ml)**
0	0.35±0.03	0.13±0.01	11.21±1.12	0.46±0.06
5	0.50±0.05	0.19±0.01	15.69±2.20	0.62±0.11
10	0.91±0.03	0.11±0.01	39.65±1.29	2.69±0.15
15	0.96±0.03	0.11±0.00	42.47±1.32	2.85±0.09
20	1.01±0.06	0.11±0.01	45.38±2.57	2.90±0.12

H.2 Data on effect of yeast concentration on phosphate solubilization of *S. haemolyticus* HCLB02

The effect of yeast concentration on the phosphate solubilization ability of *S. haemolyticus* HCLB02 were studied in the range of 0 g L^{-1} to 4 g L^{-1}. Results were tabulated in Table A.7.

Table A.7 Effect of yeast concentration on the phosphate solubilization and cell growth of *S. haemolyticus* HCLB02. Each point represents a mean value and the error bars showed the standard deviation (n=3)

Yeast concentration (g/L)	**Absorbance (P-solubilized) @ 400nm**	**Absorbance (Control) @ 400nm**	**Net concentration of soluble phosphate, ppm**	**Cell concentration (x10^8 CFU/ml)**
0	0.60±0.02	0.15±0.01	22.75±0.90	1.35±0.08
1	0.63±0.01	0.14±0.01	24.58±0.39	1.77±0.12
2	0.91±0.03	0.11±0.01	39.65±1.29	2.66±0.18
3	0.48±0.05	0.15±0.02	17.02±1.29	1.17±0.11
4	0.12±0.04	0.02±0.01	9.83±3.20	0.34±0.14

H.3 Data on effect of magnesium chloride hexahydrate concentration on phosphate solubilization of *S. haemolyticus* HCLB02

The effect of magnesium chloride hexahydrate concentration on the phosphate solubilization ability of *S. haemolyticus* HCLB02 were studied in the range of 0 g L^{-1} to 10 g L^{-1}. Results were tabulated in Table A.8.

Table A.8 Effect of magnesium chloride hexahydrate concentration on the phosphate solubilization of *S. haemolyticus* HCLB02. Each point represents a mean value and the error bars showed the standard deviation (n=3)

Magnesium chloride hexahydrate concentration (g/L)	**Absorbance (P-solubilized) @ 400nm**	**Absorbance (Control) @ 400nm**	**Net concentration of soluble phosphate, ppm**	**Cell concentration (x10^8 CFU/ml)**
0	0.62±0.04	0.13±0.01	25.09±1.80	0.97±0.10
2.5	0.69±0.04	0.15±0.01	27.20±1.51	1.05±0.14
5	0.91±0.03	0.11±0.01	39.65±1.29	2.66±0.16
7.5	0.93±0.03	0.13±0.01	40.31±1.28	2.73±0.09
10	0.94±0.02	0.11±0.01	41.53±0.82	2.75±0.10

Appendix I Data on kinetic release of *S. haemolyticus* HCLB02 from microbeads

Initial cell viability = 52.04±2.34 % ($5.77\times10^8\pm1.92\times10^7$ CFU/g)

Initial amount of microbeads used = 0.01 g

Table A.9 Raw data for kinetic release of *S. haemolyticus* HCLB02 from dried microbeads. Each point represents a mean value and the error bars showed the standard deviation (n=3)

Time (min)	**Average plate count (CFU)**	**Bacteria released ($\times10^8\pm\times10^7$ CFU/ml)**	**Withdrawn bacteria ($\times10^6\pm\times10^5$ CFU/ml)**	**Cumulative bacteria released ($\times10^8\pm\times10^7$ CFU/ml)**
0	17.3±5.4	0.18±0.56	0.18±0.56	0.18±0.56
30	34.7±6.9	0.35±0.70	0.35±0.71	0.35±0.71
60	64.0±5.1	0.64±0.51	0.65±0.52	0.64±0.52
90	112.3±6.3	1.11±0.63	1.15±0.65	1.12±0.63
120	165.3±11.0	1.62±1.08	1.70±1.13	1.63±1.10
150	247.0±9.9	2.40±0.96	2.52±1.01	2.41±0.97
180	43.0±7.5	0.41±0.72	0.44±0.76	0.44±0.73
210	31.7±4.5	0.30±0.43	0.32±0.46	0.31±0.43
240	30.0±6.5	0.28±0.61	-	0.29±0.61

Table A.10 Kinetic data for zero, first order, Higuchi, Weibull and Ritger-Peppas models. Each point represents a mean value and the error bars showed the standard deviation (n=3)

Zero order		**First order**		**Higuchi**		**Weibull**		**Ritger-Peppas**	
y-axis	**y-axis**	**x-axis**	**y-axis**	**x-axis**	**x-axis**	**x-axis**	**y-axis**	**y-axis**	**x-axis**
ln(-ln(1-F))	**F**	**t**	**ln (1-F)**	$\sqrt{t}$	**t**	**ln t**	**ln F**	**F**	**ln t**
-	0.031±0.008	0	-0.031±0.009	0.000	0	-	-	0.031±0.008	-
-2.765±	0.061±0.010	30	-0.063±0.011	5.477	30	3.401	-2.797±0.150	0.061±0.010	3.401
-2.135±	0.112±0.005	60	-0.118±0.006	7.746	60	4.094	-2.193±0.044	0.112±0.005	4.094
-1.535±	0.194±0.004	90	-0.215±0.005	9.487	90	4.500	-1.641±0.022	0.194±0.004	4.500
-1.102±	0.283±0.009	120	-0.332±0.013	10.954	120	4.787	-1.263±0.032	0.283±0.009	4.787
-0.614±	0.418±0.003	150	-0.541±0.005	12.247	150	5.011	-0.872±0.007	0.418±0.003	5.011

*only data taken up to 150min were used in kinetic model fitting

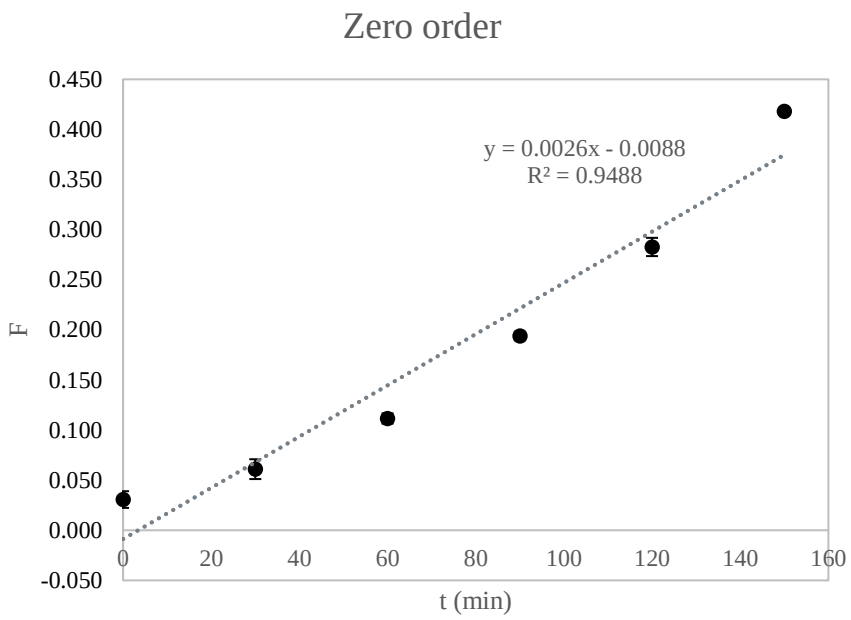

Figure A.4 Graph fitting for zero order kinetic models. Each point represents a mean value (n=3) and error bars (±SD) are shown when larger than symbol

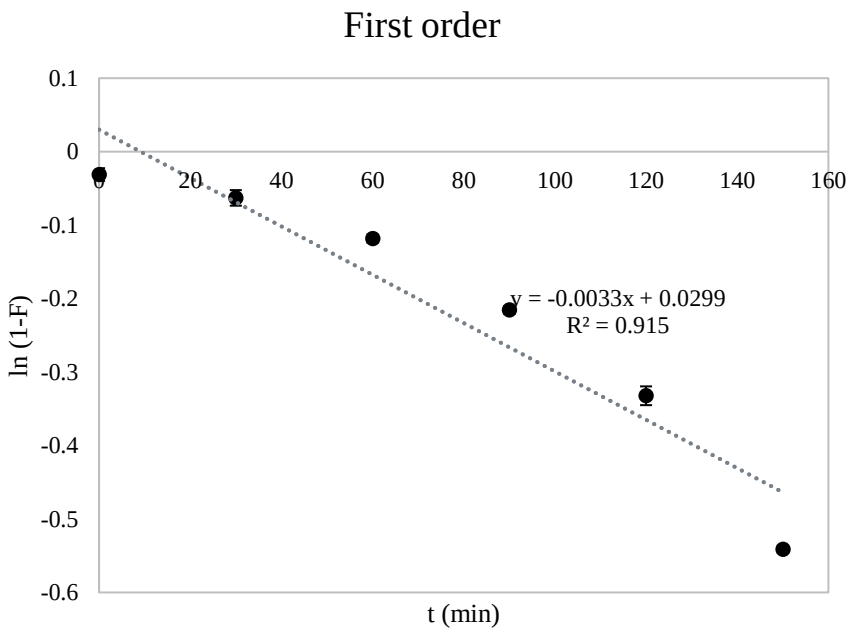

Figure A.5 Graph fitting for first order kinetic models. Each point represents a mean value (n=3) and error bars (±SD) are shown when larger than symbol

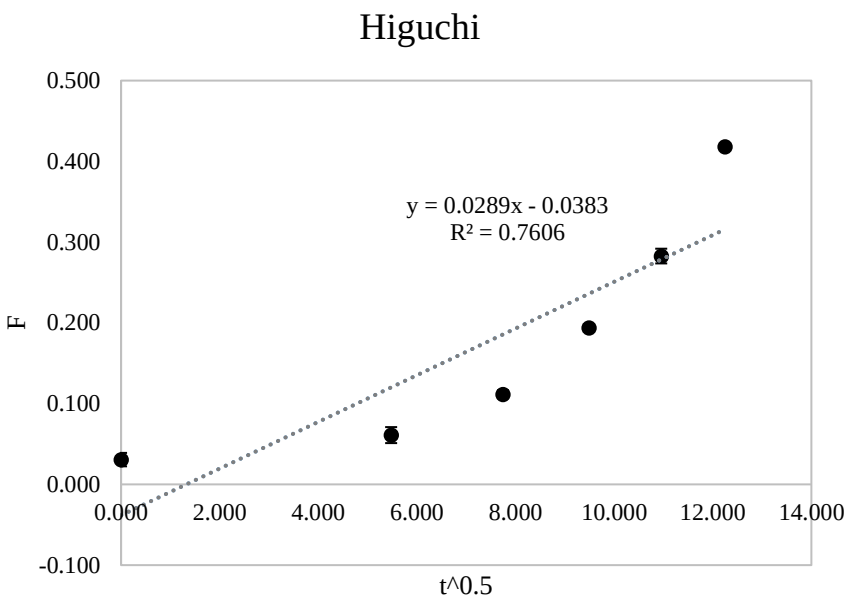

Figure A.6 Graph fitting for Higuchi kinetic models. Each point represents a mean value (n=3) and error bars (±SD) are shown when larger than symbol

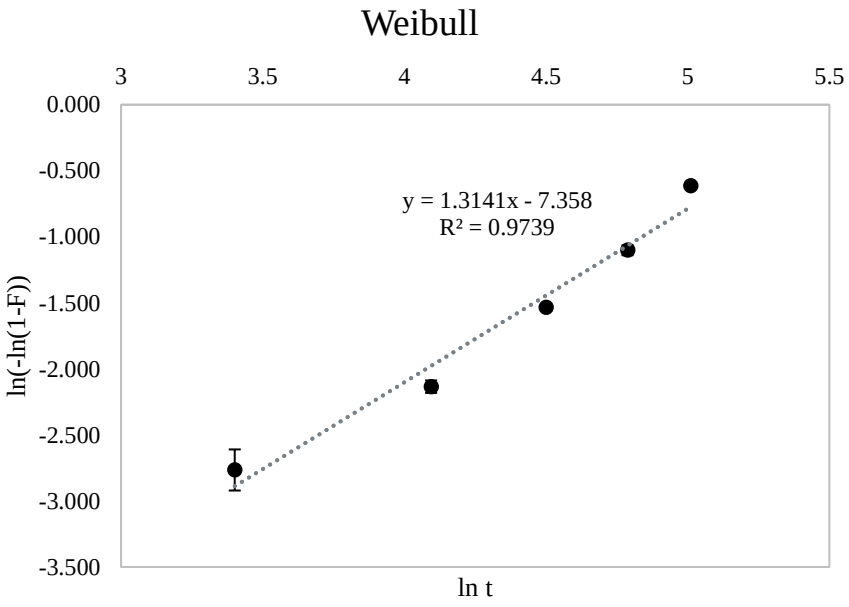

Figure A.7 Graph fitting for Weibull kinetic models. Each point represents a mean value (n=3) and error bars (±SD) are shown when larger than symbol

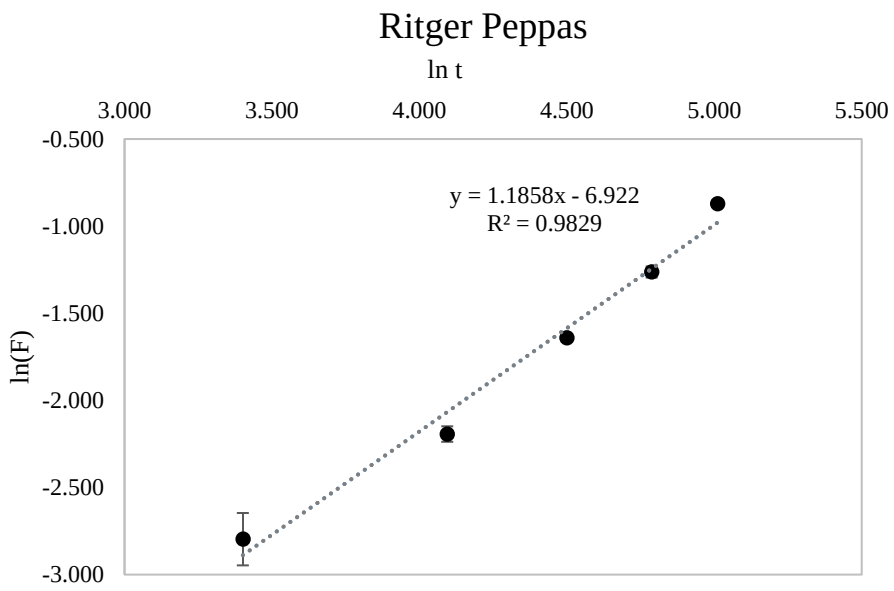

Figure A.8 Graph fitting for Ritger Peppas kinetic models. Each point represents a mean value (n=3) and error bars (±SD) are shown when larger than symbol

Appendix J Copyrights and Approval

1. Copyright from Biocatalysis and Agricultural Biotechnology

Curtin University Malaysia

YIIK SIANG HII <yiiksiang@postgrad.curtin.edu.my>

RE: Obtain permission request - Journal (1023857)
1 message

Rights and Permissions (ELS) <Permissions@elsevier.com> Wed, Jun 17, 2020 at 2:02 AM
To: "yiiksiang@postgrad.curtin.edu.my" <yiiksiang@postgrad.curtin.edu.my>

ELSEVIER

Dear Hii Yiik Siang

We hereby grant you permission to reprint the material below at no charge **in your thesis** subject to the following conditions:

1. If any part of the material to be used (for example, figures) has appeared in our publication with credit or acknowledgement to another source, permission must also be sought from that source. If such permission is not obtained then that material may not be included in your publication/copies.
2. Suitable acknowledgment to the source must be made, either as a footnote or in a reference list at the end of your publication, as follows:

   "This article was published in Publication title, Vol number, Author(s), Title of article, Page Nos, Copyright Elsevier (or appropriate Society name) (Year)."

3. Your thesis may be submitted to your institution in either print or electronic form.
4. Reproduction of this material is confined to the purpose for which permission is hereby given.
5. This permission is granted for non-exclusive world **English** rights only. For other languages please reapply separately for each one required.
6. Permission excludes use in an electronic form other than submission. Should you have a specific electronic project in mind please reapply for permission.
7. Should your thesis be published commercially, please reapply for permission.

Thanks

Akshaya

Akshaya G R

Copyrights Coordinator, GR - Copyrights

ELSEVIER | Global Book Production

+91 44 4299 4930 office

a.ganesh.1@elsevier.com

From: yiiksiang@postgrad.curtin.edu.my <yiiksiang@postgrad.curtin.edu.my>
Sent: Monday, June 15, 2020 2:24 PM
To: Rights and Permissions (ELS) <Permissions@elsevier.com>
Subject: Obtain permission request - Journal (1023857)

*** External email: use caution ***

Submission ID: 1023857
Date: 15 Jun 2020 9:53am

Name: Miss Hii Yiik Siang
Institute/company: Curtin University Malaysia
Address: CDT 250, Sarawak Malaysia
Post/Zip Code: 98009
City: Miri
State/Territory: Sarawak
Country: Malaysia
Telephone: 0105190737
Email: yiiksiang@postgrad.curtin.edu.my

Type of Publication: Journal

Title: Biocatalysis and Agricultural Biotechnology
Auhtors: Yiik Siang Hii, Chan Yen San, Shiew Wei Lau, Michael Kobin Danquah
Year: 2020
From page: 101643
To page: 101643
ISSN: 1878-8181
Volume: 26
Article title: Isolation and characterisation of phosphate solubilizing microorganisms from peat

I would like to use: Full article / chapter

I am the author of the Elsevier material: Yes
Involvement: The Elsevier author is the main author for thesis

In what format will you use the material: Print and Electronic
Translation: No

Proposed use: Reuse in a thesis/dissertation

Additional Comments / Information:

2. Copyright from Taylor and Francis for Figure 2.7

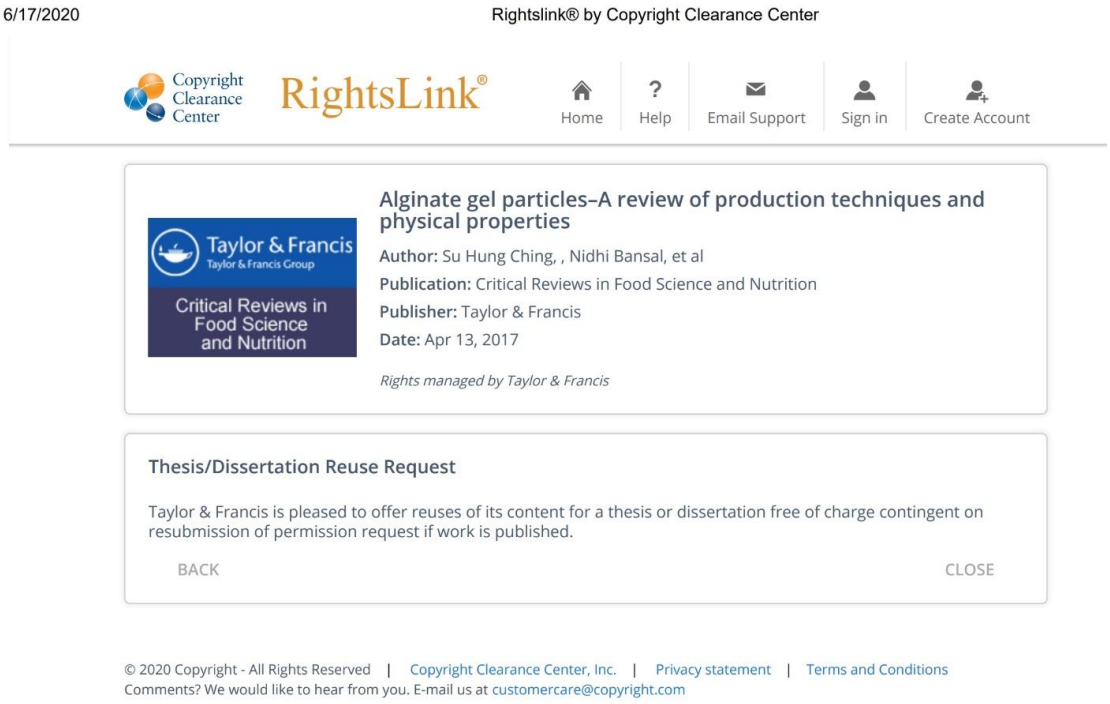

3. Copyright from Elsevier for Figure 1.3

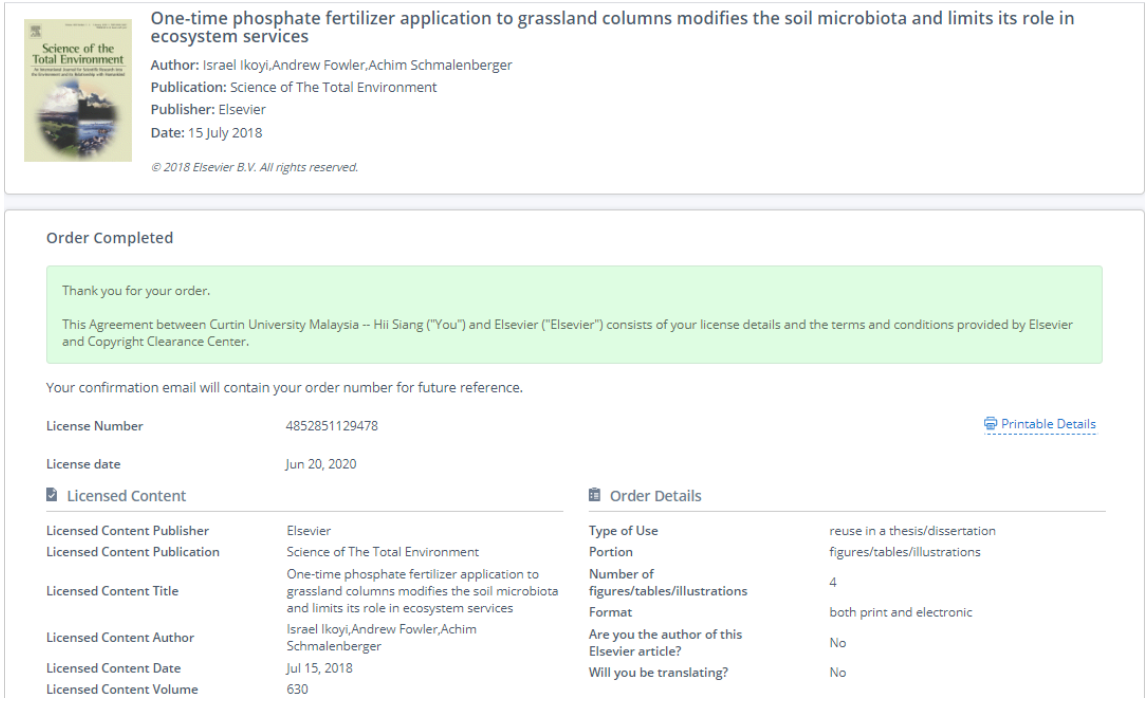

4. Copyright from Springer Nature for Figure 2.1

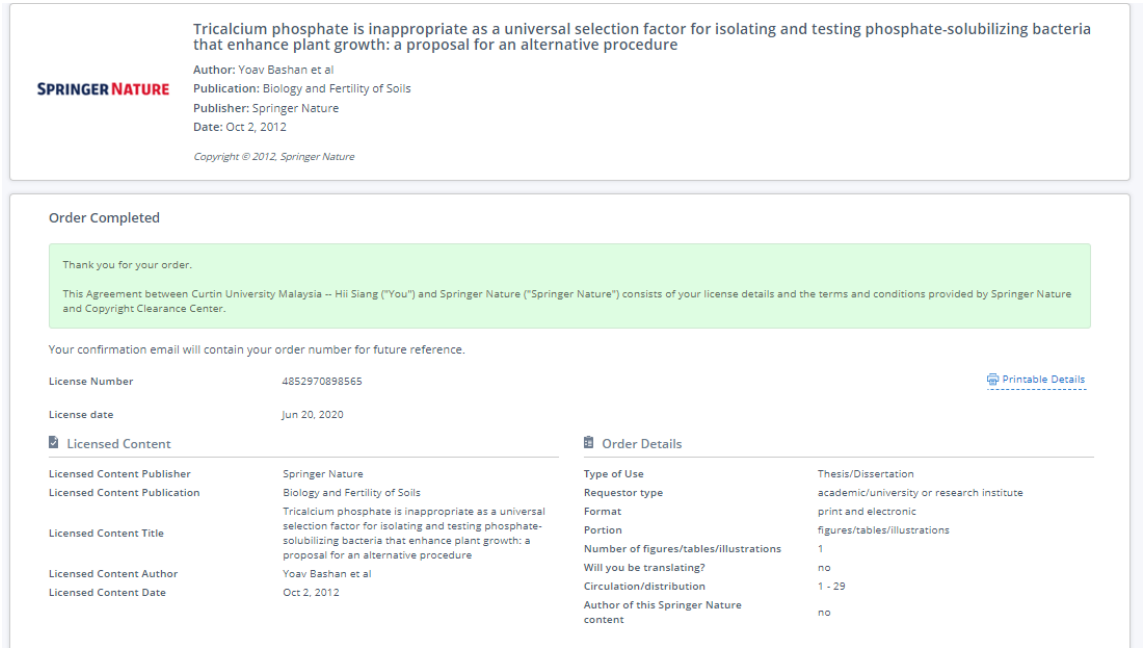

Tricalcium phosphate is inappropriate as a universal selection factor for isolating and testing phosphate-solubilizing bacteria that enhance plant growth: a proposal for an alternative procedure

Author: Yoav Bashan et al
Publication: Biology and Fertility of Soils
Publisher: Springer Nature
Date: Oct 2, 2012

Copyright © 2012, Springer Nature

Order Completed

Thank you for your order.

This Agreement between Curtin University Malaysia -- Hii Siang ("You") and Springer Nature ("Springer Nature") consists of your license details and the terms and conditions provided by Springer Nature and Copyright Clearance Center.

Your confirmation email will contain your order number for future reference.

License Number	4852970898565
License date	Jun 20, 2020

Printable Details

Licensed Content

Licensed Content Publisher	Springer Nature
Licensed Content Publication	Biology and Fertility of Soils
Licensed Content Title	Tricalcium phosphate is inappropriate as a universal selection factor for isolating and testing phosphate-solubilizing bacteria that enhance plant growth: a proposal for an alternative procedure
Licensed Content Author	Yoav Bashan et al
Licensed Content Date	Oct 2, 2012

Order Details

Type of Use	Thesis/Dissertation
Requestor type	academic/university or research institute
Format	print and electronic
Portion	figures/tables/illustrations
Number of figures/tables/illustrations	1
Will you be translating?	no
Circulation/distribution	1 - 29
Author of this Springer Nature content	no

5. Copyright from John Wiley and Sons for Figure 2.8

Comparison of an Effervescent Nozzle and a Proposed Air-Core-Liquid-Ring (ACLR) Nozzle for Atomization of Viscous Food Liquids at Low Air Consumption

Author: Heike P. Schuchmann, Volker Gaukel, Philipp Stähle
Publication: Journal of Food Process Engineering
Publisher: John Wiley and Sons
Date: Aug 11, 2015

© 2015 Wiley Periodicals, Inc.

Order Completed

Thank you for your order.

This Agreement between Curtin University Malaysia -- Hii Siang ("You") and John Wiley and Sons ("John Wiley and Sons") consists of your license details and the terms and conditions provided by John Wiley and Sons and Copyright Clearance Center.

Your confirmation email will contain your order number for future reference.

License Number	4851210693278
License date	Jun 17, 2020

Printable Details

Licensed Content

Licensed Content Publisher	John Wiley and Sons
Licensed Content Publication	Journal of Food Process Engineering
Licensed Content Title	Comparison of an Effervescent Nozzle and a Proposed Air-Core-Liquid-Ring (ACLR) Nozzle for Atomization of Viscous Food Liquids at Low Air Consumption
Licensed Content Author	Heike P. Schuchmann, Volker Gaukel, Philipp Stähle
Licensed Content Date	Aug 11, 2015
Licensed Content Volume	40
Licensed Content Issue	1
Licensed Content Pages	9

Order Details

Type of use	Dissertation/Thesis
Requestor type	University/Academic
Format	Print and electronic
Portion	Figure/table
Number of figures/tables	1
Will you be translating?	No

6. Copyright from Elsevier for Table 2.10

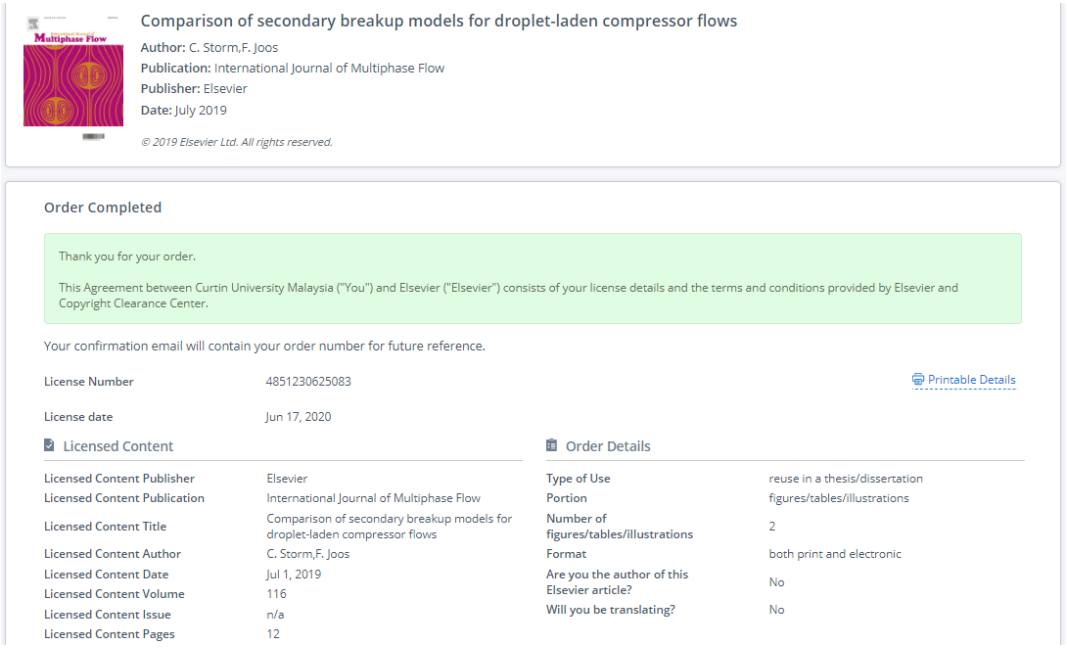

Comparison of secondary breakup models for droplet-laden compressor flows

Author: C. Storm,F. Joos
Publication: International Journal of Multiphase Flow
Publisher: Elsevier
Date: July 2019

Order Completed

Thank you for your order.

This Agreement between Curtin University Malaysia ("You") and Elsevier ("Elsevier") consists of your license details and the terms and conditions provided by Elsevier and Copyright Clearance Center.

Your confirmation email will contain your order number for future reference.

License Number	4851230625083
License date	Jun 17, 2020

Printable Details

Licensed Content

Licensed Content Publisher	Elsevier
Licensed Content Publication	International Journal of Multiphase Flow
Licensed Content Title	Comparison of secondary breakup models for droplet-laden compressor flows
Licensed Content Author	C. Storm,F. Joos
Licensed Content Date	Jul 1, 2019
Licensed Content Volume	116
Licensed Content Issue	n/a
Licensed Content Pages	12

Order Details

Type of Use	reuse in a thesis/dissertation
Portion	figures/tables/illustrations
Number of figures/tables/illustrations	2
Format	both print and electronic
Are you the author of this Elsevier article?	No
Will you be translating?	No